Electrochemical Investigations of H_2-producing Enzymes

Gabrielle Goldet

Saint John's College

Trinity 2009

A thesis submitted to the Board of the Faculty of Physical Sciences, for the degree of Doctor of Philosophy, University of Oxford

ABSTRACT

Electrochemical Investigations of H_2-producing Enzymes

Gabrielle Goldet, St. John's College
DPhil
Trinity term 2009

Hydrogenases are a family of enzyme that catalyses the bidirectional interconversion of H^+ and H_2. There are two major classes of hydrogenases: the [NiFe(Se)]- and [FeFe]-hydrogenases. Both of these benefit from characteristics which would be advantageous to their use in technological devices for H_2 evolution and the generation of energy. These features are explored in detail in this thesis, with a particular emphasis placed on defining the conditions that limit the activity of hydrogenases when reducing H^+ to produce H_2. Electrochemistry can be used as a direct measure of enzymatic activity; thus, Protein Film Electrochemistry, in which the protein is adsorbed directly onto the electrode, has been employed to probe catalysis by hydrogenases.

Various characteristics of hydrogenases were probed. The catalytic bias for H_2 production was interrogated and the inhibition of H_2 evolution by H_2 itself (a major drawback to the use of some hydrogenases in technological devices to produce H_2) was quantified for a number of different hydrogenase. Aerobic inactivation of hydrogenases is also a substantial technological limitation; thus, inactivation of both H_2 production and H_2 oxidation by O_2 was studied in detail. This was compared to inhibition of hydrogenases by CO so as to elucidate the mechanism of binding of diatomic molecules and determine the factors limiting inactivation. This allows for a preliminary proposal for the genetic redesigning of hydrogenases for biotechnological purposes to be made. Finally, preliminary investigation of the binding of formaldehyde, potentially at a site integral to proton transfer, opens the field for further research into proton transfer pathways, the structural implications thereof and their importance in catalysis.

Collaborations

Protein samples were generously donated by Dr. Thomas Happe, Prof. Juan Fontecilla-Camps and Prof. Bäbel Friedrich. Non-turnover voltammetry experiments in Chapter 4 were performed in collaboration with Dr. Alison Parkin. Experiments in Chapters 3, 5 and 6 were completed with the help of Ms. Caterina Brandmayr. The model for CO inhibition of [FeFe]-hydrogenases described in Chapter 5 was developed by Prof. Fraser Armstrong.

Acknowledgements

My first thanks should go to Fraser for eventually believing in me enough to give me a superb project, being generous and forbearing enough to put up with my irreverence, stupidity and stubbornness, for having some great ideas that form the backbone of this thesis (and some frankly laughable ones that gave me a good giggle when I needed it) and for teaching more than a thing or two. The collaborations with Christine Cavazza in the Fontecilla-Camps group, Oliver Lenz and Marcus Ludwig in the Friedrich group and Sven Stripp in the Happe group have been priceless. A particular thanks to Sven for supplying fountains of [FeFe]-hydrogenase at the drop of a hat, precious musical advice and for being approximately three million times cooler than me. Caterina deserves top marks for riding the storm of my not-so-infrequent idiocy, and tactfully coaxing me to an understanding of what was usually going on in our experiments. And for assaulting me with more data than any part II has ever subjected their supervisor to. Again, this thesis would not look like much without you.

The rest of the Armstrong group, present and past, who have also been subject to my slowness, need for explanation and lack of respect for safety, get a big high-five. A particularly painful one should go to Alison and James for answering my every question and doing a considerable amount of proofreading. My other proofreaders - Nat, Annemarie, Kylie and Chris - offered inestimable guidance. Margarida should also get a special mention for keeping me sane in the second year.

To my friends (i.e. housemates and friends thereof) who have made life bearable over the last few years of lunacy, I can't thank you enough. Lastly, but probably most importantly (cliché as it is), to my parents (et à la fratrie bien sure!), whose liberal up-bringing has allowed me to do something as utterly insane as a PhD and whose support has been unstinting.

Table of Contents

List of Figures

List of Figures

List of Figures

List of Figures

List of Abbreviations

1. Enzymes names

Abbreviated enzyme name	Organism name	Type of organism
*Av*H	*Allochromatium vinosum*	Purple-photosynthetic sulphur metabolizer, facultative anaerobe
*Ca*HydA	*Clostridium acetobutylicum*	Fermentative anaerobe
*Cr*HydA1	*Chlamydomonas reinhardtii*	Photosynthetic green algae
*Cp*I	*Clostridium pasteurianum*	Fermentative anaerobe
*Cp*II	*Clostridium pasteurianum*	Fermentative anaerobe
*Cs*HydA	*Clorococcum submarinum*	Photosynthetic green algae
*Db*H	*Desulfomicrobium baculatum*	Sulphate-reducer, facultative anaerobe
*Dd*H	*Desulfovibrio desulfuricans*	Sulphate-reducer, facultative anaerobe
*Df*H	*Desulfovibrio fructosavorans*	Sulphate-reducer, facultative anaerobe
*Dg*H	*Desulfovibrio gigas*	Sulphate-reducer, facultative anaerobe
*Df*H	*Desulfovibrio fructosavorans*	Sulphate-reducer, facultative anaerobe
*Dv*H	*Desulfovibrio vulgaris*	Sulphate-reducer, facultative anaerobe
*Re*MBH	*Ralstonia eutropha* (strain H16)	Knallgas bacteria
*Rm*MBH	*Ralstonia metallidurans* (strain CH34)	Knallgas bacteria

2. Enzymes: structural elements

Abbreviation	Name
[FeS]-	Iron sulphur cluster
[FeFe]-	Iron-iron-containing hydrogenase active site
[NiFe]-	Nickel-iron-sulphur-containing hydrogenase active site
[NiFe(Se)]-	Nickel-iron-containing hydrogenase active site
[NiFeSe]-	Nickel-iron-selenium-containing hydrogenase active site

3. Constants

Abbreviation	Name
F	Faraday's constant
K	Rate constant
k_H	Henry's constant
$K_I^{app}(CO/H_2)$	Apparent inhibition constant for inhibition of H_2 oxidation by CO
$K_I^{app}(CO/H^+)$	Apparent inhibition constant for inhibition of H_2 production by CO
$K_I^{app}(H_2/H^+)$	Apparent inhibition constant for inhibition of H_2 production by H_2
R	Gas constant
K_M	Michaelis Constant
K_{ox}	Equilibrium constant for oxidation
K_{red}	Equilibrium constant for reduction

4. Technique

Abbreviation	Name
DFT	Density functional theory
EPR	Electron paramagnetic resonance
ENDOR	Electron nuclear double resonance
ESEEM	Electron Spin Echo Envelope Modulation
EXAFS	Extended X-ray absorption fine structure
IR spectroscopy	Infrared spectroscopy
PFE	Protein film electrochemistry

5. Units

Abbreviation	Name
µA	Micro-amps
Å	Angstrom
atm	Atmospheres
°C	Degree Celsius
kDa	Kilo-Dalton
rpm	Rotations per minute
s	Seconds
scc/min	Standard cubic centimetres per minute
V	Volts
V/s	Volts per second

6. Variables

Abbreviation	Name
Ω	Electrode rotation rate
E	Potential
E_{switch}	Electrochemical switch potential
v	Scan rate
i	Current
i_{cat}	Current (catalytic)
i_{lim}	Current (limiting)
n	Number of electrons
t	Time

7. Miscellaneous

Abbreviation	Name
e^-	Electron
H_2ase	Hydrogenase
PGE	Pyrolytic graphite edge
PDB	Protein Data Bank
ROS	Reactive oxygen species
SHE	Standard Hydrogen Electrode

οὐδεὶς ἡμῶν οὐδὲν οἶδεν οὐδ᾽ αὐτὸ
τοῦτο, πότερον οἴδαμεν ἢ οὐκ οἴδαμεν « οὐδ᾽ αὐτὸ τὸ μὴ
εἰδέναι καὶ τὸ εἰδέναι οἴδαμεν (ὅτι ἔστιν) οὐδ᾽ ὅλως πότε-
ρον ἔστι τι ἢ οὐκ ἔστιν »

Metrodorus of Chios (4th century B.C.)

Chapter 1:

Introduction

"We won't run out of oil – but what will happen is that production will decline and that's when all hell will break loose"

Dr. James McKenzie, Senior Assistant on the Climate Change Programme,
World Resources Institute, Washington

The prospect of this so-called "hell", not to mention the growing concerns over the ecological consequences of burning fossil fuels,[1,2] has instigated a wave of research into renewable sources of energy as these are thought to be the only long-term solution. Hydrogen has been heralded as the fuel for the future since the early 1970's.[3] The combustion of H_2 presents a number of advantages over that of fossil fuels;[4] most obviously, it is clean as water is the only by-product of this reaction and liberates a considerable amount of energy.

$$2H_2 + O_2 \rightarrow 2H_2O + \text{energy} \qquad \text{Reaction 1.1}$$

Hydrogen is also more efficiently transported through pipelines than electricity is transmitted through power lines,[5] so an intuitive alternative would be to produce electricity from H_2 locally using fuel cells.[6]

At present, 98% of H_2 is produced by (endothermic) steam reforming of coal, naphtha and natural gas.[7,8]

$$CH_4 + H_2O \rightarrow CO + 6H_2 \qquad \text{Reaction 1.2}$$

Further H_2 can be evolved (exothermically) by reacting the by-product CO with more H_2O in the water gas shift reaction.[9]

$$CO + H_2O \rightarrow CO_2 + H_2 \qquad \text{Reaction 1.3}$$

Overall this process is endothermic and generates CO_2. Therefore, biological alternatives to this process have become an imperative.

1.1. Hydrogenases in nature and technology

The name hydrogenase was given to a family of enzyme catalysing the interconversion of H^+ and H_2 ($2H^+ + 2e^- \leftrightarrow H_2$) by Strickland and Stephenson in 1931.[10] Hydrogenases have attracted much interest of late because of their potential involvement in the generation of "green" energy.[11] They are widespread in nature and their activity is coupled to processes as diverse as methanogenesis, sulphate reduction, Fe^{3+} reduction, and denitrification,[12] as is shown in Figure 1.1.

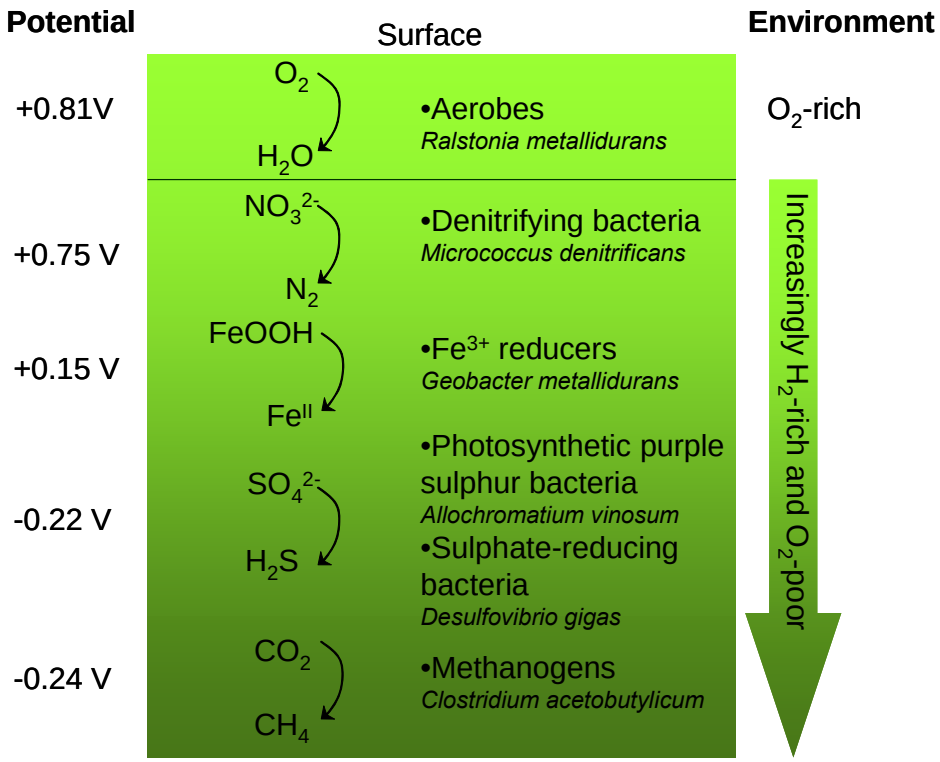

Figure 1.1: Biological H_2-cycling in wetland soils. Schematic representation of the vertical distribution of organisms with respect to the surface with the potentials of the redox reactions occurring at each level. The potentials[13] are quoted vs. the Standard Hydrogen Electrode (SHE) and are calculated for pH 7, 25 °C, 1 atm pressure for a gas. As the standard gas pressure is higher than what will be experienced by the organism *in vivo*, the potentials will vary according to the Nernst equation.

Figure 1.2 and Figure 1.3 demonstrate some of the functions performed by hydrogenases in nature:

1. **H_2-uptake hydrogenase:** these oxidise H_2 *in vivo*. Often linked to the respiratory chain,[5] these generate protons so as to set-up a proton gradient across the membrane which powers ATP synthesis.[14]
2. **H_2 producers:** these evolve H_2 *in vivo*, for example, to utilise excess reducing equivalents produced by the oxidation of lactate or pyruvate[15] or to mop up H^+ to generate the proton motive force without the expenditure of ATP.[16]
3. **Bi-directional hydrogenases:** can catalyse both processes and are thought to play a role in fermentation and/or act as electron valves during photosynthesis in cyanobacteria.[17]

In general, the more aerobic the environment, the lower the concentration of H_2 experienced by the organism and the more biased the hydrogenases expressed are to H_2 oxidation.[18] Thus, fermentative bacteria in the most anaerobic environments are excellent H_2-producers. This trend will be shown to correlate with the ability to bind H_2 in Chapters 3 and 4.

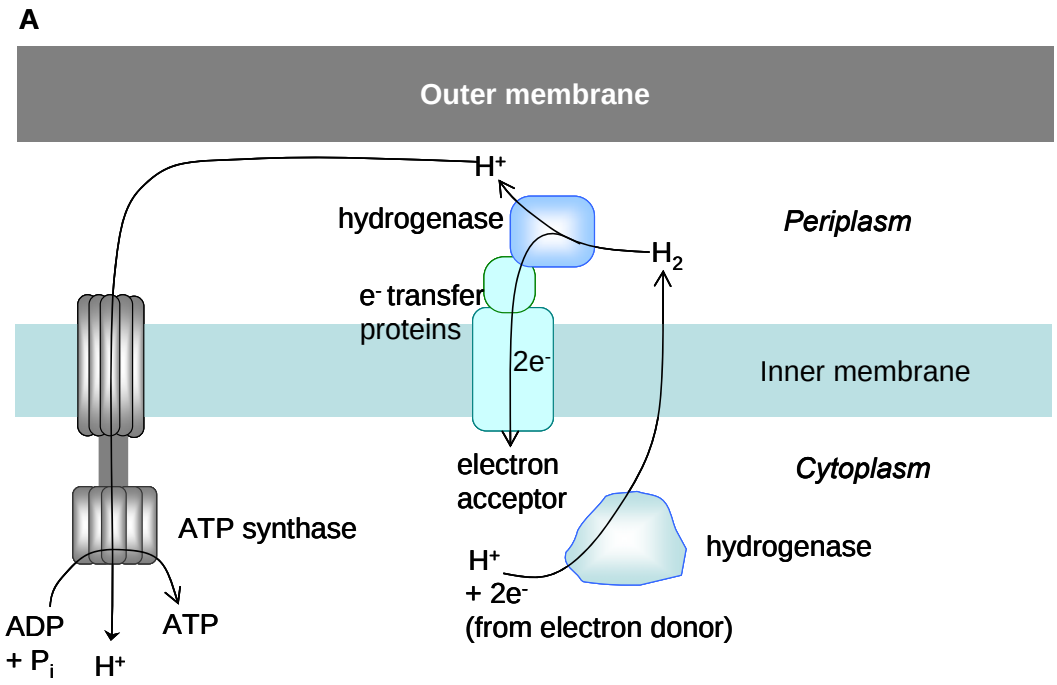

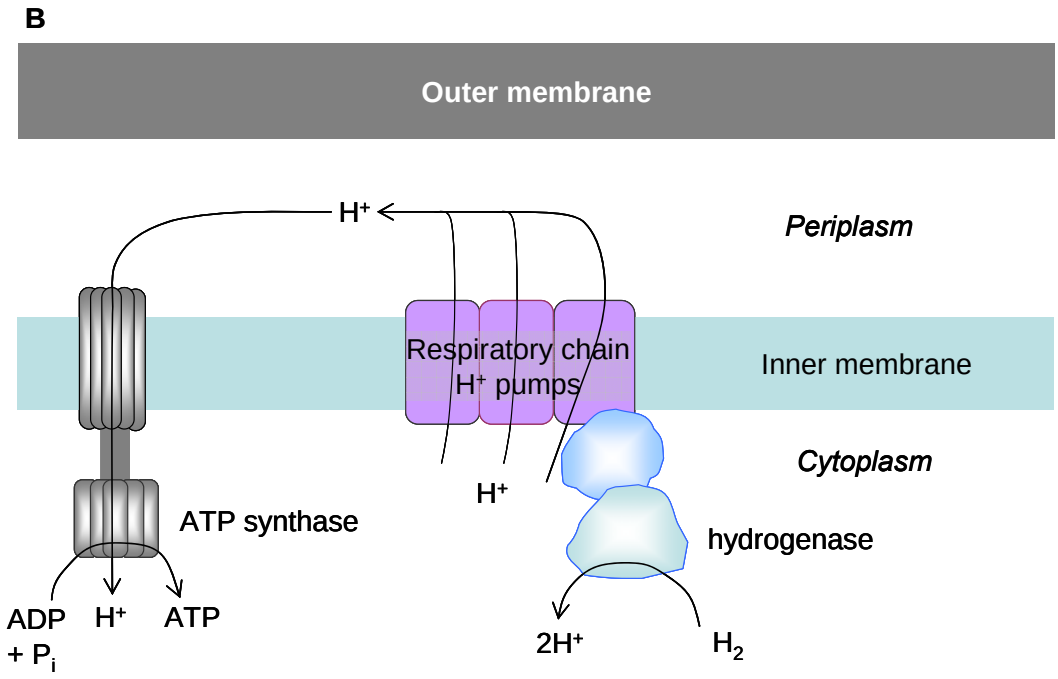

Figure 1.2: Representation of cellular energy conservation involving hydrogenases and other membrane proteins. A) In *Desulfovibrio* bacteria, H_2 is produced by a hydrogenase inside the cell and diffuses to the periplasm where it is oxidised by an uptake hydrogenase to produce protons which traverse the membrane (down their concentration gradient) through the ATP synthase thus driving ATP synthesis.[19] B) In many other species, H^+ is produced by a hydrogenase inside the cell and is pumped into the periplasm by the respiratory chain.[5] The process of H^+ diffusion back into the cytoplasm and concomitant ATP synthesis then mimics that described in panel A.

1.1.1. Biological H_2 production

Biological H_2 production[11] is either carbon neutral (in the case of fermentative H_2 production) or actually consumes CO_2 (in the case of photosynthetic H_2 production[20]). It also eliminates the need for precious metals and avoids the production of other toxic wastes such as NO_x.[5] In both photosynthetic and fermentative H_2 production, the key enzyme is hydrogenase.[21]

The mechanism for H_2 formation at the active site of hydrogenases involves the combination of protons (H^+) and electrons, and the reverse process, H_2 oxidation, occurs through heterolytic cleavage of H_2 to generate H^+ and a hydride ligand.[22]

1.1.1.1. Photosynthetic H_2 production

It is intuitive that we should exploit solar energy, as it reaches the planet at a rate of ~12 000 TW[23] which far exceeds that required by global human consumption.[24,25] Photosynthesis offers us this opportunity. Since the discovery of photosynthetic H_2 production in the green alga *Scenedesmus obliqus*[26] two other different kinds of organism were also found to produce H_2 as a by-product of the harvesting of light: cyanobacteria[27] and purple photosynthetic bacteria.[28-30]

Cyanobacterial and purple photosynthetic bacterial H_2 production

Whilst H_2 is evolved by hydrogenases in green algae, the nitrogen-reducing nitrogenase enzyme in cyanobacteria and purple photosynthetic bacteria catalyse H_2 production as a by-product of NH_3 formation according to Reaction 1.4.[13]

$$N_2 + 8e^- + 8\,H^+ + 16ATP \rightarrow 2NH_3 + H_2 + 16ADP + 16P_i \qquad \text{Reaction 1.4}$$

This reaction is atomically inefficient in terms of H_2 production, requiring 8 H^+ and 8 e^- to generate 1 H_2 molecule. In fact, the turnover numbers of nitrogenase are nearly 1000 times lower than those of [FeFe]-hydrogenases (see section 1.2.2).[31] Furthermore, these organisms also have an uptake hydrogenase that oxidises the H_2 produced at the nitrogenase and, in the case of cyanobacteria, potentially at the bidirectional hydrogenase. However, there is a growing interest in cyanobacterial H_2 production by the bidirectional hydrogenase as it is thought to be more insensitive to O_2 than algal H_2-producing hydrogenases.[32,33] This is because the cyanobacterial enzyme is a [NiFe]-hydrogenase rather than a [FeFe]-hydrogenase, and the former are considered to be more O_2-tolerant (see section 1.2 and Chapter 6). Studies directed at improving cyanobacterial H_2 production by genetic modification have shown that reducing the activity of the H_2-uptake hydrogenase in *Synechocystis* sp.[27] and *Anabeana variabilis*[34]

enhances H_2 production. However, cyanobacteria and purple photosynthetic bacteria remain inefficient H_2-producers with respect to green algae (the light efficiency of cyanobacteria and purple photosynthetic bacteria is about 6% and that of green algae is 10-13%[35]) and have not been studied in this thesis.

Photosynthetic H_2 production in algae

In contrast to cyanobacteria and purple photosynthetic bacteria, the high rates of H_2 production in the algal species *Chlamydomonas reinhardti* means its hydrogenase, *Cr*HydA1, is potentially of great technological interest and it is thus examined in greater detail in this thesis.

The established mechanism for H_2 production in algae involves water-splitting catalysed by the photosystem II complex of proteins (PSII) in the thylakoid membrane,[36] as shown in Figure 1.3. The electrons generated by this process are then activated by light in PSII and eventually transferred to photosystem I (PSI), at which point they are further activated and used to reduce a ferrodoxin (Fd) which becomes re-oxidised upon reduction of the adjacent hydrogenase. The hydrogenase then combines the electrons with protons to produce H_2.

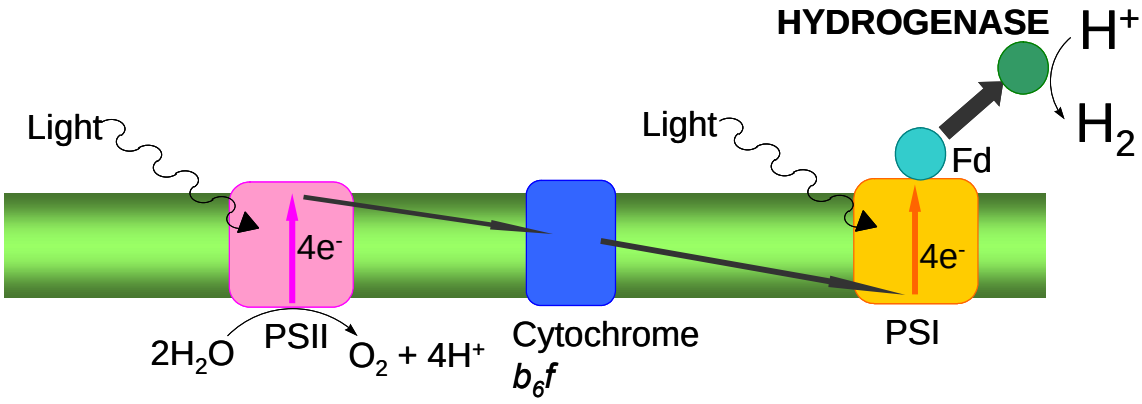

Figure 1.3: Photosynthetic chain of electron transport in green algae leading to H_2 production.

A substantial limitation of this process in terms of biotechnological applications of algal H_2 production is that the O_2 evolved from water-splitting at PSII inhibits the hydrogenase,[37] the key maturation proteins for the hydrogenase and the transcription of the genes that code for this enzyme.[38,39] Various different methods attempting to address this problem have been reported.

Improving algal H_2 production

Melis et al. showed that sulphur deprivation of algal cells results in light-induced damage of particular component of the PSII complex.[40] This cannot be repaired under sulphur-deprived conditions. As PSII is the site of water splitting, this process slows down until it eventually falls beneath the rate of aerobic respiration thus depleting the cells of O_2. The genes for the hydrogenase are then induced and the enzyme expressed begins H_2 production. However, the experimentally observed H_2 production is limited to ~25% of its maximum yield on account of a variety of different potential factors including cyclic electron transport (see below).[35]

An inducible chloroplast gene expression system developed by Surzicki et al. also makes use of the fact that diminishing the activity of another component of PSII brings anoxia about thus leading to the induction of the hydrogenase gene and H_2 production by the hydrogenase. This system involves a mutant form in which addition of copper to the cells prevents the accumulation of RNA coding for this component of PSII.[41]

Further attempts to reduce the concentration of O_2 in the chloroplasts of *Chlamydomonas reinhardtii* have lead Kruse et al. to make a mutant with an enhanced capacity for H_2 production.[42] In this mutant the issue of cyclic electron transport which

deflects electrons away from the hydrogenase (thus preventing it from reducing H^+ to produce H_2) is circumvented. This was found to induce an at least five-fold increase in H_2 evolution over the wild type.[42]

It has been suggested that expressing the hydrogenase under the control of a promoter induced by conditions other than anaerobiosis in a heterologous expression system could help to by-pass the issue of O_2 sensitivity of gene induction.[43] However the maturation proteins and hydrogenase itself still require anaerobic conditions. It has also been hypothesised that hydrogenases might be designed so that their active sites are inaccessible to O_2[43] and efforts to engineer such an enzyme are ongoing.[44] Evidence for gas channel effects on O_2 sensitivity of hydrogenases is detailed in section 1.2.3 below. Overall, gaining an understanding of the structure and the mechanisms by which hydrogenases are inactivated by O_2 is paramount in the quest to engineer enzymes better able to sustain H_2 production in the presence of O_2. Hydrogen production by wild type organisms is unlikely to produce commercially-interesting quantities of H_2,[9] even under sulphur-deprived conditions.[43]

Artificial photosynthesis

Recent results by Hambourger et al.[45] have shown that a device utilising the [FeFe]-hydrogenase from *Clostridium acetobutylicum*, *Ca*HydA, coupled to a light-harvesting material can be used to produce H_2. In their photoelectrochemical biofuel cell (Figure 1.4), the photoanode is comprised of porphyrin dye-sensitized TiO_2 particles on a transparent, conductive tin (IV) oxide support and the cathode consists of hydrogenase adsorbed onto a carbon felt electrode. The porphyrin dye (P) absorbs light and is excited up to the singlet state denoted P*. When P* relaxes back to its radical cationic

form $P^{\cdot+}$, it transfers an electron into the conduction band (CB) of TiO_2. The electrons thus generated are transmitted to the cathode where H_2 is evolved. The original P state is regenerated by concomitant oxidation of NADH to NAD^+, and NADH itself is regenerated through enzymatic oxidation of a biomass.[46] In a similar vain, a hydrogenase attached to a Ru dye-sensitized TiO_2 particle was employed to photo-produce H_2.[47]

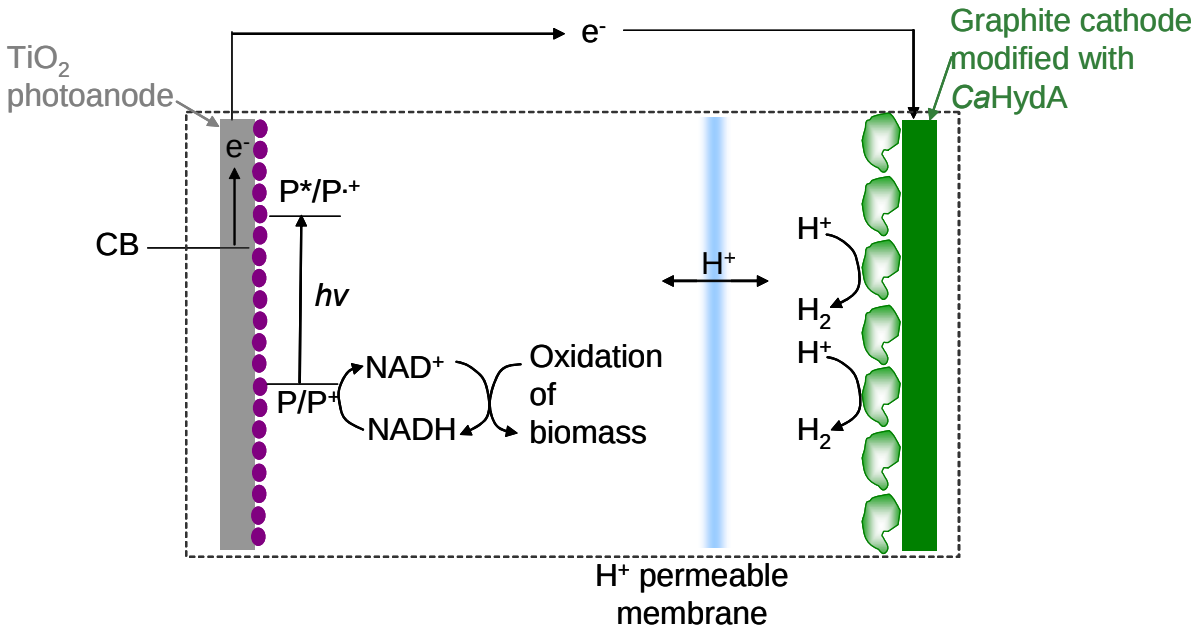

Figure 1.4: Photoelectrochemical biofuel cell reported by Hambourger et al.[45] with a dye-sensitized TiO_2 photoanode and a graphite cathode modified with the hydrogenase from *Clostridium acetobutylicum*, *Ca*HydA.

1.1.1.2. Fermentative H_2 production

Biomass obtained in the first stage of light conversion (i.e. starch found in higher plant and microalgae biomass) and, appealingly, various waste streams can be fermented by fermentative microbes to produce H_2.[9,48] However, the overall H_2 yields from these organisms are low because fermentation has evolved to produce biomass rather than H_2.[31] Another major disadvantage of fermentative H_2 production is that CO_2 is a by-product. A general scheme for the production of H_2 through fermentation is shown in

Figure 1.5. Fermentative H_2 production also occurs in green algae,[49] though it operates at 0.01% of the rate of photosynthetic H_2 production.[35] Like photosynthetic microorganisms, fermentative bacteria have also been the subject of genetic manipulation to enhance H_2 production.[50]

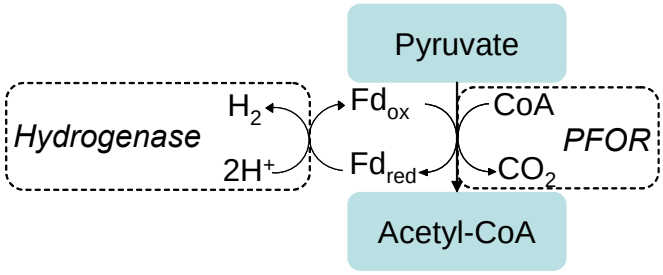

Figure 1.5: Fermentative production of H_2 as a by-product of the reaction of pyruvate to form Acetyl-CoA catalysed by pyruvate ferrodoxin oxidoreductase (PFOR).

Clostridium acetobutylicum is an example of an organism in which this fermentative process occurs and its hydrogenase, *Ca*HydA, is known to have a very high turnover for H_2 production.[51,52] It has thus been studied in detail in this thesis.

1.1.1.3. A combinatorial fermentative/ photosynthetic approach to H_2 production

A recent proposal for a photobioreactor that still under development[35] utilises green algae, photosynthetic bacteria and fermentative bacteria. Cell biomass accumulating during photosynthesis by photosynthetic microorganisms is consumed by fermentative microbes. These produce H_2 and organic acids which stimulate further biomass production by the photosynthetic organisms.

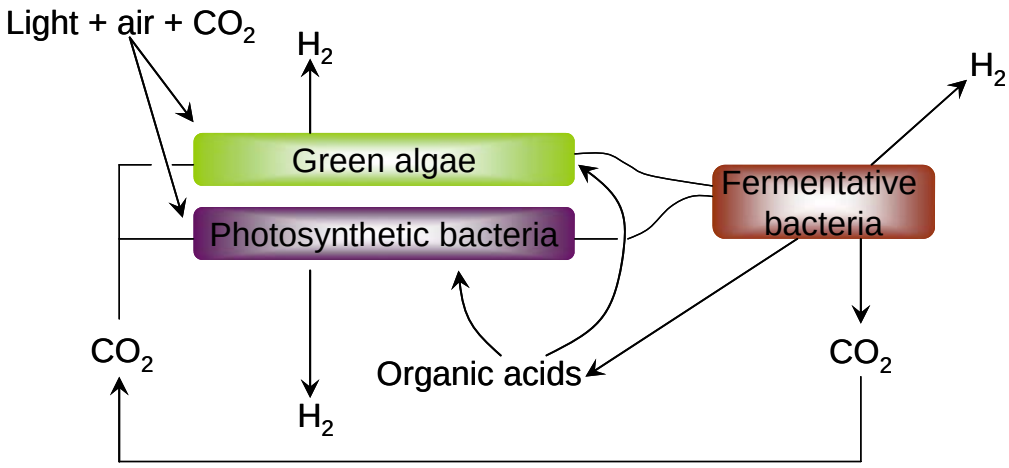

Figure 1.6: Combinatorial bioreactor under investigation by Ghirardi et al.[35]

1.1.2. Other uses of hydrogenases in biotechnology

Waste decontamination by hydrogenases is an innovative new area of research and has revealed a wealth of possible new applications. Bioremediation of chromate occurs via reduction to Cr(III) (to give products that are both less toxic and less soluble and thus can be more easily removed from solution) catalysed by hydrogenase.[53] The [FeFe]-hydrogenase from *Desulfovibrio desulfuricans* (*Dd*H) has been used to reduce the soluble pollutant Pd^{2+} to Pd^{0}. This "Bio-Pd^{0}" can then used to catalyse the reduction of Cr(VI), reductive dehalogenation of polychlorinated biphenyls or hydrogenation reactions in chemical manufacturing.[54] Decontamination of waste water from TNT using the [FeFe]-hydrogenase from *Ca*HydA has also been achieved.[55] A point of note, when considering the use of hydrogenases in waste detoxification, is the prevalence of [FeFe]-hydrogenases over [NiFe(Se)]-hydrogenases as this process exploits the bias of [FeFe]-hydrogenases towards H_2 production with respect to the [NiFe(Se)]-

hydrogenases.* The evolved H_2 is then used as a reductant in decontamination processes.

In comparison to Pt, the metal content in hydrogenases (Fe and Ni) is cheap and readily available. As a component part of electrical devices for energy generation, it is obviously important to compare the activity of hydrogenases with that of Pt in both the direction of H_2 production and oxidation. Three notable studies have been performed. Adams et al. indicated in 1979 that the activity of hydrogenases was not too far below that of Pt for H_2 evolution.[56] The photobiofuel cell devised by Hambourger in 2008[45] was as efficient with a hydrogenase coated graphite cathode as with a Pt cathode. Jones and co-workers also showed that the hydrogenase from *Allochromatium vinosum* (*Av*H) compared favourably with Pt in H_2 oxidation.[57]

Hydrogenases have also been employed as a component of a H_2 fuel cell in which they are adsorbed to a Pyrolytic Graphite "Edge" (PGE) electrode, thus forming the anode (as shown in Figure 1.7).[58,59] The electrons generated from oxidation of H_2 are then transferred to the cathode where a PGE electrode modified with an oxidase utilises them to reduce O_2 to H_2O, concomitantly consuming H^+ produced by the oxidation of H_2 on the other side of the semi-permeable membrane.

* The catalytic bias of the [NiFe(Se)]- and [FeFe]-hydrogenases for H_2 production and oxidation is discussed in Chapter 4

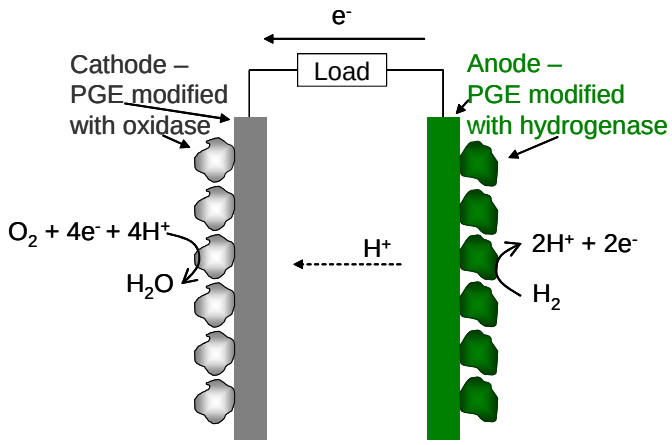

Figure 1.7: Schematic representation of a H_2/O_2 bio-fuel cell.[58,59]

One issue limiting the use of electrodes modified with hydrogenase is the size of the enzyme with respect to the platinum atom. Each enzyme molecule and Pt atom represents one reaction centre. If these two reactions centres were performing at the same rate, it is evident that an electrode of a much larger surface area would be needed for the hydrogenase than the equivalent Pt electrode for the former to function as efficiently as the latter. Moreover, the reaction of hydrogenases with our aerobic atmosphere is an important limitation in this bio-fuel cell.[60] This is thus another example of an application which would benefit from a greater understanding of the characteristics of hydrogenase that make them more susceptible to O_2.

1.2. The structure of hydrogenases

The presence of Fe in hydrogenases was established in the 1950s[61] and that of Ni in most hydrogenases in the 1980s.[62-65] There are three distinct categories of hydrogenases:[66] [NiFe(Se)]-hydrogenases, [FeFe]-hydrogenases[67] and Fe-only hydrogenases, named according to the metals present in their active site. In the [NiFe(Se)]-hydrogenases, the presence of selenium identifies the subclass of the

[NiFeSe]-hydrogenases[68] from the "standard"[†] [NiFe]-hydrogenases.[69] Ligation of the [NiFe(Se)]- active site to the protein backbone occurs through a cysteine in [NiFe]-hydrogenase and a selenocysteine in [NiFeSe]-hydrogenases. The Fe-only hydrogenases are also known as "[FeS]-cluster-free hydrogenases" because they lack the [FeS]-clusters[70] possessed by [FeFe]- and [NiFe(Se)]-hydrogenases that are thought to act as an electron relay between their active sites and their physiological partners.[71-73]

The [NiFe(Se)]- and [FeFe]-hydrogenases catalyse the interconversion of H_2 and H^+ whilst Fe-only hydrogenases catalyse the reduction of N_5,N_{10}-methenyltetrahydromethanopterine to N_5,N_{10}-methenylenetetrahydromethanopterine.[74] Despite the structural similarities between the Fe-only[‡], [NiFe(Se)]- and [FeFe]-hydrogenases in that they all contain the common structural unit $Fe(CO)_n(CN)RS$[66,75] in their active sites, strictly speaking, the former are not hydrogenases because of the fact that they catalyse a different process. They are thus not pertinent to the present discussion. The fact that the two distinct classes of enzymes which catalyse the same process, the [NiFe(Se)]- and [FeFe]-hydrogenases, evolved independently and share no sequence homology is an interesting example of convergent evolution.

A crucial aspect of the study of hydrogenases has become their response to O_2 which varies greatly from enzyme to enzyme. This will be discussed in Chapter 6. Other divisive characteristics are their bias for the two processes they catalyse, H_2 production and H_2 oxidation, and their affinity for H_2. The [FeFe]-hydrogenases are more biased towards H_2 production than the [NiFe(Se)]-hydrogenase.[5,77] These characteristics are

[†] The term "standard" [NiFe]-hydrogenase is used for convenience in this thesis to represent those enzymes which do not contain a selenium atom in their active site.
[‡] The structure of the prosthetic active site in the Fe-only hydrogenases is still unknown but it is thought to contain a single low-spin Fe atom ligated[76] to CO ligands and a cysteine.[77,78]

explored in Chapters 3 and 4. Whilst gross traits differentiate the [NiFe(Se)]-hydrogenases from [FeFe]-hydrogenases, further distinctions can be elucidated even within these two classes of enzyme.

1.2.1. The [NiFe(Se)]-hydrogenases

Unlike the [FeFe]-hydrogenase, which abound in both the prokaryotic and eukaryotic domains, the [NiFe(Se)]-hydrogenases are only found in prokaryotes. These are generally thought to be more O_2-tolerant than [FeFe]-hydrogenases.[5,18] The structures of five [NiFe(Se)]-hydrogenases – those from the bacteria *Desulfovibrio gigas* (*Dg*H),[78,79] *Desulfovibrio fructosovorans* (*Df*H),[80] *Desulfovibrio desulfuricans* (*Dd* [NiFe]-H),[81] *Desulfomicrobium baculatum* (*Db*H),[82] and *Desulfovibrio vulgaris* Miyazaki F (*Dv*H)[83] – have been solved. A vast body of spectroscopic[84-86] and electrochemical[87,88] research has concentrated on [NiFe]-hydrogenases. It has been shown that they share a number of common features:

1. Their bimetallic active-sites, which are described in greater detail in section 1.2.1.1 below.
2. They possess a chain of three [FeS]-clusters thought to act as a relay for shuttling electrons between the active site and their physiological partners.[66] Whilst many have at least one [3Fe4s]-clusters,[73] [NiFeSe]-hydrogenases only have [4Fe4S]-clusters.[89] The [3Fe4S]-cluster has a redox potential much more positive than that of the onset of H_2 oxidation, so it is usually in its reduced state during turnover.[63] The [FeS]-clusters are labelled “proximal”, “medial” and “distal” according to their position with respect to the active site.
3. They are dimeric, with the active site being located in the large subunit and the [FeS]-clusters in the small sub-unit.

Moreover, the structures of a [NiFe]-hydrogenase (from *Desulfovibrio gigas*, *Dg*H) and a [NiFeSe]-hydrogenase (from *Desulfomicrobium baculatum*, *Db*H) were shown to be highly related in terms of conservation of residues surrounding the [FeS]-clusters in the small subunit[82] even though there is overall only a 36% sequence homology between these two enzymes (Figure 1.8).[90]

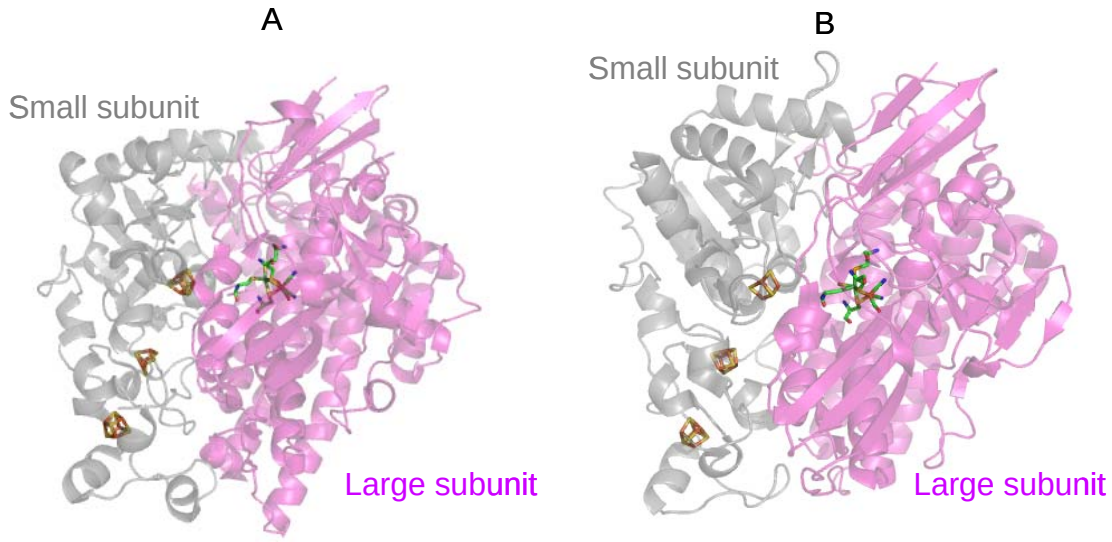

Figure 1.8: A) Cartoon representation of the oxidised form of the [NiFe]-hydrogenase from *Desulfovibrio gigas* (*Dg*H - PDB code: 1YQ9[91]). B) Cartoon representation of the reduced form of the [NiFeSe]-hydrogenase from *Desulfomicrobium baculatum* (*Db*H – PDB code: 1CC1[82]). Both A and B were constructed using PyMOL.

1.2.1.1. The active site

In both [NiFe]- and [NiFeSe]-hydrogenases, the Fe atom is coordinated by one CO and two CN ligands which fit into hydrophobic and hydrophilic pockets (respectively) around the active site.[92,93] Apart from the aforementioned ligation to the selenocysteine and slightly shorter distance between the two metals in *Db*H, its active site is almost identical to that of *Dg*H – see Figure 1.9.[82] The Ni is coordinated to two cysteines and a further two cysteines bridge the two metal atoms in the active site. In the case of the [NiFeSe]-hydrogenase, one of the terminal cysteines is a selenocysteine. Interestingly, the presence of an extra cyanide ligand bound to the Fe atom in the active site of the

soluble [NiFe]-hydrogenase from *Ralstonia eutropha* has been suggested to confer increased O_2 tolerance to this enzyme.[94]

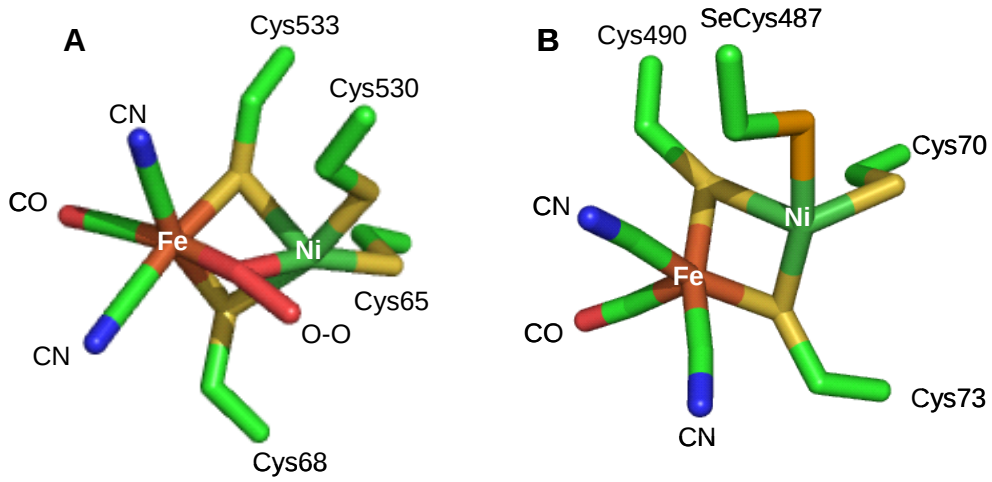

Figure 1.9: Structures of active sites of the oxidised [NiFe]-hydrogenase *Dg*H (A) (PDB code: 1YQ9[91] and reduced [NiFeSe]-hydrogenase *Db*H. (B) (PDB code: 1CC1[82]). The O-O bridging ligand is thought to be a hydroperoxo- ligand in the Ni-A state and a hydroxo ligand in the Ni-B state. Both schematics were constructed using PyMOL.

1.2.1.2. The oxidation states

The active site of [NiFe]-hydrogenases has been characterised in number of different active and inactive states as shown in Table 1.1. While Ni-A, Ni-B, Ni-C and Ni-R are EPR active, Ni-SU, Ni-SI, Ni-SR and Ni-R are not. Redox changes in the active site occur either at the O-ligand bridging the two metals or at the Ni atom; it is now widely acknowledged that the Fe atom remains in its diamagnetic +2 state.[95]

Relative no. of electrons	Structure	State
0	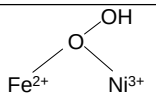	Ni-A
1	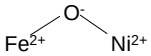	Ni-SU
2	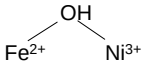	Ni-B
3	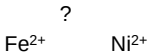	Ni-SI & Ni-SR
4	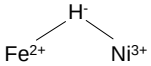	Ni-C
5	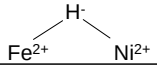	Ni-R

Table 1.1: Oxidation states of [NiFe]-hydrogenases.[66]

The relationship between these states is represented in Figure 1.10. Formation of the active states[96] Ni-C, Ni-R and Ni-SI from the more oxidised Ni-A and Ni-B state requires activation by subjecting the enzyme to H_2[97] to remove a bound O-species.[83] Oxidation of the active states to produce the inactive Ni-B under anaerobic conditions is slow[93,98] whereas reactivation of the enzyme in the Ni-B state to the active state is fast, hence its also being known as the "Ready state". In contrast, the Ni-A state generated by more strongly oxidising conditions[69,79] is also known as the "Unready" state which reflects the fact that conversion of this species to the active species is much slower than the "Ready" state.[99] Whilst the O-species present in the active site in the Ni-B state is thought to be a bridging hydroxo- ligand which becomes protonated upon activation of the enzyme,[99] a hydroperoxo-[66,91,100] species has been postulated to bridge the two metals in the Ni-A state. One-electron reduction of Ni-A and Ni-B yields their respective EPR-silent inactive states, Ni-SU (where the U stands for "Unready") and Ni-SR (where the R stands for "Ready").[101] These two states are in acid base equilibrium with the EPR-silent Ni-SI[92] and an early report suggested that protonation of an active site cysteine is central to their interconversion.[93] In any case, Ni-SI can be

generated by heating above 30 °C[102] and reduction of this state gives Ni-C. As Ni-C is converted to the EPR-silent state Ni-R by reduction with H_2, the fact that it does not spontaneously convert to Ni-R indicates that Ni-C does not catalyse the reduction of H^+ to H_2, but may instead be an important intermediate in catalysis.[103]

The so-called P state[87] characterised electrochemically by Lamle et al.[104] is thought to be a transient species in the transformation between Ni-A and the active forms of the active site. As it is not oxidised to Ni-B, it cannot be equivalent to Ni-SI. The reversible formation of the P state from Ni-A is thought to correspond to a proton transfer or a rearrangement of the bound O-species in the active site. Subsequent formation of the active state proceeds with exposure to H_2 or CO which are thought to displace the bound hydroperoxo species.[87] The "dead" state corresponds to an irreversibly inactivated form of the enzyme.[105]

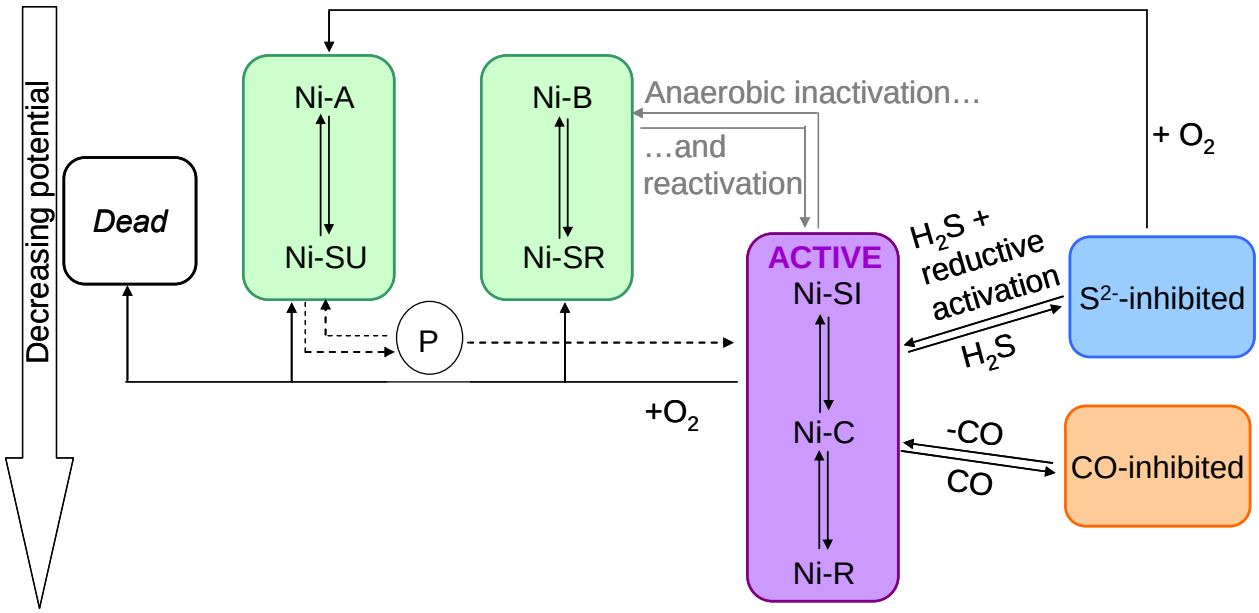

Figure 1.10: Schematic of the oxidation states of [NiFe]-hydrogenases. Vertical transitions correspond to 1 electron redox changes.

1.2.1.3. The catalytic mechanism

That the competitive inhibitor CO was found to bind to the Ni in crystallographic results on the CO-inhibited form of *Dv*H is compelling evidence for the binding of H_2 occurring at the Ni atom[106] and this has been supported by numerous other EPR studies,[103,107,108] though some computational studies has suggested that binding might occur at the Fe atom.[109,110] Cleavage of H_2 is generally thought to be heterolytic though the precise mechanism is still very much under scrutiny[36,101,111,112] – it is thought to be facilitated by back-donation of electron density from the Ni to the H_2 anti-bonding σ-orbital.[113,114] Binding of H_2 to the Ni-SI state leads to the Ni-R state with Ni-C as a transient intermediate between these two states. Two electrons and two protons are then removed to regenerate the Ni-SI.[96] The electrons are transferred to the redox partner via the chain of [FeS]-clusters and protons are transported out of the protein. The existence of a proton transfer chain is still a speculative matter, though it has been suggested that glutamate and cysteine residues in the active site pocket are involved in proton translocation.[115,116]

1.2.2. The [FeFe]–hydrogenases

Aside from the technological interest in their ability to produce H_2 at very high rates, [FeFe]-hydrogenases have the potential to allow some evolutionary insight into the prokaryote to eukaryote transition as they are found in both eukaryotes and prokaryotes.[117]

Bacterial and algal hydrogenases differ in that the former have a chain of [FeS]-clusters separated by ~11 Å[118] (see Figure 1.11), as do the [NiFe(Se)]-hydrogenases, whilst the latter possess only the [4Fe4S]-subcluster present within the H-cluster (see section

1.2.2.1 on the active site of [FeFe]-hydrogenases). Whilst the hydrogenase from *Desulfovibrio desulfuricans* (*Dd*H) and hydrogenase 1 from *Clostridium pasteurianum* (*Cp*I) are both bacterial hydrogenases, there are differences in their [FeS]-cluster content: *Dd*H has two [4Fe4S]-clusters in addition to that present in the active site[119] whilst *Cp*I has three [4Fe4S]- and an extra [2Fe2S]-cluster.[120] These two clusters are located near the surface of *Cp*I but at opposite sides of the enzyme with respect to the next [FeS]-cluster along the chain; it is thus unclear which of these engages in electron transfer with the redox partner.[66] Additionally, *Dd*H and another [FeFe]-hydrogenase from a *Desulfovibrio* species, *Desulfovibrio vulgaris* (*Dv*) Hildenborough, are dimeric whereas clostridial and algal hydrogenases are monomeric. In fact, the small subunit in *Dd*H (shown in pink in Figure 1.11A) mimics the c-terminus of the main chain of *Cp*I.[66,121]

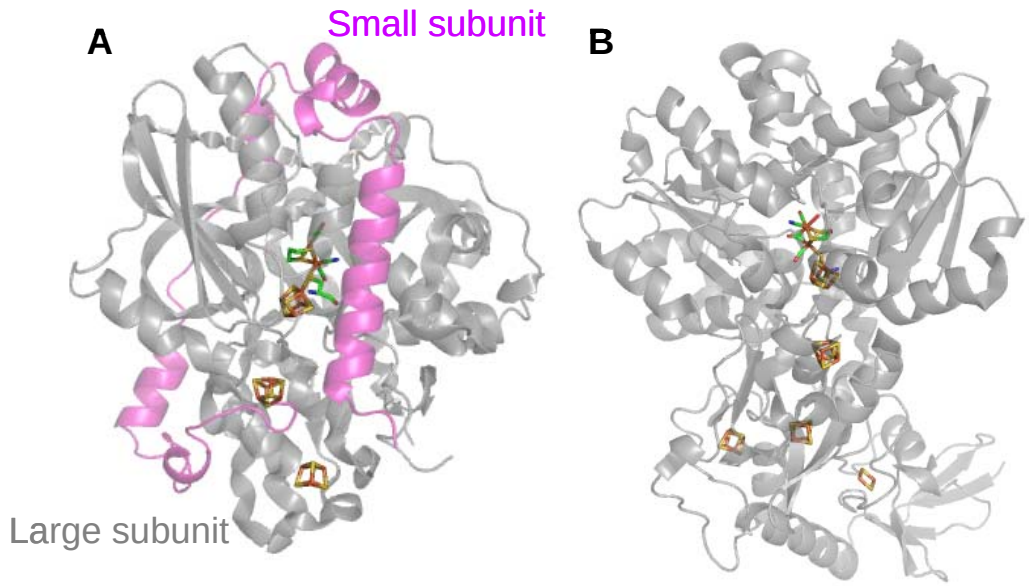

Figure 1.11: A) Cartoon representation of the reduced form of the [FeFe]-hydrogenase from *Desulfovibrio desulfuricans* (*Dd*H - PDB code: 1HFE[119]). B) Cartoon representation of the oxidised form of the [FeFe]-hydrogenase from *Clostridium pasteurianum* (*Cp*I - PDB code: 3C8Y[122]). Structures constructed using PyMOL.

1.2.2.1. The active site

The active site – the so-called "H-cluster"[123] - of bacterial [FeFe]-hydrogenases has been shown to be highly related to that of eukaryotic algal [FeFe]-hydrogenases.[124] Both have a binuclear [2Fe]-subcluster in which the two Fe atoms are labelled Fe_P (for "proximal") and Fe_D (for "distal"), denoting their relationship in space to the ligated [4Fe4S]-cluster (see Figure 1.12).[125]

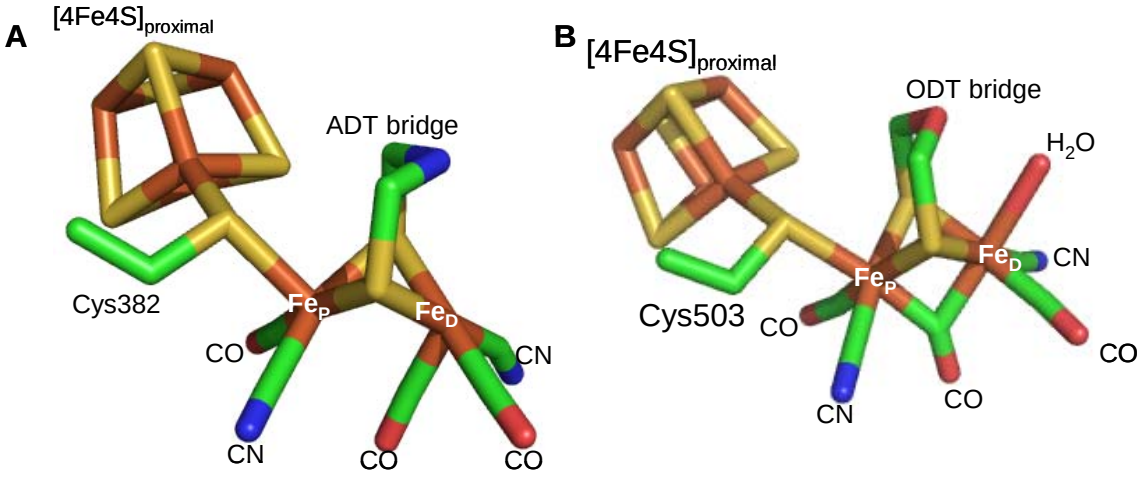

Figure 1.12: Structures of the H-clusters of the [FeFe]-hydrogenase from A) *Desulfovibrio desulfuricans* (*Dd*H) and B) *Clostridium pasteurianum* (*Cp*I) constructed using PyMol. A) Reduced *Dd*H active site (structure from ref.[126]). B) Oxidised *Cp*I active site (PDB code: 3C8Y[122]). Structures constructed using PyMOL.

As in the [NiFe(Se)]-hydrogenases, the two Fe atoms in the binuclear [FeFe]-subcluster are coordinated to CO and CN ligands[127] thought to be important in tuning the electronic structure of the active site and stabilising the low-spin state of the Fe atoms.[128,129] They are also ligated to a cysteine bridging to the [4Fe4S]-subcluster[67] and a bidentate ligand whose identity is still under discussion. Initially modelled as a propanedithiolate (PDT) ligand,[119] it was later postulated to be an aminedithiolate (ADT) ligand. The possibility of the N in ADT acting as a base and conjugate acid with an appropriate pKa to transmit H^+ to the active site was suggested.[126,130] This is supported by ENDOR and ESEEM studies which have shown the presence of two N

atoms close to the active site[131-133] as well as a recent pulse EPR study.[134] Whilst one signal was reminiscent of imidazole the other is expected to be from the CN ligand.[135] As there are no histidines close to the active site, the former signal could thus be assigned as the bridgehead N atom in an ADT ligand.[66] The most recent crystallographic data in conjunction with DFT studies on *Cp*I indicate that an oxodithiolate (ODT)[122] is more likely than an ADT bridge for this enzyme. It has been suggested that the identity of this moiety has a considerable effect on the electronic structure of the [FeFe]-subcluster.[136]

The assignment that both the Fe atoms are ligated to one CN and one CO was made on the basis of the presence of an amino acid residue close to each of the Fe atoms that could hydrogen-bond ligands such as CN; the second diatomic ligand thus had to be incapable of H_2-bonding, hence the assignment of CO.[119] The two first published structures of an [FeFe]-hydrogenase ascribed a different position to one of the CO ligands bound to Fe_D (see Figure 1.12). Whilst Peters and co-workers found it to bridge between the two Fe atoms of the binuclear site of *Cp*I,[120] Nicolet et al.[119] assigned it as a terminal ligand bound to Fe_D. Later crystallographic data have indicated that this discrepancy can be attributed to the different oxidation states of the two samples that were used in these studies.[126,137,138] The sample of *Dd*H was purified under more reducing conditions than that of *Cp*I. It was thus postulated that the CO shifts from a bridging position in the more oxidised state to terminal in the more reduced state[137] though it has also been argued that the position of the CO is semi-bridging rather than purely terminal in this reduced state.[139] The more electron-rich the Fe which binds CO is, the stronger the binding[66] because of back-bonding from the Fe atom to the CO ligand – in fact Fe^{3+} is not expected to bind CO which is a strong π–electron *accepting*

ligand.[140] In the terminal conformation, back-bonding is facilitated therefore it is intuitive that the more reduced the oxidation state, the more terminal binding should be favoured. The increased steric blockage around Fe_D with terminally-bound CO may affect the ability of the H_{red} state to bind inhibitors; this will be discussed further in Chapter 5.

1.2.2.2. The oxidation states

A number of states of the [FeFe]-hydrogenase active site have been described, as illustrated in Figure 1.13. The aerobic purifications of the [FeFe]-hydrogenases from *Desulfovibrio vulgaris* and *Desulfovibrio desulfuricans*[141-143] generated an EPR- and catalytically-inactive state now known as H_{ox}^{inact}. Upon monoelectronic reduction, a transient EPR-active state denoted H_{trans} is formed[141] which converts irreversibly to the catalytically-active H_{ox} state under more reducing conditions.[142] The nature of the structural and electronic changes that take place during this reduction are still under discussion;[66,129,144] one hypothesis is that an oxidised Cys-SOH ligated to the active site in the H_{trans} is reduced to Cys-SH in the H_{ox}.[139] A further one-electron reduction of the H_{ox} state yields the EPR-inactive but catalytically active H_{red} state, as indicated by EPR[67,143] and IR spectroscopy.[139] Super-reduction of the H-cluster to a state more reduced than H_{red} at potentials below -487 mV vs. SHE has also been reported from IR-spectroscopy results.[139] The state known as H_{ox}^{air} (the active site after exposure to O_2, labelled "dead" in Figure 1.13) is generated upon oxidation of the active states. The H_{ox}-CO state is formed upon exposure of active enzyme to exogenous CO.[129,138] The consensus on the oxidation states of the active sites of [FeFe]-hydrogenases from DFT calculations[145] and EPR[146] and IR spectroscopy,[139,147,148] is as follows: $Fe(II)_DFe(II)_P$ in H_{ox}^{inact}, $Fe(II)_DFe(I)_P$ in H_{ox} and $Fe(I)_DFe(I)_P$ (or H^--$Fe(II)_DFe(I)_P$[139]) in H_{red}.[66] A super-

reduced state (H_{sred}) of *Dd*H, in which the [4Fe4S]-subcluster (rather than the [2Fe]-center) is reduced with respect to H_{red}, has also been observed in infrared spectrospcopy upon reduction below -0.54 V vs. the Normal Hydrogen Electrode.[139] At the other end of the scale, the nature of the O-species present in the active site upon oxidative inactivation remains to be resolved conclusively, though some speculate that it may be a water ligand[149] or an OH bound to Fe_D.[145] It is long-established that prolonged exposure to O_2 causes irreparable damage to the H-cluster[67] possibly due to reaction of partially reduced Reactive Oxygen Species (ROS) with the thiolate ligands.[66]

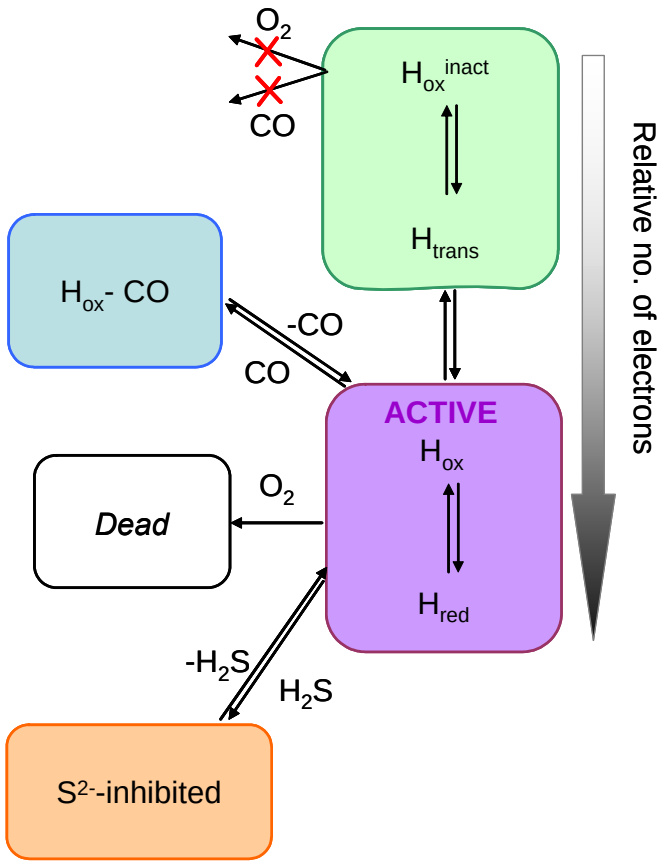

Figure 1.13: Schematic of the oxidation states of [FeFe]-hydrogenases.

1.2.2.3. The catalytic mechanism

The catalytic cycle of [FeFe]-hydrogenases remains a speculative field[139,150,151] which has inspired numerous computational studies.[145,149,152-154] Two possibilities for the mechanism are shown in Figure 1.14, one of which actually involves binding of H_2 to

Fe_P.[144] Another possible mechanism involves a cysteine residue in the active site environment assisting in the heterolytic cleavage of H_2 by accepting a proton from the Fe-H_2 complex formed when H_2 binds by displacement of the water ligand on Fe_D.[155] The binding of H_2 at the H-cluster has been postulated to occur at Fe_D from EPR data[146] and the fact that the competitive inhibitor CO binds in this position.[138] Possibilities for residues involved in proton transfer to the active site are lysine and cysteine residues that are conserved in *Cp*I and *Dd*H. Proton transfer from the surface of the protein to these residues is believed to take place through pathways involving charged and polar amino acid side chains.[66]

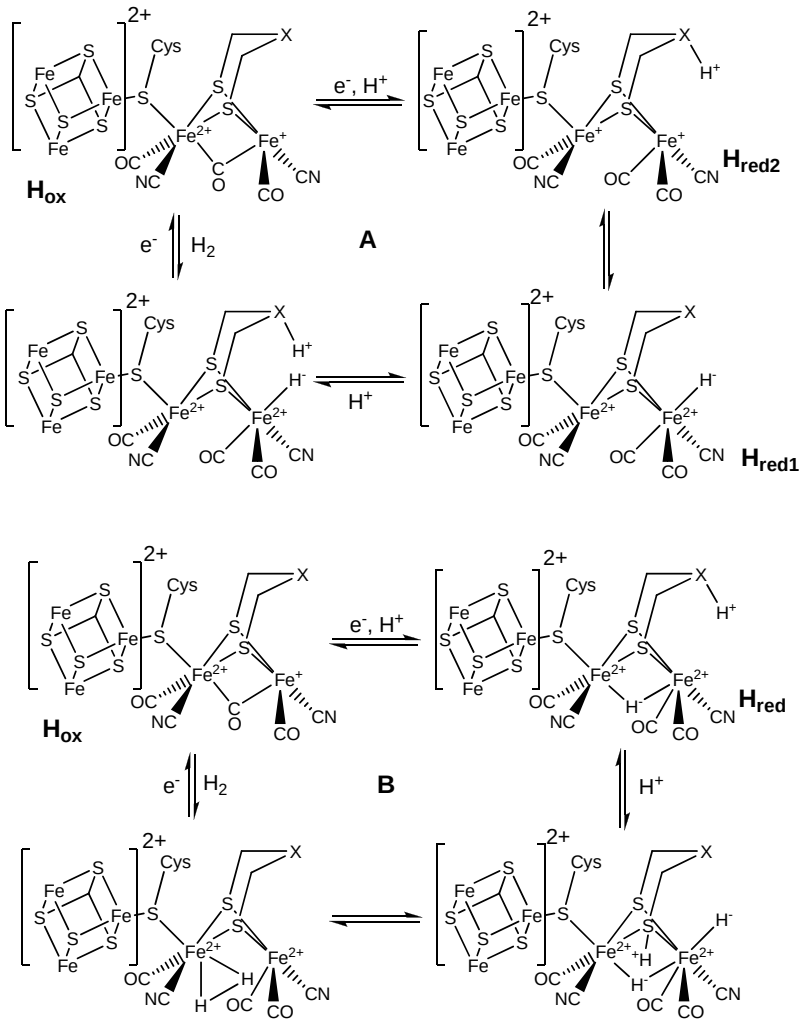

Figure 1.14: Two possible mechanisms for catalysis by the [FeFe]-hydrogenases.[144]

In fact, it has even been suggested that [FeFe]-hydrogenases bind H_2 cooperatively from the results of kinetic experiments performed on *Dv*H.[156] In this study, Van Haaster et al. demonstrated that one molecule of H_2 is required to activate the enzyme isolated in the resting state before a second can be bound and catalytically oxidised at the active site.

1.2.3. Gas channels in hydrogenase and O_2 sensitivity

The existence of a hydrophobic channel through which O_2 could travel in [FeFe]-hydrogenases has been reported.[119,130,157] Efforts to genetically modify [FeFe]-hydrogenases to narrow their gas channel are ongoing as it has been proposed that this might limit diffusion of O_2 to the active site and thus increase O_2 tolerance.[43,158]

The presence of hydrophobic gas channels in [NiFe]-hydrogenases has been investigated in a number of different enzymes. The first results published were on *Db*H,[159] *Df*H and *Dg*H.[160] Both Texeira[161] and Montet[160] noted that the putative gas channel lead specifically to the Ni in the active site, thus supporting the hypothesis that the Ni atom is the site of H_2 binding. For *Dg*H molecular dynamics simulations were used to prove that diffusion of H_2 to the active site was not rate-limiting.[160] However, it was shown by Léger et al.[162] that the gas channel of *Df*H could be tuned by genetic modification of the protein main-chain environment close to the active site at the entry of the putative gas channel such that a dramatic effect on the rate of inactivation by O_2 was observed. In fact, such an "active site" mutant of *Df*H was much more slowly inactivated by O_2 than the wild type.[162] Conversely, widening the gas channel of the regulatory hydrogenase in *Ralstonia eutropha* increased its O_2 sensitivity.[163]

1.3. Synthetic hydrogenase mimics

A vast library of structural and/or functional synthetic mimics of hydrogenase exists.[164-167] One interesting challenge for chemists involved in this research is that the metals present in the hydrogenase active site are first row transition metals which generally have low affinities for H_2.[168] Compounds relating to the H-cluster of the [FeFe]-hydrogenases are more common than those relating to the [NiFe]-active site, in part due to the added difficulty of synthesising *hetero*bimetallic compounds.

Structural mimics have been used in laboratory-based and *in silico* experiments to corroborate numerous hypotheses regarding the structure of the H-cluster and the [NiFe]-active site. For example, the various oxidation states of the H-cluster were confirmed through a set of DFT calculations on a biomimetic compound.[169] In addition, model compounds of the binuclear [2Fe]-subcluster with ODT and ADT bridges have demonstrated that these bridges may promote enhanced H_2 production over a PDT bridge.[170] One study particularly supported the assignment of ADT.[171] Structural studies have also added weight to the idea that the role of the Fe atom in [NiFe]-hydrogenases is as a Lewis acid which stabilises the bridging hydride, rather than as the catalytic metal atom of the two present in the active site.[166]

Attempts at mimicking the *activity* of hydrogenases in H_2 production have notoriously been hampered by the high overpotentials required by the analogues used,[172] a problem with which hydrogenases do not contend.[88] However, some progress has been made in this area with cobalt macrocyclic glyoxime and tetraimine complexes.[173]

1.4. Aims of this thesis

This thesis aims to identify the features of a hydrogenase that might help it survive damage from inhibitors: do gas channels play a part in preventing the access to the active site?[160,162] Computational studies have described pathways for O_2 and H_2 across *Cp*I involving packing defects in the enzyme[157] – how important are these in protecting hydrogenases from inactivation by O_2? What knowledge can be gleaned from the rate and degree of inhibition of hydrogenases by different inhibitors, specifically O_2 and CO? Can the results on [FeFe]- and [NiFe(Se)]-hydrogenases outlined above be corroborated by further electrochemical studies? **All in all, how would we design the perfect hydrogenase for H_2 production?**

Chapter 2:

Protein Film Electrochemistry and

The Electrochemical Set-up

2.1. Abstract

This chapter outlines the technique of Protein Film Electrochemistry (PFE). The evolution and advantages of PFE over traditional solution electrochemistry are described, with an emphasis on the theories underlying this technique. The electrochemical set-up and some key control experiments for experiments detailed in Chapter 6 are also described.

2.2. Protein film electrochemistry and its origins

Electrochemistry is a very useful tool for studying redox enzymes as the current is related to the rate of reaction. In mediated solution electrochemistry of proteins, mediators (small redox-active molecules) either accept or donate electrons to the protein and the subsequent regeneration of the mediator in its original state by redox at the electrode is observed as a current wave.[174] As the recorded current in traditional solution electrochemistry is limited by slow protein diffusion, the relationship between current and rate of reaction is convoluted. In 1977 two groups found a way of circumventing the problems of diffusion limitations that beset solution electrochemistry. Hill[175] and Kawana[176] attached the protein directly to the electrode and Protein Film Voltammetry[177] (PFV, since given the more general name of Protein Film Electrochemistry, PFE) was born. The active site of the protein is thus wired to the surface of the electrode.

The schematic shown in Figure 2.1 represents the underlying principle of PFE. The advantages of PFE[178] are as follows:

1. High rates of interfacial electron transfer between the protein and the electrode[87,179,180] circumvent the problem of sluggish diffusion of the enzyme to the electrode's surface. Changes in potential (*E*) *instantly* affect the enzyme therefore allowing for details of the energetics (and thus the mechanism) to be elucidated.[181]
2. It only requires minuscule amounts of protein – a substantial benefit when one considers the cost of proteins and the laborious task of protein purification when the protein in question is not commercially available. In fact, one study reported the observation of an electrochemical response from as little as 50 molecules adsorbed on a modified gold surface.[182] In the experiments reported in this thesis, the coverage of the enzyme on the electrode is expected to be within the picomolar range.[183]
3. As the electrode on which the protein is adsorbed can easily be removed from solution and placed in another solution, the protein can effectively be instantly dialysed.
4. Some proteins have redox centres of potentials that are outside the range of that accessible to mediators.

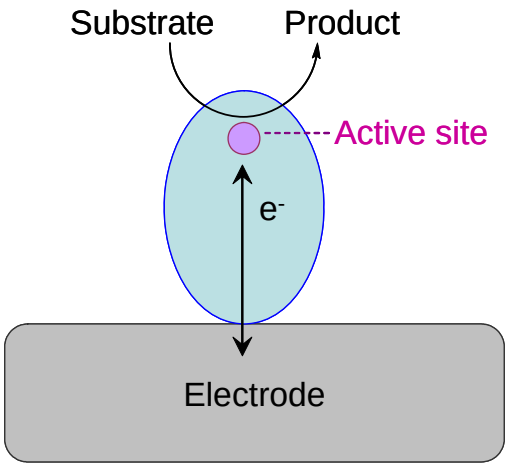

Figure 2.1: Schematic of the principle of PFE: electrode with an enzyme film adsorbed onto it.

However, PFE cannot be employed to study all the proteins (electron-transfer proteins or redox-active enzymes) that can be examined using electrochemistry. If a protein does not have an active site within the electron-tunnelling distance (~14 Å[184]) of its surface (as does, for example, cytochrome *c* peroxidase) or an electron relay chain linking the surface to a buried active site (i.e. hydrogenase),[181] it cannot engage in electron transfer with it.

2.3. Electrode surfaces and protein binding

The first report of adsorbtion of proteins onto pyrolytic graphite-edge (PGE) electrodes[185] was a substantial improvement on the previous reports of adsorption onto tin-doped indium oxide[176] and gold[175] because it described a method of attaching proteins to electrodes without the need to modify the surface. (Since then, protein adsorption on unmodified gold *has* been observed.)[186,187] Graphite electrodes also offer the advantages of being cheap, having a wide potential window (+1.0 V to -0.9 V vs. SHE)[§] and relatively inert electrochemistry.[188] For the method of adsorption of enzymes onto PGE used in the experiments reported in this thesis, see Appendix I.

However, graphite adsorption of proteins is by no means perfect and the phenomenon of "film loss"[189] is still a considerable limitation in PFE. "Film loss" is characterised by a decrease in current that is expected to be the result protein desorption, denaturation, reorientation of the protein on the surface such that its active site is no longer wired to the electrode or any combination of the above. Various different methods of stabilising the protein on the electrode have provided a means of tackling this problem.

[§] A note on potential: all potentials quoted in this thesis are referenced versus the Standard Hydrogen Electrode (SHE).

Attachment of groups to the surface of graphite that structurally mimic the substrate in the case of the laccases from *Trametes versicolor* and *Pycnoporus cinnabarinus*[190] has not only improved the long-term stability of the enzymes - possibly as a result of an increased number of "docking" sites on the surface to adhere to the enzyme's substrate binding pocket - but has also increased the magnitude of the currents recorded. A hydrogenase (*Dg*H) has also been ligated to PGE surface by direct covalent attachment.[191] Modifications of gold by alkane-thiols such that the surface resembles the physiological redox partner have also proved beneficial.[192-194]

2.4. The two contributions to the current recorded in protein film electrochemistry

2.4.1. Non-faradaic current

The non-faradaic current results from non-redox electrochemistry. It is observed as a background current as seen in the cyclic voltammogram of a bare PGE electrode (Figure 2.2). It arises from the rearrangement of ions in solution to compensate for build-up of charge at the electrode; this results in the formation of an electrical double-layer surrounding the surface of the electrode which acts as a capacitor. The magnitude of this capacitive current is a function of the electrode area, scan rate, temperature and solution composition.[195] In chronoamperometry (see section 2.7.1 below) it is defined by Equations 2.1 in which E is the magnitude of the potential step, R_s is the resistance of the resistor, t is time, and C_d is the capacitance of the capacitor.

$$i = \frac{E}{R_S}\exp^{\frac{-t}{R_s C_d}} \qquad \text{Equation 2.1}$$

In cyclic voltammetry (see section 2.4.2), the capacitive current is defined as in Equation 2.2, where v is the scan rate (i.e. the rate at which the potential is swept in V/s), E_i is the initial potential at the beginning of the potential ramp, and R_s, C_d and t are as above.

$$i = vC_d + \left[\left(\frac{E_i}{R_S} - vC_d\right)\exp(-t/R_sC_d)\right] \qquad \text{Equation 2.2}$$

2.4.2. Introducing cyclic voltammetry

Cyclic voltammetry consists of applying a saw-toothed potential ramp (see Figure 2.2A) to a working electrode and measuring the current thereby induced. Figure 2.2B shows a cyclic voltammogram of an unmodified PGE electrode in which the hysteresis between the forward oxidative and backward reductive sweeps is evident. This profile results from charging of the double–layer as described in section 2.4.1 and is present as a background in all the cyclic voltammetry experiments reported in the following chapters.

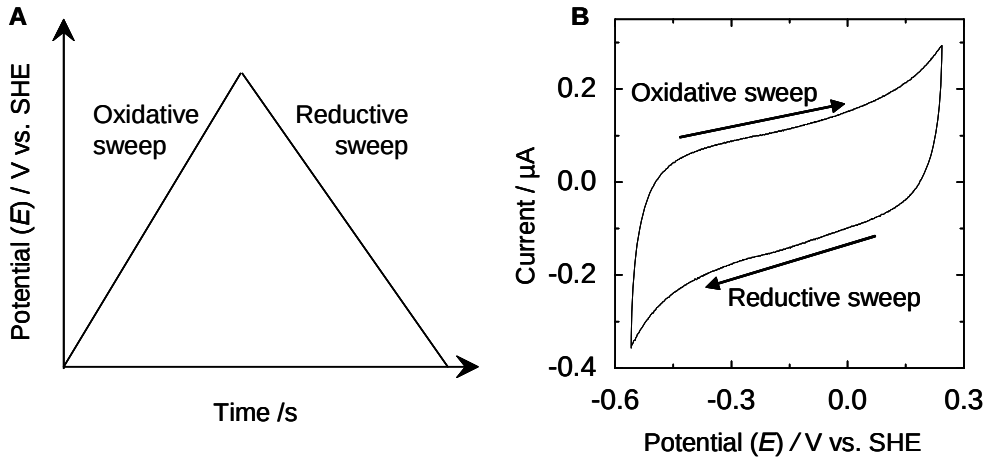

Figure 2.2: A) Graphical representation of the potential ramp as the potential is swept in a cyclic voltammogram, an example of which is shown in B. B) A cyclic voltammogram of a bare graphite electrode recorded at 20 mV/s in pH 6 buffer, 20 °C, exhibiting only a non-faradaic (capacitive) current.

While the time and potential domains are convoluted in cyclic voltammetry, a considerable amount of information can extracted from a single voltammogram which can be recorded in a very brief period of time depending on the rate at which the potential is swept between the two vertices (the scan rate) and the size of the potential window (i.e. the voltage separating the two vertices). The catalytic activity of proteins, as reported by the current, is a function of potential thus a cyclic voltammogram affords insight into the effect of a spectrum of potentials on the protein (see section 2.5.3). Moreover, it allows us to determine the potentials at which various redox processes occur, an example of which is the signals arising from reduction and oxidation of the [FeS]-clusters in hydrogenase as described below (section 2.5.2).

2.4.3. Faradaic current

The faradaic current is a consequence of redox-active species (such as redox enzymes or electron transfer proteins) becoming reduced or oxidised and withdrawing electrons from or donating them to the electrode. This is the contribution of interest in PFE.[196]

In the simplest case, interconversion of an oxidised (Ox) and a reduced (Red) species on an electrode can be described by Reaction 2.1 where $E^{\circ\prime}$ is the reduction potential, k_{ox} is the rate of oxidation and k_{red} is the rate of reduction.

$$\mathrm{Ox} + \mathrm{ne^-} \underset{k_{red}}{\overset{E^{\circ\prime},\ k_{ox}}{\rightleftharpoons}} \mathrm{Red}$$

Reaction 2.1

Current (i) is a measure of the rate of flow of electrons and can be defined by Equation 2.3 in which A is the electrode area, F is the Faraday constant, and j is the flux of electrons reaching the electrode's surface in moles(unit area)$^{-1}$s^{-1}.

$$i = AFj \qquad \text{Equation 2.3}$$

Furthermore, we can define j_{ox} (the flux in the oxidative direction) and j_{red} (the flux in the reductive direction) by Equations 2.4A and 2.4B which can be used to derive Equations 2.5A and 2.5B defining the currents for those processes.

$$j_{ox} = nk_{ox}\Gamma_{red} \qquad \text{Equation 2.4A}$$

$$j_{red} = nk_{red}\Gamma_{ox} \qquad \text{Equation 2.4B}$$

$$i_{ox} = nFk_{ox}\Gamma_{red}A \qquad \text{Equation 2.5A}$$

$$i_{red} = nFk_{red}\Gamma_{ox}A \qquad \text{Equation 2.5B}$$

Here, Γ_{ox} are Γ_{red} are the electroactive coverages of the oxidised and reduced species respectively per unit area and n is the number of electrons.

2.5. The three resistors limiting the faradaic current in PFE

A model has be designed to describe the processes that may limit the current corresponding to enzymatic catalysis[197] (see Figure 2.3).

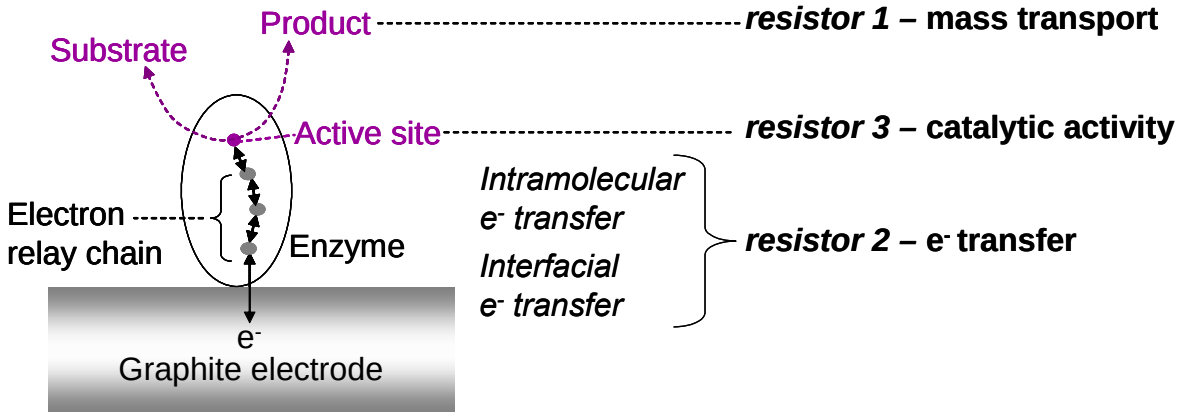

Figure 2.3: Schematic of PFE in which the components of an enzyme-modified electrode that will limit the rate of reaction are modelled as three resistors.

In this model the observed current i_{obs} is related to the overall resistance ($1/i_{obs}$) which can be described as the sum of the three resistors shown in Figure 2.3.

$$\frac{1}{i_{obs}} = \frac{1}{i_{ET}} + \frac{1}{i_{cat}} + \frac{1}{i_{Lev}} \qquad \text{Equation 2.6}$$

The first resistor, $1/i_{Lev}$ (where i_{Lev} is the Levich current for a mass-transport controlled reaction) corresponds to mass-transport of the substrate from the bulk solution to the enzyme and the diffusion of the product away from the enzyme (see section 2.5.1). A key feature of the experiments described in this thesis is that the electrode is rotated at high speeds (~3000 rpm). This hydrodynamically drives substrate to the electrode and product away from it thus ensuring a constant supply of substrate and removal of product. This limitation is therefore effectively non-existent in the experiments described herein.

Resistor 2, $1/i_{ET}$ (where i_{ET} is the current corresponding to electron transfer), consists of resistance to electron transfer between the electrode and the enzyme (intermolecular e^- transfer) and resistance to electron transfer across the enzyme (intramolecular e^- transfer). This is modelled by the Butler-Volmer equation (Equation 2.7A) which is based on transition-state theory. In this model, i_0 is the standard exchange current, the value of α varies from 0 to 1 reflecting the character of the transition state of the reaction, E is the applied potential, $E^{\circ\prime}$ is the standard potential, R is the gas constant and T is the temperature.

$$i = i_0\left(\exp\left[\frac{(1-\alpha)F(E-E^{\circ\prime})}{RT}\right] - \exp\left[\frac{\alpha F(E-E^{\circ\prime})}{RT}\right]\right) \qquad \text{Equation 2.7}$$

Intermolecular electron transfer is considered to contribute little to the resistance as it has been observed to be very rapid in many cases.[87,180] Intramolecular electron transfer has also been shown to be extremely fast[184] (5000 s^{-1} or faster[198]). However, signals

arising from redox at these relay centres can be observed under certain conditions as described in section 2.5.2.

This leaves resistor 3, $1/i_{cat}$, which is a measure of the rate of catalysis at the active site (see section 2.5.3). Often this is assumed to be the rate-controlling centre as catalysis at the active site is slower than electron transfer and mass-transport of substrate when the electrode is being rotated at high speeds.

2.5.1. Mass-transport control: resistor 1

As mentioned above, rotation of the electrode ensures supply of substrate to the enzyme film and removal of product. However, when the electrode is not rotated rapidly enough, the (mass-transport limited) current (i_{Lev}) recorded is dependent on the rate of rotation (ω) of the (planar) electrode such that the relationship between i_{Lev} and ω is given by the Levich equation (Equation 2.8) in which [S] is the concentration of the substrate in the bulk, F is Faraday's constant, A is the electrode area, D is the diffusion coefficient and v is the kinematic viscosity.

$$i_{Lev} = 0.62nFAD^{2/3}\nu^{-1/6}\omega^{1/2}[S] \qquad \text{Equation 2.8}$$

Thus, the current is proportional to the square root of rotation rate. As resistor 1 is inversely proportional to the square root of the rate of rotation, mass-transport becomes increasingly insignificant as the rate of rotation is raised.

2.5.2. Non-turnover voltammetry: detecting the intramolecular component of resistor 2

When catalysis is suppressed, signals arising from redox within the components of the electron relay chain (*intra*molecular e^- transfer in resistor 2 in Figure 2.3) may be observed. These are known as non-turnover signals.[199] Returning to the simplest case, described by Reaction 2.1, the current arising from redox at these centres can be defined by Equation 2.9 so long as the protein is bound to the surface.

$$i = -nFA\frac{d\Gamma_{ox}}{dt} = nFA\frac{d\Gamma_{red}}{dt} \qquad \text{Equation 2.9}$$

Under equilibrium conditions, the Nernst equation can be used to define Γ_{ox} and Γ_{red} so long as the oxidised and reduced species do not interact with each other.

$$E = E^{\circ\prime} + \frac{RT}{nF}\ln\left(\frac{\Gamma_{ox}}{\Gamma_{red}}\right) \qquad \text{Equation 2.10}$$

E is the potential as it is being swept throughout the experiment and $E^{\circ\prime}$ is the redox potential of the (redox-active) centre in question. As the total electroactive coverage is $\Gamma = \Gamma_{ox} + \Gamma_{red}$, the Nernst equation can be rearranged to determine Γ_{red} and Γ_{ox}.

$$\Gamma_{red} = \frac{\Gamma}{1+\exp\left(\frac{nF\left(E-E^{\circ\prime}\right)}{RT}\right)} \qquad \text{Equation 2.11A}$$

$$\Gamma_{ox} = \frac{\Gamma}{1+\exp\left(\frac{nF\left(E-E^{\circ\prime}\right)}{RT}\right)} \qquad \text{Equation 2.11B}$$

By differentiating Equations 11A and 11B with respect to time to determine $d\Gamma_{red}/dt$ and $d\Gamma_{ox}/dt$ and inserting the result into Equation 2.9, Equation 2.12 which describes the shape of non-turnover peaks as a function of the total coverage of protein on the electrode is obtained.[174] For a full derivation, see Appendix II.

$$i = \frac{\pm n^2 F^2 v A \Gamma}{RT} \left(\frac{\exp\left(\frac{nF\left(E - E^{\circ\prime}\right)}{RT} \right)}{\left(1 + \exp\left(\frac{nF\left(E - E^{\circ\prime}\right)}{RT} \right) \right)^2} \right) \qquad \text{Equation 2.12}$$

In Equation 2.12, a positive current corresponds to oxidative process and a negative current is recorded for the reductive process, and v is the scan rate. Non-turnover signals are recorded by employing cyclic voltammetry. The clarity of these signals depends on a number of factors, with size of the protein being an important factor. Non-turnover signals are more easily discerned when there are more protein molecules on the surface, as is the case with smaller protein molecules which give high electroactive coverages, e.g. ferrodoxin.[185] Conversely, signals from larger proteins are harder to obtain[179] but a number of studies on large enzymes have been performed.[183,200-202] Chapter 4 describes the detection of such signals for the [NiFeSe]-hydrogenase from *Desulfomicrobium baculatum* (*Db*H).

2.5.3. Catalytic voltammetry: exploring resistor 3

An enzyme attached to an electrode at a potential which is being swept will not be at equilibrium. For example, let us consider H^+ reduction by hydrogenase. Below the thermodynamic potential, the enzyme feels a driving force that pushes it to reduce H^+, thus becoming oxidised. It withdraws electrons from the electrode to become reduced again so as to continue catalysing H^+ reduction, thus giving rise to a *negative* current. As the driving force increases (the potential becomes more negative), this process can occur more rapidly and the magnitude of the current generated increases. The converse is true for H_2 oxidation, which corresponds to a *positive* current. This is illustrated in Figure 2.4.

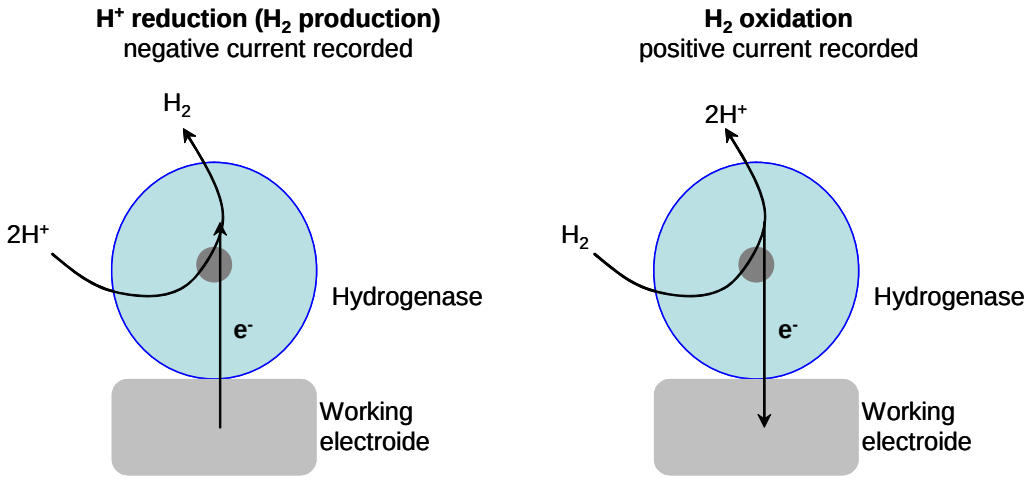

Figure 2.4: Schematic representation of electrocatalytic H_2 production and H_2 oxidation by a hydrogenase adsorbed on the working electrode.

The ideal dependence of current on potential for an enzyme attached to a rotating electrode is shown in Figure 2.5A. At low overpotentials, when the driving force for electron transfer is low, resistor 2 controls the rate of catalysis for some enzymes and the current increases exponentially as the potential becomes more positive. On the other end of the scale, as the driving force increases, electron transfer ceases to be rate-limiting, and the catalytic current is no longer a function of potential. At this point, a plateau is reached at a current denoted i_{cat} and the active site is said to be the control centre. The direct relationship between the rate of catalysis and the current (i) which underpins the advantages of PFE is expressed by the electrochemical adaptation of the Michaelis-Menten equation, (Equation 2.13) which reduces down to Equation 2.14 when the substrate concentration is saturating. Under such conditions, the maximal catalytic rate is obtained, i.e. $i = i_{cat}$, and k_{cat}^{max} is the catalytic rate constant in the absence of electron transfer and mass-transport limitations (i.e. when the substrate concentration is saturated).

$$\frac{1}{i} = \frac{K_M}{i_{cat}[S]} + \frac{1}{i_{cat}} \qquad \text{Equation 2.13}$$

$$i_{cat} = nFA\Gamma k_{cat}^{max} \qquad \text{Equation 2.14}$$

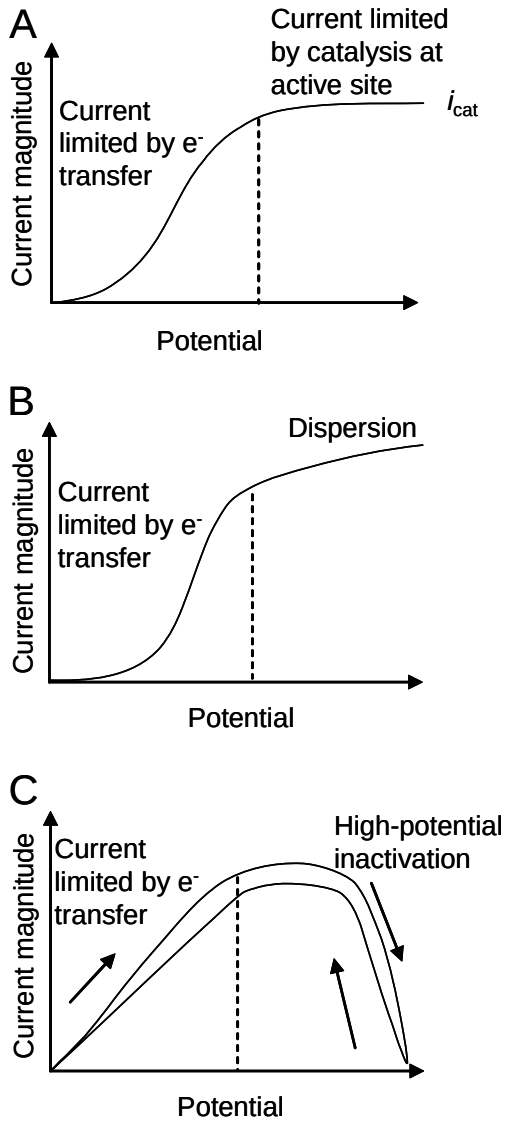

Figure 2.5: Schematic representations of the catalytic wave shape in the absence of mass-transport limitations. A) The "classic" sigmoid reflecting current controlled by electron transfer (and thus potential) and then catalysis at the active site above a given potential. B) The sigmoid is altered by dispersion of enzyme molecules such that no plateau is reached at high potential. C) Representation of the catalytic wave shape in the instance where high potentials induce anaerobic inactivation on the forward sweep and lowering the potential on the backward sweep reactivates the enzyme.

Two further features that can modulate the catalytic wave are relevant to cyclic voltammetry of hydrogenases. A study performed by Léger et al.[203] showed that, at high overpotentials at which electron transfer should no longer be limiting the recorded current, there was a residual increase in current due to H_2 oxidation by *Av*H; a

schematic is shown in Figure 2.5B. This was modelled as the result of inhomogenous adsorption of enzyme on the electrode, thus molecules adsorbed in conformations in which the interfacial electron transfer was slow could only contribute to the catalytic current at higher overpotentials.** Therefore, as the potential increases, the current still continues to increase, albeit at a slower rate. This behaviour is evident in the case of the [FeFe]-hydrogenase from *Clostridium acetobutylicum* (*Ca*HydA) – see Figure 3.3.

In the event that the current reaches a maximum as the oxidative sweep progresses (e.g. Figure 2.5C), as is the cases for most hydrogenases that have been studied electrochemically (at least under certain conditions such as low hydrogen concentration[88,97,204,205]), this is indicative of formation of a catalytically inactive form of the enzyme. This is known as the "Ready" or "Ni-B"-state for the [NiFe]-hydrogenases (section 1.2.1.2 in Chapter 1) and H_{ox}^{inact} for the [FeFe]-hydrogenases (section 1.2.2.2). Anaerobic inactivation of [FeFe]-hydrogenases is discussed further in Chapter 3. Another feature, illustrated in Figure 2.5C, that distinguishes cyclic voltammograms of hydrogenase from that modelled in Figure 2.5A is the rise in current at potentials slightly more positive (in the case of H_2 oxidation) or negative (in the case of H^+ reduction) than the thermodynamic potential of the $2H^+/H_2$ couple. For most (but not all, see Chapter 3, section 3.3.1) hydrogenases, the catalytic wave increases in a linear fashion as the potential is made either more negative or more positive than the zero-current potential rather than increasing in a sigmoidal fashion. This is evidence of the rapid electron transfer between the electrode and the enzyme exhibited by many hydrogenases, indicating that they are not subject to Butler-Volmer kinetics.[87]

** Note there is an exponential decay in the rates of electron transfer with respect to the distance between the electrode surface and adjacent redox-center as this distance increases.

2.6. The electrochemical set-up

The experiments described in this thesis have been carried out in a three-electrode cell as illustrated in Figure 2.6 and Figure 2.7. The potential is applied to the working electrode and measured at the reference electrode. The current generated at the working electrode passes through the counter electrode instead of the reference electrode so that the reference potential remains constant.[195,206]

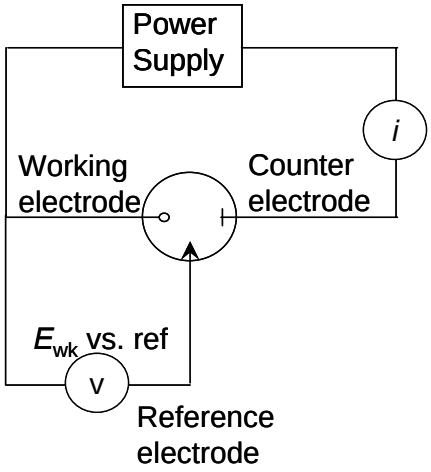

Figure 2.6: The three-electrode cell[195] in which the potential of the working electrode vs. the reference electrode is E_{wk} vs. ref.

Figure 2.7 shows a schematic of the sealed all-glass electrochemical cell used. The reference electrode, a Saturated Calomel Electrode (SCE), is connected to the cell through a Luggin side-arm which effectively brings the reference electrode closer to the working electrode, thus minimising resistance between the two.[207] A Pt wire is used as the counter electrode. The cell is surrounded by a water-jacket connected to a water-circulator so that reactions happening within it are under precise thermostatic control. For experiments in which it was important to ensure that the enzyme was not subject to light, the cell was blocked out with black electrochemical tape. For the photolability experiments described in section 5.3.3.6, the cell was placed on top of a light source (a Kodak 150 W projector projecting a full solar spectrum, though the borosilicate glass of

the electrochemical cell absorbs the far UV wavelengths) which could be turned on and off

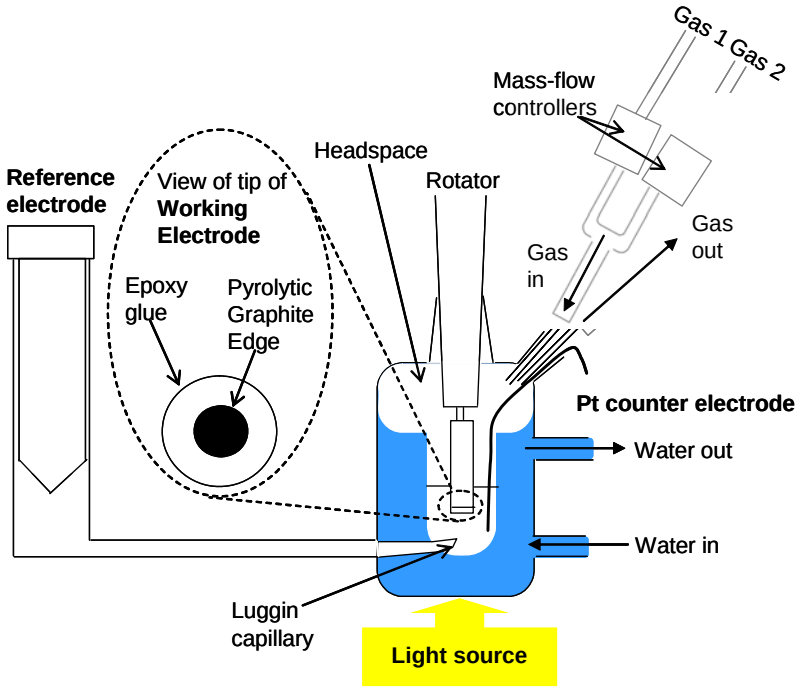

Figure 2.7: Schematic of the electrochemical set-up involving a three-electrode cell with an optional light source. The inset shows a cartoon of the end of the PGE electrode.

2.7. Studying hydrogenases using protein film electrochemistry

Hydrogenases have been studied extensively by PFE.[87,88,181] Whilst the exact mechanism of catalysis by the [NiFe(Se)]-hydrogenases is not known, Léger et al. proposed that the mechanisms of H_2 oxidation and H_2 production were different (involving different catalytic intermediates) from results of PFE experiments.[208] It is thus reasonable to suggest that different catalytic cycles are involved in H_2 production and oxidation by the [FeFe]-hydrogenases too. By poising the electrode at a particular potential, PFE imposes the population of certain states in the catalytic cycle and allows for the study of the reactions of these intermediates.

2.7.1. Chronoamperometry

Chronoamperometry is the measuring of current under potentiostatic control as a function of time.[178] In one experiment, the potential can be stepped such that the effect of a variety of driving forces on the kinetics and thermodynamics of enzymatic catalysis can be interrogated. As the time and potential domains are deconvoluted, this technique allows for a direct examination of the rate at which a given process occurs, be it inactivation by the application of high potentials, exposure to inhibitors or reactivation by the reversal of these processes. Thus, it is a very useful technique for observing changes in resistor 3, as represented in Figure 2.8.

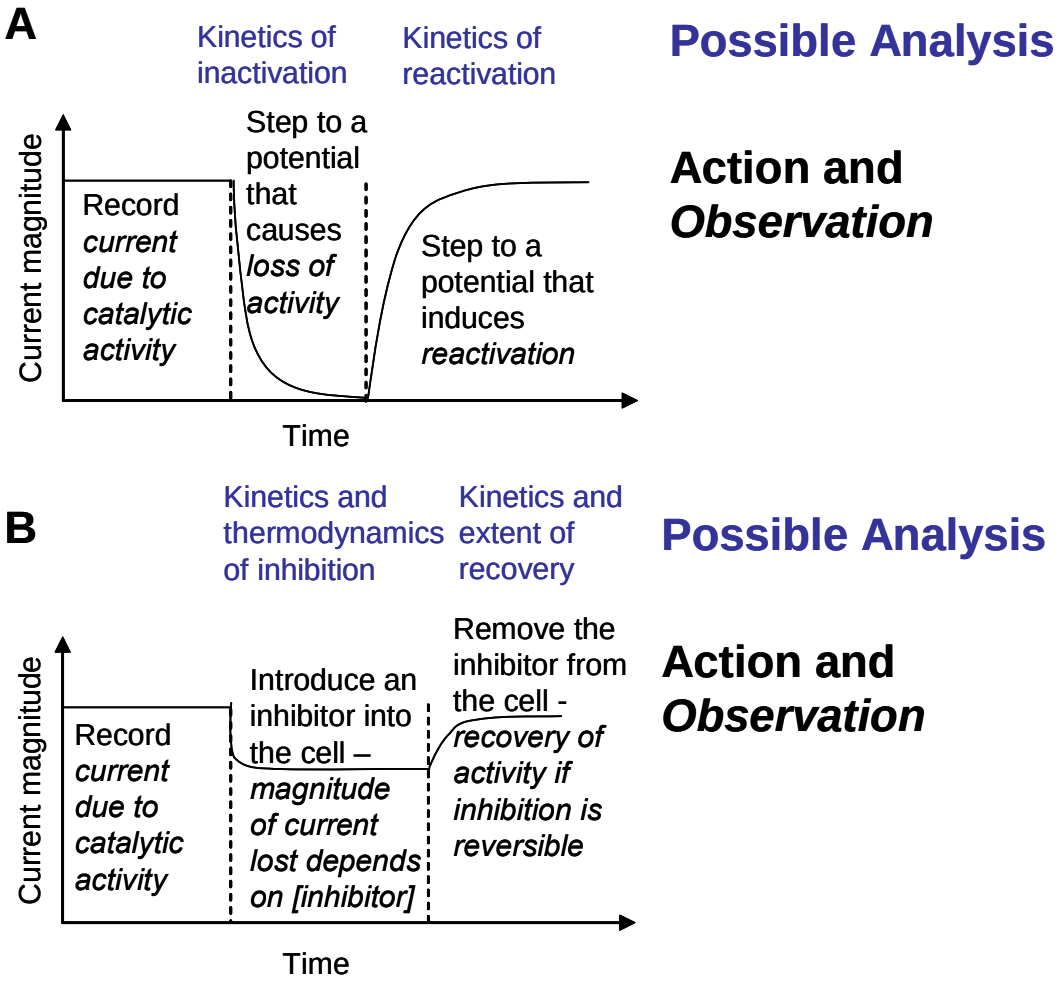

Figure 2.8: Chronoamperometry and its uses. A) Schematic representation of chronoamperometric experiment in which the potential is *stepped* to induce inactivation and reactivation of the enzyme. B) Schematic representation of a chronoamperometric experiment in which the potential remains constant and changes in activity of the enzyme are caused by introduction and removal of an inhibitor.

As the current reports on the rate of the enzyme-catalysed process, the dependence of the increase or decrease in current on time can be used to report on the kinetics of the changes occurring at the enzyme following a change in conditions, for example recovery from inhibition following the removal of inhibitor from solution. The rate constants for these processes can easily be determined when the rate of change in activity is first order by performing a log transformation. Let us consider the simple case of recovery of activity following oxidative inactivation of a hydrogenase (a process explored at length in Chapter 3), as described by Reaction 2.2, where k_1 is the rate at which the enzyme reactivates and k_{-1} is the rate at which the enzyme is inactivated.

$$\text{Inactive} \underset{k_{-1}}{\overset{k_1}{\rightleftharpoons}} \text{Active} \qquad \text{Reaction 2.2}$$

The first order rate law is given by Equation 2.15 which integrates and is rearranged to Equation 2.16 in which [Inactive] is the concentration of the inactive species and $[\text{Inactive}]_0$ is the concentration of inactive species at $t = 0$.

$$\frac{d[\text{Inactive}]}{dt} = -k_1[\text{Inactive}] \qquad \text{Equation 2.15}$$

$$\text{Log}[\text{Inactive}] = -k_1 t + \text{Log}[\text{Inactive}]_0 \qquad \text{Equation 2.16}$$

As the limiting current (i_{lim}) recorded in a chronoamperometry experiment is reached when all the inactive enzyme has reactivated to form the "Active" species and the current (i) is a proportional to [Active] as the enzyme is reactivating, Equation 2.16 can be electrochemically interpreted (Equation 2.17). See Appendix V for a complete derivation.

$$\text{Log}(i_{\text{lim}} - i) = -k_1 t + \text{Log} i_{\text{lim}} \qquad \text{Equation 2.17}$$

Thus, k_1 can be determined from the gradient of a Log(i_{lim}-i) vs. t plot.

2.8. Graphite reduction of O_2

The study of the damage that O_2 causes to hydrogenases is of critical import when considering these enzymes for potential biotechnological applications. However, calculating the rates at which inactivation occurs is hampered by the fact that O_2 reacts easily with components of the experiment set-up other than the hydrogenase. For example, in mediated solution electrochemistry, O_2 reacts with the mediators thus preventing electron transfer between the enzyme and the electrode. In PFE, O_2 reacts with a number of electrode materials including Pt and graphite thus compounding the contribution of the hydrogenase-catalysed process with that of the electrode reduction of O_2.

2.8.1. Control experiments for the experiments probing H_2 production in the presence of O_2

A novel method for investigating the possibility of continued H_2 production by hydrogenase in the presence of O_2 is developed in this thesis.[205,209] A schematic is shown in Figure 2.9 and the experiments themselves are described in detail in Chapter 6.

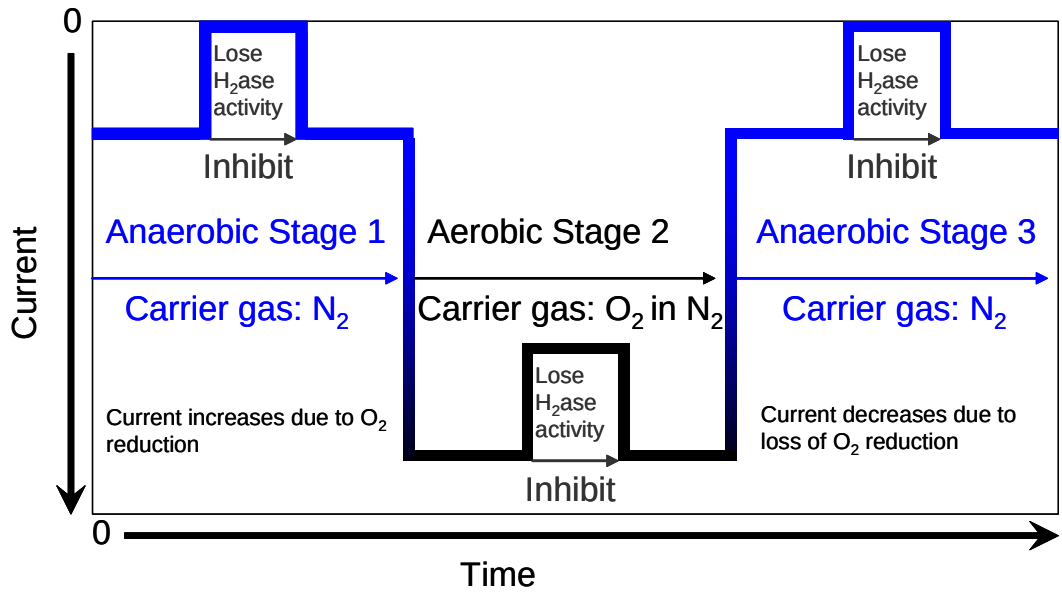

Figure 2.9: Schematic representation showing the three stages of the experiments investigating H_2 production by hydrogenase in the presence of O_2. The term "Carrier gas" refers to the gas mixture that remains constant throughout each stage of the experiment. The term H_2ase is short-hand for hydrogenase.

An important concept in these experiments is that hydrogenases can be reversibly inhibited by at least two gaseous inhibitors, CO and H_2 (product inhibition). In the presence of O_2, the current at potentials at which hydrogenases catalyse H_2 production is the result of the current corresponding to the enzymatic process and that due to O_2 reduction by graphite. Thus, selective inhibition of the hydrogenase resulting in a drop in current is a means of distinguishing between these two contributions and the magnitude of this current decrease is representative of the activity of the hydrogenase prior to exposure to the reversible inhibitor. Stage 1 of the experiment is anaerobic; the enzyme is inhibited with CO or H_2 depending on which inhibitor is more effective (see section 5.3.1) and the inhibitor is removed from solution so that the enzyme recovers activity. This allows for comparison with the effect of repeating this inhibition in Stage 2 in the presence of O_2 to inform on the degree to which the enzyme is active under aerobic conditions. Stage 3, a repetition of Stage 1, confirms the activity of the enzyme after O_2 has been purged from the cell. It is obvious that control experiments proving

that the presence of H_2 and CO does not affect the magnitude of the current due to O_2 reduction are necessary to ensure that no artefacts complicate the experimental results described in Chapter 6. Control experiments such as those shown in Figure 2.10 prove that these inhibitors are selective for the enzyme rather than the electrode.

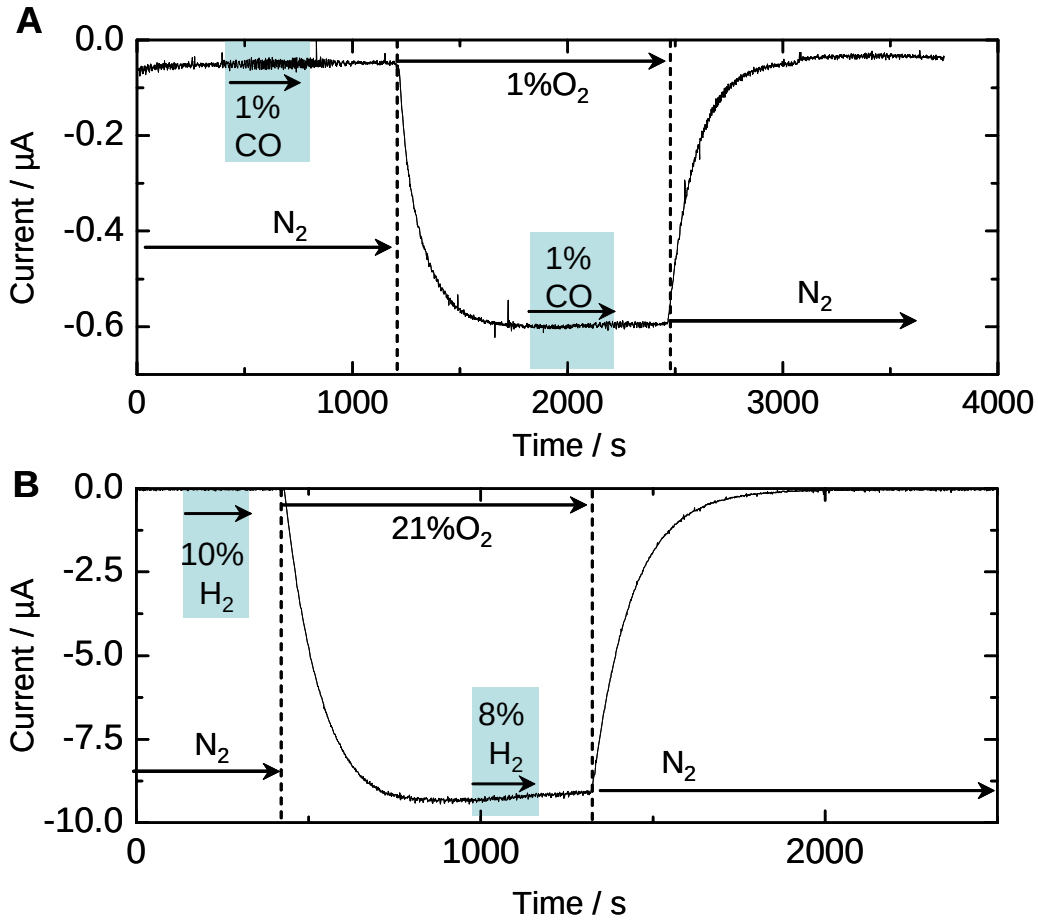

Figure 2.10: Control experiments for the experiments investigating the possibility of continued H_2 production by a hydrogenase in the presence of O_2 (see Chapter 6). Experimental conditions for both A and B: 30 °C, electrode rotation rate 3000 rpm, -0.45 V, gas mixtures as indicated with N_2 as the carrier gas, electrode surface area 0.3 cm^2. A) Control for the experiments in which CO was used as the inhibitor (pH 6). B) Control for the experiments in which H_2 was used as the inhibitor (pH 5.5).

Both experiments begin under N_2 and no current is recorded as there are no electroactive species present. The atmosphere of the cell is exchanged for 1% CO in N_2 in panel A or 10% H_2 in N_2 in panel B and then returned to N_2. In these "blank" experiments, this does not engender a change in current. However, when O_2 (1% in panel A and 21% in panel B) is introduced into the cell, the current increases until it

reaches a steady level indicating that the O_2 in the headspace of the cell has fully equilibrated with that in solution. When H_2 or CO are reintroduced into and removed from the cell, again this does not induce a change in current signifying that the presence of this gas does no poison the process of reduction of O_2 by graphite. Therefore, we can be sure that in the experiments shown in Chapter 6 a decrease in current in the presence of O_2 and H_2 (for the membrane-bound [NiFe]-hydrogenase from *Ralstonia eutropha*, *Re*MBH) or CO (for all the other hydrogenases) is indeed the result of inhibition of the enzyme and this allows us to gauge its activity at that point.

As O_2 is reduced by graphite, it is necessary to assess the degree to which this occurs so as to ascertain how much O_2 is not removed from solution by graphite. The results from the experiments shown in Figure 2.11 enabled the estimation of a lower limit for the concentration of O_2 that would be sensed by the hydrogenase under each particular case of potential, rotation rate and temperature in the experiments described in Chapter 6. The assumption underlying the experiments used to determine this concentration was that, below a certain potential, the reduction of graphite reduction was no longer limited by the driving force but rather by mass-transport of O_2 (resistor 1) and PGE's inherent capacity to reduce O_2 and a plateau would be reached in the cyclic voltammogram (see Figure 2.5A).[209] Voltammograms such as those shown in Figure 2.11 were recorded over a wide potential range and at different temperatures and partial pressures of O_2. These showed that the O_2 reduction current is strongly controlled by mass transport at –0.81 V. Above a certain rotation rate, mass-transport becomes increasingly insignificant; in fact the cyclic voltammograms recorded at an electrode rotation rate of 5000 and 6000 rpm practically overlay each other. This indicates that mass-transport has essentially been overcome at 6000 rpm. It is therefore assumed that the majority of

the available O_2 at the electrode surface is being consumed at the lowest potential recorded in these voltammograms, -0.81 V. This negative limit of the potential was chosen as a compromise between the appearance of curvature in the voltammograms, signifying the approach of potential-independent electrode kinetics, and the onset of solvent breakdown by graphite giving rise to large negative currents. The lower limit for the proportion of O_2 in the headspace actually sensed by the enzyme ($[O_2]_{enzyme}$) was calculated by taking the ratio of the current due to O_2 reduction at -0.81 V at the potential (-0.4 V or -0.45 V) and rotation rate (3000 rpm) that were used in the experiments in Chapter 6 ($i_{-0.4\ V}/i_{-0.81\ V}$) and removing it from 1. The corresponding concentration is then calculated by multiplying this proportion by the Henry's constant[††] (k_H,[210] which gives a measure of the gas solubility in solution) as shown in Equation 2.18.

$$[1-(i_{-0.4\ V})/(i_{-0.81\ V})]*k_H = [O_2]_{enzyme} \qquad \text{Equation 2.18}$$

As an example, let us consider an O_2 fractional pressure of 1% as is the case in Figure 2.11, which is expected to give a solution concentration of 16 μM at 10 °C according to Henry's Law. At 3000 rpm, the reduction current at -0.4 V is -0.35 μA and the reduction current at -0.81 V is -1.26 μA, therefore the actual concentration must be greater than 11 μM. The approximate $[O_2]_{enzyme}$ determined for the experiments described in Chapter 6 are tabulated below. It is assumed in this model that the footprint of the enzyme on the electrode is so slight that the presence of an enzyme film will not significantly alter the O_2-reduction currents from those recorded in the absence of the film which are used to calculate the $[O_2]_{enzyme}$ values below.

[††] Throughout this thesis, k_H is used to determine the concentration of CO, H_2 and O_2 in solution.

Temperature / °C	pH	$[O_2]$ in headspace / %	$[O_2]_{enzyme}$ / µM
10	6	1	11
10	6	5	73
20	6	1	11.5
20	6	10	115
30	6	1	9
30	5.5	2	16
40	5.5	21	138

Table 2.1: Minimum values for the O_2 concentrations available in solution to be sensed by the enzyme ($[O_2]_{enzyme}$) under the various conditions used in the experiments in Chapter 6.

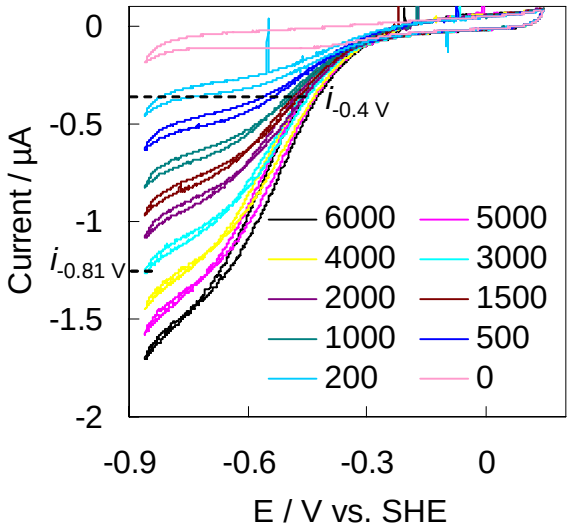

Figure 2.11: Control for calculation of concentration of O_2 sensed by the enzyme in the experiments described in Chapter 6. Experimental conditions: pH 6, 10 °C, 1% O_2 in N_2, scan rate 20 mV/s, electrode surface area: 0.03 cm^2. The rate of electrode rotation (in rpm) is as indicated.

2.8.2. Control experiments for the calculation of rates of inactivation of H_2 oxidation

Experiments described in Chapter 6 have also examined the kinetics of O_2 inactivation of hydrogenases at potentials at which they oxidises O_2. Two different experimental designs were utilised. For the experiments performed on the *Ca*HydA, the enzyme was subjected to O_2 by flushing O_2 through the headspace of the cell. However, the [FeFe]-hydrogenases from *Chlamydomonas reinhardtii* (*Cr*HydA1) and *Desulfovibrio desulfuricans* (*Dd*H) were found to react much more rapidly with O_2, thus the rates observed for the inactivation process were limited by the rate of equilibration of the

headspace gas with solution. So as to ensure that the delivery of O_2 was as instantaneous as was required for the experiments performed on these last two enzymes, O_2 was introduced into the cell by concomitant injection of O_2-saturated buffer into the cell and gas exchange of the headspace of the cell (as in the experiments carried out on C*a*HydA).

At this higher potential (-0.05 V), graphite reduction of O_2 is almost negligible, but it should still be taken into account when assessing the rates at which O_2 inactivates hydrogenase-catalysed H_2 oxidation. Two different kinds of control experiments were performed to adjust for this contribution. The control experiment was then subtracted from the raw experiment to give an "adjusted" version of the experiment. Figure 2.12 shows the two different kinds of control experiments employed to remove the background O_2 contribution in the experiments detailed in Chapter 6. For the experiments performed on *Dd*H and *Cr*HydA1, the relevant control experiments involved introduction of the O_2 into the cell by simultaneous injection of O_2-saturated buffer and gas exchange. Figure 2.12A shows that the current increases instantaneously on injection of O_2-saturated buffer and remains at a fairly steady level whilst O_2 is flushed through the headspace of the cell. When the O_2 is removed from the cell, the current decreases. In the case of *Ca*HydA for which a simplified experimental technique in which O_2 was introduced into the cell by gas exchange without concomitant injection of O_2-saturated buffer, the control experiment involved only gas exchange (Figure 2.12B). As expected, the increase in O_2-reduction current is slower here than it is in Figure 2.12A.

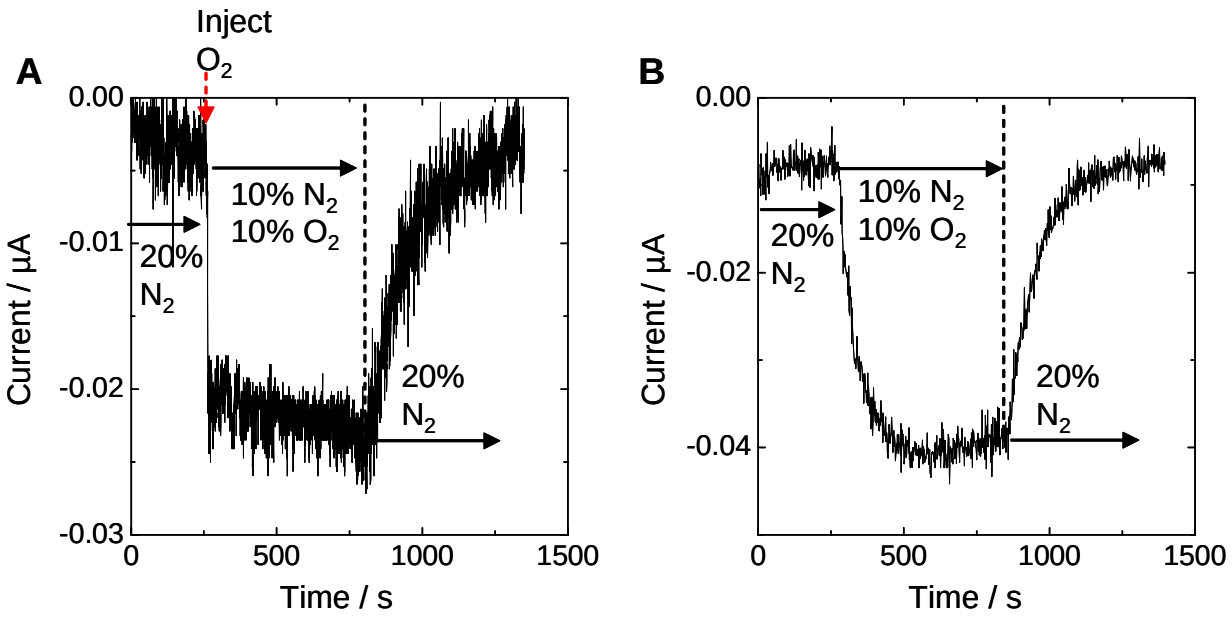

Figure 2.12: Example of control experiments for the experiments examining the rates of O_2 inactivation of H_2 oxidation by hydrogenase performed at -0.05 V described in Chapter 6. A) Simultaneous injection of 2 mL 20% O_2-saturated buffer (into the 2 mL of buffered electrolyte already present in the cell such that 10% O_2 was present after injection) and flushing with 10% O_2 . B) Simple gas exchange experiment. Other conditions: pH 6, 10 °C, electrode rotation rate 3000 rpm, -0.05 V, gases as indicated with the remaining 80% of the atmosphere being H_2 as in most of the experiments in Chapter 6, electrode surface area: 0.03 cm^2.

As reduction of O_2 by graphite is not a clean process, the products are likely to be a mixture of O-species, including peroxide. To verify that H_2O_2 would not survive in solution at the potentials at which O_2 is being reduced, cyclic voltammograms of H_2O_2 dissolved in the electrolytic buffer were recorded. Figure 2.13 shows cyclic voltammograms of an unmodified electrode in pH 6 buffer (dashed line), an unmodified electrode in pH 6 buffer with 1% O_2 in N_2 flushing through the headspace (thin line) and an unmodified electrode in pH 6 buffer containing 1% H_2O_2. That a negative current is recorded over the -0.55 V to +0.24 V potential range strongly suggests that any peroxide formed at the electrode would be reduced and thus would not complicate the rates obtained for inactivation of the enzyme by O_2. While this experiment does not inform on the rates of reduction of H_2O_2 relative to its production by reduction of O_2, it lends credence to the notion that the species with which the enzyme reacts is O_2 and not H_2O_2.

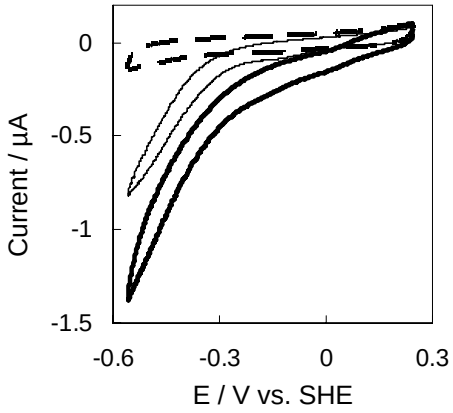

Figure 2.13: Control experiments performed to compare the electrochemical response of a PGE rotating disk electrode to O_2 and H_2O_2. The electrode is placed in cell containing a buffered solution under N_2 (dashed line) or 1% O_2 in N_2 (thin line). The bold line shows the response of the electrode to 1% (volume for volume) H_2O_2 under a 100% N_2 atmosphere. Other conditions: pH 5.5, 30 °C, 20 mV/s, electrode surface area: 0.03 cm^2.

Chapter 3:

Electrochemical Characterization of The [FeFe]-Hydrogenases

3.1. Abstract

Electrocatalysis by the [FeFe]-hydrogenase from *Clostridium acetobutylicum* (*Ca*HydA) and the algal [FeS]-cluster-free [FeFe]-hydrogenases *Chlamydomonas reinhardtii* (*Cr*HydA1) and *Chlorococcum submarinum* (*Cs*HydA) was studied using PFE. The efficiency of electrocatalysis by *Cr*HydA1 and *Cs*HydA demonstrates that [FeS]-clusters are not necessary to observe electrocatalysis, though a small overpotential (absent in the case of enzymes with an [FeS]-cluster chain) is observed. The catalytic bias is probed and the K_M for H_2 oxidation and apparent inhibition constant for inhibition of H_2 production (H^+ reduction) by H_2 ($K_I^{app}(H_2/H^+)$) are determined and used in conjunction with the catalytic bias to further our understanding of the requisite characteristics for efficient H_2 production. Finally, the process of anaerobic inactivation is investigated and it is shown that this process differs considerably for *Cr*HydA1 and *Cs*HydA from that reported[204] for *Dd*H. Uniquely amongst the [FeFe]-hydrogenases, *Ca*HydA only inactivates very slowly. Whilst anaerobic inactivation is completely reversible for *Dd*H, it is only partially so for *Cr*HydA1 and *Cs*HydA. Moreover, there is a greater complexity of reversibly inactivated states formed by the algal hydrogenases and these are characterized by their pH-, [H_2]- and reactivation potential- dependences.

3.2. Introduction

As previously mentioned, the increasing interest in the [FeFe]-hydrogenases stems from their high turnover of H_2 production,[77] between 6000 and 9000 s^{-1}.[35]

3.2.1. Structural and Catalytic background

As electrocatalysis by a hydrogenase lacking an electron relay chain has not been described before, it is pertinent to begin by discussing the structure of the algal (eukaryotic) [FeFe]-hydrogenases *Cr*HydA1 and *Cs*HydA relative to those of electrocatalytically characterized[18,204] [FeFe]-hydrogenases that do have an electron transfer chain of [FeS]-clusters. Crystallographic structures are available for two [FeFe]-hydrogenases, that of *Dd*H (small subunit 10 kDa, large subunit 46 kDa), and *Cp*I, (one subunit, 64 kDa). The two structures are shown in Figure 1.11. The large subunit of (periplasmic) *Dd*H shares only 39 % sequence identity with (cytoplasmic) *Cp*I. Both possess a relay chain of [FeS]-clusters in addition to the H-cluster: in *Dd*H there are an extra two [4Fe4S]-clusters, and in *Cp*I there are three [4Fe4S]-clusters and an additional [2Fe2S]-cluster. The algal *Cr*HydA1 enzyme (one subunit, 48.7 kDa) shares 34% sequence identity with *Cp*I and 33% with the large subunit of *Dd*H, with the notable difference that it does not contain a [FeS]-cluster relay chain.[211] In fact, the C-termini of [FeFe]-hydrogenases (which comprise the H-cluster in the case of algal hydrogenases[212]) exhibit a great degree of conservation.[35] A structural model for *Cr*HydA1 prepared using PyMOL (by Sven Stripp, University of Bochum) is shown in Figure 3.1; this is based on the structures of the C-termini of *Dd*H and *Cp*I. The bacterial *Ca*HydA enzyme shares a 71% sequence similarity with *Cp*I[16] and the model shown in Figure 3.1 is prepared using *Cp*I as a template.

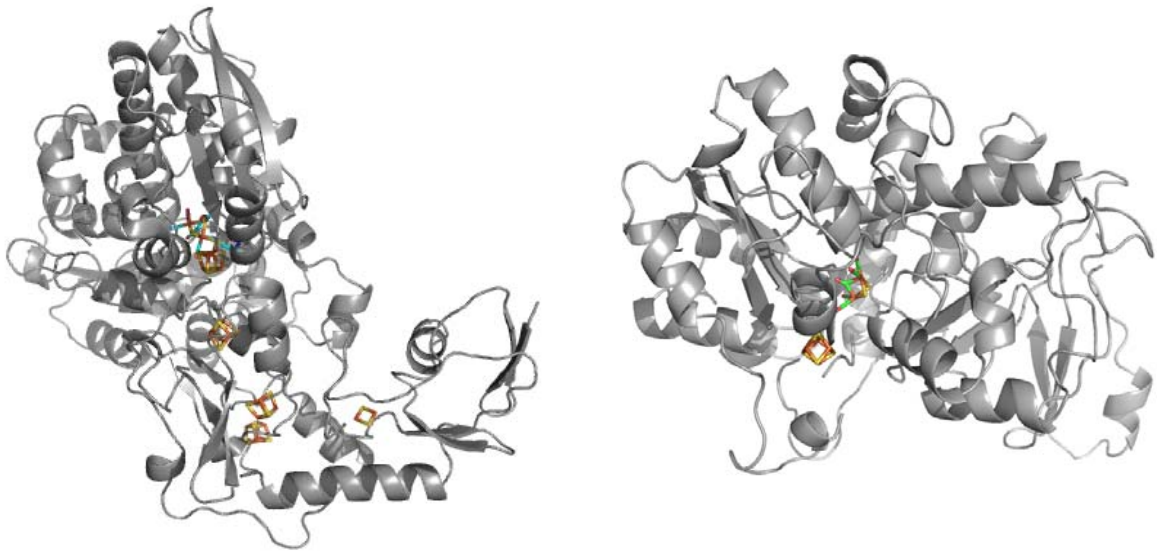

"Bacterial" *Ca*HydA **"Algal" *Cr*HydA1**

Figure 3.1: Model structures of *Ca*HydA (based on the structure of *Cp*I, prepared using the internet-based program Modbase[213] accessed at http://modbase.compbio.ucsf.edu/ModWeb20-html/modweb.html) and *Cr*HydA1 (modelled by Sven Stripp (U. Bochum) using PyMOL).

Aside from being noted to be more catalytically active in the direction of H_2 production than [NiFe(Se)]-hydrogenases, it has also been observed that [FeFe]-hydrogenases have lower binding affinities for H_2.[214] Two notable exceptions exist within the [FeFe]-hydrogenases: *Cp*II[215] and *Dv*H,[214] which have very low K_M values. In the case of *Dv*H, Van Haaster postulates that this is related to its physiological function as a H_2 oxidiser,[214] but the role of *Cp*II has not been clearly established.

3.2.2. Electrochemical studies of [FeFe]-hydrogenases

The [NiFe]-hydrogenases have received much greater electrochemical attention[57,59,97,162,203,205,208,209,216-218] than the [FeFe]-hydrogenase. A broad-spectrum electrochemical characterization of *Dd*H described features such as irreversible inactivation by O_2 and anaerobic inactivation acting as a protective mechanism against this (as previously suggested by Van Dijk[219]) as well as the reversible inhibition by CO

and the photolability of the exogenous CO-ligand.[204] In this study, Parkin et al. showed that anaerobic inactivation involved an electron at pH < 6 and a proton and an electron at pH > 6. It was also demonstrated that reactivation is pH-dependent (the rate of reactivation increases with decreasing pH) and is accelerated at more negative potentials. Extensive comparisons are drawn between the algal enzymes *Cs*HydA and *Cr*HydA1 and *Dd*H in this chapter.

Baffert et al. have also used PFE to characterize an [FeFe]-hydrogenase – the bacterial *Ca*HydA enzyme - by determining an approximate K_M value and noting that H_2 does not inhibit H_2 production by this enzyme.[220] Hambourger et al. have adsorbed this hydrogenase onto a graphite electrode in a photovoltaic device to produce H_2, noting that the enzyme is only marginally inhibited by H_2.[45] There is thus some disagreement in the literature as regards product inhibition of H_2 production catalysed by *Ca*HydA.

Both *Dd*H and *Ca*HydA have been shown to engage in very efficient electrocatalysis when adsorbed as a film on a graphite electrode. Since the shortest distance from the surface of the protein to the buried active site is greater than about 15 Å, it is highly unlikely that electrons are exchanged directly between the active site and the electrode,[184] so it is assumed that, as with the physiological partner, the active site exchanges electrons with the electrode only via the chain of [FeS]-clusters. Experiments in this chapter probe the capacity of *Cr*HydA1 and *Cs*HydA (which lack the [FeS]-cluster relay chain) to engage in direct electron transfer and electrocatalysis at a graphite electrode.

The work presented here aims to further our knowledge of some basic characteristics of [FeFe]-hydrogenases by examining the catalytic bias of *Cs*HydA, *Cr*HydA1, *Ca*HydA and *Dd*H and their behaviour at highly oxidising potentials. Their binding affinity for H_2 both in terms of the apparent inhibition constant for H_2 in H_2 production ($K_I^{app}(H_2/H^+)$) and the Michaelis constant (K_M) for binding of H_2 in H_2 oxidation are also determined and compared to those measured for [NiFe(Se)]-hydrogenases (also see Chapter 4). The availability of a given enzyme sample in the laboratory dictated which experiments were performed on which enzyme but, as a rule, experiments were carried out on as many hydrogenases as possible. Note that all experiments on [FeFe]-hydrogenases described in this thesis were performed in a cell that was blacked out with black electrochemical tape to avoid convoluting the results with light-activated processes[204] (see section 5.3.3.6).

3.3. Results

3.3.1. The point of inflection

A cyclic voltammogram recorded for a film of *Cr*HydA1 on a PGE rotating disk electrode under 100% H_2 (~0.8 mM) at pH 6, 20 °C is shown in Figure 3.2. The vertical grey line shows the potential of the $2H^+/H_2$ couple corrected for these conditions, -0.349 V. At potentials below this value, a negative current is recorded as the hydrogenase catalyses H^+ reduction to form H_2, and in the potential region above -0.349 V, a positive current is recorded as the enzyme oxidises H_2. These electrocatalytic currents show that electrons must be able to exchange rapidly between the active site and the electrode even though *Cr*HydA1 does not contain an [FeS]-cluster relay chain, and this is the first observation of direct electrocatalysis for a

hydrogenase with no [FeS]-relay. Thus, the distance between the electrode and the active site is apparently sufficiently small for electrons to enter it directly. However, there is a detectable point of inflection at the thermodynamic potential of the $2H^+/H_2$ couple (which is also visible for *Cs*HydA in Figure 3.3), indicating that there is a small overpotential for both H_2 oxidation and H^+ reduction catalysed by these algal hydrogenases.[221] This is in contrast to observations for the [FeFe]-hydrogenases from *Dd*H[18,204] or *Ca*HydA (see below, Figure 3.3), and the [NiFe(Se)]-hydrogenases studied to date,[87,88] for which the electrocatalytic current cuts the zero-current axis cleanly at to the $2H^+/H_2$ potential indicating that electron transfer is so efficient for these enzymes that they electrocatalysis is not subject to the Butler-Volmer equation (Equation 2.7). The additional driving force required for catalysis by these two hydrogenases is thus likely to be imposed by the electron tunnelling distance between the active site and the electrode rather than being an inherent electronic property of the active site.

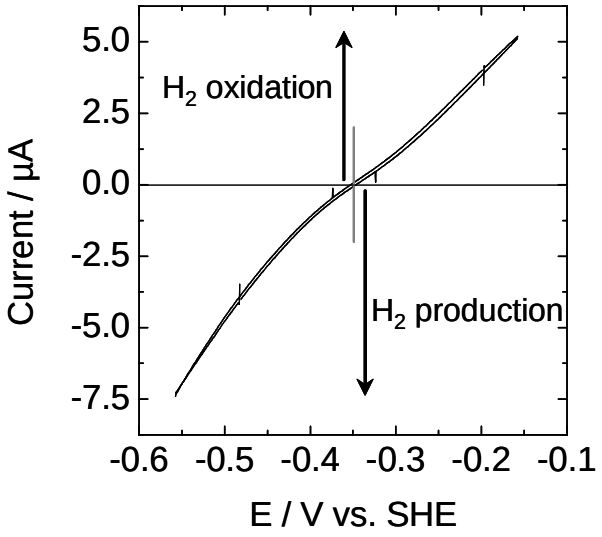

Figure 3.2: Cyclic voltammogram for *Cr*HydA1 on a PGE rotating electrode under 100% H_2 at pH 6, 20 °C. The potential of the $2H^+/H_2$ couple corrected for these conditions is shown as the vertical grey line. The black arrows indicate increasing H_2-oxidation and H_2-production activity. Other conditions: scan rate 20 mV/s, electrode rotation rate 3000 rpm.

3.3.2. Catalytic bias

Figure 3.3 shows cyclic voltammograms recorded under 100% H_2, pH 6 to compare the catalytic activity of four [FeFe]-hydrogenases (*Dd*H, *Cs*HydA1, *Cr*HydA1 and *Ca*HydA) in the direction of H_2 oxidation with respect to that in the direction of H_2 production (termed the catalytic bias). Under these conditions, the rate of H^+ reduction and H_2 oxidation by *Cr*HydA1 and *Cs*HydA is similar for a given driving force (marked by the vertical red lines) on either side of thermodynamic potential (marked by the vertical grey line). In contrast, the catalytic bias for *Ca*HydA lies strongly in favour of H^+ reduction and the ratio of the currents at the positive overpotential : negative overpotential is about 1:2; although the current cuts sharply through the axis at the thermodynamic potential, H_2 oxidation activity rapidly tends towards a plateau as the potential is raised, suggesting that a chemical rate-determining step, rather than electron transfer, governs the catalytic rate and (consequently) the catalytic bias. Physiologically, *Dd*H is the only one of the four enzymes to function in the direction of H_2 oxidation. It is thus apt that it is the most biased towards H_2 oxidation (the ratio of the currents at the positive overpotential : negative overpotential is about 3:2). Also marked (by a star) on Figure 3.3 is the potential above which *Dd*H, *Cs*HydA and *Cr*HydA1 anaerobically inactivate; anaerobic inactivation will be discussed further in section 3.3.4. As expected, the bias in all cases is strongly dependent on pH.

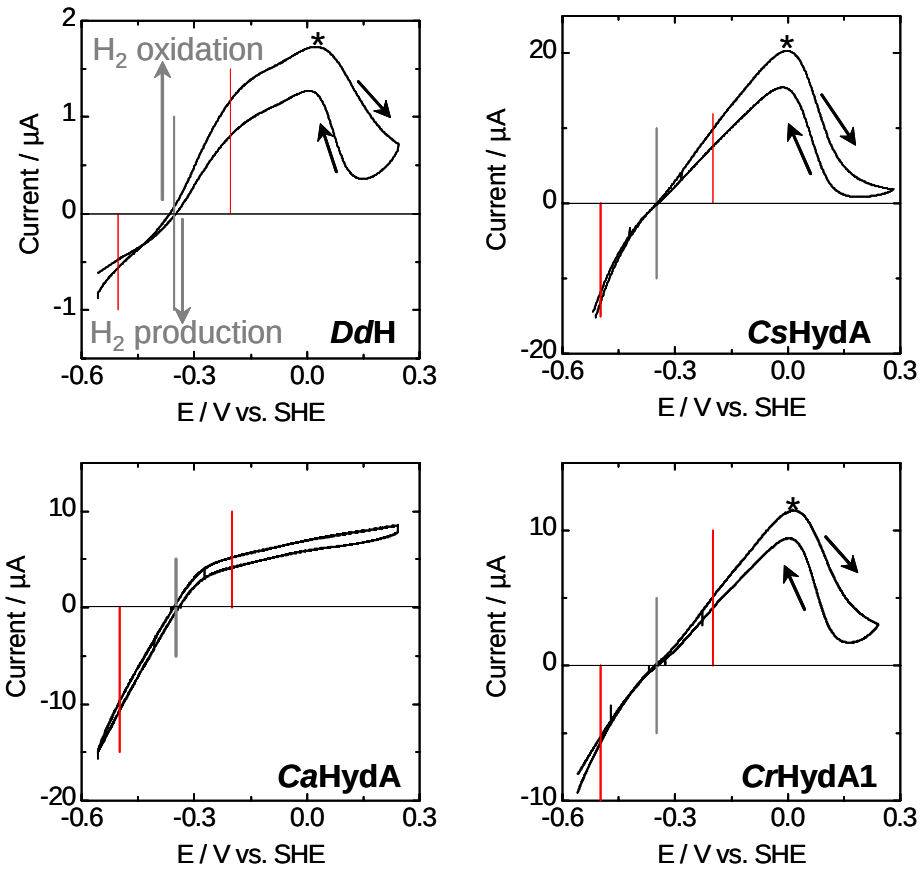

Figure 3.3: Cyclic voltammograms showing the catalytic bias of *Dd*H (courtesy of Dr. Alison Parkin), *Cr*HydA1, *Cs*HydA and *Ca*HydA under 100% H_2, pH 6. The stars mark the potential above which *Dd*H, *Cr*HydA1 and *Cs*HydA anaerobically inactivate. The black arrows mark the direction of the reductive and oxidative sweeps. The vertical grey lines mark the thermodynamic potential of the $2H^+/H_2$ couple. The vertical red lines mark the points on the catalytic waves that are at overpotentials 0.15 V more positive and negative than the thermodynamic potential. The grey arrows indicate increasing H_2-oxidation and H_2-production activity. Other conditions for *Ca*HydA, *Cs*HydA and *Cr*HydA1: 20 °C, electrode rotation rate: 3000 rpm, scan rate 20 mV/s. Other conditions for *Dd*H: 25 °C, electrode rotation rate 2500 rpm, 10 mV/s.

3.3.3. Binding of H_2 - K_M and $K_I^{app}(H_2/H^+)$

In order to obtain a broader perspective on catalytic bias, the affinity of one bacterial and one algal enzyme for H_2 was evaluated in terms of the K_M for H_2 as substrate in H_2 oxidation and the inhibition constant $K_I^{app}(H_2/H^+)$ for H_2 as an inhibitor of H^+ reduction (i.e. product inhibition). Experiments such as the one shown in Figure 3.4A to determine the K_M for H_2 oxidation of (bacterial) *Ca*HydA and (algal) *Cr*HydA1 were conducted by varying the ratio of H_2 to N_2 in the headspace of the cell using mass-flow

controllers and allowing time for equilibration with the cell solution at each concentration of H_2. The experiments were performed at -0.05 V to avoid inactivation of the hydrogenases. It was also important to carry out the experiments under conditions where the current was limited by the catalytic rate of the enzyme rather than mass-transport of substrate to the electrode or removal of product from the electrode. For this reason the experiments were carried out at a low temperature (10 °C) to slow the rate of catalysis. The low temperature also minimises film loss. At the highest and lowest of the H_2 concentration, the rotation rate of the electrode was stepped between 3000 and 5000 rpm to ensure that the current (and thus the rate of reaction) was independent of rotation rate (i.e. mass-transport of H_2). Values for K_M were calculated from the *x*-intercept of the electrochemical version of the Lineweaver-Burk plot shown in Figure 3.4B and are summarised in Table 3.1. See Appendix IV for more information on the mathematical basis for the electrochemical calculation of K_M. The slow film loss, as traced by the dashed grey line, is taken into account in calculating the error bars quoted in Table 3.1.

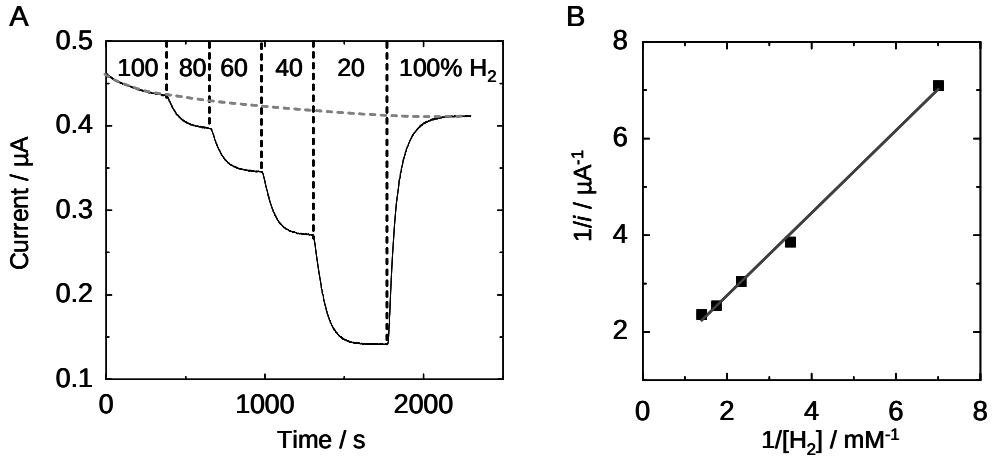

Figure 3.4: Calculation of K_M for *Ca*HydA. A) Chronoamperometric experiment performed at -0.05 V, at pH 6, 10 °C. The concentration of H_2 in N_2 in the headspace of the cell is indicated in the figure. The rotation rate was varied from 3000 to 4000 and 5000 rpm under 100 % H_2 and 20% H_2 to ensure that the catalysis was not mass-transport limited; under 80, 60 and 40% H_2 the rotation rate was 5000 rpm. The horizontal dashed grey line visually traces the progression of film loss. B) Electrochemical Lineweaver-Burk plot of $1/i$ against $1/[H_2]$.

Experiments to obtain values of $K_I^{app}(H_2/H^+)$ (defined in Equation 3.1 where K_M^{H+} is the K_M for binding of the substrate H^+, and $K_I(H_2/H^+)$ is the real inhibition constant) for *Ca*HydA and *Cr*HydA1 were conducted at -0.45 V using a similar method to that described above. In Figure 3.5A (which, again, shows an experiment carried out on *Ca*HydA), the H_2 concentration was varied from 100% to 0% in the headspace and the rotation rate was varied at each concentration step when the current had settled to a steady level. Again, the fact that no change in current was observed on changing the rotation rate confirms that mass-transport of [H_2] was not limiting its reaction with the enzyme. The values of $K_I^{app}(H_2/H^+)$ were calculated using an adaptation of a method based on Michaelis-Menten kinetics pioneered by Léger (Figure 3.5B) – see Chapter 4 and Appendix IV for further details of the mathematical basis of this work.[216] The $K_I^{app}(H_2/H^+)$ can be calculated using Equation 3.2, in which i_{N_2} is the current recorded under N_2 and that obtained at each given concentration of H_2 is i_{H_2}. Figure 3.5B shows a plot of (i_{N_2}/i_{H_2} -1) vs. [H_2], fitted to a straight line, the slope of which is the reciprocal of the average $K_I^{app}(H_2/H^+)$ value. Thus, the accuracy of the fit gives some indication as to the accuracy of each measurement of $K_I^{app}(H_2/H^+)$. The values obtained along with the error bars taking film loss into account are quoted in Table 3.1.

$$K_I^{app}(H_2/H^+) = \frac{K_I(H_2/H^+)[H^+]}{K_M^{H^+}}\left[1+\frac{K_M^{H^+}}{[H^+]}\right] \qquad \text{Equation 3.1}$$

$$\left(i_{N_2}/i_{H_2}\right)-1 = \frac{[H_2]}{K_I^{app}(H_2/H^+)} \qquad \text{Equation 3.2}$$

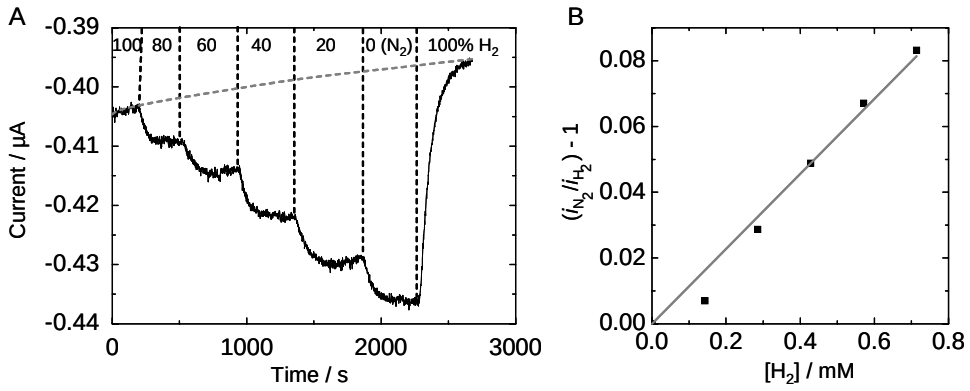

Figure 3.5: Calculation of $K_I^{app}(H_2/H^+)$ for *Ca*HydA. A) Chronoamperometric experiment performed at -0.4 V, at pH 6, 10 °C. The concentration of H_2 in N_2 in the headspace of the cell is indicated in the figure. The rotation rate was varied from 3000 to 4000 and 5000 rpm at each concentration of H_2 to ensure that the inhibition was not mass-transport limited. B) Léger-type plot from which the $K_I^{app}(H_2/H^+)$ can be calculated. The horizontal dashed grey line visually traces the progression of film loss throughout the experiment.

Enzyme	K_M / mM	$K_I^{app}(H_2/H^+)$ / mM
Algal *Cr*HydA1	0.19 ± 0.03	3.7 ± 0.6
Bacterial *Ca*HydA	0.46 ± 0.06	6.2 ± 1.1

Table 3.1: The K_M and $K_I^{app}(H_2/H^+)$ values for *Cr*HydA1 and *Ca*HydA calculated at pH 6, 10 °C from the experiments shown in Figure 3.4 and Figure 3.5. The K_M and $K_I^{app}(H_2/H^+)$ were calculated at -0.05 V and -0.4 V, respectively.

The values reported above are not perfectly accurate due to a shifting of the thermodynamic potential as the concentration of H_2 varies. Thus, as the thermodynamic potential changes from -0.337 V under 100% H_2 to -0.317 V at 20% H_2, the driving force for H_2 oxidation (-0.05 V in the K_M experiments) and H_2 production (-0.4 V in the $K_I^{app}(H_2/H^+)$ experiments) also change by 0.02 V. However, these data are still usefully representative of the $K_I^{app}(H_2/H^+)$ and K_M values for these enzymes since -0.4 V represents 'driving potentials' (with respect to the thermodynamic potential) of -0.063 V (at 100% H_2) and -0.083 (at 20% H_2) and -0.05 V represents a 'driving potential' of °0.287 V (at 100% H_2) or +0.267 V (at 10% H_2), so the 0.02 V shift is small or fairly insignificant (in the case of the calculation of K_M) relative to these driving potentials.

Unfortunately, films of *Dd*H are much less stable on the electrode than those of *Ca*HydA and *Cr*HydA1 and this prevented uncomplicated analysis of experiments such as those shown in Figure 3.4 and Figure 3.5 because the current decreased rapidly throughout the experiment due to film loss. However, some sense of the comparative degree of inhibition of these three enzymes by H_2 can be attained by performing a simple experiment in which the enzyme-modified electrode is poised at -0.4 V and the gas in the headspace of the cell is changed from N_2 to H_2 and back N_2. In Figure 3.6, the current is normalised to the level recorded under N_2 prior to inhibition in all three cases.

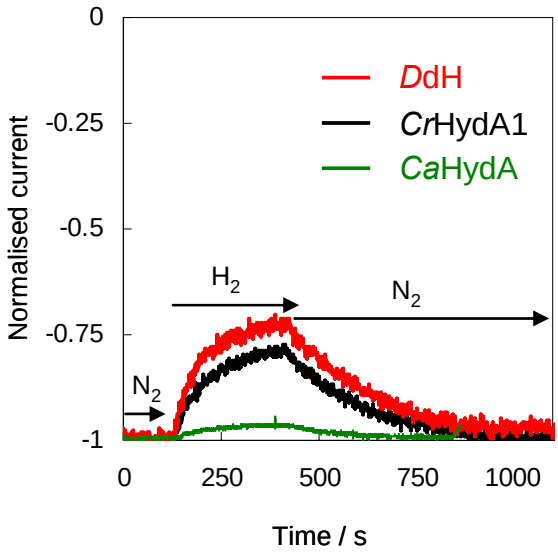

Figure 3.6: Comparison of the effect of H_2 on H_2 production by *Dd*H, *Cr*HydA1 and *Ca*HydA. Experimental conditions: pH 6, 10 °C, -0.4 V, electrode rotation rate 3000 rpm, headspace atmosphere as indicated.

The magnitude of the current lost on inhibition of *Dd*H is slightly larger than that of *Cr*HydA1 and much more pronounced than that of *Ca*HydA. Therefore, *Dd*H (whose physiological function is H_2 oxidation) is more inhibited by H_2 than either of the other two [FeFe]-hydrogenases that function as H_2-producers *in vivo*.

3.3.4. Observing anaerobic inactivation

It is apparent from the decrease in H_2 oxidation current as the potential is swept above 0 V (marked by * in Figure 3.3) that the bacterial enzyme *Dd*H and the algal enzymes *Cr*HydA1 and *Cs*HydA inactivate at high potential; in contrast *Ca*HydA appears not to inactivate the same degree, therefore it is not studied any further.

Figure 3.7 shows cyclic voltammograms that depict the effects of scan rate (A), H_2 concentration (B) and pH (C) on anaerobic inactivation of *Cr*HydA1. In panel A, three experiments performed at pH 6 under 100% H_2 in the headspace are shown: one scan recorded at 20 mV/s (black trace), one recorded at 1 mV/s (green trace) and one recorded at 0.1 mV/s (red trace). Panel B shows three cyclic voltammograms recorded at 20 mV/s at pH 6: one under 100% H_2 (black trace), one under 50% H_2 (green trace) and one under 10% H_2 (red trace). The effect of pH on anaerobic inactivation is demonstrated in panel C. Two cyclic voltammograms (one at pH 6 (black trace) and one at pH 8 (red trace)) recorded under 100 % H_2 at 20 mV/s are overlaid. In all cases, the current is normalised to the maximum value measured on the oxidative scan.

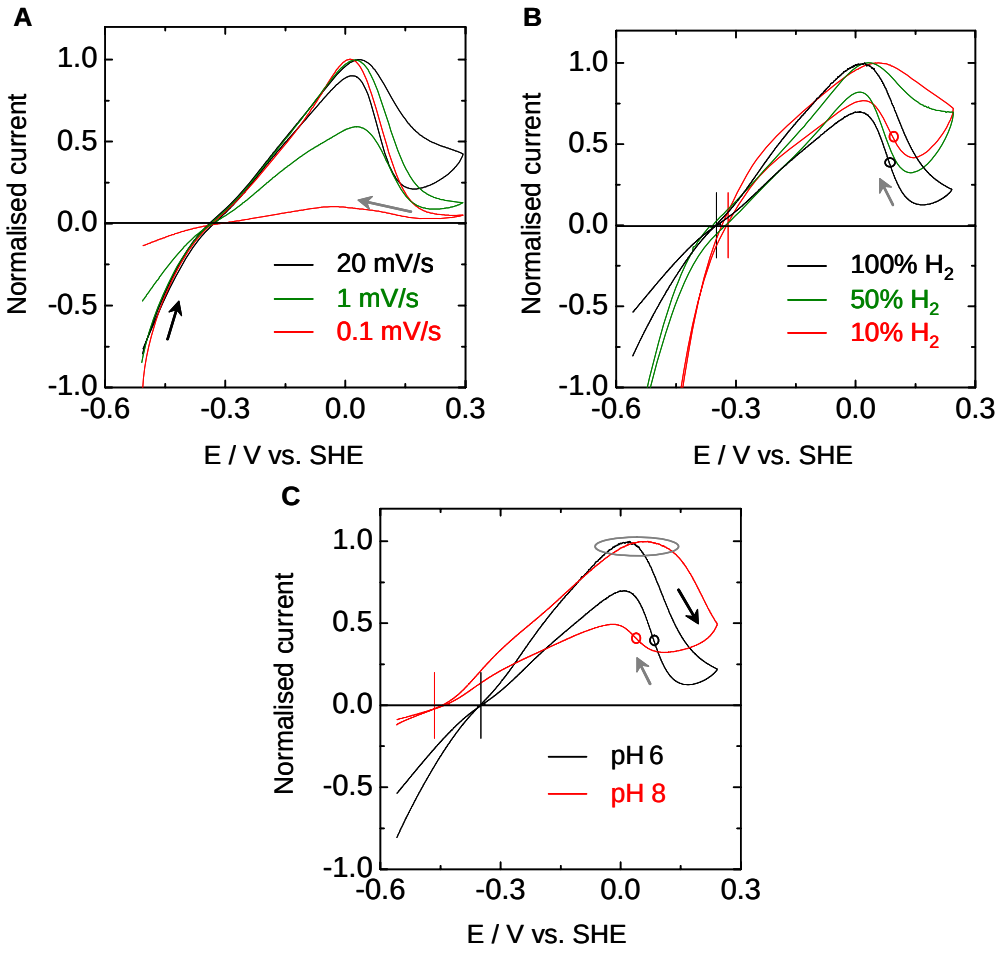

Figure 3.7: Anaerobic inactivation of *Cr*HydA1 as viewed by cyclic voltammetry at different scan rates (A), under different concentrations of H_2 in the headspace (B) and at different pH values (C). A) Experimental conditions: pH 6, 20 °C, 100% H_2 atmosphere, electrode rotation rate 3000 rpm, scan rates as indicated. B) Experimental conditions: pH 6, 20 °C, H_2 percentage in the headspace as indicated, electrode rotation rate 3000 rpm, scan rate 20 mV/s. C) Experimental conditions: pH 6 (black trace) or pH 8 (red trace), 20 °C, 100% H_2 atmosphere, electrode rotation rate 3000 rpm, scan rate 20 mV/s. The vertical black lines in panels B and C indicate the thermodynamic potential at pH 6 under 100% H_2. The vertical red line in panels B and C marks the thermodynamic potential at pH 6, 10 % H_2 in N_2 atmosphere, and the thermodynamic potential at pH 8, 100% H_2, respectively. The circles mark the point in the reductive scans at which E_{switch} is reached – see the main text for the definition of E_{switch}. The grey oval highlights the maxima reached on the oxidative scans at pH 6 and pH 8 in panel C. Black and grey arrows mark the directions of the oxidative and reductive scans, respectively.

Panel A demonstrates that decreasing the scan rate increases the extent of inactivation as the current recorded at +0.3 V is lower when the potential was swept at 0.1 mV/s (red trace) than it was when the potential was swept at 1 mV/s (green trace) which in turn was lower than when the scan rate was set to 20 mV/s (black trace). This is because lowering the scan rate increased the period of time for which *Cr*HydA1 experienced

highly oxidising potentials thus increasing the degree of inactivation. The maximum current corresponding to H_2 oxidation recorded on the reductive sweep (marked by the grey arrow) was lower for the scan recorded at 0.1 mV/s than it was for the scan recorded at 1 mV/s. The greatest normalised H_2-oxidation current on the reductive scan was obtained in the scan measured at 20 mV/s. This is the consequence of two factors. Firstly, as the scan rate is lowered, film loss is allowed more time to progress thus decreasing the magnitude of the current obtained on the reductive sweep. Secondly, as will be discussed in sections 3.3.6 and 3.3.7, anaerobic inactivation of the algal hydrogenases (*Cr*HydA1 and *Cs*HydA) is not completely reversible, thus the slower the scan, the more time allowed for *irreversible* inactivation to take place, the lower the current recovered on the reductive sweep.

Panels B and C are shown above to depict the effect of changing the concentration of H_2 and H^+ on shifting the thermodynamic potential and thus the entirety of the catalytic wave, including E_{switch}. For other hydrogenases E_{switch} has been identified as the point of steepest change in current on the reactivation sweep (i.e. the maximum in the derivative plot di/dE for the return sweep). This describes the point at which half the molecules that have inactivated at high potential have become *re*activated by applying more reducing potentials. The pH dependence of E_{switch} is examined further in section 3.3.5 below. The values of E_{switch} calculated in section 3.3.5 do not match up exactly with those marked in panel C; the complexity of the process of anaerobic inactivation of the algal hydrogenases which underlies this effect is discussed in greater detail in section 3.4.3. Suffice it to note that altering the thermodynamic potential by shifting from pH 6 to pH 8 and from a concentration of 10% H_2 to 100% H_2 in the headspace shifts the entire catalytic wave and this has some bearing on the results described below.

3.3.5. Thermodynamics of reversible anaerobic inactivation and reactivation

As discussed in sections 3.3.6 and 3.3.7, anaerobic inactivation of *Cr*HydA1 and *Cs*HydA is not always completely reversible. The analysis of the thermodynamics of anaerobic inactivation discussed below is only relevant to the species that is reversibly inactivated by the application of high potential. As outlined in Appendix III, log-transform plots (panels C and D of Figure 3.8) of the reductive sweep in the potential region in which the enzyme is observed to reactivate from high potential inactivation (panels A and B of Figure 3.8) can be used to calculate the number of electrons (n) involved in inactivation and reactivation.

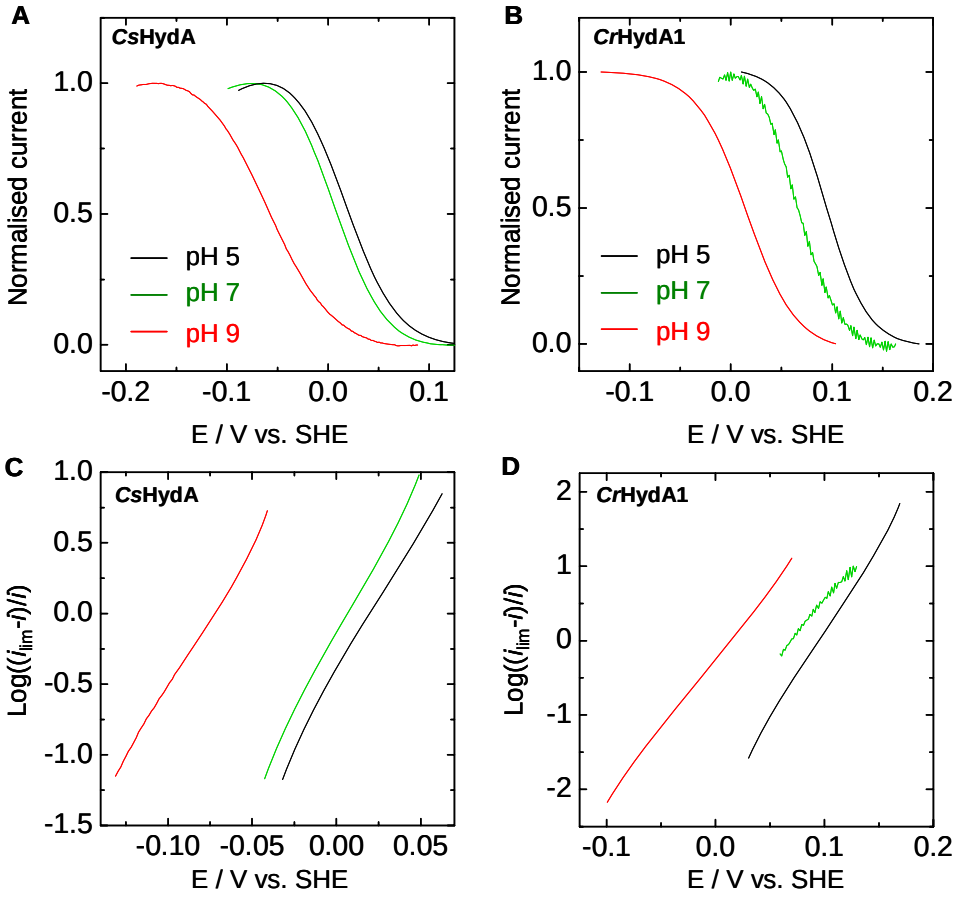

Figure 3.8: "Reactivation" sweeps after 1000 s of inactivation of A) *Cs*HydA and B) *Cr*HydA1 at +0.29 V. The corresponding log-transform plots to calculate the value of n are shown in panels C and D. Experimental conditions: 100% H_2, 20 °C, electrode rotation rate 3000 rpm, scan rate 30 mV/s for *Cr*HydA1 and 10 mV/s for *Cs*HydA.

An *n* value of 1 was determined for these processes throughout the pH range only when the potential was swept at 30 mV/s for *Cr*HydA1 and 10 mV/s for *Cs*HydA. The significance of the scan rate in determining the *n* value is discussed further in section 3.4.3 of the Discussion of this chapter.

The pH dependence of E_{switch} reports directly on the mechanisms of inactivation and reactivation (see Appendix III). Therefore, a set of experiments including those shown in Figure 3.8 were conducted to determine E_{switch} at a range of pH values for *Cr*HydA1 and *Cs*HydA. As in Figure 3.8, the potential was held at +0.29 V for 1000 s prior to sweeping to more negative potentials and the minimum in the first derivative of this "reactivation" sweep (i.e. E_{switch}) was calculated. In the Pourbaix diagrams shown in Figure 3.9, the values of E_{switch} are plotted against pH.

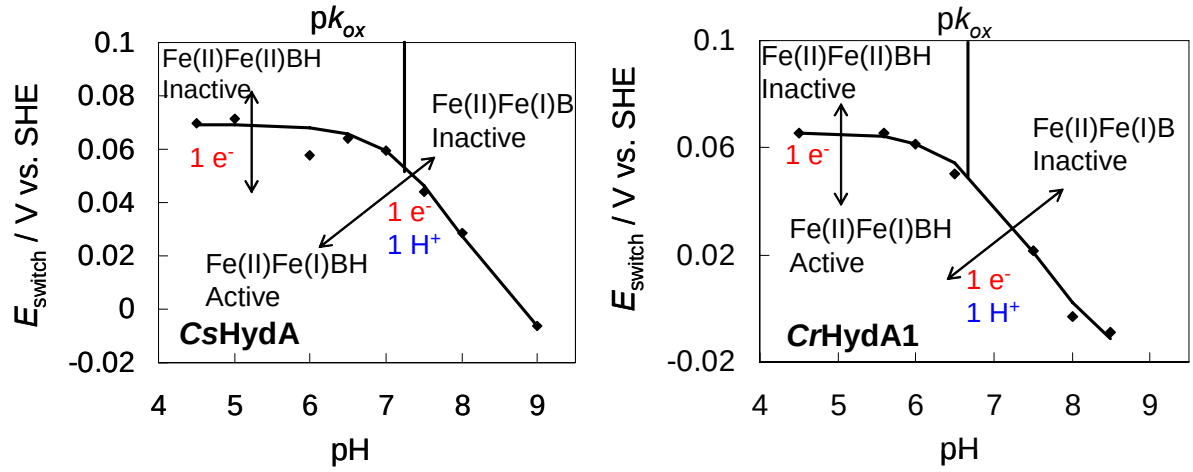

Figure 3.9: Pourbaix diagrams for *Cs*HydA and *Cr*HydA1 depicting the dependence of E_{switch} calculated from experiments such as those shown in Figure 3.8 on pH.

The Pourbaix diagrams demonstrate that E_{switch} is dependent on pH at pH > pK_{ox} but independent of pH below this value for both enzymes.[‡‡] This indicates that two different mechanisms are involved in the interconversion of the active form and H_{ox}^{inact}

[‡‡] K_{ox} is defined as the proton dissociation constant for interconversion of the two oxidised species (see Appendix III).

at different pH values, as was observed for *Dd*H.[204] Above pH 6.7 in the case of *Cr*HydA1 and pH 7.2 for *Cs*HydA, an electron and a proton are required for reactivation but below this pH, only an electron is necessary.

3.3.6. Irreversibility of anaerobic inactivation

Anaerobic inactivation of *Cr*HydA1 and *Cs*HydA1 is essentially reversed as the potential is swept back to more negative potentials so long as the enzyme is not subject to high potentials for more than approximately 30 s (judging from the scans recorded at 20 mV/s shown in Figure 3.7A). As will be shown below, the application of potentials higher than 0 V to these two enzymes for longer periods of time induces some loss of activity that is not recovered at lower potentials.

To probe the relationship between irreversible inactivation and the enzyme being subject to high potentials (>0 V) and isolate this relationship from the artefact of film loss (which will lead to a greater loss of current between the forward and backward scans at slower scan rates in the experiments shown in Figure 3.7A), two further experiments were performed on *Cr*HydA1 and *Cs*HydA. In Figure 3.10A for *Cr*HydA1 and Figure 3.10C for *Cs*HydA, a scan (shown in black) was recorded and the potential was held at +0.24 V for 5 minutes (marked by the dashed rectangle) before the reductive return sweep was allowed to proceed. A second cyclic voltammogram, shown in red, was then recorded. The same procedure was employed for the experiments shown in Figure 3.10B and Figure 3.10D, except that the potential was held at -0.51 V instead of +0.24 V (again marked by the dashed rectangle). In all cases the currents are normalised to the maximum value obtained on the oxidative sweep in the first (black) scan. The maximum normalised current obtained on the red scan (marked by the

dashed red line) can then be used to evaluate how much the current had decreased whilst the potential was held constant.

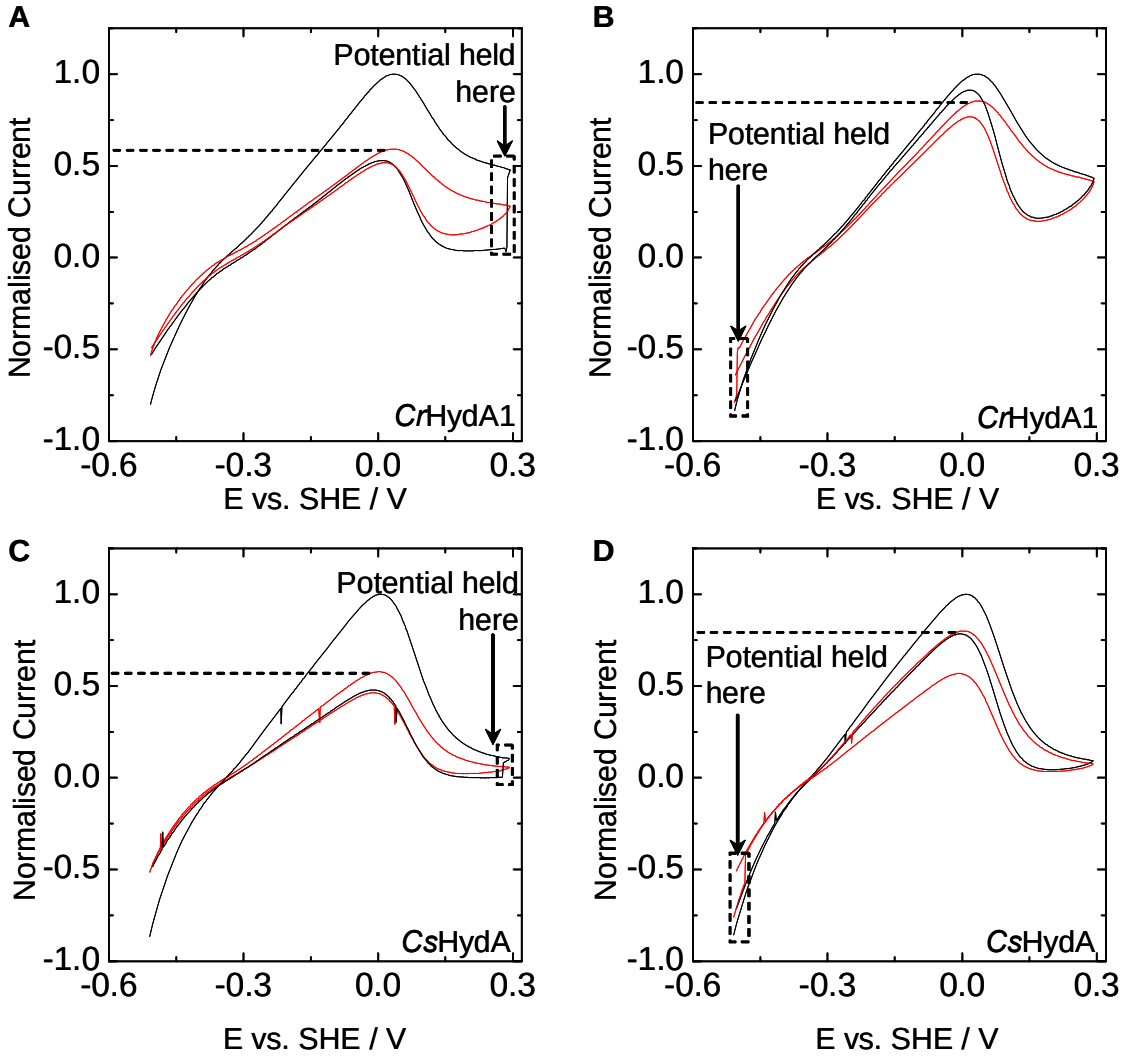

Figure 3.10: Investigation of the irreversibility of the high-potential inactivation of *Cs*HydA and *Cr*HydA1. Experimental conditions: pH 6, 20 °C, 100% H_2, electrode rotation rate 3000 rpm, scan rate 20 mV/s.

It is evident from Figure 3.10 that the normalised current obtained after the potential was held at a high value (0.59 for *Cr*HydA1 and 0.58 for *Cs*HydA) is much lower than that recorded after the potential was held at low value (0.85 for *Cr*HydA1 and 0.80 for *Cs*HydA). That this is the case for both enzymes reinforces the idea that some irreversible damage has occurred at high potential.

The conditions favouring this irreversibility were investigated further using chronoamperometric step experiments. These included the dependence of the degree of irreversible anaerobic damage on the potential at which the enzyme was inactivated (termed here E_{inact} for convenience), that at which it was reactivated (E_{react}), pH and concentration of H_2 in the headspace. The basic protocol for all the experiments was the same. The experiment begins at a potential E at which a catalytic current is recorded (step 1). The potential is stepped up to E_{inact} (step 2) and then to E_{react} (step 3). Importantly, E_{react} is equal to E so that the currents recorded in steps 1 and 3 can be compared fairly to assess the proportion of activity lost by stepping the potential to E_{inact} in step 2.

3.3.6.1. Dependence of extent of irreversible high-potential damage on E_{inact}

Figure 3.11 shows three experiments performed on *Cs*HydA in which the dependence of the extent of irreversible anaerobic damage on E_{inact} was probed at pH 6 under 100% H_2 at 20 °C. The potential is stepped from E = -0.05 V to E_{inact} = +0.19 V (red trace), +0.29 V (green trace) or +0.39 V (blue trace), at which point the current drops quickly due to anaerobic inactivation, before being stepped back to E = -0.05 V to reactivate the enzyme. Comparing the currents recorded in the two steps at -0.05 V (steps 1 and 3) informs on the degree to which the activity of the enzyme has recovered after being inactivated.

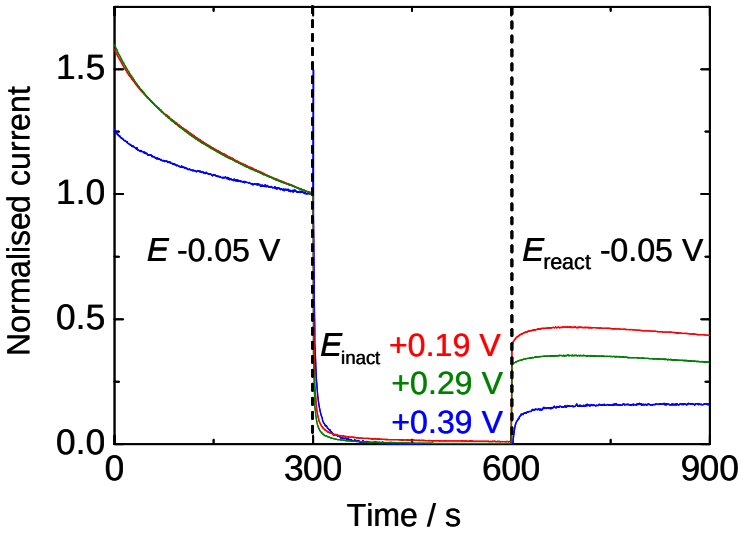

Figure 3.11: Dependence of the extent of irreversible anaerobic inactivation of *Cs*HydA on E_{inact}. Experimental conditions: pH 6, 20 °C, 100% H_2 atmosphere, electrode rotation rate 3000rpm, potentials as indicated. In all three cases the current is normalised to the value recorded at -0.1 V at t = 299 s, just before the potential step to E_{inact}.

Even though the film loss is more rapid in the experiments in which the enzyme was inactivated at +0.19 V and +0.29 V than it was in that at which E_{inact} was +0.39 V (as is evident from the relative decrease in current in the first 300 s of the three experiments), more activity is recovered than in the +0.39 V experiment. Therefore, these experiments do not require adjustment from film loss because it does not obscure the trend. The percentages of recovered activity were calculated to be 16% for inactivation at +0.39 V, 36% for inactivation at +0.29 V and 47% for inactivation at +0.19 V, thus subjecting *Cs*HydA to more oxidising conditions lowers the degree to which it is able to reactivate.

3.3.6.2. Dependence of extent of irreversible high-potential damage on E_{react}

Experiments were designed to probe the dependence of the degree of reversibility on the potential at which *re*activation of *Cs*HydA was induced. The experimental design

involving the three potential steps was similar to that of the experiments shown in Figure 3.11, but E_{inact} was set at +0.29 V, and E_{react} was either -0.05 V (green trace), -0.2 V (blue trace) or -0.4 V (red trace). The data in Figure 3.12 are represented in terms of "normalised activity" rather than "normalised current" as in Figure 3.11. This is because E_{react} in the -0.4 V experiment is low enough to drive enzymatic H_2 production, recorded as a *negative* current, but the other two experiments are performed at E_{react} values at which *Cs*HydA catalyses H_2 oxidation, corresponding to a *positive* current. Therefore, so that all three experiments could be shown on the same scale for ease of visual interpretation, the two steps of the E_{react} = -0.4 V experiment (steps 1 and 3) were multiplied by -1 as well as being normalised.

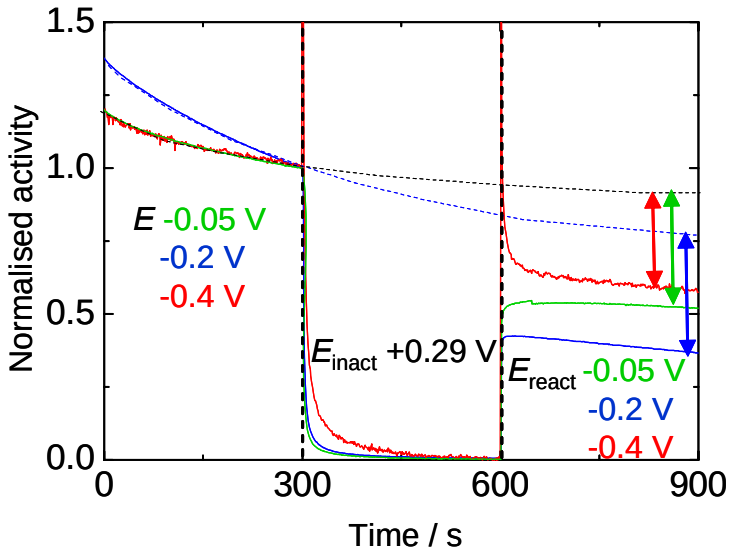

Figure 3.12: Dependence of the extent of irreversible anaerobic inactivation of *Cs*HydA on E_{react}. Experimental conditions: pH 6, 20 °C, 100% H_2 atmosphere, electrode rotation rate 3000 rpm, potentials as indicated. The current is normalised to the value recorded at t = 299s, just before the potential was stepped to +0.24 V. The dotted blue line gives a visual indicator of the projection of film loss through the experiment where reactivation was caused by poising the electrode at -0.2 V. The dotted black and blue lines give a visual indicator of the projection of film loss through the experiment where reactivation was caused by poising the electrode at -0.4 V (and -0.05 V) and -0.2 V.

Whilst it is not possible to control the degree of film loss convoluting a given experiment, it *is* possible to estimate the decrease in current over time due to film loss, Thus, the fact that the three experiments shown exhibit different rates of film loss does

not complicate the analysis too much. The "trajectory" of film loss is represented by the dotted blue line for the E_{react} = -0.2 V experiment in which the film loss was faster and the dotted black line for the E_{react} = -0.4 V and -0.05 V experiments. The approximate percentages for irreversible damage caused by the three experiments (as depicted by the double-headed arrows) are as follows: E_{react} = -0.05 V, 55%; E_{react} = -0.2 V, 50%; E_{react} = -0.4 V, 67%. Not only are these percentages quite similar (the difference that there is being the result in natural variation in results) but there is no obvious correlation between E_{react} and extent of irreversible damage, thus the degree of reversibility is independent of E_{react}. This implies that the irreversible damage occurs during the inactivation process rather than being an artefact of the potential at which the enzyme is reactivated.

3.3.6.3. Dependence of extent of irreversible high-potential damage and kinetics of inactivation and reactivation on pH

Another intriguing facet of the process of irreversible anaerobic damage is its pH dependence. Experiments analogous to those shown in Figure 3.11 and Figure 3.12 were performed at pH 6 (in red) and pH 8 (in blue) on both *Cr*HydA1 (panel A) and *Cs*HydA (panel B) under 100% H_2 at 20 °C. As above, the current is normalised to the value recorded at t = 299 s in Figure 3.13. The potential step sequence was -0.05 V, +0.29 V, -0.05 V.

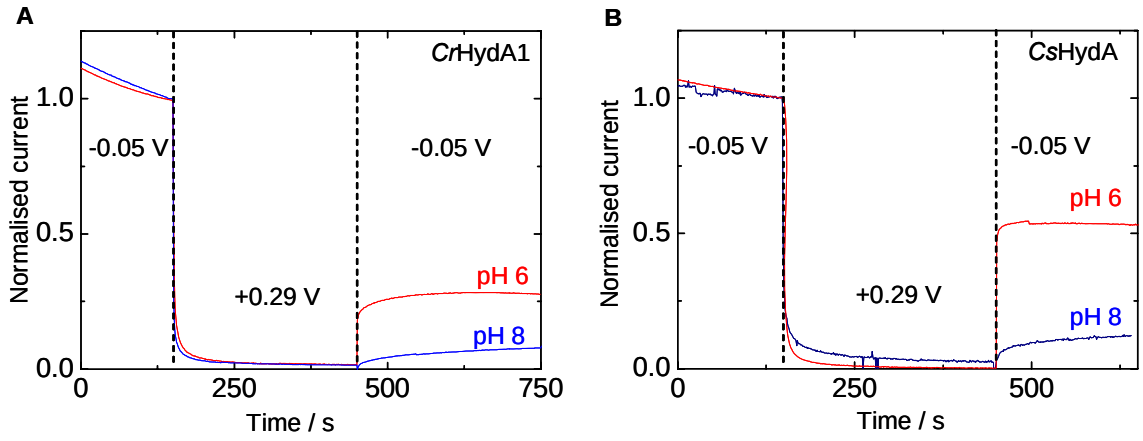

Figure 3.13: Dependence of the extent of irreversible anaerobic damage of A) *Cr*HydA1 and B) *Cs*HydA on pH. Experimental conditions: 20 °C, 100% H_2 atmosphere, electrode rotation rate 3000 rpm, pH and potentials as indicated.

Although the cyclic voltammograms shown in Figure 3.7C demonstrate that increasing the pH shifts the entire catalytic wave to the left, the potential at which the enzymes were reactivated in step 3 (-0.05 V) is more negative than the E_{switch} values calculated at *both* pH 6 and pH 8 and the inactivation potential (+0.29 V) is more positive than the E_{switch} at both pH values, thus direct comparison of the rates of inactivation and reactivation is valid. Examination of the current-time attributes of the second and third steps in Figure 3.13 informs on these rates. Whilst there is not an obvious pH dependence of the rate of inactivation (see step 2), there is a clear increase in rate of reactivation at pH 6 over pH 8 for both *Cs*HydA and *Cr*HydA1. The pH dependence of the kinetics of reactivation is further interrogated in section 3.3.7.

For both *Cs*HydA and *Cr*HydA1, Figure 3.13 demonstrates that the degree of irreversible damage was greater at pH 8 than at pH 6 when they are inactivated at the same potential. This indicates that the availability of H^+ can protect the enzyme from this process. However, applying the same E_{inact} at pH 6 and at pH 8 means the enzyme was inactivated at an overpotential that is 0.12 V higher with respect to the

thermodynamic potentials at pH 8 than at pH 6. Moreover, Figure 3.11 shows that the degree of reversibility is dependent on the E_{inact}. Thus, a further experiment in which *Cr*HydA1 was inactivated at the same overpotential at pH 8 as it was at pH 6 (+0.64 V) in Figure 3.13 was performed. These two experiments are overlaid in Figure 3.14.

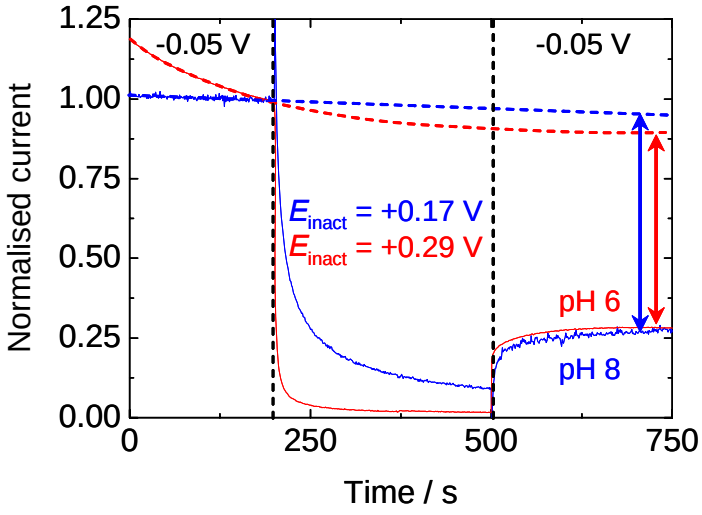

Figure 3.14: Dependence of the extent of irreversible anaerobic inactivation of *Cr*HydA1 at an overpotential of +0.64 V (with respect to the thermodynamic potential) on pH. Experimental conditions: 20 °C, 100% H_2 atmosphere, electrode rotation rate 3000 rpm, pH and potentials as indicated. A visual guide of the progression of film loss is indicated by the dashed red and blue lines (pH 6 and pH 8 respectively).

A number of features immediately obvious in Figure 3.14, including the disparity in the rates of inactivation at pH 6 and pH 8 (examined in section 3.3.8), are worthy of discussion. Within the 300 s allowed for inactivation, more activity is lost at pH 6 than at pH 8. However, when the potential was lowered to -0.05 V and the enzyme was allowed to reactivate, a nearly identical normalised current was recorded at pH 6 and pH 8. Therefore, even though the inactivation at pH 6 was more complete (the decrease in current when E_{inact} was applied was greater), a greater current was recovered at -0.05 V when film loss is taken into account, thus indicating that a much greater proportion of the reversible species was formed at pH 6 than at pH 8.

3.3.6.4. Dependence of extent of irreversible high-potential damage on [H_2]

Figure 3.15 shows an experiment utilising the protocol described above. Changing the concentration from 100% H_2 to 10 % H_2 at 20 °C shifts the thermodynamic potential from -0.35 V to -0.32 V, therefore only shifting the whole catalytic wave by 0.03 V (see Figure 3.7B). The value of E_{switch} under 10% H_2 will thus be in the range of +0.08 V, therefore the potential of step 3 (-0.05 V) is more negative than E_{switch} at both 100% and 10% H_2, so, again, the comparison of the degree of reversibility is fair.

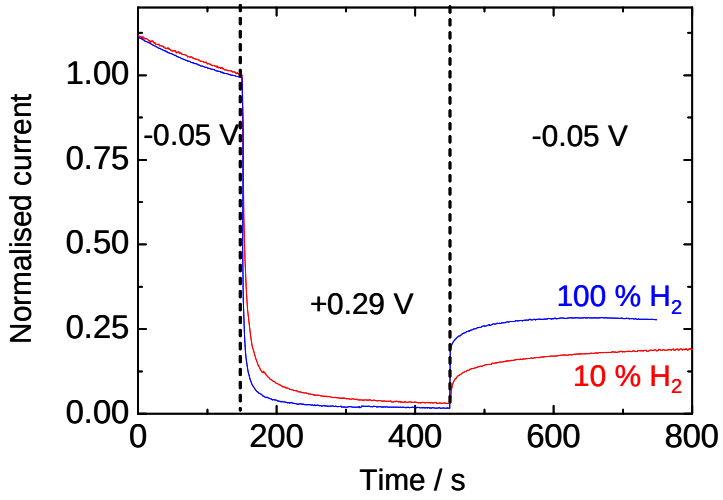

Figure 3.15: Dependence of the extent of irreversible anaerobic inactivation on [H_2] for *Cr*HydA1. Experimental conditions: pH 6, 20 °C, electrode rotation rate 3000 rpm, potentials and [H_2] (in N_2) as indicated.

The dependence of the extent of irreversibility on [H_2] indicates that H_2 can also protect *Cr*HydA1 from irreversible anaerobic damage. Figure 3.15 thus shows that the degree of recovered activity at -0.05 V in step 3 is greater for the experiment performed under 100% H_2 than for that under 10% H_2 (90% N_2).

3.3.7. Further characterization of the species formed upon anaerobic inactivation

Chronoamperometric experiments examining the rates at which *Cr*HydA1 reactivated from anaerobic inactivation at different potentials revealed yet another novel characteristic of this enzyme. Unlike *Dd*H,[204] reactivation appears to be slower than inactivation, and the rate of reactivation actually decreases as the potential is made more negative between +0.1 V and -0.05 V. The experiment carried out on *Cr*HydA1 shown in Figure 3.16 demonstrates that at least two reversibly inactivated species are produced by the application of high potentials at pH 6 and 8. The experiments begins at -0.05 V at which a current due to H_2 oxidation is monitored. A step to +0.29 V inactivates the enzyme. The potential is then stepped to +0.1 V and a rapid reactivation is observed (for clarity, the species that recovers at this potential is termed the "high-potential" species). When the potential is stepped to -0.05 V, a further and much slower reactivation is detected (this species is termed the "low-potential species"); in fact reactivation of the "low-potential" species is much slower than that of any other anaerobically-inactivated hydrogenase reported to date.[18] The proportions of the three species formed on inactivation at pH 8 and pH 6 are indicated on panels A and B respectively and the log transforms of the reactivation at the two reactivation steps are shown in panel C (pH 8) and D (pH 6).

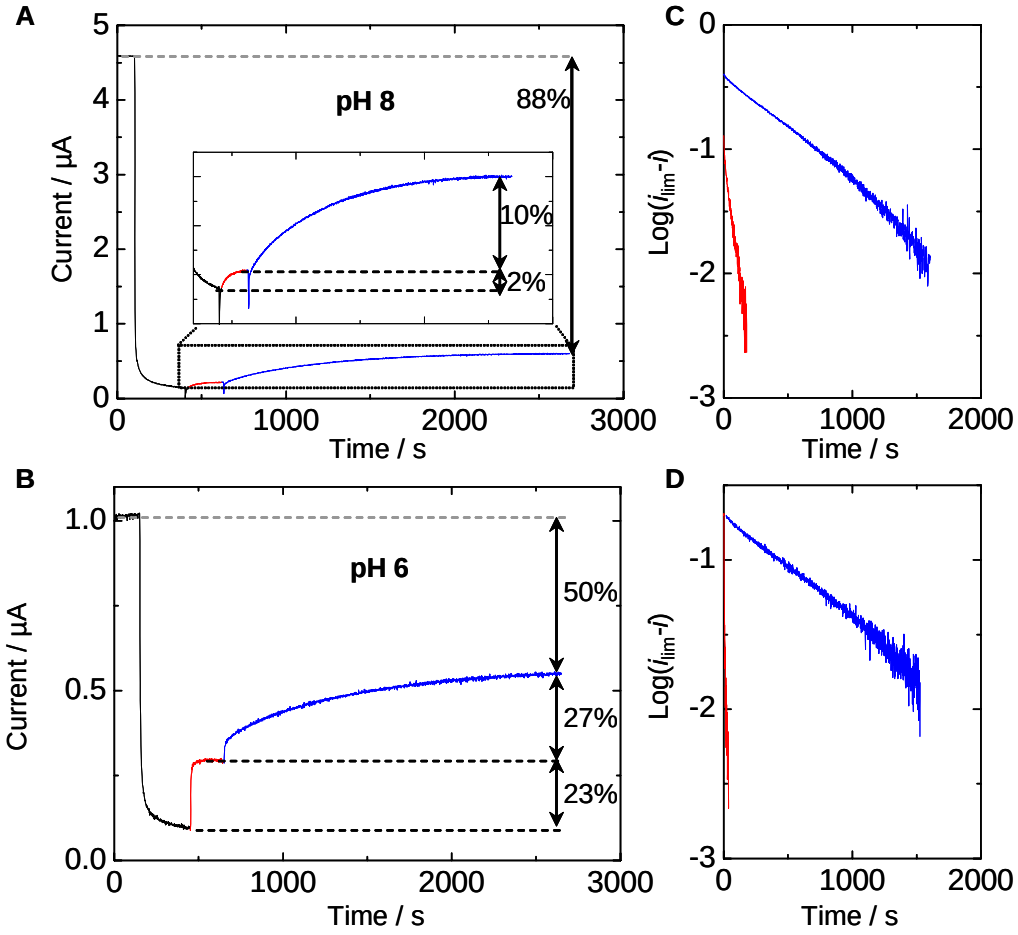

Figure 3.16: Chronoamperometric study of the species formed upon anaerobic inactivation of *Cr*HydA1 at pH 8 (A) and pH 6 (B). Experimental conditions: pH as indicated, 20 °C, electrode rotation rate 3000 rpm, 100% H_2 atmosphere, the potential step sequence is -0.05 V, +0.29 V, +0.1 V, -0.05 V. The reactivation step occurring at +0.1 V is shown in red and that occurring at -0.05 V is shown in blue in panels A and B, as are the corresponding log transforms in panels C and D. The dashed grey lines give a visual guide to the progression of film loss and the percentages quoted for the proportion of the three species formed are approximates based on this guide.

Thus, Figure 3.16 demonstrates that the proportion of the two species (as evidenced by the level the current reaches once reactivation at a given potential is complete) is a function of pH. Both the reversible forms are favoured by inactivation at pH 6 (as expected from the data shown in Figure 3.13) over inactivation at pH 8, especially the "high-potential" species. However, at pH 6, the first reactivation step at +0.1 V is just below E_{switch} (+0.11 V) whereas it is more positive than E_{switch} at pH 8 (+0.07 V). The

significant effect this disparity has on the proportion of species formed upon anaerobic inactivation is discussed further in the Discussion (section 3.4.3) of this chapter.

	pH 6			pH 8
	10% H_2	**50% H_2**	**100% H_2**	**100% H_2**
K at +0.1 / s^{-1}	0.010	0.056	0.091	0.017
K at -0.05 / s^{-1}	0.004	0.002	0.002	0.002

Table 3.1: Rate constants (quoted to three decimal places) obtained for reactivation of *Cr*HydA1 from the experiments shown in Figure 3.16 and Figure 3.17.

Panels C and D of Figure 3.16 show log-transform plots of the two reactivation steps in panels A and B respectively (where i is the normalised current and i_{lim} is the normalised limiting current reached at each potential once reactivation at that level was complete). The linearity of these plots signifies that the reactivation processes fit well to first-order kinetics. The rate constants reported in Table 3.1 are obtained from the gradients of these plots. These data demonstrate that the kinetics of reactivation of the two reversible species are also a function of pH. It is evident that the "high-potential" species, like *Dd*H, reactivates more rapidly at pH 6 than at pH 8 and that the opposite is true (albeit to a much lesser extent) for the "low-potential" species.

The proportion of the three species is also affected by the concentration of H_2 as shown in Figure 3.17. The experimental protocol was identical to that of the experiments shown in Figure 3.16 (A and B), but the pH was set to 6 and three different concentrations of H_2 were tested: 100% H_2 (shown in Figure 3.16B), 50% and 10% H_2 (shown in Figure 3.17A and B respectively).

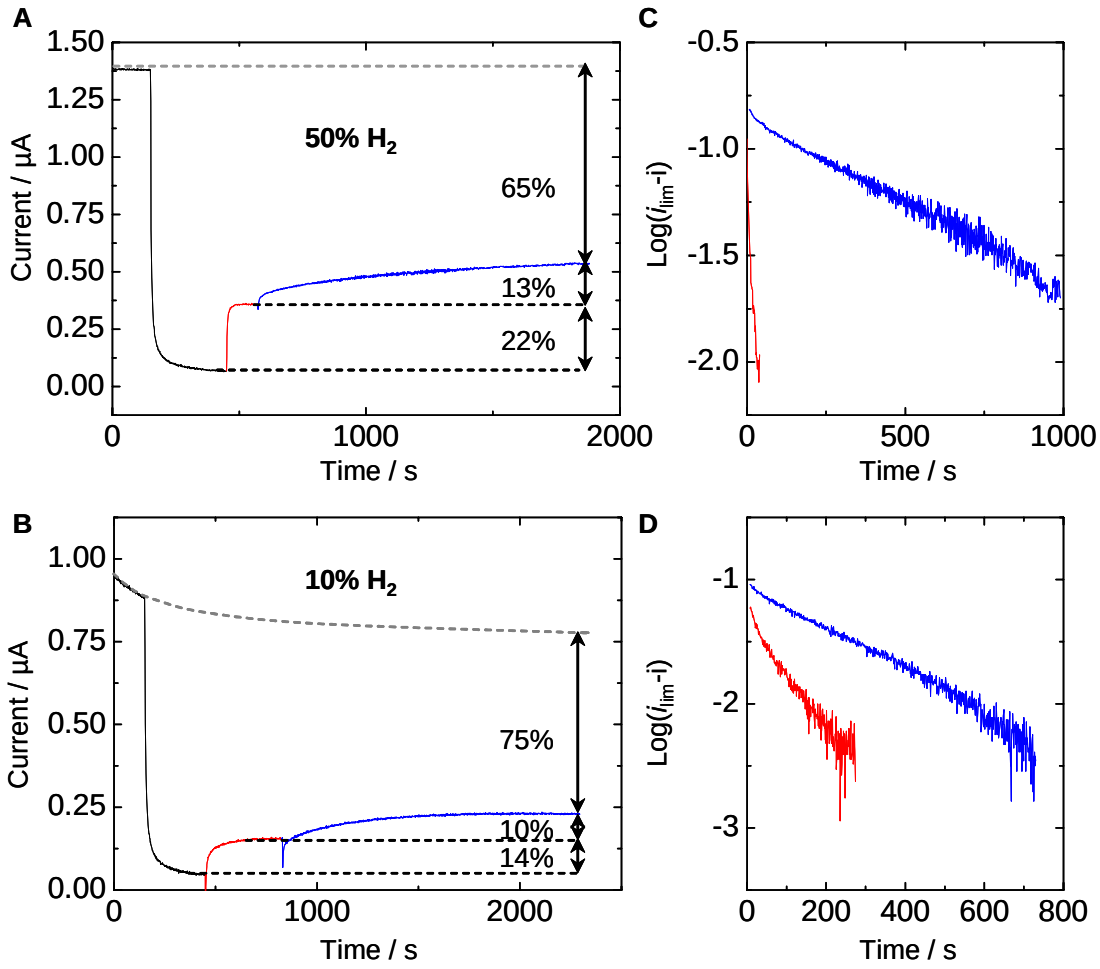

Figure 3.17: Chronoamperometric study of the effect of the concentration of H_2 on the two species formed upon anaerobic inactivation. Experimental conditions: pH 6, 20 °C, rotation rate 3000 rpm, 50% H_2, 50% N_2 in A and 10% H_2, 90% N_2 in B and the potential step sequence is -0.05 V, +0.29 V, +0.1 V, -0.05 V. The reactivation step occurring at +0.1 V is shown in red and that occurring at -0.05 V is shown in blue in panels A and B, as are the corresponding log transforms in panels C and D. The dashed grey lines give a visual guide to the progression of film loss and the percentages quoted for the proportion of the three species formed are approximates based on this guide.

High [H_2] thus favours the formation of both the reversibly bound species (as expected from the data shown in Figure 3.15). Lowering the concentration of H_2 diminishes the proportion of "low-potential" species first (the proportion drops from 27% to 13% as [H_2] is lowered from 100% to 50%) and then reduces the proportion of the "high-potential" species (which remains approximately the same when [H_2] is lowered from 100 to 50 % but drops to 14% when the [H_2] is lowered to 10%). The value of E_{switch} at 100%, 50% and 10% is calculated as +0.11, +0.10, and +0.08 V, respectively, according

to the shift in the thermodynamic potential. Again, the effect this has on the rates obtained for reactivation at +0.1 V and -0.05 V (shown in Table 3.1) as well as the proportion of the species generated by anaerobic inactivation is discussed in section 3.4.3 of the Discussion.

3.3.8. Kinetics of anaerobic inactivation

The experiments shown in sections 3.3.6 and 3.3.7 above were analysed to calculate the pH- and [H_2]-dependence of the rate anaerobic inactivation of *Cr*HydA1 at +0.3 V. A similar method for the determination of the rate constant to that shown in Figure 3.16 (C and D) and Figure 3.17 (C and D) i.e. a log transformation (Log(i-i_{lim}), where i_{lim} is the minimal current reached on inactivation) was applied to the data. As the fits were curved, this analysis could not be used to examine the conditions affecting anaerobic inactivation. Examples of this behaviour at three different pH values are shown in Figure 3.18. As log transforms such as these linearise first order processes, the non-linearity of the log transforms shown in Figure 3.18 is in keeping with the fact that multiple products result from anaerobic inactivation, therefore there must be multiple different processes occurring.

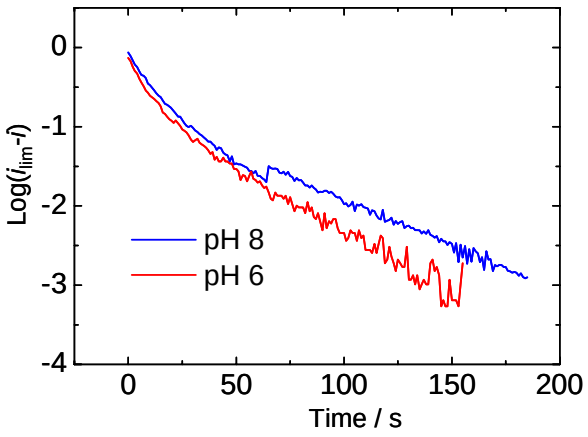

Figure 3.18: Log-transform plots for inactivation of *Cr*HydA1 at +0.3 V at pH 6 and pH 8. The experiments are shown in Figure 3.13A.

In contrast, let us consider the rates of inactivation at pH 6 and pH 8 when E_{inact} was set to the same overpotential with respect to the thermodynamic potential (E_{inact}(pH 6) = +0.29 V, E_{inact}(pH 8) = +0.17 V, Figure 3.14). By considering the degree of overlap of the current-time traces at these two pH values as the enzymes are being inactivated, a qualitative evaluation of the rates of inactivation can be made. These experiments clearly show that inactivation is more rapid at pH 6 than at pH 8 and that, within the 300 s period allowed for inactivation, more activity is lost at pH 6 than at pH 8. This coincides with the fact that the maximum reached on the oxidative scan in Figure 3.7C (marked by the grey circle) is at a higher potential at pH 8 than at pH 6, i.e. a greater driving force is required to drive inactivation at higher pH. In the context of the H_{ox}^{inact} species (the "high-potential" species, see Discussion below), Parkin et al. attributed the relative slowness of inactivation at higher pH as a consequence of the need for both an electron and a proton transfer at pH values between pK_{ox} and pK_{red} (like at pH 8) rather than just an electron transfer at pH values outside of this range (as at pH 6).

3.4. Discussion

In summary, this chapter has explored some basic electrochemical characteristics of [FeFe]-hydrogenases using *Cr*HydA1, *Cs*HydA and *Ca*HydA as examples. Chapter 4 will compare some of these characteristics to those exhibited by [NiFe(Se)]-hydrogenases so as to determine the qualities of a hydrogenase that dispose it towards H_2 production.

3.4.1. Potential profile for activity

Though *Cr*HydA1 and *Cs*HydA have no [FeS]-cluster relay, they still catalyse H_2 oxidation and production on the electrode. This implies that the [FeS]-cluster relay chain is not essential for electrocatalysis. However, these two enzymes do differ from all previously electrochemically-characterised hydrogenases[87,88] in that an overpotential is required for the onset of catalysis. This may reflect an energetic barrier to electron transfer from the electrode to the enzyme or a potential barrier presented by the lone [4Fe4S]-cluster. However, for this latter proposition to be worthy of consideration, the redox potential of the [4Fe4S]-cluster would have to fall exactly on the thermodynamic potential because the overpotential is observed both in the direction of H_2 oxidation and H_2 production.

The bacterial *Ca*HydA enzyme is more strongly biased toward H_2 production than H_2 oxidation compared with *Cr*HydA1 and *Cs*HydA which in turn are more biased towards H_2 production than *Dd*H. In fact, though the physiological function of *Cr*HydA1 and *Cs*HydA is H_2 production, these enzymes are as biased towards H_2 production as H_2 oxidation at pH 6 and their bias for H_2 oxidation becomes more pronounced at higher pH. On the other hand, *Ca*HydA is biased towards H_2 production throughout the pH range.

3.4.2. Affinity for H_2 and relation with the catalytic bias

The values calculated for the K_M of *Ca*HydA and *Cr*HydA1 are very much higher than those calculated for [NiFe]-hydrogenases that oxidise H_2 *in vivo* – for example *Df*H has a K_M of 0.5 μM (at pH 6, 40 °C),[216] and *Rm*MBH which only experiences trace H_2 in its

environment, has K_M of 0.2 μM (at pH 5.5, 30 °C).[222] The values calculated for *Ca*HydA and *Cr*HydA1 coincide well with those reported[214] for other [FeFe]-hydrogenases. These were found to be 286-669 μM for *Cp*I, and 100 μM, 170-269 μM, and 152 μM for the [FeFe]-hydrogenases from *Thermotoga maritima*, *Megasphaera elsedenii* and *Trichomonas vaginalis*, respectively.

The K_M for *Ca*HydA is larger than that for *Cr*HydA1. This is commensurate with the fact that the catalytic bias for the latter lies more towards H_2 oxidation than it does for the former. Unfortunately, the K_M for *Dd*H could not be calculated using PFE because the degree of film loss throughout the experiment is so high that the data is highly convoluted. It would be interesting to be able to confirm the trend of low K_M values correlating to an increased bias towards H_2 oxidation by obtaining a K_M value for this enzyme since the same trend holds (generally speaking, see Chapter 4) for the [NiFe(Se)]-hydrogenases.

Generally, the relative $K_I^{app}(H_2/H^+)$ values also correlate to the K_M values and the catalytic bias, as previously suggested;[214] thus, a good H_2-oxidiser binds H_2 tightly (exhibiting a low K_M) and is poor at H_2 production since the enzyme is highly product inhibited (low $K_I^{app}(H_2/H^+)$). The paradigm of the relationship between affinity for H_2 and catalytic bias is the difference in the behaviour of *Cp*I and *Cp*II. Whilst the former produces H_2 *in vivo*, has a K_M of 310 μM and is not significantly inhibited by H_2, the latter exhibits much lower H_2 production activity, has a K_M of 32 μM and is more highly inhibited by H_2 when evolving H_2.[215]

As with the K_M values, the $K_I^{app}(H_2/H^+)$ values obtained for these enzymes were much higher than the comparative published values for *Df*H (approximately 160 μM)[216] and *Rm*MBH (10 μM).[209] As with the calculation of K_M, the $K_I^{app}(H_2/H^+)$ could not be determined for *Dd*H using PFE, though Figure 3.6 suggests that *Dd*H is slightly more inhibited by H_2 that *Cr*HydA1, which is in turn more noticeably inhibited by H_2 than *Ca*HydA and this is reflected in the relative $K_I^{app}(H_2/H^+)$ values for these two enzymes. When considering both the catalytic bias and inhibition by H_2, *Ca*HydA is the better H_2 producer. Both characteristics are important in exploiting hydrogenases for H_2 production.

3.4.3. Anaerobic inactivation

Anaerobic inactivation of *Ca*HydA is so slow as to have made attempts at investigating its dependence on pH and [H_2] impossible. High-potential inactivation of *Cs*HydA and *Cr*HydA1 is a complex process, involving the generation of three species: an irreversibly-inactivated species, and two reversibly inactivated species (the "low-potential" and "high-potential" species).

The dependence of E_{switch} of *Cr*HydA1 and *Cs*HydA (determined at particular scan rates) on pH mimics that of *Dd*H.[204] The species formed on high-potential inactivation of *Dd*H was reported to be the H_{ox}^{inact} state – i.e. Fe(II)Fe(II) with a possible bound OH^- ligand[145] - and a 1 e^- reactivation mechanism was determined from PFE experiments.[204] However, only at certain scan rates were *n* values of 1 obtained throughout the pH range for *Cr*HydA1 and *Cs*HydA, implying that a mechanism of reactivation (and thus the species formed on anaerobic inactivation) similar to that of *Dd*H can only be observed

when the potential is swept at particular rates. Scanning more slowly than 30 mV/s for *Cr*HydA1 (as was attempted in early experiments to determine the value of *n*) allowed enough time for more than one species to reactivate in the time period of the reductive scan, therefore complicating the calculation of the value of *n* and yielding *n* values that drifted further from 1 as the pH was raised above pH 6. As the species having an *n* value of 1 probably being interrogated at lower pH is the "high potential" species (which is favoured under these conditions – see below), the observation that *n* drifts from 1 as the pH is raised is consistent with a greater proportion of the "low-potential" species being formed at higher pH values. Additionally, the recovery of activity in the reverse (reductive) sweep after a very slow oxidative forward sweep was incomplete, indicating the generation of a third, irreversibly-inactivated species. This was corroborated in numerous chronoamperometry experiments.

Reactivation of *Dd*H at +0.041 V from anaerobic inactivation at +0.341 V is complete within 25 s (at pH 7, 10 °C).[204] Reactivation of *Cr*HydA1 at +0.1 V (the "high-potential") proceeded with a half-life of 7 s at pH 6, and 69 s at pH 8, thus falling in the range reported for *Dd*H. Therefore, the kinetic and thermodynamic behaviour of the "high-potential" species reflects that expected from the results on *Dd*H, suggesting that this species is H_{ox}^{inact}.

For the experiments performed at 30 mV/s for *Cr*HydA1 and 10 mV/s for *Cs*HydA examining the *Dd*H-like (H_{ox}^{inact}) species, reactivation was favoured by lower pH values as evidenced by the fact that E_{switch} becomes increasingly positive as the pH is lowered from pH 9 to pH 6; below pH 6, E_{switch} is no longer dependent on pH. This points to a

mechanism involving only an electron transfer below pH 6 and both a proton and an electron transfer above pH 6.

In terms of the kinetics, Figure 3.16 demonstrated that, unlike the "low-potential" species which was shown to reactivate faster at pH 8 than at pH 6 (see Table 3.1), the "high-potential" species reactivated more slowly at pH 8 than it did at pH 6 and was formed in greater proportion at pH 6 than at pH 8 in these fundamental experiments. The potential used to probe the "high-potential" species was in the range of E_{switch} at pH 6 (around +0.1 V) but more positive than E_{switch} at pH 8 (between 0 and +0.02 V), therefore at pH 8, these experiments may be convoluted by the electrochemical driving force being insufficient to reactivate all the enzyme molecules in the "high-potential" form. The fact that the "low-potential" species appears to be present in higher proportions at pH 8 than the "high-potential" species (H_{ox}^{inact}) from the data presented in Figure 3.16 is also still under investigation since these preliminary experiments could be complicated by the fact that, at -0.05 V, two reactivation processes are occurring. As +0.1 V (the first reactivation step) is a less reducing potential than E_{switch} at pH 8, this driving force was not sufficient to reactivate all the H_{ox}^{inact} (i.e. the "high-potential") species; consequently, stepping down to -0.05 V induced reactivation of this species as well as the "low-potential" species, thus enhancing the proportion of species reactivating at -0.05 V. A similar convolution affects the evaluation for the proportion of the two species at different concentrations of H_2. However, on the whole, it can be stated that lower pH and higher concentrations of H_2 favour the formation of both the reversible species.

The "low-potential" species, reactivates more slowly at -0.05 V than at +0.1 V at pH 6. The rate of reactivation does not vary greatly with pH (0.0017 s^{-1} at pH 6 and 0.0020 s^{-1} at pH 8) nor [H_2] (0.0038 s^{-1}, 0.0019 s^{-1}, and 0.0017 s^{-1} under 10%, 50% and 100% H_2, respectively). The fact that both these trends are opposite to those observed for the H_{ox}^{inact} species is noteworthy and further characterizes this species from the H_{ox}^{inact} species.

The increase in rate of reactivation of the "high-potential" species of *Cr*HydA1 on increasing the H_2 concentration is commensurate with the infrared spectroscopy results[139] - from experiments performed on *Dd*H in the H_{ox}^{inact} state - suggesting that reactivation requires three electrons. Whilst the data presented in section 3.3.5 indicates that reactivation from anaerobic inactivation is a 1 electron process, H_2 is a 2 electron reductant.[204] Therefore, the fact that binding of H_2, favoured by higher concentrations of H_2, helps to drive reactivation suggests that the state of *Cr*HydA1 being examined here is also H_{ox}^{inact}. This dependence can be explained in the context of the putative inhibitory ligand such as H_2O[149] or -OH[145] is bound to Fe_D in the H_{ox}^{inact} state. Upon application of a potential at which the enzyme reactivates, binding of H_2 thus helps to displace this ligand and allows catalysis to proceed. As CO and H_2 are thought to bind at the same place (Fe_D), further evidence for the hypothesis that an inhibitory ligand is present in the H_{ox}^{inact} state was provided by the electrochemical study of *Dd*H[204] showing that this state was protected from CO binding.

As the conditions of inactivation have such dramatic effects on the nature and proportions of the three species formed, it is no surprise that the E_{switch} values shown in the cyclic voltammograms in Figure 3.7 differ from those which were calculated by

fully inactivating the enzyme film and applying conditions that probably only reactivated the high-potential (H_{ox}^{inact}) species (section 3.3.5). Thus, whilst the two reversible species may have been reactivating at the same time in the experiments shown in Figure 3.7, those shown in Figure 3.8 specifically target reactivation of the H_{ox}^{inact} species.

The structures of the "low-potential" and irreversible species are as yet unknown. High-potential degradation of [4Fe4S]-clusters to [3Fe4S]-clusters has been demonstrated in PFE studies,[223,224] so it may be that this kind of damage is occurring here, though which species is thereby generated remains a speculative matter. Whether the possibility that the H-cluster [4Fe4S]-cubane is degraded by anaerobic inactivation is related to the fact that these enzymes do not contain an extended electron-relay chain and are the only hydrogenases for which anaerobic inactivation is (partially) irreversible is a subject that should be of great interest to spectroscopists. Whilst it is unlikely that the enzyme should experience potentials positive enough for the process of *an*aerobic inactivation to be physiologically relevant, the possibility of high-potential damage to the [4Fe4S]-cluster is of interest in the context of *aer*obic inactivation, as will be discussed in Chapters 6 and 7.

Chapter 4:

What Characterises A Good H_2 Producer?

4.1. Abstract

This chapter presents studies carried out to establish the ability of O_2-tolerant [NiFe]-hydrogenases from *Ralstonia* sp. to catalyze H_2 production in addition to H_2 oxidation. These hydrogenases are not noted for H_2-evolution activity, and this is partly due to strong product inhibition. However, as with other hydrogenases electrocatalytic H_2 production proceeds with minimal overpotential – a significant observation because lowering this activation barrier is seen as crucial in developing small-molecule catalysts for H_2 production. The inhibition of *Rm*MBH and *Re*MBH and a mutant thereof by H_2 was quantified in terms of the apparent inhibition constant $K_I^{app}(H_2/H^+)$. The mutant, which had a high K_M for H_2 oxidation, did not prove to be a better H_2 producer nor did it have a higher $K_I^{app}(H_2/H^+)$ relative to the wild type, thus suggesting that weak binding of H_2 in H_2 oxidation does not itself confer a tendency to favour H_2 production within enzymes of a given species. However, a high K_M does correlate with a high $K_I^{app}(H_2/H^+)$ across hydrogenases from different species, which confirms the notion that a factor other than binding of H_2 as an inhibitor is responsible for the *Ralstonia* enzymes being poor H_2 producers. Finally, electrochemical signals representing the chain of the three [4Fe4S]-clusters (also thought to be present in the [FeFe]-hydrogenases that produce H_2 *in vivo*) in the [NiFeSe]-hydrogenase *Db*H are recorded and used to add weight to the EPR and X-ray crystallography characterization of these clusters.

4.2. Introduction

This chapter aims to investigate a number of features that are relevant to the context of H_2 production for a broad spectrum of hydrogenases: ranging from those isolated from

Knallgas bacteria that oxidise H_2 *in vivo*, to the [FeFe]-hydrogenases, utilised by nature to absorb high potential electrons and in so doing, perform the reverse reaction, H_2 production. The [NiFeSe]-hydrogenase *Db*H is also examined as its H_2/HD exchange activity has been shown to occupy a middle-ground between that of the [NiFe]-hydrogenases and the [FeFe]-hydrogenases.[225] This notion was confirmed through a variety of spectroscopic and biological assay techniques.[89] It should also be noted that the *Db*H shares a significant portion of its sequence with the [NiFeSe]-hydrogenase from *Desulfovibrio vulgaris* Hildenborough (67% for the large sub-unit and 60% for the small sub-unit), which was also found to have an unusually high H_2 production activity.[89] Two characteristics of hydrogenases are considered in this chapter. The *functional* capacity for H_2 production is defined by the catalytic bias for this process and the ability to bind H_2. Additionally, a potentially crucial *structural* element, the [FeS]-cluster content, is considered.

4.2.1. Quantifying H_2 production

It has long been known that [NiFe]-hydrogenases have lower K_M values for H_2 than the [FeFe]-hydrogenases.[69] In H_2 production, product inhibition is a substantial limitation to technological applications, especially for the [NiFe(Se)]-hydrogenases which are shown to be more easily inhibited by H_2 than [FeFe]-hydrogenases herein. Whilst [NiFe(Se)]-hydrogenases benefit from the ability to recover from oxidative damage (see Chapter 6), utilising them in any such technology involves overcoming this important hurdle.

Quantifying inhibition of H_2 production allows us to draw comparisons between enzymes and to catalogue their suitability for use in technological devices. There are

various techniques for determining the apparent inhibition constant ($K_I^{app}(H_2/H^+)$), one of which was described in Chapter 3. Another electrochemical technique was reported by Léger et al.[216] and is used to determine the $K_I^{app}(H_2/H^+)$ values of *Db*H, *Dg*H, *Rm*MBH, *Re*MBH and its C81A mutant.[209] In this instance, this technique was deemed more appropriate for these [NiFe(Se)]-hydrogenases as it is better-suited to enzymes with low $K_I^{app}(H_2/H^+)$ values whilst that described in Chapter 3 suits those with high $K_I^{app}(H_2/H^+)$ values. To observe changes in the level of inhibition an enzyme that exhibits a high $K_I^{app}(H_2/H^+)$ large changes in inhibitor concentration must be made; this is easily carried out by changing the composition of the headgas (as shown in Figure 3.5). On the other hand, an enzyme with a low value of $K_I^{app}(H_2/H^+)$ will be fully inhibited by even small concentrations of inhibitor, therefore subtle changes in inhibitor concentration are required to determine the extent to which each inhibits the enzyme. These low concentrations are more precisely delivered by injection of [H_2]-saturated buffer in the Léger-type experiments described below than by flushing the headspace of the cell with an atmosphere containing H_2 as detailed in Chapter 3 because the error margins in gas composition are higher when delivering the inhibitor by flushing with mass-flow controllers.

The technique pioneered by Léger[216] involves injecting known quantities of buffer solutions saturated with a gaseous inhibitor (such as CO or H_2) and recording the recovery of enzymatic current as the inhibitor is flushed out of solution in the continuous flow of an inert gas in the headspace of the cell by rotation of the electrode. Control experiments showed that the concentration of gases dissolved in solution varies exponentially with time as the gas is removed from the cell after injection (according to

Equation 4.1, in which C_t is the concentration of inhibitor as it varies with time, C_0 is its concentration just after injection, t is time and τ is a time constant related to the rate of diffusion of the gas from solution).[216]

$$C_t = C_o e^{(-t/\tau)} \qquad \text{Equation 4.1}$$

One such control experiment is shown in Figure 4.1A. Here, O_2-saturated buffer is injected into the cell when it is poised at a potential at which graphite reduces O_2. The current corresponding to O_2 reduction by the bare graphite electrode increases instantaneously and then, as the O_2 is flushed from solution, the current decreases to zero. The linearity of the log plot shown in Figure 4.1B confirms that this is indeed an exponential decay.

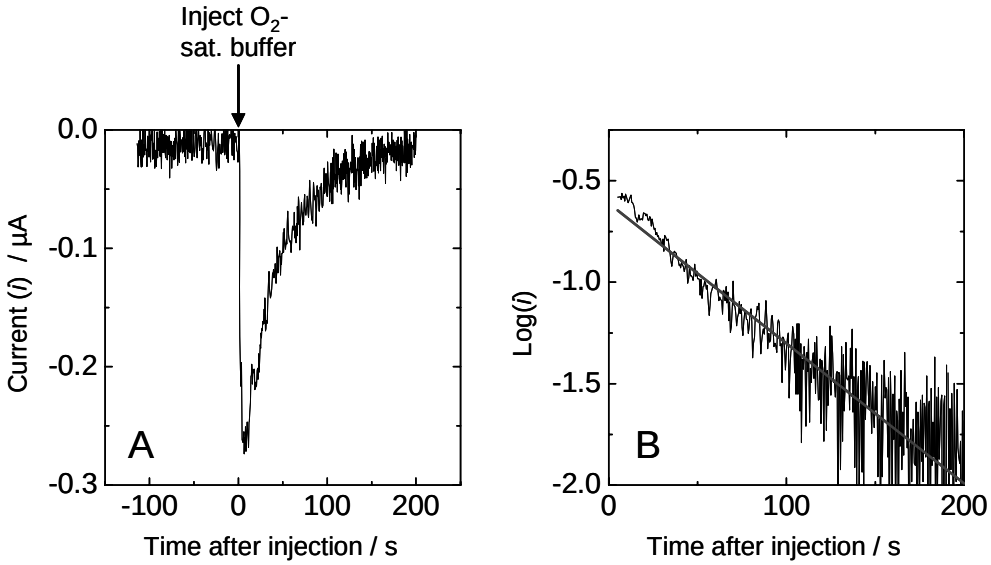

Figure 4.1: Control experiments performed to determine the dependence of concentration of O_2 (representative of the concentration of H_2 in the experiments in this chapter) in solution on time after injection. A) Chronoamperometric experiment at -0.25 V under a 100% Ar atmosphere. The injection of O_2-saturated buffer at $t = 0$ s initially brought the O_2 concentration in the cell to 231 µM before it was flushed out of the cell. Other conditions: 23 °C, pH 6.3, electrode rotation rate 3000 rpm. B) Log-transform plot of the experiment shown in A.

4.2.2. Non-turnover voltammetry

Lastly, this chapter will present preliminary data which highlights the possible importance of the nature of the [FeS]-electron relay chain in determining the bias of a

hydrogenase towards H_2 production. Electrochemical signals corresponding to the [FeS]-cluster electron relay chain are not observed under catalytic conditions as the catalytic current completely overwhelms these small signals. However, under conditions at which catalysis is suppressed, these signals may be elucidated. They can be used to identify both how many different kinds of [FeS]-clusters are present, and also the total coverage of the enzyme on the electrode, which can in turn be used to calculate the catalytic turnover frequency. As these signals are by their nature hard to observe, these experiments require a high coverage of enzyme on the electrode therefore they can only be performed on certain hydrogenases as different hydrogenases adsorb to PGE to different extents.

4.3. Results

4.3.1. Cyclic voltammetry profile of H_2 production and oxidation by hydrogenases

Cyclic voltammetry under H_2 and N_2 distinguishes [NiFe]-hydrogenases from [FeFe]-hydrogenase and the [NiFeSe]-hydrogenase. Figure 4.2 shows the catalytic profile of *Re*MBH, *Rm*MBH, *Dg*H, *Db*H and *Ca*HydA recorded under H_2 and N_2. Importantly, for each enzyme, the scans under H_2 and N_2 were recorded on the same film (i.e. the enzyme film was not "regrown" between the two scans) within 10 minutes of each other; this eliminates artefacts relating to the total coverage of enzyme on the electrode (which changes with time and from film to film) having a significant bearing on the magnitude of the current recorded. This allows for a qualitative appraisal of these five hydrogenases as H_2 producers.

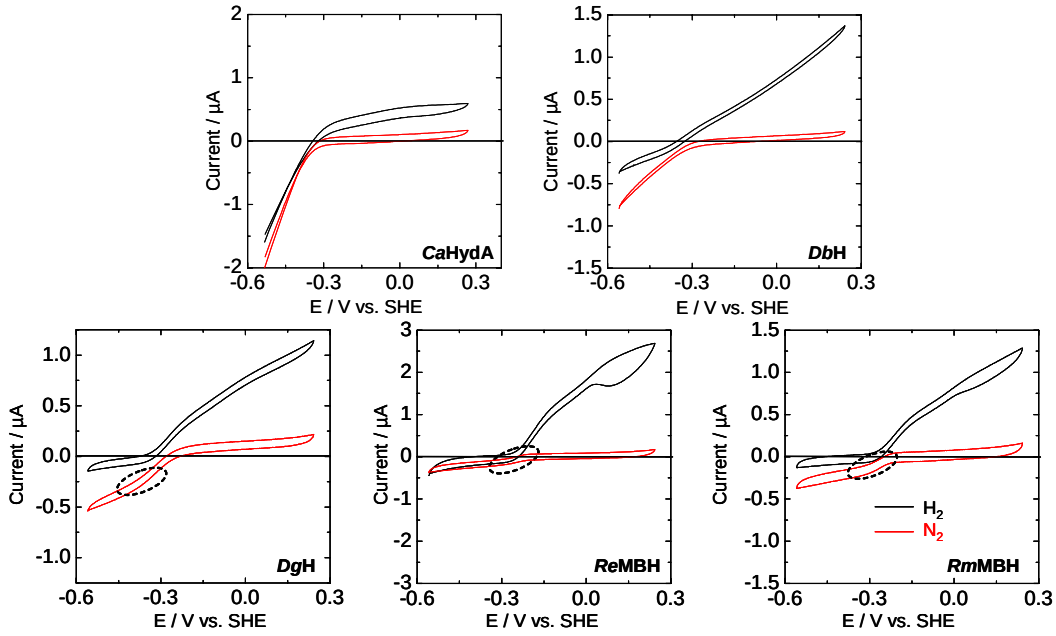

Figure 4.2: Comparison of catalytic bias for *Db*H, *Ca*HydA *Re*MBH, *Rm*MBH, and *Dg*H, under 100% H_2 (black line) and 100% N_2 (red line). Other conditions: pH 5.5, 30 °C, scan rate 20 mV/s, electrode rotation rate 3000 rpm. The zero-current line is set to the middle of the plot in each case so as to make the interpretation of the catalytic bias visually intuitive.

It is clearly demonstrated that, as expected, the [FeFe]-hydrogenase *Ca*HydA is the most biased towards H_2 production as the proportion of negative current representing H_2 production to positive current corresponding H_2 oxidation is the highest, with the [NiFeSe]-hydrogenase *Db*H coming a close second in terms of bias towards H_2 production. This is in agreement with previous results comparing the activity of [FeFe]- and [NiFeSe]-hydrogenases.[225] The proportion of H_2 oxidation to production current is the highest for the hydrogenases from *Ralstonia* species.

As the potential is swept into the potential domain in which hydrogenases catalyse H_2 production in the cyclic voltammograms of *Dg*H, *Re*MBH, and *Rm*MBH under H_2, no negative current is recorded indicating that these enzymes do not exhibit H_2 production activity in the presence of H_2. Furthermore, as the potential is swept to more negative values in the experiments performed on these last three enzymes, there is a clear

inflection point at -0.4 V. This feature is absent in the voltammograms of *Db*H and *Ca*HydA. This implies that there is a potential-dependent limitation to H_2 production by these [NiFe]-hydrogenases which does not apply to the two enzyme more biased towards H_2 production (*Db*H and *Ca*HydA). However, the potential of the onset of H_2 production is the most positive for the *Ralstonia* enzymes, implying that this onset is not limited by an electrochemical step.

4.3.2. Calculation of $K_I^{app}(H^+/H_2)$ for inhibition of H_2 production by H_2

In the experiments performed to determine the values of the inhibition constant, the current transients obtained after injection of the inhibitor vary exponentially with time as there is a linear relationship between the level of inhibition of the enzyme and the concentration of inhibitor in solution so long as a low enough concentration is injected.[§§] The transient can then be modelled using an adaptation of Michaelis-Menten kinetics for inhibition (Equation 4.2, in which v_0 is the rate, v_{max} is the maximal rate, [S] is the concentration of substrate – H^+ in this case, calculated from the pH – and [I] is the concentration of inhibitor (H_2)) using current (i) as a measure of rate (Equation 4.3[216]).

$$v_0 = \frac{v_{max}}{[S] + K_M(1 + [I]/K_I)} \qquad \text{Equation 4.2}$$

$$i_t = \frac{i_0}{1 + \frac{C_0 e^{(-t/\tau)}}{K_I^{app}(H_2/H^+)}} \qquad \text{Equation 4.3}$$

Here, i_t is the current as it varies with time after the injection, i_0 and C_0 are the current and the concentration of inhibitor just after the injection, respectively, and $K_I^{app}(H_2/H^+)$

[§§] Larger quantities of inhibitor able to saturate the active site cause a sigmoidal recovery of H_2-production current rather than an exponential one. The model described by Léger is designed to fit an exponential. An exponential recovery from inhibition results from a lesser degree of inhibition therefore low concentrations of H_2 were injected in the experiments described in this chapter.

is the apparent inhibition constant defined in Equation 3.1. Equation 4.3 can be linearised so as to extract the value of $K_I^{app}(H_2/H^+)$ by applying a log transform, as shown in Equation 4.4.

$$\mathrm{Log}((i_0/i_t)-1) = \mathrm{Log}(C_0/K_I^{app}(H_2/H^+)) - t/\tau \qquad \text{Equation 4.4}$$

This technique was used to determine the $K_I^{app}(H_2/H^+)$ for *Db*H, *Dg*H, *Rm*MBH, *Re*MBH and a variant of *Re*MBH. Figure 4.3A shows a chronoamperometric experiment carried out on *Rm*MBH. The electrode was poised at -0.45 V under a headspace of Ar such that a current due to H_2 production was recorded. Four sequential injections of different volumes of buffer saturated with 5% H_2, 95% N_2[***] were performed such that the current transients recorded after the injection could be analysed as described above. The log transforms of these transients are shown in Figure 4.3B. The anti-log of the *y*-intercept of these log transforms can be used to determine the $K_I^{app}(H_2/H^+)$ (Equation 4.5). These values can also be plotted against the concentration of H_2 and the fit to a straight line reflects the scatter of the data. Figure 4.3C thus demonstrates that there is little scatter in the results.

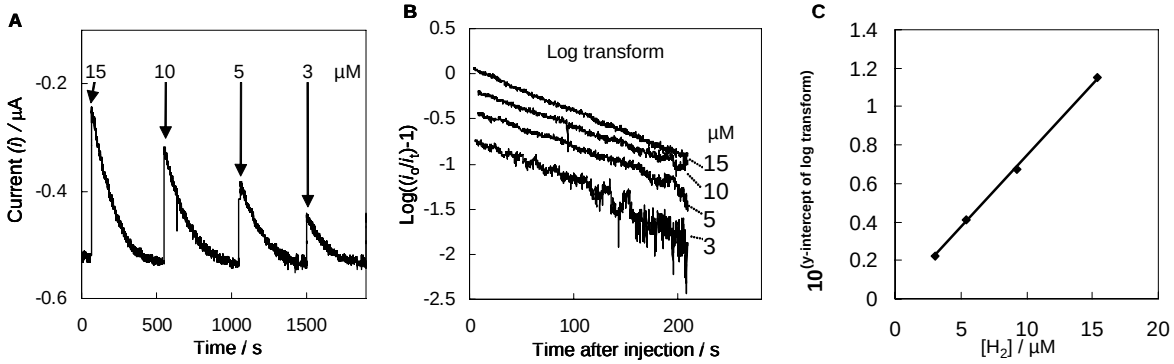

Figure 4.3: Calculation of $K_I^{app}(H_2/H^+)$ for *Rm*MBH. A) Chronoamperometric experiment involving four sequential injections of H_2-saturated buffer such that the concentration of H_2 in the cell just after the injection as indicated on the figure. B) Log transforms of the individual transients recorded in (A). The anti-logs of the *y*-intercept of the log transforms in panel B are plotted against [H_2] and

[***] The pH 5.5 buffer solutions to be injected were saturated with 5% H_2 rather than 100% H_2 as higher concentrations of H_2 caused complete inhibition such that the recovery of activity with time was sigmoidal rather than exponential so this measure ensured that the transients could be analysed using the reported method.[216]

fitted to a straight line. Other conditions: pH 5.5, 30 °C, 100% Ar atmosphere, -0.45 V, electrode rotation rate 3000 rpm.

The $K_I^{app}(H_2/H^+)$ values determined for a number of enzymes are shown in Table 4.1 (including the values for the [FeFe]-hydrogenases determined in section 3.3.3). The trend in $K_I^{app}(H_2/H^+)$ values confirm that the [NiFe]-hydrogenases are more easily inhibited by H_2 than the [FeFe]-hydrogenases. Moreover, the *Ralstonia* hydrogenases have the lowest $K_I^{app}(H_2/H^+)$ values, demonstrating that these enzymes suffer the most from inhibition by H_2 within the [NiFe]-hydrogenases. Among the [NiFe(Se)]-hydrogenases, the [NiFeSe]-hydrogenase *Db*H has one of the two highest $K_I^{app}(H_2/H^+)$ values.

Enzyme	Type of hydrogenase	Physiological function	$K_I^{app}(H_2/H^+)$ / μM	K_M
*Re*MBH	[NiFe]	H_2 oxidation	7.1	6.1[a]
*Rm*MBH	[NiFe]	H_2 oxidation	10.8	0.57[a]
C81A *Re*MBH	[NiFe]	H_2 oxidation	15	~300
*Dg*H	[NiFe]	H_2 oxidation	80	-
*Df*H	[NiFe]	H_2 oxidation	170[b]	~5[c]
*Db*H	[NiFeSe]	H_2 oxidation	150	280
*Cr*HydA1	[FeFe]	H_2 production	3700	190
*Ca*HydA	[FeFe]	H_2 production	6000	460

Table 4.1: Values for $K_I^{app}(H_2/H^+)$ and K_M for H_2 in H_2 oxidation of eight hydrogenases from experiments described in Chapters 3 and 4 and from the literature: a – Ludwig et al.[222] (30 °C, pH 5.5, -0.1 V). b – Léger et al. (40 °C, pH 6.1, -0.16 V).[216] c – Léger et al. (40 °C, pH 6, -0.66 V).[216]

4.3.3. Potential dependence of $K_I^{app}(H^+/H_2)$ for *Rm*MBH

As mentioned section 4.3.1, the current due to H_2 production by the [NiFe]-hydrogenases *Dg*H, *Rm*MBH and *Re*MBH is curtailed below a certain potential (about -0.4 V). To explore whether tighter binding of the produced H_2 below this potential was the source of this feature, potential-step experiments analogous to those described above

were performed over a range of potentials that targeted this change in catalytic ability to produce H_2, i.e. between -0.28 V and -0.45 V. The potential was thus stepped between these values and an injection of 5% H_2-saturated buffer was performed at each potential (Figure 4.4A). The analysis described above was then used to determine the $K_I^{app}(H_2/H^+)$ at each potential. These are plotted against potential in Figure 4.4B.

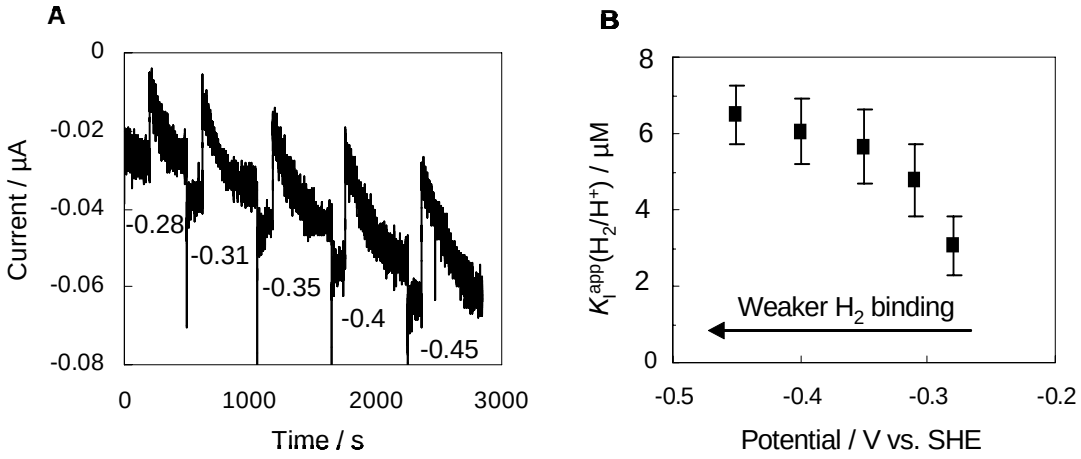

Figure 4.4: Potential dependence of K_I^{app} (H_2/H^+) for *Rm*MBH. A) Chronoamperometric trace in which the potential was stepped from -0.28 V down to -0.45 V as indicated on the figure. B) The $K_I^{app}(H_2/H^+)$ values are plotted against the potential at which they were determined. Error bars are estimated from the experimental error in injection and the signal-to-noise ratio. Other conditions: pH 5.5, 30 °C, 100% Ar atmosphere, electrode rotation rate 3000 rpm.

The fact that the $K_I^{app}(H_2/H^+)$ values actually increase as the potential is lowered can be seen in Figure 4.4B. This implies that the curtailment of the current in this potential region is in fact not due to inhibition by H_2. This mirrors the potential dependence of $K_I^{app}(CO/H^+)$ for inhibition of proton reduction by *Df*H by CO[216] and thus introduces a running theme throughout this thesis: that lowering the potential disfavours the binding of inhibitory molecules such as H_2, CO and O_2.

4.3.4. Ability of a *Re*MBH mutant having a high K_M for H_2 oxidation to produce H_2

Looking across the spectrum of hydrogenases from the [FeFe]-hydrogenase to the [NiFe(Se)]-hydrogenases, high K_M values for H_2 in H_2 oxidation generally correlate with high $K_I^{app}(H_2/H^+)$ values for inhibition by H_2 in H_2 production for a given enzyme. A mutant of a membrane-bound hydrogenase from *Ralstonia* sp. having a high K_M might thus be a better H_2 producer than the wild type whilst still benefiting from the increased tolerance to O_2 that distinguishes the *Ralstonia* enzymes and therefore make an interesting subject for technological investigation. To that end, the catalytic bias under N_2 and H_2 and the $K_I^{app}(H_2/H^+)$ of the C81A mutant (K_M ~ 300 µM) of *Re*MBH (K_M = 6.1 µM)[222] were examined.

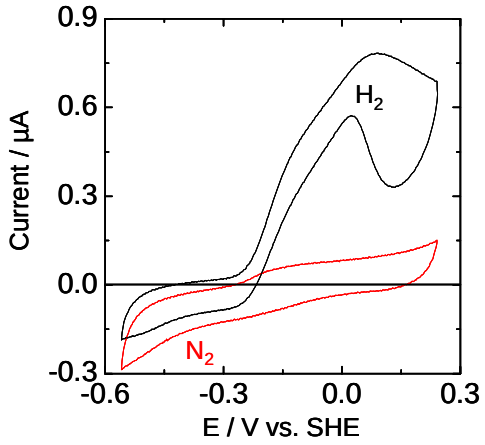

Figure 4.5: Catalytic bias of the C81A mutant of *Re*MBH under 100% H_2 (black) and 100% N_2 (red). Other conditions: pH 5.5, 30 °C, 20 mV/s, electrode rotation rate 3000 rpm.

Figure 4.5 clearly demonstrates that this enzyme does not exhibit enhanced H_2 production in terms of its catalytic bias with respect to the wild type. The $K_I^{app}(H_2/H^+)$ determined for this variant using the method described in section 4.3.2 (15 µM) was also within the range of those calculated for the wild type and for *Rm*MBH thus

indicating that it is inhibited to the same degree as enzymes of the same genus (see Table 4.1 above).

4.3.5. Attempts at calculating the K_M for *Db*H

Experiments were performed to try to determine the K_M of *Db*H to obtain a complete picture of the relationship between physiological function, catalytic bias, K_M for binding H_2 in H_2 oxidation and $K_I^{app}(H_2/H^+)$ for inhibition by H_2 in H_2 production, thus allowing for comparisons to be drawn across a spectrum of hydrogenases. Initially, a technique described by Léger[216] that utilises the same principle of electrochemically adapting Michaelis-Menten kinetics as that used to calculate the $K_I^{app}(H_2/H^+)$ was employed (see Appendix IV). The experiment performed at -0.05 V commenced under an atmosphere of N_2 and a volume of H_2-saturated buffer large enough to bring the concentration of H_2 in solution to >50% was injected into the cell (Figure 4.6).

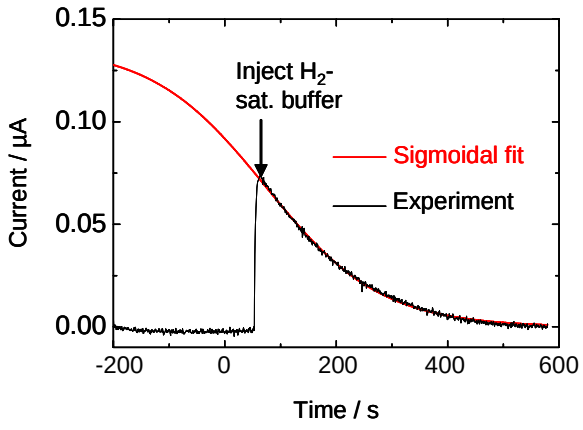

Figure 4.6: Approximate calculation of the K_M for H_2 of *Db*H. The cell was flushed with a 100% N_2 and an injection which brought the concentration of H_2 in solution to 410 µM was performed at $t = 0$ s. Other conditions: pH 5.5, 30 °C, electrode rotation rate 3000 rpm, -0.05 V.

The current increased immediately as the enzyme sensed an increase in substrate but then decreased as the substrate H_2 flushed (exponentially) out of the cell. In

experiments on other [NiFe]-hydrogenase (such as *Df*H[216] and the *Ralstonia* hydrogenases), such a concentration of H_2 in solution was easily sufficient to "saturate" the active site such that the subsequent decreases in current due to the loss of substrate H_2 from the cell was sigmoidal. Whilst these enzymes continue to catalyse H_2 at a rapid rate for a given period after the H_2-saturated buffer is injected into the cell (i.e. above a given level of H_2, the rate of H_2 oxidation of *Df*H and the *Ralstonia* hydrogenases is nearly independent of the concentration of H_2), the exponential loss of current which was observed in the case of *Db*H indicates that the rate of reaction is directly proportional to the concentration of H_2 in solution and thus that *Db*H has a lower affinity to H_2 i.e. *Db*H must have a higher K_M than the aforementioned [NiFe]-hydrogenases. The observation of an exponential decrease in current in a similar experiment performed on *Dd*H[226] allows us to draw further parallels between the [FeFe]- and the [NiFeSe]-hydrogenases. Léger's model for the calculation of K_M (unlike that for the calculation of $K_I^{app}(H_2/H^+)$) fits a sigmoidal decrease in current after injection, thus only the lower part of the sigmoid predicted by this model fits the experiment shown above. Whilst this means that the value calculated for K_M carries large error bars (280 ± 100 μM), it is representative of the range in which this value falls for *Db*H.

The second method used was that described in Chapter 3 (section 3.3.3). Rapid film loss exhibited by this enzyme throughout this experiment (not shown) prevented the application of this method from yielding useful results. Unfortunately, the low quantity of *Db*H available in the laboratory meant that it was not possible to continue these experiments. However, the observation that this enzyme has a lower affinity for H_2 than the other [NiFe]-hydrogenases discussed in this chapter is important and

commensurate with the fact that it is also less inhibited by H_2 when catalysing H_2 production (as evidenced by the fact that it has a higher $K_I^{app}(H_2/H^+)$ than other [NiFe]-hydrogenases).

4.3.6. Non-turnover voltammetry of *Db*H

Experiments under non-catalytic conditions can illuminate redox occurring at sites other than the active site in an enzyme. PFE studies of hydrogenases have helped to elucidate their [FeS]-cluster content (for example, *Av*H[183]). The enzymes chosen for the experiments described herein were *Db*H and *Ca*HydA. Other enzymes studied in this chapter were omitted from this study for a number of reasons, ranging from the quality of the sample available being too low to adsorb a film good enough for these experiments (e.g. *Dg*H) to the lack of an inhibitor to inhibit the enzyme completely (e.g. the *Ralstonia* enzymes). The algal *Cr*HydA1 enzyme only has one [FeS]-cluster. As the current from redox occurring at distinct centres but at the same potentials is additive, it is much easier to elucidate signals arising from a number of [FeS]-clusters undergoing redox at the same potential than from a single [FeS]-cluster. This makes the observation of non-turnover peaks corresponding to *Cr*HydA1's only [FeS]-cluster very unlikely.

Figure 4.7 shows a cyclic voltammogram in which the *Db*H-modified electrode was subjected to conditions which inhibit catalysis: 100% CO was flushed through the headspace of the cell and the temperature was set to 2 °C to stop catalysis and enhance stability of the enzyme on the electrode surface.

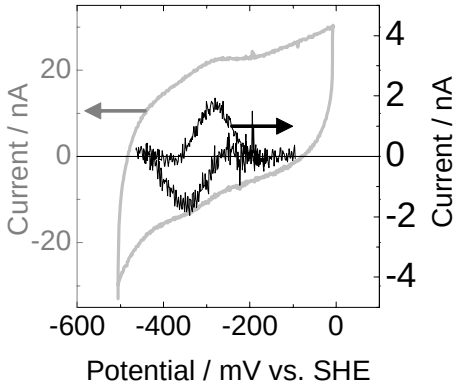

Figure 4.7: Non-turnover digital step cyclic voltammetry of *Db*H. The grey trace shows the raw experiment and the black trace shows the baseline subtracted data revealing the non-turnover peaks. Experimental conditions: pH 6, 2 °C, 100% CO atmosphere, 5 mV/s, electrode rotation rate 3000 rpm.

By subtracting the baseline contribution (modelled as a 6th order polynomial) from the capacitance of the electrode using the in-house program SOAS, only one oxidation and one reduction peak are elucidated (around -300 mV) in the range of -550 to +250 mV.[205] This indicates that only one type of [FeS]-cluster is present, as was observed in the EPR. Moreover, the potentials at which these peaks appear coincide well with those reported by Teixeira et al. for the [4Fe4S]-clusters in *Db*H which was -315 ± 20 mV at pH 7.6.[227]

Attempts at utilising this method on *Ca*HydA did not reveal non-turnover signals. This suggests that the electroactive coverage of the enzyme on the electrode was too low. Enhancing the adsorption of *Ca*HydA by, for example, covalently attaching the enzyme to the electrode[190,191] may help to record these signals in future experiments.

4.4. Discussion

4.4.1. Catalytic bias and favourability of binding of H_2

A number of trends, evident from Table 4.1, are depicted in Figure 4.8. For enzymes from *different species*, the K_M values are generally proportional to those of $K_I^{app}(H_2/H^+)$ [†††]. The [FeFe]-hydrogenases have the largest K_M and $K_I^{app}(H_2/H^+)$ values. A high value of $K_I^{app}(H_2/H^+)$ will obviously be advantageous to an enzyme whose physiological function is H_2 production. It is also intuitive that a low K_M will not be of great benefit to such an enzyme. However, for *Rm*MBH, *Re*MBH and its C81A mutant, which come from Knallgas bacteria, their low K_M allows them to scavenge H_2 so as to be able to oxidise it from an environment in which it is only present in low concentrations. The fact that these enzymes are strongly inhibited by H_2 when electrocatalytically producing H_2 is of little consequence to them in nature. The [NiFeSe]-hydrogenase *Db*H has a very high K_M for a [NiFe(Se)]-hydrogenase. The profile of the cyclic voltammogram of *Db*H under N_2 (Figure 4.2D) points to a similarity with the [FeFe]-hydrogenases (as previously suggested by Fauque et al.[89,225]) as this hydrogenase lacks the curtailment of the current below -0.35 V observed for the [NiFe]-hydrogenases (Figure 4.2 and Figure 4.5, though in this latter case – the C81A mutant of *Re*MBH – the H_2 production current is so low that the effect is very subtle).

[†††] The obvious exception here is *Df*H which has a relatively high $K_I^{app}(H_2/H^+)$ and/or a low K_M. It should be noted that the conditions under which these value were recorded[216] were different to those of the experiments performed on the other [NiFe]-hydrogenases i.e. the temperature was 40 °C (rather than 30 °C), the potential was -0.66 V rather than -0.45 V for the calculation of $K_I^{app}(H_2/H^+)$.

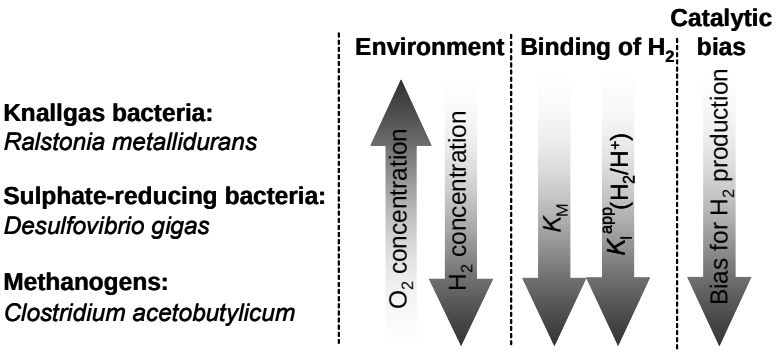

Figure 4.8: Schematic of the relationship between the physiological environments of three representative organisms expressing a hydrogenase, the degree to which these hydrogenases favour binding of H_2 and the catalytic bias.

The results for the C81A mutant of *Re*MBH are a departure from the trend that a high K_M is accompanied by bias towards H_2 production: this mutant is no more efficient at H_2 production than the wild type. This indicates that some inherent characteristic of the *Ralstonia* enzymes limits catalysis in H_2 production. Furthermore, this suggests that in the event of such a limitation, the binding of H_2 as a substrate in H_2 oxidation no longer correlates with the binding of H_2 as an inhibitor. Thus, whilst the mutation appears to have deteriorated the mutant's capacity for H_2 oxidation (in terms of its ability to scavenge H_2 from the native low-H_2 environment of *Ralstonia* sp. as demonstrated by the fact that it has a larger K_M), it has not improved its ability to produce H_2.

4.4.2. Electron transfer

It has been shown that the [NiFeSe]-hydrogenase from *Desulfovibrio vulgaris* Hildenborough actually bears a greater sequence similarity to the [NiFe]-hydrogenases from other *Desulfovibrio* species that only contain [4Fe4S]-clusters than to the [NiFe]-hydrogenases found in *Dv* Hildenborough that also contain a [3Fe4S]-cluster.[89] Whilst the lack of a high potential [3Fe4S]-cluster (common to the [NiFe]-hydrogenases) in *Db*H and the [FeFe]-hydrogenase may be coincidental, it could also suggest the absence

of this [FeS]-cluster is important in favouring H_2 production. In fact, it was reported[228] that the construction of a mutant of *Db*H containing a medial [3Fe4S]-cluster like the [NiFe]-hydrogenases rather than a [4Fe4S]-cluster decreased its activity in H_2 oxidation with respect to the wild type tenfold, though this study did not examine H_2-production activity. Whether the [FeS]-content is a crucial determinant in the overall structure, (which in turn enhances H_2 production) or whether the high turnover rates of H_2 production by the [NiFeSe]-hydrogenase *Dv*H[89] and the lack of the [3Fe4S]-cluster are coincidental remains to be seen.

4.4.3. Proton transfer

Another point worthy of consideration is whether the presence of the Se in *Db*H enhances its ability to produce H_2. The species R-Se-H is known to have a lower pKa (pKa 5.2)[229] than R-S-H (pKa 8)[230] which suggests that a proton bound as R-Se-H would more easily be lost or donated to the active site to be reduced to H_2, thus promoting H_2 production by this enzyme.[82] Similarly the bridging ligand present in the active site of *Dd*H which has been modelled as di(thiomethyl)amine has been hypothesised to be important in the transfer of protons to and from the active site.[66] Thus, a group with a low pKa in the active site may be crucial in encouraging H_2 production.

4.4.4. Concluding remarks

This chapter has aimed to examine some of the characteristics of hydrogenases that might predispose them towards H_2 production. The catalytic bias depicted by cyclic voltammetry under H_2 and N_2 gave an immediate image of the bias towards H_2

production, and from this perspective, the [FeFe]-hydrogenase *Ca*HydA won out over the [NiFe(Se)]-hydrogenases. The values of K_M and $K_I^{app}(H_2/H^+)$ defined the degree of binding of H_2 in H_2 oxidation and production, and binding of H_2 was found to be favoured by the [NiFe]-hydrogenases over the [FeFe]-hydrogenases, with the [NiFeSe]-hydrogenase *Db*H occupying the middle ground. The non-turnover signals observed for *Db*H examined a possible connection between the nature of the [FeS]-clusters and the propensity for H_2 production. In sum, these observations point to the importance of the [FeFe]-active site and the presence only of [4Fe4S]-clusters in enhancing the ability of a hydrogenase to produce H_2.

Chapter 5:

Inhibition of Hydrogenases by CO and Formaldehyde

5.1. Abstract

As CO and O_2 have similar Lennard-Jones radii (3.69 Å and 3.47 Å, respectively[231]), CO may be useful as probe to determine the underlying kinetics of the process of binding of an inhibitor (via its transfer through the protein architecture to the active site of hydrogenases) that does not induce the more permanent and complex modifications to the active site engendered by O_2. Inhibition of a range of [NiFe(Se)]-hydrogenases and [FeFe]-hydrogenases by CO is investigated quantitatively through measurements of inhibition constants. Two methods (previously described in Chapters 3 and 4) for the measurement of $K_I^{app}(CO/H_2)$ are employed. The enzymes are also qualitatively characterized by the comparative effect that H_2 and CO have on their H_2-production activity. For each enzyme, inhibition by CO is compared qualitatively to inhibition by H_2. More detailed studies are performed on the [FeFe]-hydrogenases to probe the nature of the CO-bound state. It is shown that CO inhibits H_2 oxidation more rapidly than H_2 production. It is also demonstrated that the reaction of *Cr*HydA1 and *Ca*HydA with CO at -0.4 V is partially irreversible – the first electrochemical proof that CO does not always act as a competitive inhibitor of hydrogenases. Comparison of the rates at which CO is bound and removed from the enzyme allows for conclusions to be drawn on the nature of the limitations (formation of the Fe-Inhibitor bond vs. transport through the protein) to binding of diatomic molecules. Lastly, preliminary experiments demonstrating the effect that formaldehyde has on *Cr*HydA1 are described; these pave the way for a variety of further spectroscopic and electrochemical investigations.

5.2. Introduction

Competitive inhibition of hydrogenases by CO is a well-documented process.[59,143,209,216,232-235] Whilst CO is not present in nature to a significant degree (0.05

to 0.35 ppm in the atmosphere[236,237]), it may be a poison present in the cell. In fact, a number of "hydrogenogenic" bacteria, for example *Carboxydothermus hydrogenoformans*,[238] couple [NiFe]-hydrogenase-catalysed H_2 production with CO-dehydrogenation, thus the hydrogenase enzyme must be able to function in the presence of CO. As such the reactions of this inhibitor with hydrogenases have physiological relevance. Moreover, CO is a reactant in the water gas shift reaction (Reaction 1.3), the process by which H_2 is industrially produced. Thus, it is present in trace quantities in purified H_2 so the study of inhibition of hydrogenases by CO has relevance to the use of these enzymes as H_2 oxidisers in fuel cells (such as that shown in Figure 1.7).

5.2.1. Inhibition of the [NiFe(Se)]-hydrogenases

Complete inhibition of both H_2 oxidation and H_2 production by the [NiFe(Se)]-hydrogenases by CO has been reported for *Av*H[59] and can be predicted for *Df*H[216] and *Dg*H (see below) from their low apparent inhibition constants for H_2 oxidation ($K_I^{app}(CO/H_2)$) and H_2 production ($K_I^{app}(CO/H^+)$). In fact, the only known [NiFe(Se)]-hydrogenases that resist complete inhibition of H_2 production and oxidation even under 100% CO are the *Ralstonia* membrane-bound hydrogenases.[59,239,240]

Results of an IR-spectroscopy study performed by de Lacey et al. revealed that only the active states of *Df*H were able to bind CO, whilst "Unready" Ni-A, "Ready" Ni-B, Ni-SU and Ni-SR were protected from CO,[241] perhaps because the bound O-species present in these states blocks the binding site of CO,[79] and that the CO bound to the Ni atom which is thought to lie closer to the mouth of the gas channel than the Fe atom.[160,161] In agreement with these results, Ogata et al. demonstrated that inhibition of [NiFe]-hydrogenases occurred at the Ni atom[106] by publishing a structure of the CO-inhibited

state of *Dv*H in 2002 in which the exogenous CO binds in a bent Ni-C-O conformation (see Figure 5.1).

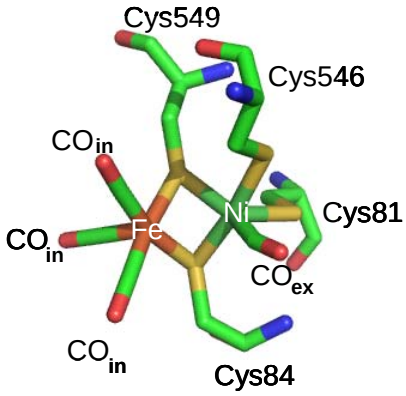

Figure 5.1: Structure of CO-inhibited active site of *Dv*H prepared using PyMOL (PDB code: 1UBL). The ligands bound to the Fe atom are "tentatively assigned as CO".[106] The intrinsic CO ligands are labelled CO_{in} and the extrinsic CO ligand is labelled CO_{ex}.

5.2.2. Inhibition of the [FeFe]-hydrogenases

A number of kinetic,[235] spectroscopic,[147] and electrochemical[204,220] studies on the inhibition of [FeFe]-hydrogenases by CO have been reported. There is some variation in results depending on the article and the [FeFe]-hydrogenase in question. For example, Erbes et al. used solution assays of the [FeFe]-hydrogenase from *Clostridium pasteurianum* to demonstrate that binding of CO was reversible and competitive, though in this early work, it had not yet been determined that this organism in fact expressed two [FeFe]-hydrogenases, thus the identity of the enzyme used in this study is not known.[233] Later research on the reversibility of CO inhibition of the two *Clostridium pasteurianum* hydrogenases appears to be contradictory,[67,215,242] and recent EPR results[243] have called the claim (made by Adams in 1987[242]) that a catalytic intermediate of *Cp*I binds CO irreversibly into question.

There is a substantial body of evidence indicating that exposure to CO yields the H_{ox}^{CO} state, either by only binding to the H_{ox} state or by forming the H_{ox}^{CO} state from the H_{red} state.[129,243] However, it has been shown that the *process* of H_2 production by [FeFe]-hydrogenases is inhibited by CO.[155,215,243,244] Terminal binding of CO to Fe_D[139,147] at the site suggested to coordinate H_2 in such a way that Fe_D is co-ordinately-saturated provides a rational explanation for the mechanism of inhibition by CO.[244]

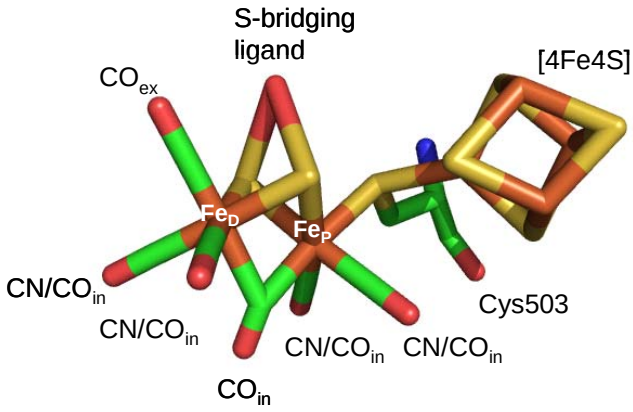

Figure 5.2: Structure of the CO-inhibited active site of *Cp*I prepared using PyMOL. (PDB code: 1C4C).[244] The intrinsic CO (labelled CO_{in}) and CN ligands have not been assigned in the crystal structure. The extrinsic CO-ligand is labelled CO_{ex}. The bridging S-ligand was modelled without the $-CH_2-$ groups connecting the bridging S atoms to the heteroatom (in red).

Comparison of infrared studies on inhibition of *Dd*H[147] and *Dv*H[127] by CO suggests that binding of extrinsic CO occurs in a similar fashion in these enzymes, though the effect on the spin density of binding an extrinsic CO ligand differs in *Dd*H and *Cp*I.[124,245] Moreover, it has been shown that exogenously-bound CO in a number of [FeFe]-hydrogenases including *Cp*I and *Dd*H is photolabile.[139,148,204,234,235,246] Later studies highlighted certain differences occurring at the active site. For example, the shift in the CN vibrations upon exposure to CO is different in these two enzymes; it has been suggested[246] that this may be attributed to the difference in the species (i.e. the residues) with which the CN ligands in *Dd*H[119] and *Cp*I[122] hydrogen-bond.

5.2.3. CO as a probe

Reactions with O_2 are complicated for both the [NiFe(Se)]-hydrogenases and the [FeFe]-hydrogenases. Recovery of activity of the enzyme requires reductive reactivation[18,104,247] and, in the case of the [FeFe]-hydrogenases only occurs to a small degree (see Chapter 6). Unlike O_2, CO is not redox-active. Therefore, the reactions of hydrogenases with CO are thought to be simpler than those with O_2, in that they do not affect the oxidation state of the active site. As CO is of a similar size to O_2, it can be used to separate the more complicated processes occurring at the active site when O_2 is present from those relating to transfer of the inhibitor into the active site from the environment outside the protein. If we consider this process to be limited by the size of the molecule rather than any polar interactions it may have with the protein environment or the favourability of the formation of the Fe-CO bond with respect to the Fe-O_2 adduct, the rates of inhibition by CO can be used as a "baseline subtraction" to isolate the reaction of O_2 at the active site from transfer of the diatomic molecule to the active site.

Furthermore, as was mentioned in Chapter 2 and will be discussed further in Chapter 6, CO can also be used as an inhibitor to prove the continued activity of hydrogenases in the direction of H_2 production when O_2 is present in the electrochemical cell. It is thus important to understand how and the degree to which hydrogenases are inhibited by CO.

5.3. Results

5.3.1. Qualitative comparison of inhibition of H_2 production by H_2 and CO

5.3.1.1. The [NiFe(Se)]-hydrogenases

Figure 5.3 shows chronoamperometric experiments in which the electrodes modified with four [NiFe(Se)]-hydrogenases are poised at a potential at which they catalyse H_2 production under an inert atmosphere of N_2 and the headspace of the cell is changed from N_2 to CO and H_2. This allows for a qualitative comparison of the degree of inhibition of H_2 production by H_2 relative to CO for a given enzyme. This is represented by the selection factor reported in Table 5.1.

In all cases the cell solution was equilibrated with N_2 at the beginning of the experiment. When the cell atmosphere was changed to CO, a decrease in current magnitude was observed as the enzymes became inhibited. Removal of the inhibitor by flushing with N_2 restored the current to its original level under N_2. Introduction of H_2 caused another decrease in current which was reversed by flushing with N_2.

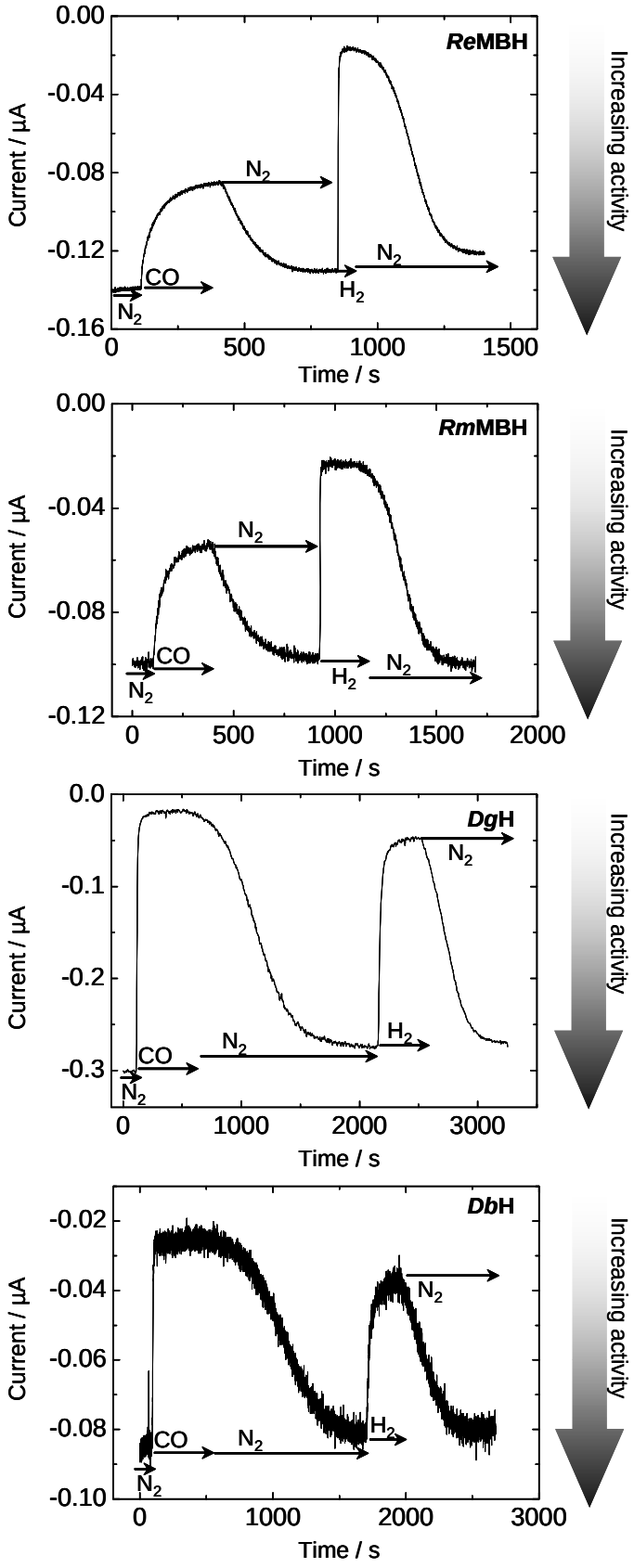

Figure 5.3: Chronoamperometric traces showing inhibition of H_2 production by H_2 and CO for *Re*MBH, *Rm*MBH, *Dg*H and *Db*H. Experimental conditions: pH 5.5, 30 °C, electrode rotation rate 3000 rpm, 100% atmospheres of gases as indicated. The potential for the experiments performed on *Rm*MBH, *Re*MBH, and *Dg*H was -0.45 V and that for the experiment on *Db*H was -0.4 V.

A striking feature of Figure 5.3 is that CO is a poor inhibitor of *Re*MBH and *Rm*MBH relative to *Dg*H and *Db*H. Moreover, the presence of H_2 terminates H_2 production by the *Ralstonia* enzymes (the remaining 0.025 μA of current under H_2 are due to a small current offset at this potential[216]) whilst a very small H_2-production current is recorded for *Dg*H and *Db*H under H_2 (0.05 μA). Thus, *Re*MBH and *Rm*MBH are much more strongly inhibited by H_2 than CO and are inhibited by H_2 to a greater extent than *Db*H and *Dg*H (see Chapter 4). These last two enzymes are totally inhibited by 100% CO (1 mM in solution) and the recovery of current as the CO is flushed out of the cell is sigmoidal rather than exponential as observed for H_2-inhibition of the *Ralstonia* hydrogenases. A sigmoidal recovery indicates saturation of the enzyme with the inhibitor. As the concentration of the inhibitor in solution drops below a certain level, the rate of recovery increases significantly and becomes exponential.

5.3.1.2. The [FeFe]-hydrogenases

Similar experiments were performed on the [FeFe]-hydrogenases *Dd*H, *Cr*HydA1 and *Ca*HydA. These enzymes were found to recover very slowly from inhibition by CO, so they were inhibited by flowing 1% CO through the cell rather than 100% CO. In these experiments, the enzymes were inhibited by H_2 before being inhibited by CO. As will be discussed in greater detail in section 5.3.3.1, CO causes some irreversible damage, especially pronounced for *Cr*HydA1 and *Ca*HydA, when they are poised at potentials at which they produce H_2. This is evidenced by the fact that the current recorded after exposure to CO at the end of the experiments is lower than that recorded prior to inhibition by CO. It was thus advantageous to perform this phase of the experiment after the H_2 phase to retain as much activity as possible for the most part of the experiment.

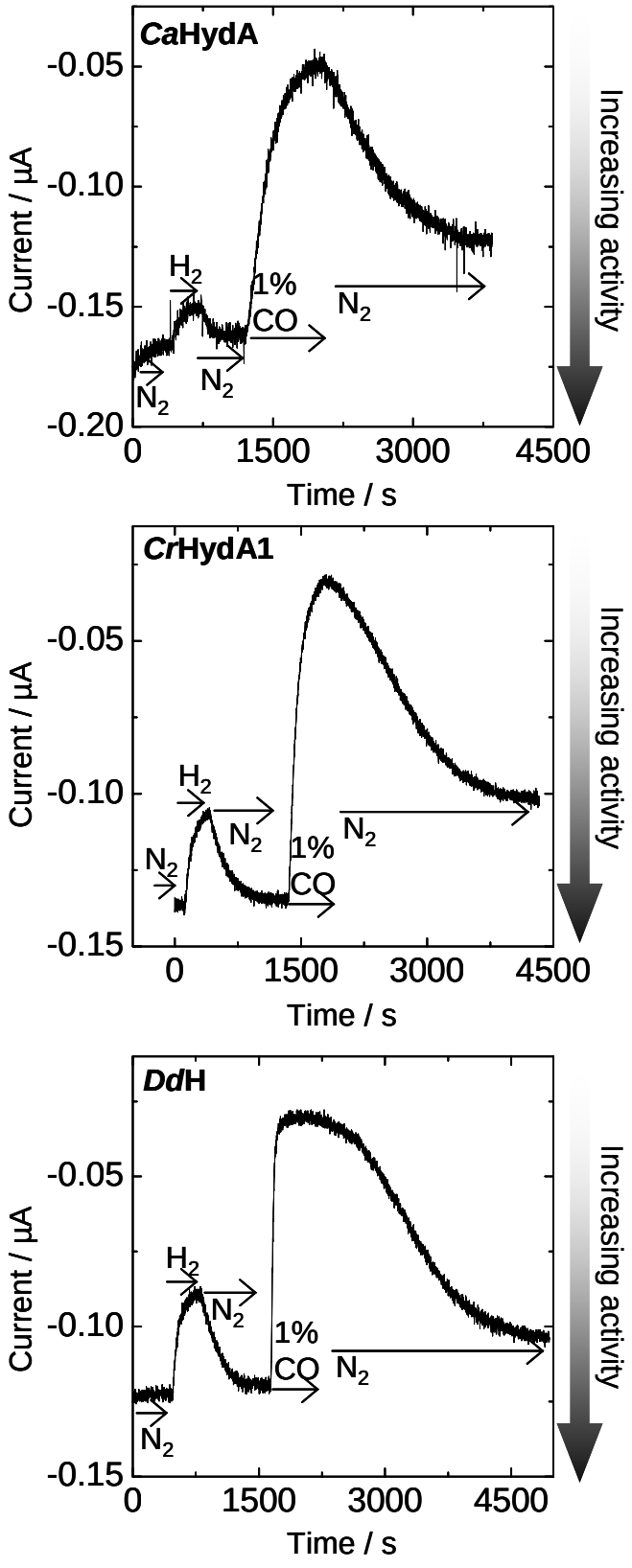

Figure 5.4: Comparison of inhibition by H_2 and 1% CO for *Ca*HydA, *Cr*HydA1 and *Dd*H. Experimental conditions: pH 6, 10 °C, -0.4 V, electrode rotation rate 3000 rpm, gases as indicated (1% CO is in N_2).

The behaviour of these three enzymes is an extension to that of *Db*H: CO is a much better inhibitor of H_2 production than H_2 which does not inhibit these enzymes completely. In fact even *1%* CO has a greater effect on the activity than *100%* H_2. Also, whilst *Dd*H is inhibited by 1% CO immediately, inhibition of *Ca*HydA and *Cr*HydA1 is much slower. The relative kinetics of inhibition of these three enzymes by CO are examined in greater detail in section 5.3.3.3. As inhibition of H_2 production of *Ca*HydA and *Cr*HydA1 (and perhaps *Dd*H) by CO is partially irreversible, it is not appropriate to quantify this inhibition in terms of $K_I^{app}(CO/H^+)$ values, which in turn means that a numerical "selection factor", reported for the [NiFe]-hydrogenases in Table 5.1, could not be determined. However, a qualitative comparison of the relative binding of CO and H_2 for the three enzymes can be made. These experiments demonstrate that *Dd*H is the most inhibited by H_2 (also see Figure 3.6) *and* by CO (see section 5.3.3.2) and *Ca*HydA the least inhibited by both H_2. The characteristics of the irreversible CO-adduct is investigated further in section 5.3.3.

5.3.2. Quantifying inhibition of the [NiFe(Se)]-hydrogenases

5.3.2.1. Calculation of $K_I^{app}(CO/H^+)$

As with the determination $K_I^{app}(H_2/H^+)$ for inhibition of H_2 production by H_2, different techniques were appropriate for different enzymes. For the *Ralstonia* enzymes,[209] *Dg*H and *Db*H, the method described in Chapter 4 for inhibition of H_2 production by H_2 pioneered by Léger[216] was employed. The values obtained for $K_I^{app}(CO/H^+)$ are shown in Table 5.1. Figure 5.5A shows an experiment performed on *Rm*MBH in which four sequential injections of CO-saturated buffer (final concentration in solution = 502,

288, 159, 73 μM CO) were performed under an inert atmosphere of Ar which was flushing through the cell, with time allowed between each injection for the CO to flush out of solution and the activity to recover to its original level. Panel B shows the log transforms of each of the transients following the injection and panel C shows the dependence of the anti-logs of the *y*-intercepts of the log transforms in panel B on the concentration of CO. The accuracy of the fit of the straight line to the data can be used to estimate the degree of scatter in the value of $K_I^{app}(CO/H^+)$, thus attesting to the accuracy of the data. This technique was also employed on *Re*MBH, *Dg*H and *Db*H.

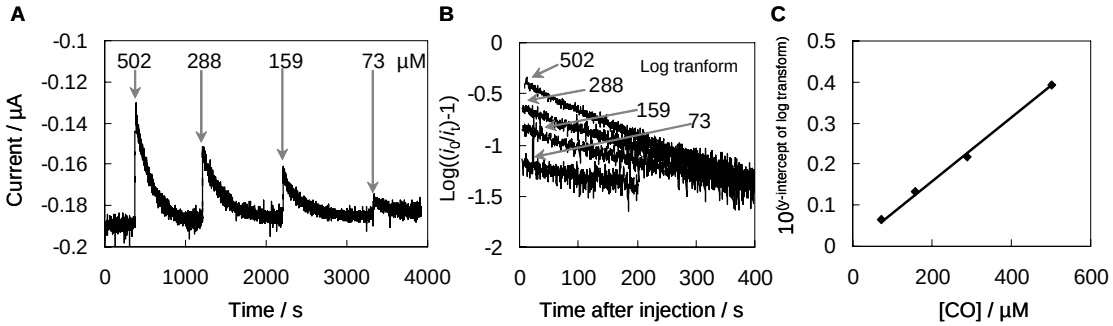

Figure 5.5: Calculation of $K_I^{app}(CO/H^+)$ for *Rm*MBH. A) Chronoamperometric experiment at -0.45 V in which four sequential injections of CO saturated buffer were performed with final concentrations of CO in the cell as indicated. Other conditions: pH 5.5, 30 °C, electrode rotation rate 3000 rpm, 100% atmosphere of Ar. B) Log-transform plots of each injection. C) Plot of the anti-logs of the *y*-intercepts of the log transforms shown in B vs. [CO] fitted to a straight line.

The "selection factor" (Table 5.1) is the ratio of the $K_I^{app}(H_2/H^+)$ for inhibition of H_2 production by H_2 (calculated in Chapter 4) and the $K_I^{app}(CO/H^+)$ and indicates the degree to which a given enzyme preferentially binds (or disfavours binding of) CO over H_2. This illustrates the strength of binding of H_2 relative to that of CO for the *Ralstonia* hydrogenases and the opposite observation for *Dg*H, *Df*H and *Db*H.

Enzyme	Type of hydrogenase	$K_I^{app}(H_2/H^+)$ / µM	$K_I^{app}(CO/H^+)$ / µM	"Selection factor"
*Re*MBH	[NiFe]	7.1	1700	4×10^{-3}
*Rm*MBH	[NiFe]	10.8	1300	9×10^{-3}
*Dg*H	[NiFe]	80	3	27
*Df*H[a]	[NiFe]	170	~5	34
*Db*H	[NiFeSe]	150	1	150

Table 5.1: Comparison of various $K_I^{app}(CO/H^+)$ and $K_I^{app}(H_2/H^+)$ values (taken from Chapter 4) for the [NiFe(Se)]-hydrogenase. a) these data are taken from ref.[216]

5.3.2.2. Potential dependence of CO inhibition of H_2 production

The potential dependence of $K_I^{app}(CO/H^+)$ was determined for *Rm*MBH[209] using the method described in Chapter 4 (section 4.3.3). At each of five potentials (-0.26 V, -0.28 V, -0.31 V, -0.37 V, and -0.43 V), an injection of CO-saturated buffer was performed in the experiment shown in Figure 5.6A and the resulting transients of recovery were analysed as above. The calculated $K_I^{app}(CO/H^+)$ values are plotted against potential in Figure 5.6B. The dependence on potential was found to mimic that of $K_I^{app}(H_2/H^+)$ for *Rm*MBH (see Chapter 4) and that published for $K_I^{app}(CO/H^+)$ for *Df*H. Thus, binding of CO to *Rm*MBH is weakened by inhibiting the enzyme at a more negative potential.

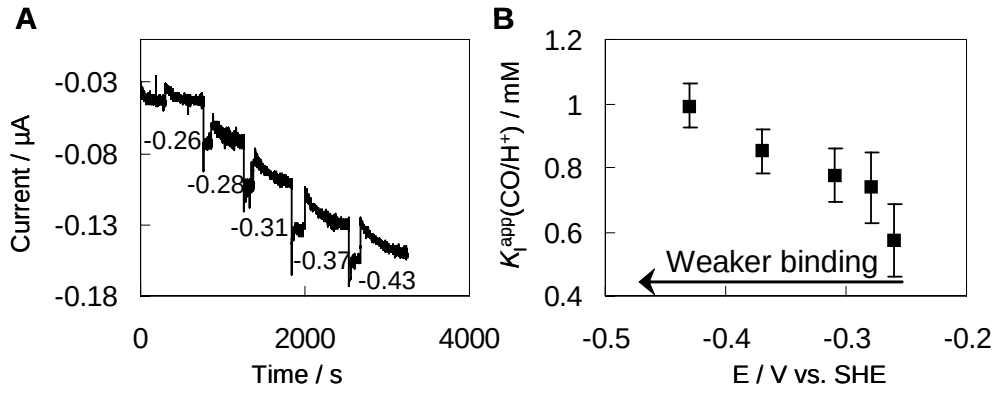

Figure 5.6: Potential dependence of $K_I^{app}(CO/H^+)$ for *Rm*MBH. A) Potential-step experiment performed pH 5.5, 30 °C, potentials as indicated (V vs. SHE). Other conditions: electrode rotation rate 3000 rpm, 100% Ar flowing through the headspace of the cell. Volumes of 0.5, 0.6, 0.83, 1.18, 1.58 mL of CO-saturated buffer were injected into the cell which originally contained 1.5 mL (thus giving a CO-concentration just after each injection of 25%, i.e. 230 µM) at -0.26, -0.28, -0.31, -0.37, and -0.43 V respectively. B) Plot of $K_I^{app}(CO/H^+)$ vs. potential demonstrating that the binding of CO is weakened by lowering the potential. The error bars are based on the error in injection concentration and signal-to-noise ratio.

The instantaneous nature of the reaction of H_2 and CO with these [NiFe(Se)]-hydrogenases is key in allowing for this method for calculating the $K_I^{app}(CO/H^+)$. In fact, the reaction is so rapid that the rate of inhibition is incalculable.

5.3.3. CO Inhibition of [FeFe]-hydrogenases

Two mechanisms of CO inhibition are discussed below: one reversible and one irreversible occurring only in the potential range at which the [FeFe]-hydrogenases produce H_2. The reversible process is assumed to proceed according to Scheme 5.1, with a second-order rate constant ($k_{inhibit}$/[CO], units = $M^{-1}s^{-1}$) and first order rate constant ($k_{recover}$, units = s^{-1}) being a measure of how fast the forward and reverse reactions (respectively) occur. The rate constants for transport of CO in and out of the enzyme are k_{in} and k_{out}, respectively. The elementary binding of CO to Fe_D is characterised by k_2 and k_{-2} for the forward and backward reactions, respectively.

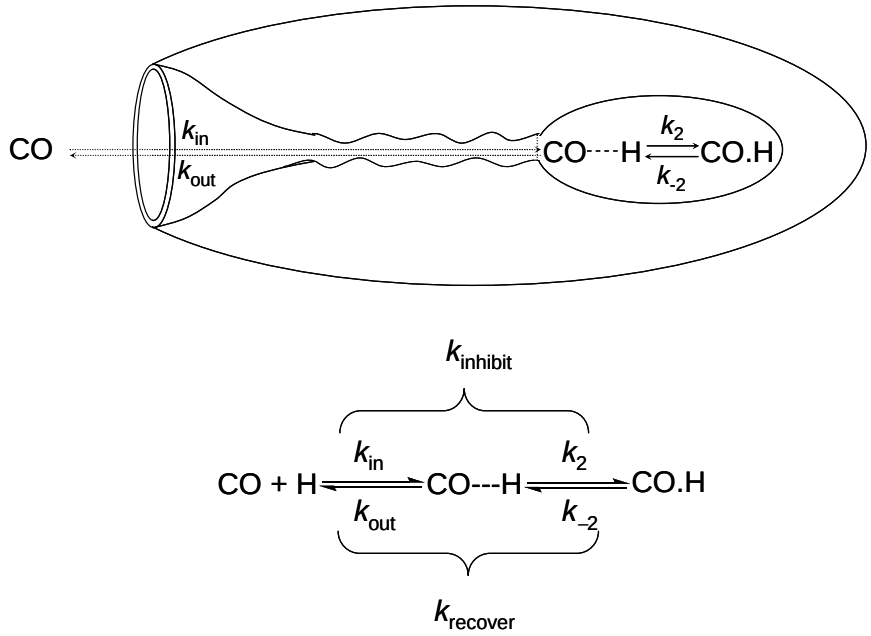

Scheme 5.1: A) Diagrammatic representation of the simplified enzyme with a single gas filter. B) Scheme of reversible CO inhibition of hydrogenases (represented by H) in which CO.H is the CO inhibited form of the enzyme and CO---H is a catalytically active form in which CO is present in the enzyme. The rate constants are as defined in the text.

5.3.3.1. Irreversible CO inhibition of H_2 production by *Cr*HydA1 and *Ca*HydA

As evoked by Figure 5.4, a particularity of *Ca*HydA and *Cr*HydA1 is their partially irreversible inhibition by CO when poised at potentials at which they produce H_2. Determining whether or not this irreversibility was specific to one state of the enzyme – i.e. that which predominates at this low potential rather than that predominating at a potential at which the enzyme is *oxidising* H_2 – is crucial when trying to elucidate a possible mechanism for this reaction. Thus, experiments at -0.05 V were performed on *Dd*H, *Cr*HydA1 and *Ca*HydA (Figure 5.7) to probe whether or not this irreversible state was formed. The electrode was first held under an atmosphere of 80% H_2[‡‡‡], 20% N_2 which was then changed to 80% H_2, 19.8% N_2, 0.2% CO in the experiment on *Dd*H,

[‡‡‡] Many of the experiments in this chapter and Chapter 6 in which different concentration of CO or O_2 are used to inactivate an enzyme are performed under 80% H_2. This level of H_2 was chosen because H_2 is explosive in air when at levels between 4 and 80%.

80% H_2, 19% N_2, 1% CO in the experiments performed on *Cr*HydA1 and 80% H_2, 10% N_2, 10% CO *Ca*HydA. (The concentrations of CO used in the experiments shown in Figure 5.7 and Figure 5.8 reflect the thermodynamic (section 5.3.3.2) and kinetic (section 5.3.3.3) favourability of CO binding of these three enzyme: *Dd*H is the most easily inhibited so the lowest concentration of CO was employed in the experiments shown in Figure 5.7A and Figure 5.8A whereas the highest concentration of CO was used in the experiments in Figure 5.7C and Figure 5.8C on *Ca*HydA because this enzyme is the least inhibited by CO.) Once a minimum in the activity had been reached, the atmosphere was returned to 80% H_2, 20% N_2 in all three cases.

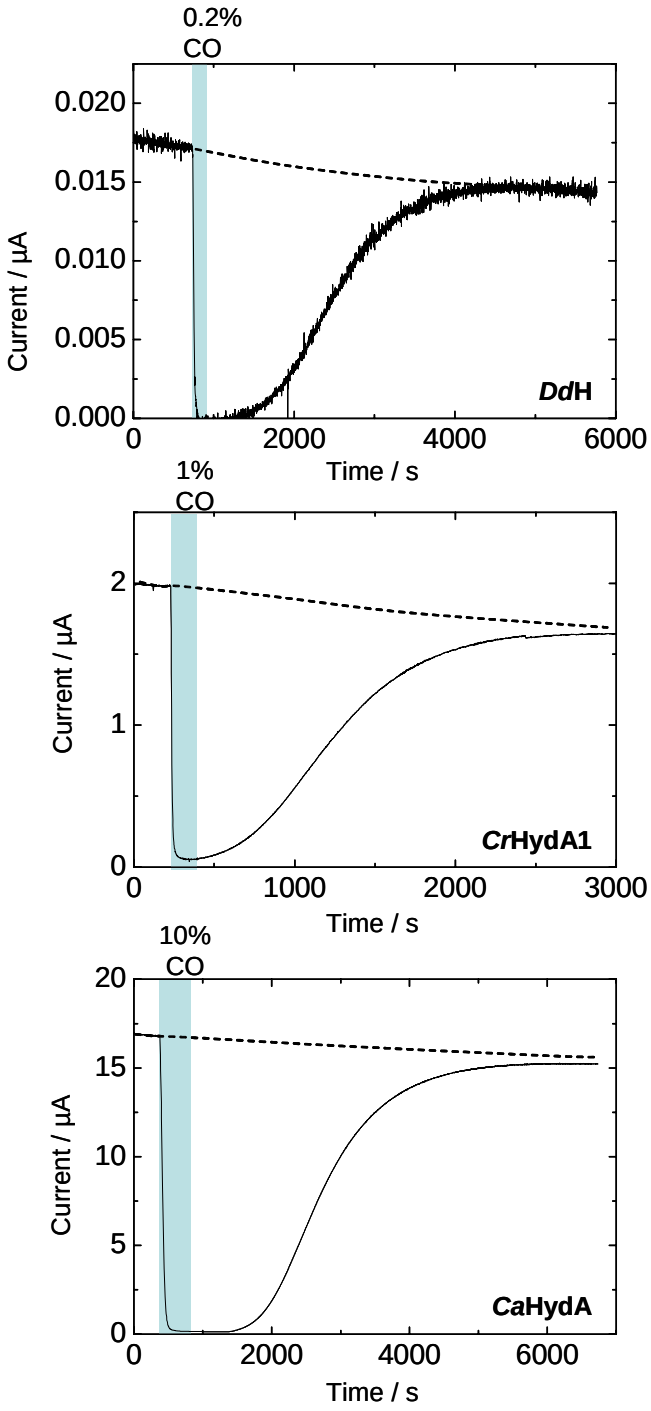

Figure 5.7: Comparison of CO inhibition of H_2 oxidation by A) *Dd*H, B) *Cr*HydA1, and C) *Ca*HydA. The headspace of the cell was flushed with 80% H_2 and the remaining, 20% was composed of N_2 or a mixture of N_2 and CO during the periods of time indicated by the blue boxes. Inhibition was induced under 0.2% CO / 19.8% N_2 for *Dd*H, 1% CO / 19% N_2 for *Cr*HydA1 and 10% CO / 10% N_2 for *Ca*HydA. The dashed lines give a visual guide of the projection of film loss in each case. Experimental conditions: pH 6, 10 °C, electrode rotation rate 3000 rpm, -0.05 V.

For all three enzymes, when the CO is flushed out of solution, the current returns to that recorded prior to introduction of CO into the cell minus natural film loss (as shown by

the dashed in Figure 5.7). This demonstrates that the reaction with CO at this potential is reversible, and that the irreversibility observed at -0.4 V as observed in Figure 5.4 (and Figure 5.8 below) is specific to the state generated at this potential.

To observe H_2 oxidation, it was necessary for the experiments shown in Figure 5.7 to be performed in the presence of H_2. As CO competes with H_2, experiments probing the irreversibility of CO inhibition of H_2 production were performed under 80% H_2 as well for consistency (Figure 5.8). Though H_2 is an inhibitor of H_2 production, it is such a weak inhibitor of these enzymes in comparison to CO (see Figure 5.4) that inhibition by CO was still observable in the presence of H_2. The experimental protocol was identical to that described for the experiments shown in Figure 5.7 except the potential was set to -0.4 V.

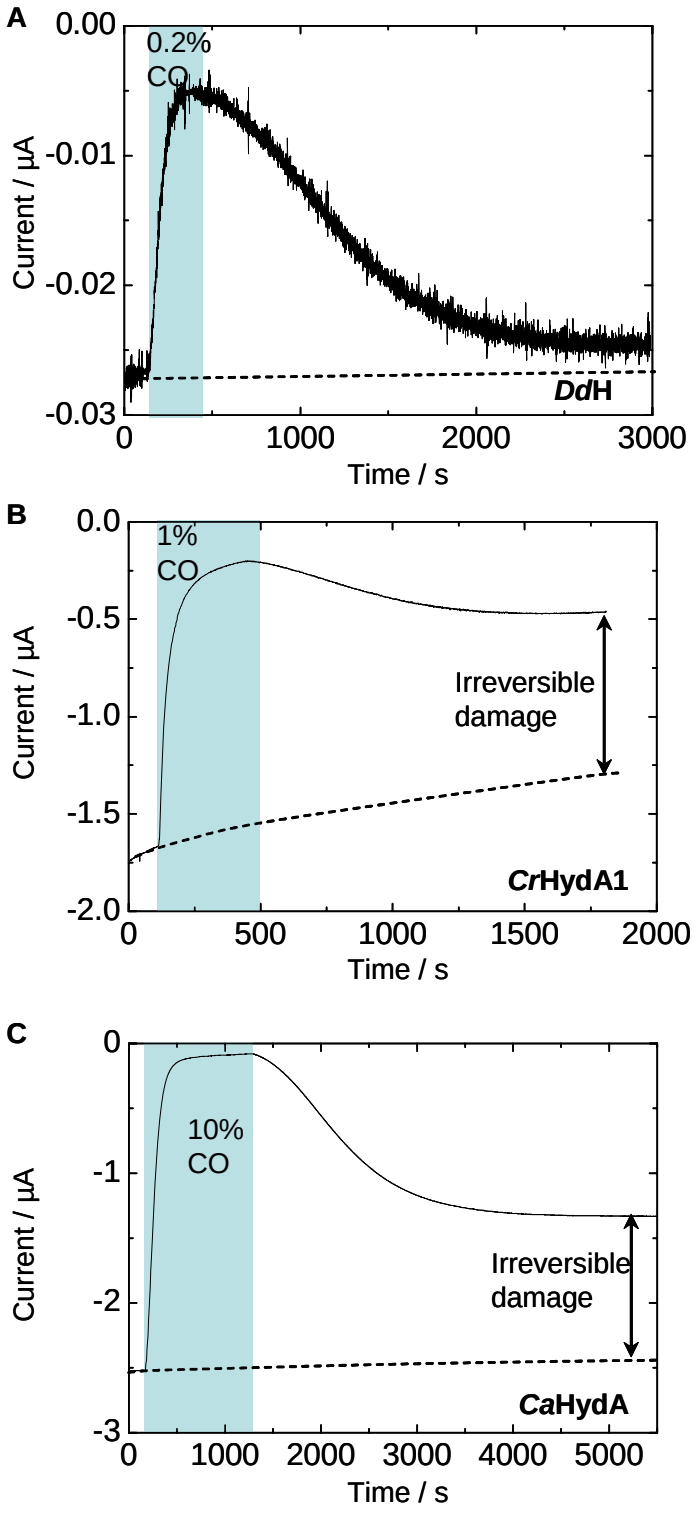

Figure 5.8: Comparison of CO inhibition of H_2 production by *Dd*H, *Cr*HydA1, and *Ca*HydA. The headspace of the cell was flushed with 80% H_2 and the remaining, 20% was composed of N_2 or a mixture of N_2 and CO during the periods of time indicated by the blue boxes, i.e. inhibition was induced under 0.2% CO, 19.8% N_2 for *Dd*H, and 1% CO, 19% N_2 for *Cr*HydA1 and 10% CO, 10% N_2 *Ca*HydA. The dashed lines give a visual guide of the projection of film loss. Experimental conditions: pH 6, 10 °C, electrode rotation rate 3000 rpm, -0.4 V.

It is evident from Figure 5.8 that the reaction of *Cr*HydA1 and *Ca*HydA (and perhaps *Dd*H) with CO at -0.4 V is not fully reversible from the fact that the current recovered after CO is flushed out of the cell eventually settles to a lower value than that expected by taking film loss into account. The fact that this irreversibility is noted both under a N_2 (see Figure 5.4) and 80% H_2 atmosphere indicates that neither the presence nor the absence of H_2 prevent the formation of the irreversible CO-adduct.

Two further experiments were performed to investigate the potential conditions that lead to the formation of the irreversibly bound CO-adduct and whether or not this seemingly irreversible damage *could* be reversed. Figure 5.9 shows an experiment, carried out on *Ca*HydA, designed to examine the reversibility of CO binding when the enzyme is first subjected to CO at a potential at which it binds this inhibitor reversibly (-0.05 V) before stepping the potential down to a level at which binding is partially irreversible. This informs on the potential at which the irreversible adduct is generated. The experiment commenced under 20% N_2 at -0.05 V and the enzyme was inhibited with 20% CO at t = 500 s. As with the experiments described above, 80% H_2 was maintained in the headspace throughout. The potential was then stepped down to -0.4 V (a potential at which *Ca*HydA produces H_2) for 100 s before being stepped back to -0.05 V. The inhibitor was then flushed out of the cell and the activity was allowed to recover.

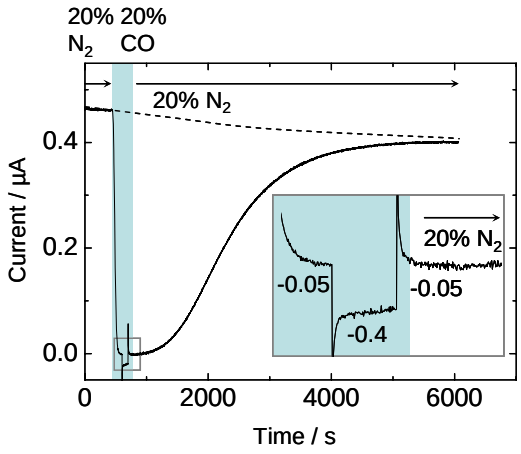

Figure 5.9: Probing the conditions leading to the formation of the irreversibly-bound CO-adduct. A) The potential at the start of the experiment is set to -0.05V. The headspace of the cell was flushed with 80% H_2, 20% N_2 then 80% H_2, 20% CO for the period of time highlighted by the blue box. Once the current had dropped to zero, a potential step down to -0.4 V was performed. The potential was returned to -0.05 V after a further 200 s and the CO was flushed out of the cell with 80% H_2, 20% N_2. The dashed line gives a visual guide of the projection of film loss. Experimental conditions: pH 6, 10 °C, electrode rotation rate 3000 rpm.

The reversibility of binding of CO to *Ca*HydA exhibited in the experiment in Figure 5.9 attests to the fact that exposing the enzyme to CO at -0.05 V leads to the formation of the reversible adduct and that this adduct cannot be converted into the irreversible adduct. Stepping down to a potential at which the irreversible form is generated (when inhibition by CO initially occurred at a potential in the H_2 oxidation range) did not engender the formation of this species. Thus, the potential at which the enzyme is first exposed to CO is the key condition in determining whether or not the irreversible adduct is generated.

Figure 5.10 shows an experiment testing whether or not stepping up to a potential at which *Ca*HydA oxidises H_2 (and binds CO reversibly) after inhibition of the enzyme at a potential at which it produces H_2 (and binds CO *ir*reversibly) can induce a return of the apparently permanently lost activity. The cell solution was pre-equilibrated with an atmosphere of 80% H_2, 20% N_2 at the start of the experiment which was then changed

to 80% H_2, 19% N_2, 1% CO for 600 s so as to inhibit the enzyme. As expected, when the CO was subsequently removed from the cell, the current recorded was lower (0.7 μA) than that detected prior to inhibition (1.3 μA). The potential was then stepped up to -0.05 V for 500 s at t = 4600 s before being stepped back down to -0.4 V.

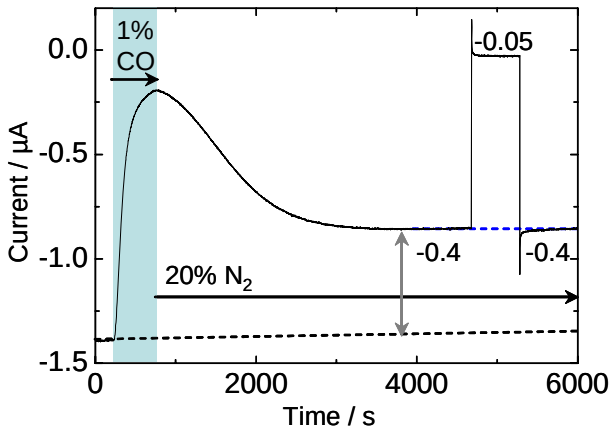

Figure 5.10: Probing the possibility of reversing irreversible CO-damage to *Ca*HydA. The potential at the start of the experiment is -0.4 V. The headspace of the cell is flushed with 80% H_2, 20% N_2 then 80%, 19% N_2, 1% CO for the period of time highlighted by the blue box then 80% H_2, 20% N_2 at which point the potential is stepped up to -0.05 V, held at this level for 500 s and then returned to -0.4 V. The dashed black line gives a visual guide of the projection of film loss. The dashed blue line indicates the level of the current recorded at -0.4 prior to stepping to -0.05 V. The double-headed grey arrow marks the irreversible loss of activity due to CO inhibition. Experimental conditions: pH 6, 10 °C, electrode rotation rate 3000 rpm. Potentials as indicated.

Stepping the potential up to one at which the enzyme oxidises H_2 did not return the activity lost on inhibition of *Ca*HydA by 1% CO at -0.04 V (as marked by the double-headed grey arrow in Figure 5.10). This reinforces the case that the potential at which the enzyme was subjected to CO is the all-important factor in modulating the nature of the species formed.

The potential dependence of irreversibility is demonstrated by the fact that irreversibility is only observed in the potential range in which *Cr*HydA1 and *Ca*HydA produce H_2. As an extension to this, experiments were performed at a lower potential (-0.6 V) on *Cr*HydA1 and *Ca*HydA than that applied in the experiments shown in

Figure 5.8 to probe whether or not lowering the potential had an effect on the reversibility of binding of CO. The experiments shown in Figure 5.11 were commenced under an atmosphere of 80% H_2, 20% N_2 which was then changed to 80% H_2, 20% N_2 with a concomitant injection of CO-saturated buffer[§§§] to observe inhibition of the hydrogenases.

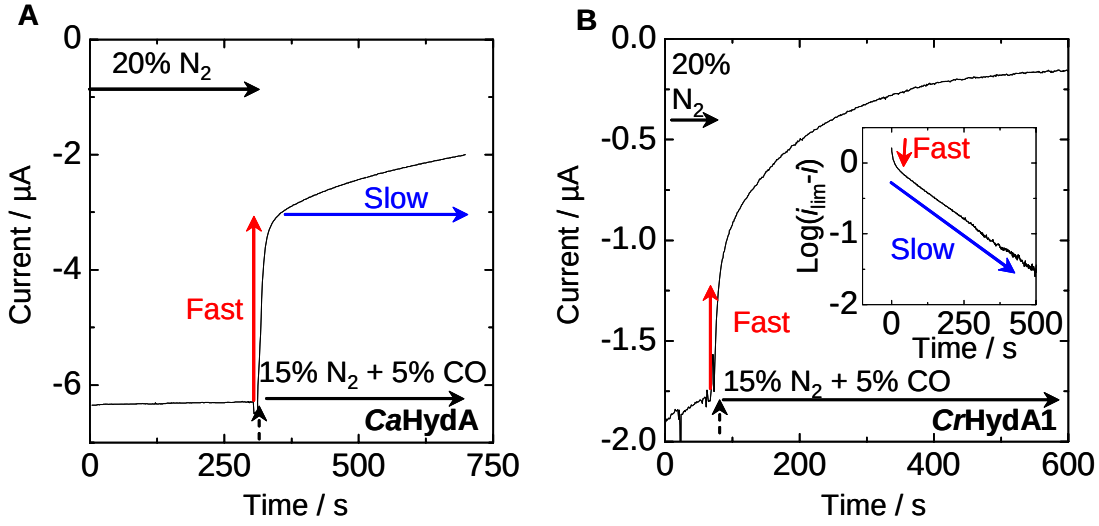

Figure 5.11: Examination of the reversibility of CO inhibition of A) *Ca*HydA and B) *Cr*HydA1 at -0.6 V. The headgas was composed of 80% H_2 throughout and the remaining 20% is as indicated. The dashed arrows mark the point at which 0.67 mL buffer saturated with 80% H_2, 20% CO were injected into the 2 mL of buffered electrolyte initially present in the cell. Experimental conditions: pH 6, 10 °C, electrode rotation rate 3000 rpm. The inset in B shows the log transform of the trace from the point of introduction of CO.

As will be shown in 5.3.3.3, the kinetics of inhibition of *Dd*H, *Cr*HydA1 and *Ca*HydA can approximately be analysed by first-order kinetics. However, the results shown in Figure 5.11 do not lend themselves to such analysis as they are biphasic; this is particularly conspicuous in the case of *Ca*HydA. For *Cr*HydA1, this is evidenced by the fact that there is an inflection in the log-transform plot in the inset of Figure 5.11B. This is to be expected in the case where two mechanisms of inactivation (one reversible, one irreversible) are taking place. The extent of the irreversible loss of activity will be

[§§§] This experimental technique was adopted so that these experiments could be compared fairly with those described in 5.3.3.3.

time-dependent as the irreversible CO-adduct accumulates over time, so this probably gives rise to the slow process observed in Figure 5.11 whereas the fast process results from reversible binding of CO. The fact that this biphasic nature of CO-binding is more pronounced at -0.6 V than at -0.4 V suggests that the irreversible process becomes more important as the potential is lowered.

5.3.3.2. Thermodynamics of reversible CO inhibition

Contrary to the [NiFe(Se)]-hydrogenases, the method described in Chapter 4, which is dependent on immediate inhibition of the enzyme by injection of inhibitor-saturated solution, was unsuitable for the [FeFe]-hydrogenases which were found to react much more slowly with CO (see section 5.3.3.5). Therefore, a method akin to that described in Chapter 3 was employed to obtain figures for the CO inhibition constant. Equation 5.1 is identical to Equation 3.2, except that i_{H_2} is replaced by i_{CO} (i.e. the current recorded at each concentration of CO) and that i_{N_2} no longer represents the current observed under 100% N_2 but rather that observed 80% H_2, 20% N_2. The constant for inhibition of H_2 oxidation by CO is $K_I^{app}(CO/H_2)$.

$$i_{N_2}/i_{CO} - 1 = \frac{[CO]}{K_I^{app}(CO/H_2)} \qquad \text{Equation 5.1}$$

Figure 5.12 shows chronoamperometric experiments in which *Cr*HydA1 (A) and *Ca*HydA (B) were held at -0.05 V under an atmosphere of 80% H_2 throughout the experiment. This concentration of H_2 was maintained throughout so as to eliminate any effect of diluting the substrate H_2 when the CO is brought into the cell. The current in the various experiments is normalised to that recorded prior to inhibition by CO (i.e. i_{N_2} is set to 1). At the start of the experiment, the remaining 20% of the headspace gas was

N_2 and this was then exchanged for a mixture of CO and N_2 (as indicated on the figure). Panel C shows the plot of Equation 5.1, and the fit of the straight line to the data can be used to estimate the degree of scatter in the value of $K_I^{app}(CO/H_2)$. The value of i_{CO} is determined when the current has stabilised in the presence of CO, as marked on Figure 5.12 by the dashed lines. As *Dd*H was fully inhibited by even the lowest concentration of CO that could accurately be delivered in these experiments (see Figure 5.13), the $K_I^{app}(CO/H_2)$ could not be calculated.

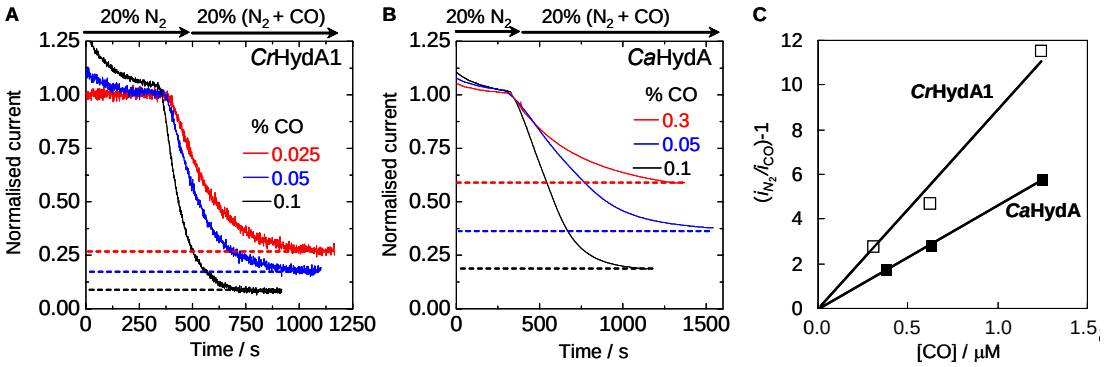

Figure 5.12: Calculation of $K_I^{app}(CO/H_2)$ for A) *Cr*HydA1 and B) *Ca*HydA. The headspace of the cell was flushed with 80% H_2 throughout all experiments. The remaining 20% was composed of N_2 at the start of all experiments, then changed to a mixture of N_2 and CO as indicated. The dashed lines mark the i_{CO} values at each concentration of CO. Panel C shows the (i_{N_2}/i_{CO})-1 vs. [CO] plots for *Cr*HydA1 (□) and *Ca*HydA (■). Experimental conditions: pH 6, 10 °C, electrode rotation rate 3000 rpm, electrode potential -0.05 V.

The values of $K_I^{app}(CO/H_2)$ for *Ca*HydA, and *Cr*HydA1 are shown in Table 5.3; these values fall within the range reported for inhibition of *Cr*HydA1 (0.9 ± 0.8 µM).[232] As displayed in Figure 5.12, the degree of inhibition of *Cr*HydA1 is greater that that of *Ca*HydA for a given concentration of CO and this is reflected in the fact that the $K_I^{app}(CO/H_2)$ value for *Cr*HydA1 is smaller than that of *Ca*HydA. Although the $K_I^{app}(CO/H_2)$ of *Dd*H could not be calculated, it can at least be asserted that this value is lower than that obtained *Cr*HydA1 and *Ca*HydA which were not fully inhibited by these low concentrations of CO. Biological assay experiments performed by Hatchikian

et al.[143] determined a $K_I^{app}(CO/H_2)$ for *Dd*H (0.16 μM) that was in fact slightly larger than that calculated for *Cr*HydA1 (0.1 μM). However, this could be the consequence of the different experimental conditions used (30 °C rather than 10 °C, and pH 8 rather than pH 6).

	***Cr*HydA1**	***Ca*HydA**
$K_I^{app}(CO/H_2)$ / μM	0.1 ± 0.04	0.3 ± 0.1

Table 5.3: $K_I^{app}(CO/H_2)$ values for *Cr*HydA1 and *Ca*HydA calculated at 10 °C, pH 6 from the experiments shown in Figure 5.12.

As the inhibition constant is only relevant to the mechanism of competitive inhibition, it could not be calculated for inhibition of H_2 production of these enzymes by CO because this process is partially irreversible.

5.3.3.3. Kinetics of CO inhibition

The rates at which H_2 oxidation by *Dd*H, *Cr*HydA1 and *Ca*HydA were inhibited by CO were obtained by analysis of the data presented in Figure 5.13A, B and C. The delivery of CO into the cell solution by simultaneous injection of CO-saturated buffer and gas exchange of the headspace was essential for instant and sustained delivery of the inhibitor throughout the time necessary to inhibit each enzyme. The dependence of the normalised current corresponding to H_2 oxidation by these three enzymes on time as CO is brought into the cell (i) is exponential, therefore it can be linearised by applying a log function (see Chapter 2, section 2.7.1). The value of i_{lim} is determined when the current has reached a stable value in the presence of CO. The agreement with first order kinetics is confirmed by the linearity of the log transforms for at least two half-lives (Figure 5.13D, E and F). The pseudo-first order rate constants ($k_{inhibit}$ in Scheme 5.1) obtained at each concentration of CO for *Dd*H, *Cr*HydA1 and *Ca*HydA calculated from

the slope of these plots are plotted against the concentration of CO in Figure 5.13G and the second order rate constants ($k_{inhibit}$/[CO]) for all three enzymes are shown in Table 5.4

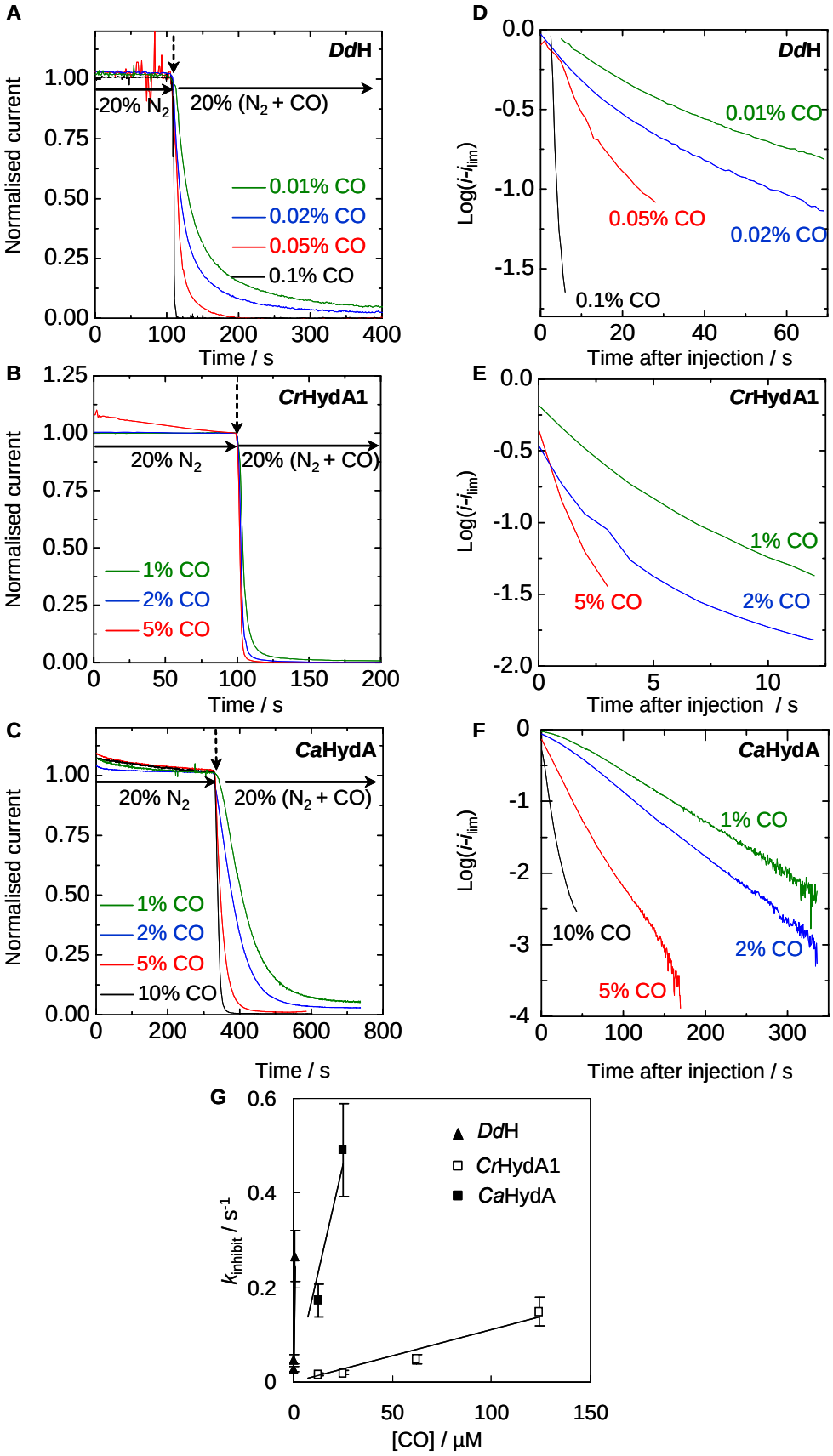

Figure 5.13: Investigating the kinetics of CO inhibition of H_2 oxidation of A) *Dd*H, B) *Cr*HydA1 and C) *Ca*HydA. Panels A, B, and C: the headspace of the cell was flushed with 80% H_2 throughout all

experiments and the remaining 20% was composed of N_2 at the start of all experiments then changed to a mixture of N_2 and CO concomitantly to performing an injection of CO-saturated buffer of the appropriate concentration, at the point indicated by the dashed arrow. Experimental conditions: pH 6, 10 °C, electrode rotation rate 3000 rpm, -0.05 V. Panels D, E, and F show log-transform plots of the normalised chronoamperometric traces shown in panels A, B and C, respectively, from the point at which CO is introduced into the cell. G) Pseudo-first order rate constants for inhibition ($k_{inhibit}$) plotted against [CO] for *Dd*H (▲), *Cr*HydA1 (□), and *Ca*HydA (■) fitted to a straight line for which the *y*-intercept was set at zero.

As the rates of inhibition of *Dd*H by 0.1% CO (i.e. 1.2 μM in solution) and *Cr*HydA1 by 5 and 10% CO (65 and 124 μM in solution) were too rapid to be accurately determined, these data have not been included in Figure 5.13G. What can be deduced from the relative rates of inhibition of these three [FeFe]-hydrogenases is that *Dd*H reacts with the greatest speed, followed by *Cr*HydA1 and then *Ca*HydA. Therefore, binding of CO to *Dd*H is both kinetically (and thermodynamically – see section 5.3.3.2 above) favoured over binding of CO to *Cr*HydA1 which is in turn favoured over binding of CO to *Ca*HydA.

The rates of inhibition of H_2 production at -0.4 V of *Ca*HydA, *Cr*HydA1 and *Dd*H by CO were obtained as described above, employing the same experimental design of inhibition by simultaneous gas exchange and injection of CO-saturated buffer (Figure 5.14, panels A, B, and C). The corresponding log transformations are shown in Figure 5.14, panels D, E, and F. The rates obtained are plotted against [CO] on Figure 5.14G. These pseudo-first order rate constants ($k_{inhibit}$) are approximates because two processes of inhibition are occurring in the case of *Cr*HydA1 and *Ca*HydA (one reversible, one irreversible, see section 5.3.3.1).

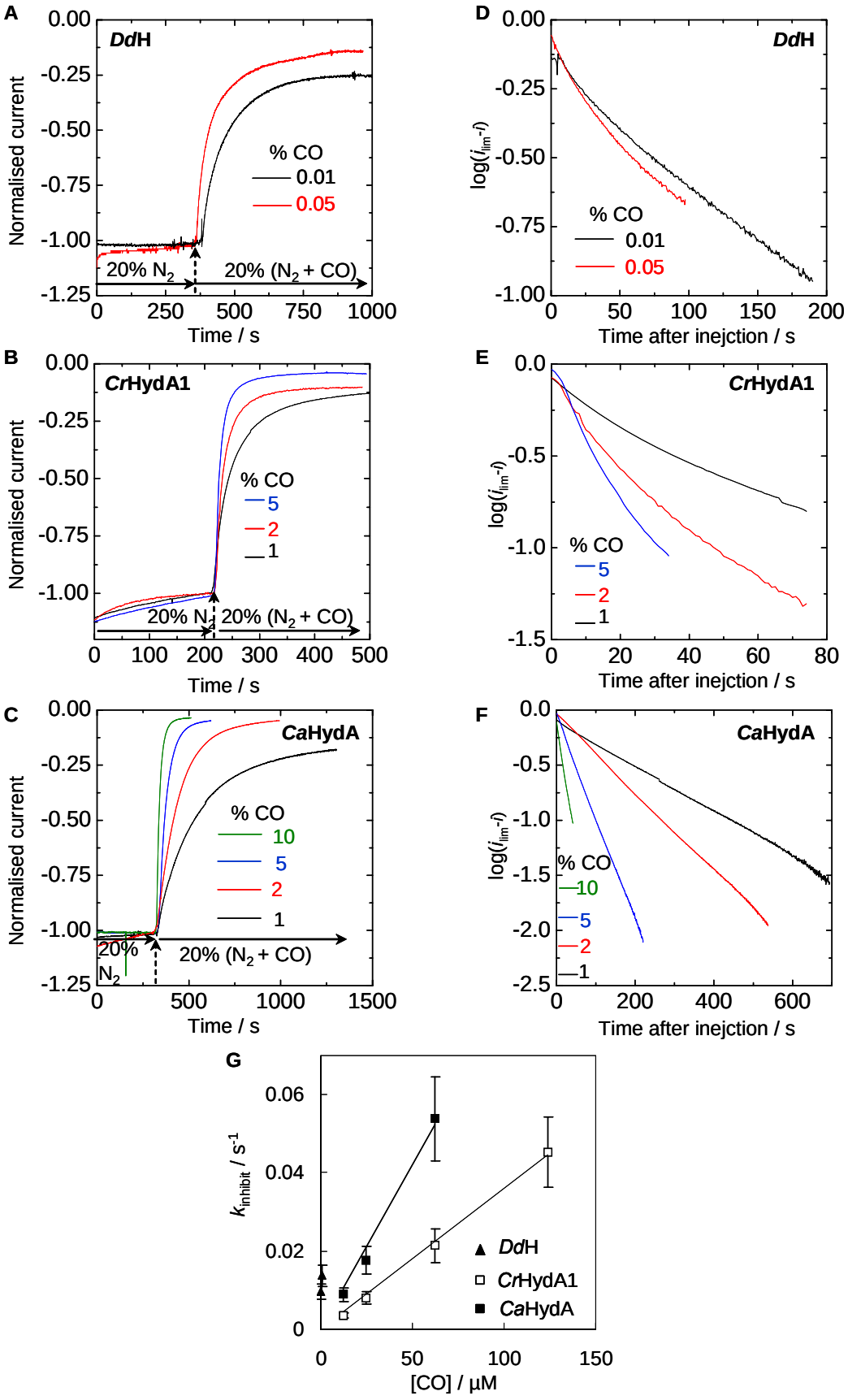

Figure 5.14: Investigating the kinetics of CO inhibition of H_2 production by A) *Dd*H, B) *Cr*HydA1 and C) *Ca*HydA. Panels A, B and C show experiments in which the headspace of the cell was flushed with

80% H_2 throughout. The remaining 20% was composed of N_2 at the start of all experiments then changed a mixture of N_2 and CO concomitantly to performing an injection of CO-saturated buffer of an appropriate concentration. Experimental conditions: pH 6, 10 °C, electrode rotation rate 3000 rpm, -0.4 V. Panels D, E, and F show log-transform plots of the normalised chronoamperometric traces shown in panels A, B and C, respectively, from the point at which CO is introduced into the cell. G) Pseudo-first order rate constants for inhibition ($k_{inhibit}$) plotted against [CO] for *Dd*H (▲), *Cr*HydA1 (□), and *Ca*HydA (■) fitted to a straight line for which the *y*-intercept was set at zero where necessary (*Cr*HydA1 and *Ca*HydA).

Table 5.4 summarises the numeric conclusions for the kinetic studies described above. The same trend for the kinetics of CO inhibition of H_2 oxidation of *Dd*H, *Cr*HydA1 and *Ca*HydA was observed for the kinetics of inhibition of H_2 production with *Dd*H binding CO the most rapidly followed by *Cr*HydA1 then *Ca*HydA. What is also evident from Table 5.4 is that binding of CO is more rapid when these [FeFe]-hydrogenases are oxidising H_2 than when they are producing H_2 and the extent of this is characterised by the $k_{inhibit}(H_2\ oxidation)/k_{inhibit}(H_2\ production)$ ratio.

Enzyme	H_2 oxidation $k_{inhibit}/[CO]$ ($s^{-1}\mu M^{-1}$)	H_2 production $k_{inhibit}/[CO]$ ($s^{-1}\mu M^{-1}$)	$\frac{k_{inhibit}(H_2\ oxidation)}{k_{inhibit}(H_2\ production)}$
*Dd*H	5×10^{-1}	8×10^{-3}	63
*Cr*HydA1	2.5×10^{-2}	8×10^{-4}	31
*Ca*HydA	1×10^{-3}	4×10^{-4}	3

Table 5.4: Second order rate constants for CO inhibition of H_2 production and oxidation by *Dd*H, *Cr*HydA1 and *Ca*HydA calculated from the data shown in Figure 5.13 and Figure 5.14. The kinetic discrimination characterising the inhibition of H_2 oxidation relative to H_2 production is given by $k_{inhibit}(H_2\ oxidation)/k_{inhibit}(H_2\ production)$.

The first order rate constants governing the rate of recovery from CO inhibition ($k_{recover}$ in Scheme 5.1) were calculated by performing log transformations on the latter part of the recovery from CO (i.e. the first 600 s after the CO had been removed from the headspace of the cell are omitted from the analysis) in experiments such as those shown in Figure 5.7 and Figure 5.8. This measure ensures that the analysis is performed on the portion of the experiment in which CO is absent from the cell solution and therefore the forward reaction (i.e. inhibition of the hydrogenase) is no longer taking place. Typical log transforms are shown in Figure 5.15.

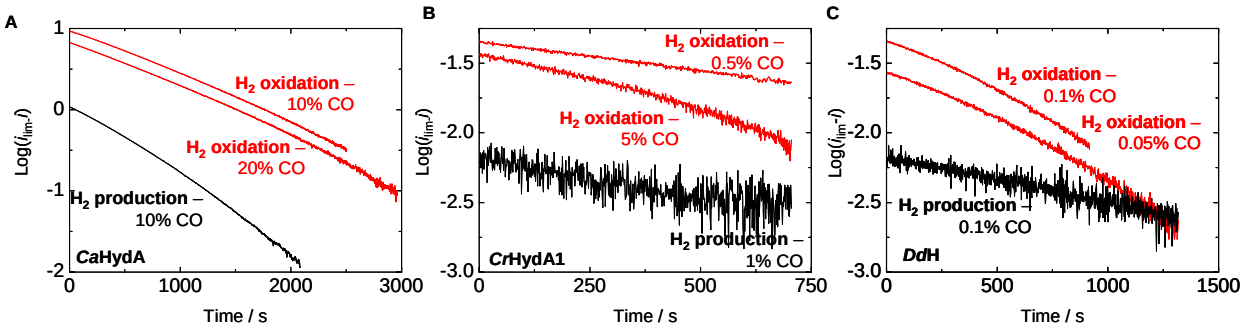

Figure 5.15: Log transforms of experiments to determine the rate constants of recovery from CO inhibition ($k_{recover}$) of H_2 oxidation (in red) and H_2 production (in black) by A) *Ca*HydA, B) *Cr*HydA1 and C) *Dd*H. These log transforms are analyses of the latter part of the recovery phase of experiments such as those shown in Figure 5.7 and Figure 5.8 in which CO is no longer present in the cell. Experimental conditions: pH 6, 10 °C, electrode rotation rate 3000 rpm, H_2 production potential -0.4 V, H_2 oxidation potential -0.05 V, 80% H_2, 20% N_2 atmosphere. Inhibition was achieved by the concentrations indicated on the figure, with 80% H_2 present at all times and N_2 making up the remaining % of the headspace.

As predicted by Scheme 5.1, the first order rate constants governing the rate of recovery from inhibition from CO were found to be independent of the concentration of CO, as illustrated by the fact that the log transforms of recoveries from inhibition under different concentrations of CO for *Ca*HydA, *Cr*HydA1 and *Dd*H run approximately parallel (Figure 5.15). Moreover, the slopes of the log transforms of the experiments performed at -0.4 V are also fairly similar, indicating that the rate of recovery is independent of potential, which in turn implies recovery from the same inactive species (presumably H_{ox}^{CO}). Overall, the value of $k_{recover}$ determined for all three enzymes after inhibition under different concentrations of CO and at the two different potentials was found to be 0.002 ± 0.0015 s^{-1}. This is in direct contrast with $k_{inhibit}$ which was dependent on the enzyme, [CO] and potential. This will be discussed further in the section 5.4.1.1 in the Discussion of this chapter. Additionally, based on predictions from the experiments in Figure 5.7 and Figure 5.8 (and depending on the enzyme and potential), only at < µM levels of CO is $k_{recover}$ larger than $k_{inhibit}$, i.e. inhibition is fast relative to recovery. This observation is consistent with the < µM values of $K_I^{app}(CO/H_2)$ determined in the experiments shown in Figure 5.12 (0.3 µM for

*Ca*HydA and 0.1 μM for *Cr*HydA1) as well as the kinetic interpretation of the inhibition constant ($K_I = k_{recover}/k_{inhibit}$), for *Cr*HydA1 which is 0.12 μM (though this approximation fails for *Ca*HydA for which the kinetic K_I = 1.6 μM).

5.3.3.4. Potential dependence of CO binding to the [FeFe]-hydrogenases

More in-depth explorations of the effect of potential on the binding of CO to [FeFe]-hydrogenases were performed using cyclic voltammetry. Figure 5.16 shows experiments in which *Cr*HydA1, *Ca*HydA and *Dd*H were inhibited by CO and sequential cyclic voltammograms (shown in different colours in Figure 5.16) were recorded as the CO was removed from solution by flushing with H_2.[248] These long experiments were performed at 10 °C in the case of *Cr*HydA1 and *Dd*H so as to favour stability of the film. However, it was advantageous to increase the temperature (to 32 °C) in the experiment performed on *Ca*HydA as this enzyme is the least biased towards H_2 oxidation and the crucial features in these experiments (see below) are recorded in the H_2-oxidation potential domain. Thus, the higher temperature amplifies the H_2-oxidation current (as well as the H_2 production current) and allows for a clear elucidation of this feature. The entire experiment performed on *Cr*HydA1 is shown – i.e. every scan between the first (in red) after inhibition by CO (recorded five minutes after CO inhibition) and the last (in black) when the recovery of activity was complete – demonstrating that the final profile of cyclic voltammogram resembled that expected from *Cr*HydA1 under 100% H_2 (see Figure 3.3). For simplicity, only the first and last scans are shown in the case of *Ca*HydA and *Dd*H. The features of interest are highlighted in the inset plots in the case of *Cr*HydA1 and *Ca*HydA but this was not necessary for *Dd*H.

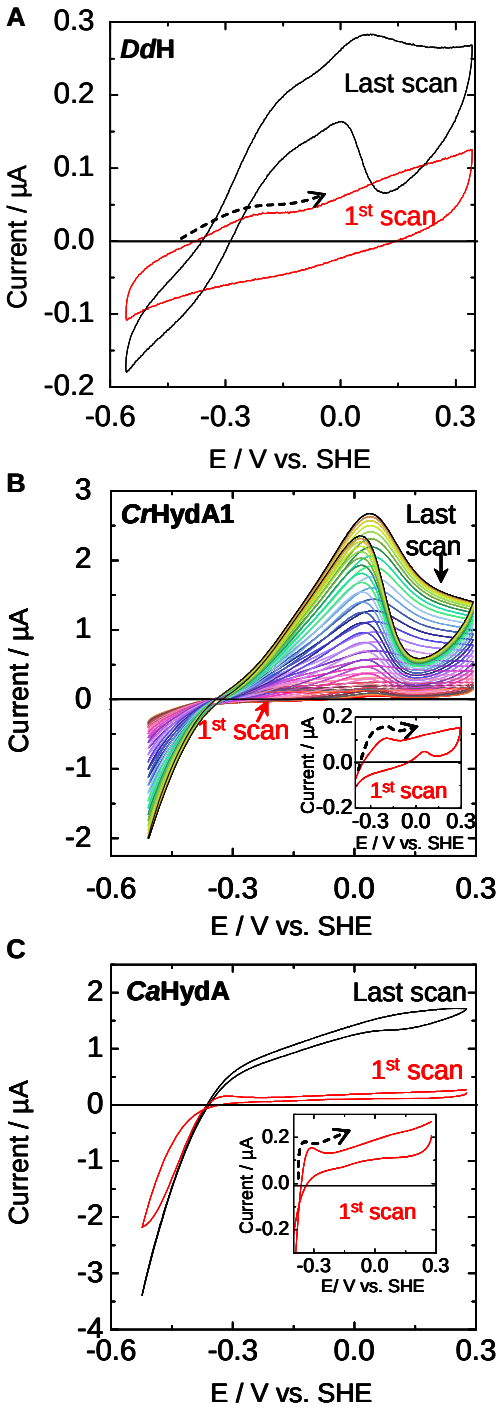

Figure 5.16: Cyclic voltammograms charting the recovery of A) *Dd*H, B) *Cr*HydA1, and C) *Ca*HydA from inhibition by CO at pH 6 under 100% H_2. A) Experimental conditions for *Dd*H (performed by Alison Parkin): 10 °C, electrode rotation rate 2500 rpm, scan rate 10 mV/s, inhibition was achieved by injection of CO-saturated buffer to give an instant concentration of 30 µM CO in solution 5 minutes prior to the first scan. B) Experimental conditions for *Cr*HydA1: 10 °C, electrode rotation rate 3000 rpm, scan rate 20 mV/s, inhibition was achieved by injection of CO-saturated buffer to give an instant concentration of 100 µM CO in solution 5 minutes prior to the first scan. C) Experimental conditions for *Ca*HydA: 32 °C, electrode rotation rate 3000 rpm, scan rate 20 mV/s, inhibition was achieved by flushing 100% CO through the cell 5 minutes prior to the first scan.

An obvious feature common to the portion of the first scans (despite the difference in experimental conditions) when the potential is swept from -0.35 V to +0.24 V (indicated by the dashed arrows) of the experiments performed on *Cr*HydA1, *Ca*HydA and *Dd*H is that the current initially increases as the driving force increases. However, there is a marked decrease in current above (approximately) -0.28 V for all three enzymes, indicative of an inactivation process. This implies that binding of CO occurs more readily at higher potentials, either because it can happen more rapidly or because binding at these potentials is thermodynamically favoured over binding at potentials more negative than -0.3 V. As time passes and the CO flushes out of solution, this feature becomes less evident and it is absent from the last scans which have the expected profiles for H_2 oxidation and production at pH 6 under 100% H_2 (Figure 3.3).

Chronoamperometric experiments performed on *Ca*HydA, *Dd*H and *Cr*HydA1 shown in Figure 5.17 further confirm the notion that binding of CO to the state of the enzyme present at potentials above -0.3 V (predominantly H_{ox}) is favoured over binding to that predominating below this potential (at which point H_{red} becomes favoured). This was achieved by scrutinising the comparative recovery from CO at potentials at which the enzyme is oxidising and producing H_2.

Timelines of the experiments are shown in Figure 5.17 panels D, E, and F. The experiments commenced under H_2 at -0.05 V (95% H_2 in the case of *Ca*HydA, 80% H_2 for *Cr*HydA1 and *Dd*H, with N_2 constituting the remaining percentage of the headspace gas) and a positive current due H_2 oxidation was recorded. At t = 400 s, CO was introduced into the cell (0.01% in the case of *Dd*H, 1% for of *Cr*HydA1 and 5% for *Ca*HydA – reflecting the degree to which each enzyme is inhibited by CO) and the

inhibition of the enzymes was recorded as the current dropped nearly to zero. The CO was then removed from the headspace by flushing with the original mixture of H_2 and N_2. As the inhibitor was flushed out, H_2-oxidation activity recovered. A time period of 1000 s was allowed to elapse so that all the inhibitor had been removed from solution before a potential step to -0.4 V was made (at which point a negative current corresponding to H_2 production was recorded). This ensured that comparison of the rates at which the activity was recovered (i.e. the slope of the increase in current with time) at -0.05 V prior to and after the step to -0.4 V was not convoluted by the possibility of trace CO in solution re-binding to the species present at -0.05 V. Another step to a potential at which the enzyme produces H_2 (-0.5 V in this case) was performed at t = 2000 s. Again, the potential was stepped back to -0.05 V, and the recovery of inhibition was allowed to conclude at this potential. The insets in Figure 5.17A, B and C show the portion of the experiment, marked out by the dashed ovals, during which these two potential steps were performed. The red and blue lines show the expected trace of current recovery had it continued at the exponential rate at which it had been increasing prior to the potential steps to -0.4 V and -0.5 V, respectively.

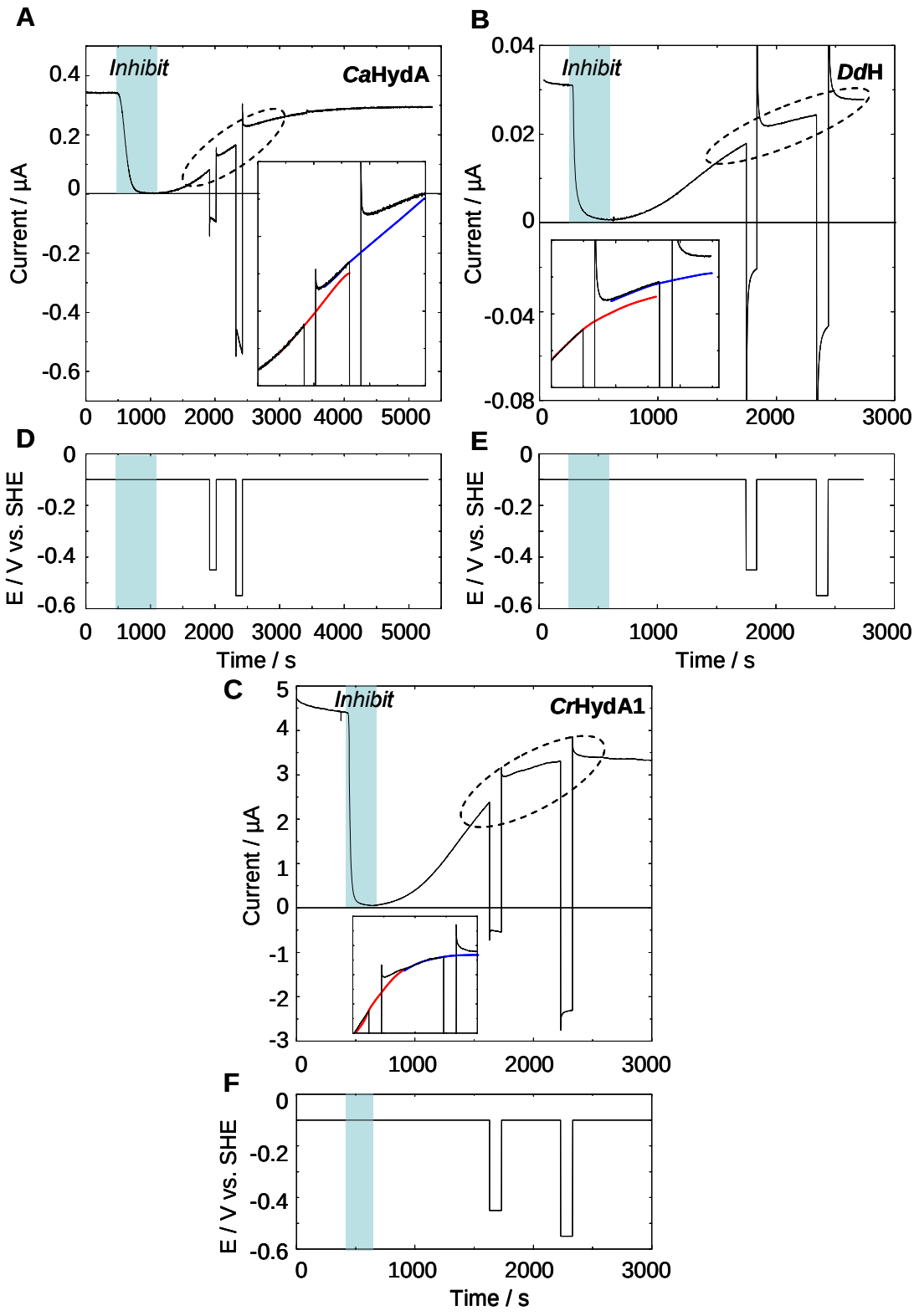

Figure 5.17: Comparison of rates of recovery from inhibition for H_2 production and oxidation by chronoamperometric experiments on A) *Ca*HydA, B) *Dd*H and C) *Cr*HydA1 and the corresponding timeline of potential steps (in panels D, E, and F, respectively). Other conditions: pH 6, electrode rotation rate 3000 rpm, 10 °C. The gas in the headspace contained 80% H_2 at all times for *Dd*H and *Cr*HydA1 or 95% H_2 for *Ca*HydA. The blue boxes mark out the periods of time in which CO is flushing through the cell. Inhibition of *Ca*HydA was achieved by flushing 5% CO into the cell, *Dd*H by flushing 0.01% CO and *Cr*HydA1 by flushing 1% CO. N_2 made up the remainder of the atmosphere in the cell at all times.

The insets in Figure 5.17A, B and C are very informative. That the current recorded after the potential step to -0.4 V was greater than expected (i.e. with respect to the red line) is more obvious in the case of *Dd*H and *Ca*HydA than it is for *Cr*HydA1. However, a subtle increase in current over that which was expected was noticeable for *Cr*HydA1 after the potential was returned to -0.05 V for the second time (as compared to the blue line), or rather, stepping down to -0.5 V had completed the process of reactivation such that, when the potential was returned to -0.05 V, the current no longer continued to increase. This was also the case for *Dd*H. These experiments show that the enzymes were more active after the potential step than expected. Thus, *Dd*H, *Ca*HydA and *Cr*HydA1 recovered more easily in the intervening steps to low potential then they did at -0.05 V. As stated in section 5.3.3.3, the rates of recovery from CO inhibition are effectively independent of potential (consistent with binding of CO to H_{ox} only). This suggests that this relative ease of recovery at lower potential results from a thermodynamic rather than a kinetic effect.

5.3.3.5. Evidence for a physical "filter" in the [FeFe]-hydrogenases

Experiments on *Dd*H, *Cr*HydA1 and *Ca*HydA in which a very low concentration of CO-saturated buffer was injected into the cell solution were conducted.[248] Figure 5.18A shows the effect of injecting 0.2 mL 5% CO (95% H_2)-saturated buffer (giving a final concentration of 4 μM in solution) on these three [FeFe]-hydrogenases when they are poised at a potential at which they *oxidise* H_2 and allowing the inhibitor to be flushed out by H_2. Figure 5.18B shows an equivalent set of experiments carried out at a potential at which they *produce* H_2. A control experiment performed to determine the timescale of the removal of CO from solution is shown in Figure 5.18C. In this

experiment, the blank electrode was poised at -0.4 V and 0.2 mL 5% O_2 (95% N_2)-saturated buffer (giving a final concentration of 5 µM in solution) were injected into the cell. The current was monitored as the O_2 was removed from solution by a steady stream of N_2 in the headspace. The grey line shows the fit of the data to an exponential decay. This fit is multiplied by -1 to model the concentration of CO throughout the experiments, as shown on the right-hand axes of panels A and B.

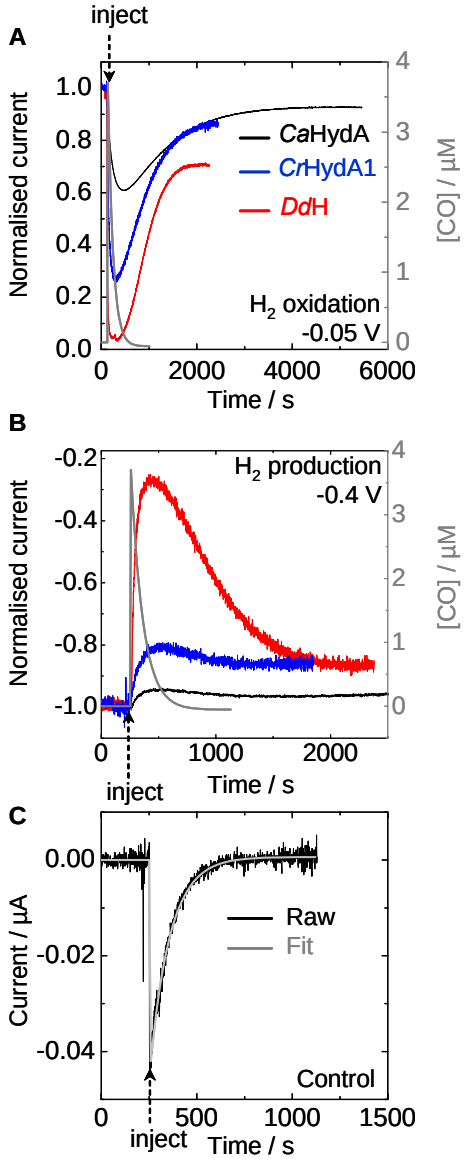

Figure 5.18: Effect of injecting 6 µM CO into the cell on *Dd*H, *Cr*HydA1 and *Ca*HydA. A) H_2 oxidation experiment performed at -0.05 V. B) H_2 production experiment performed at -0.4 V. C) Control experiment performed by injecting 0.2 mL, 5% O_2 in N_2 in the cell (initially containing 3 mL of electrolyte) and recording the change in current due to O_2 reduction at graphite. The potential was set to -0.4 V. Experimental conditions: pH 6, 10 °C, 100% H_2 in the headspace, electrode rotation rate 3000 rpm.

These results show how differently the [FeFe]-hydrogenase (Figure 5.18) and [NiFe(Se)]-hydrogenase (Figure 5.5[209] and ref.[162,216]) respond to such an injection. As the injection occurs in the experiments performed on the [NiFe(Se)]-hydrogenases, the current drops instantaneously to a minimum and then immediately begins to increases as the inhibitor is flushed out of solution indicating that inhibition is directly proportional to the concentration of CO in solution at any given point. However, for the [FeFe]-hydrogenases, the current reaches a minimum much more slowly even though the enzymes are being subjected to exponentially-decreasing concentrations of CO. This implies that there is some kind of barrier retarding access of the CO to the active site because if it were able to reach it immediately, the current would arrive at its minimum instantaneously as it does for the [NiFe(Se)]-hydrogenases. Of the three enzymes, *Dd*H is the most rapidly and/or completely inhibited by the injection of CO and *Ca*HydA is the least inhibited (in agreement with the data presented in sections 5.3.3.2 and 5.3.3.3). The recovery from inhibition by CO is also markedly longer for the [FeFe]-hydrogenases than for the [NiFe(Se)]-hydrogenases. Whilst, the slowness of the recovery from inhibition by CO could also be commensurate with there being a barrier to diffusion of CO in the enzyme (as also suggested by the experiments performed on *Cp*I by Lemon et al. showing that CO may remain trapped within the enzyme[155]), the experiments described below imply that scission of the Fe-CO bond is the rate-determining step, at least for *Dd*H and *Cr*HydA1 if not for *Ca*HydA (see section 5.3.3.6 and the Discussion of this chapter).

5.3.3.6. Photolability of CO-adduct

Preliminary experiments performed on *Cr*HydA1 and *Ca*HydA were conducted to assess the effect of light on the rate of recovery from CO inhibition (Figure 5.19A and

B) relative to its effect on catalysis (Figure 5.19C and D).[248] The electrode potential was set to -0.05 V to observe H_2 oxidation and 80% H_2, 20% N_2 was flushed through the cell. In panels A and B, an aliquot of CO-saturated buffer was then injected into cell (giving a final concentration of 50 μM) and the CO was flushed out of the cell by the stream of 80% H_2, 20% N_2 for the remainder of the experiments. The cell was illuminated (see cell design, Figure 2.7) through a window in the black electrical tape covering the cell for the periods of time highlighted in yellow. Panels C and D show control experiments examining the effect of switching the light on (during the period highlighted in yellow) and off on the H_2-oxidation activity of *Cr*HydA1 and *Ca*HydA (respectively) without prior inhibition by CO.

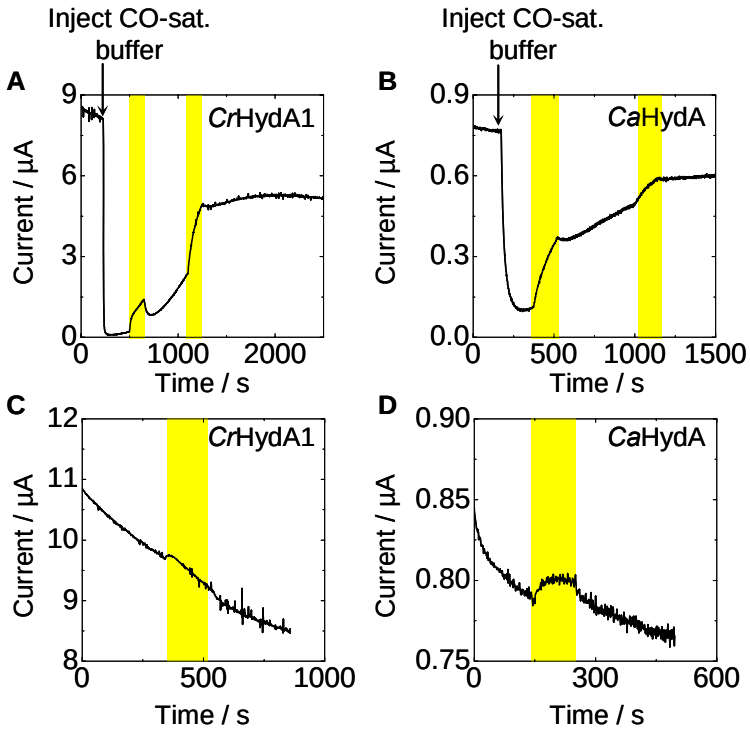

Figure 5.19: Experiments examining the photolability of the CO-adduct of *Cr*HydA1 and *Ca*HydA. In both panels A and B, *Cr*HydA1 and *Ca*HydA (respectively) were inhibited by injecting 0.5 mL 20% CO (80% H_2)-saturated solution into the cell that initially contained 2 mL of electrolyte, giving a concentration of 50 μM CO and the light was switched on in two phases (highlighted in yellow) and off as the enzymes were recovering from CO inhibition. The CO was flushed out of the cell by the stream of 80% H_2, 20% N_2 running throughout the experiments. Panels C and D show control experiments performed on *Cr*HydA1 and *Ca*HydA (respectively) in which the light was switched on (during the phase highlighted in yellow) and off as the enzymes were simply catalysing H_2 oxidation. Experimental conditions: pH 6, 10 °C, -0.05 V, electrode rotation rate 3000 rpm.

The experiments shown in panels A and B clearly demonstrate that light amplifies the increase in current with time as *Cr*HydA1 (panel A) and *Ca*HydA (panel B) recover from CO inhibition. The effect on increasing the H_2-oxidation activity (without prior CO inhibition) of these two enzymes is less pronounced, as shown in panels C and D. Thus, whilst catalysis is enhanced in the light, the rate of recovery from CO inhibition is much more pronounced (i.e. $k_{recover}$ (Scheme 5.1) increases). This is consistent with the electrochemical observation of the photolability of the CO-adduct of *Dd*H.[204]

Whilst the photolability of Fe-CO bonds is well established,[249-251] it is not expected that light should have an effect on the conformation of the gas channel. The fact that illumination, which should thus affect k_2 and k_{-2} rather than k_{in} and k_{out} (see Scheme 5.1), enhances the rate of recovery strongly suggests that (at least in the dark) this process is limited by the kinetics of the making and breaking the Fe_D-CO bond rather than transfer of CO across the protein. As the H-clusters of *Dd*H, *Cr*HydA1 and *Ca*HydA are expected to exhibit a fair degree of conservation,[124] this hypothesis provides a rationale for the similarity in the rates of recovery from CO inhibition of these three enzymes (in the dark, see Figure 5.15).

When the light was switched off after illumination in Figure 5.19A and B, the current dropped slightly before continuing to increase. This is especially obvious after the first illumination of *Cr*HydA1 (Figure 5.19A). This is the consequence of re-binding of CO either trapped in the enzyme (as suggested by Lemon[155]) or from traces left in solution. From control experiments such as that shown in Figure 5.18, it was possible to estimate that there would be approximately 1 μM CO left in solution at the point at which the light was switched off the first time. Considering that the $K_I^{app}(CO/H_2)$ values were

determined to be 0.1 and 0.3 μM for *Cr*HydA1 and *Ca*HydA, respectively, (see section 5.3.3.2), 1 μM CO is sufficient to cause an attenuation in the activity of both these enzymes. It is thus not possible to state whether the drop in current after illumination is due to re-binding of CO trapped within the enzyme scaffold or from solution.

5.3.4. Inhibition by formaldehyde

Inhibition by formaldehyde was investigated to address the possibility that the irreversibly-bound CO-adduct generated at potentials at which *Cr*HydA1 and *Ca*HydA produces an -(CO)-H adduct was formed by insertion of CO into a Fe-H bound as in Reaction 5.1.

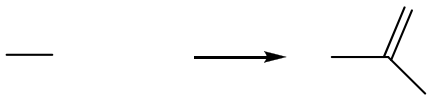

Reaction 5.1

The formation of this adduct would only be possible when the Fe-H moiety was present, which could be dependent on potential, hence explaining the formation of the irreversible adduct only at low potentials. Studies of the reactions of hydrogenases with formaldehyde have not previously been reported. In fact, it was not possible to prove in the study presented here whether or not formaldehyde is the irreversible adduct formed by CO inhibition of H_2 production because formation of formaldehyde at the active site by migratory insertion may involve a completely different mechanism to the binding of exogenous formaldehyde; the experiments described below are thus still very much in their infancy. However, two very intriguing results are noteworthy.

The first experiments investigated the effect of injecting formaldehyde (45 mM) into the cell and measuring the response of H_2 oxidation (Figure 5.20A) and H_2 production (Figure 5.20B) by *Cr*HydA1. As formaldehyde (H_2CO) is in equilibrium with

$H_2C(OH)_2$ in solution with a K_{eq} of 2280 (i.e. the aquated product is much more stable), the concentration of H_2CO is expected to be 20 μM after injection. Subsequent to injection, the experiment was stopped. The electrode was removed from the cell and the cell and electrode were rinsed thoroughly. Fresh buffer (free from formaldehyde) was added to the cell and the electrode was placed back into position and the experiment was restarted. The chronoamperometric traces showing the current recovered after inhibition by and removal of formaldehyde at -0.05 and -0.4 V are shown in Figure 5.20C and D, respectively.

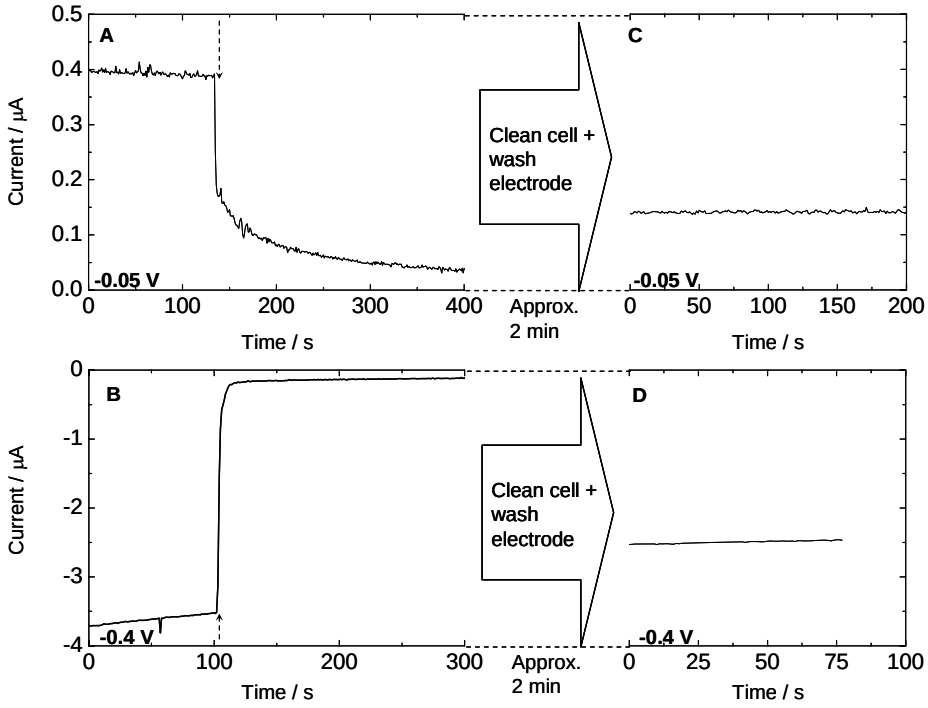

Figure 5.20: Chronoamperometric experiments at A) -0.05 V and B) -0.4 V investigating the inhibition of *Cr*HydA1 by an injection of formaldehyde (marked by the dashed arrows) to give a final concentration of 45 mM in solution. The formaldehyde solution was saturated with H_2 prior to injection. Taking the equilibrium constant for aquation of formaldehyde into consideration, this leaves 20 μM. Panels C and D show the recoveries of current at -0.05 V and -0.4 V, respectively. Prior to this, the electrode was removed from the cell and both the cell and electrode were thoroughly rinsed; fresh buffer was then placed in the cell and the electrode was re-inserted into the cell. Experimental conditions: pH 6, 20 °C, 100% H_2 atmosphere, electrode rotation rate 3000 rpm, potentials as indicated.

Upon injection of formaldehyde to a final concentration of 45 mM, the current dropped significantly at both potentials. The current decreased almost immediately to zero at

-0.4 V, however the activity at -0.05 V did not drop to that degree or at least not immediately. The decrease in current between t = 200 s and 400 s was substantially slower than in the initial 50 s after injection at -0.05 V, to the point of being indistinguishable from the current decrease due to film loss (as observed prior to injection). Removal of the formaldehyde resulted in a partial recovery of current at both -0.05 V and -0.4 V (Figure 5.20C and D). These experiments show that formaldehyde-inhibition is at least partially reversible in both H_2 oxidation and H_2 production. It is not possible to quantitatively assess the *degree* of reversibility in these experiments because the process of cleaning the cell and electrode could substantially affect the film loss. However, the results strongly suggest that the *rate* of recovery from H_2CO is fast. In fact, the current did not increase during the second parts of the experiments (Figure 5.20 C and D), indicating that simply removing H_2CO from the environment of the protein was sufficient to recover activity (thus, when the electrode was replaced in the cell, no further increase in current was observed) unlike inhibition by CO which is slow to be reversed even in the absence of CO.

In the experiments shown in Figure 5.21, the greater extent of inhibition of H_2 production over H_2 oxidation noted in the experiments shown in Figure 5.20 (panels A and B) was probed. This effect was investigated by injecting aliquots of formaldehyde into the cell at A) -0.5 V, B) -0.15 V and C) +0.24 V whilst the potential was swept between -0.55 V and +0.24 V. The first (black) traces are shown to depict the normal profile of a cyclic voltammogram of *Cr*HydA1 at pH 6. The injection, performed at the potentials indicated in the second (red) scans, resulted in a rapid decrease in current. The third (blue) scans, also shown in panels D, E, and F, inform on the effect of

formaldehyde on the catalytic activity and bias of *Cr*HydA1 in the presence of formaldehyde.

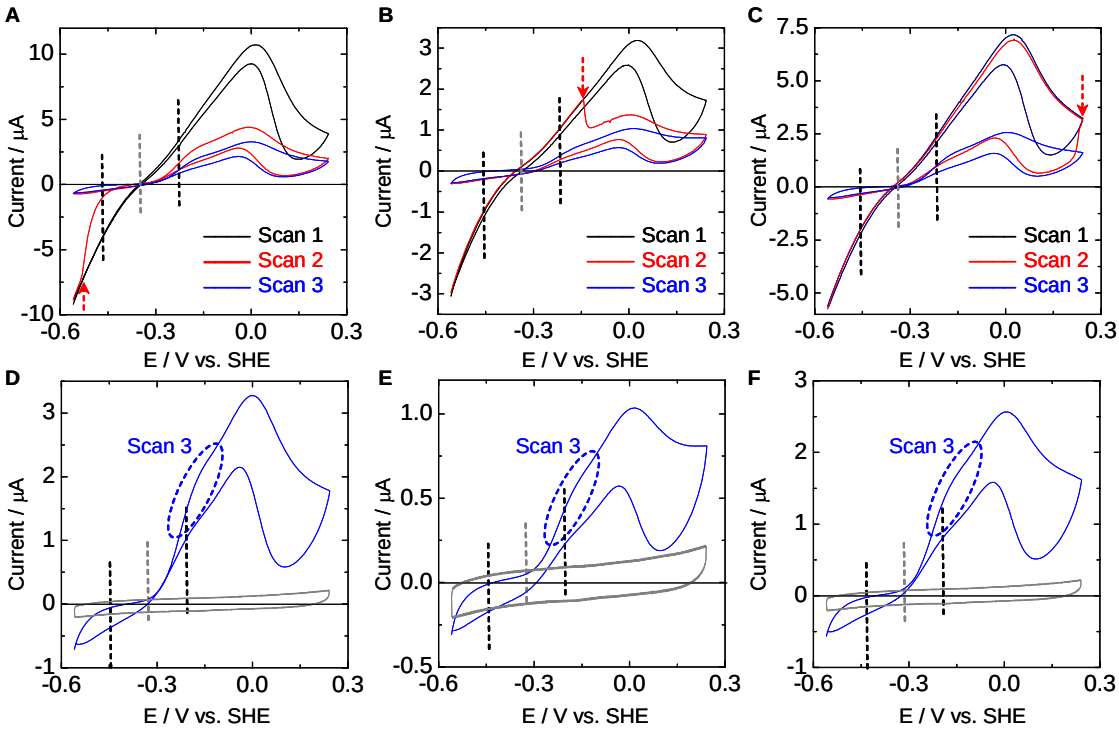

Figure 5.21: Cyclic voltammetry experiments investigating the effect of inhibiting *Cr*HydA1 by injecting formaldehyde at A) -0.5 V, B) -0.15 V and C) +0.24 V. Three scans were recorded in each set and the injection of 45 mM formaldehyde (saturated with H_2) in solution was performed during the second (red) scan at the point marked by the dashed red arrow. The third (blue) scans in A, B, and C, are shown in panels D, E, and F respectively. Experimental conditions: pH 6, 10 ºC, 100% H_2 atmosphere, electrode rotation rate 3000 rpm, 20 mV/s. The vertical dashed grey line marks the thermodynamic potential and the two dashed black lines mark the points in the cyclic voltammograms that are at overpotentials of 0.13 V more negative and more positive than the thermodynamic potential. The features in the dashed blue circles in panels D, E, and F are discussed in the main text. The grey voltammogram in panels D, E and F shows the response of the unmodified electrode in the presence of 45 mM formaldehyde (pH 6, 10 °C, 20 mV/s).

Comparison of panels D, E, and F indicates that similar profiles of the cyclic voltammograms in the presence of formaldehyde (blue scans) resulted from injection at the three different potentials. However, the profile in the presence of formaldehyde differed significantly from that recorded in the absence of formaldehyde (the black scans); a marked shoulder was recorded in the oxidative scans (circled in Figure 5.21D, E, and F) and, to some extent, in the reductive scans too. This feature cannot result from formaldehyde electrochemistry at graphite because it is absent from the scan of the

unmodified electrode (grey line in Figure 5.21D, E, and F). Moreover, in all cases H_2 production was suppressed with respect to H_2 oxidation.[****] Therefore, though the degree of inhibition is potential dependent, the potential at which inhibition initially occurs does not affect catalytic bias in the presence of H_2CO. The catalytic bias was determined by examining the comparative magnitudes of the currents at a given overpotential either side of the thermodynamic potential in the first (black) and third (blue) scans as a measure of the catalytic bias. This ratio was about 1:1 H_2 oxidation: H_2 production in the first scans but increased to approximately 2:1 in the third scans. This is in direct contrast with binding of CO which preferentially suppresses H_2 oxidation (see section 5.3.3.3).

5.4. Discussion

5.4.1. Inhibition by CO

5.4.1.1. Reversible CO inhibition

Quantitative measurements of the inhibition of H_2 production by CO in the form of the $K_I^{app}(CO/H^+)$ were made for a variety of [NiFe(Se)]-hydrogenases and it was found that the *Ralstonia* hydrogenases were the least affected by CO. The values of $K_I^{app}(CO/H_2)$ for the [FeFe]-hydrogenases were found to be very low (< μM). These findings follow perfectly from what has long been known about hydrogenases, that the [NiFe]-hydrogenases are less inhibited by CO than the [NiFeSe]-hydrogenases which are in turn more insensitive to CO than the [FeFe]-hydrogenases.[225] It was also shown that the [FeFe]-hydrogenases are inhibited by CO more slowly than the [NiFe(Se)]-

[****] Verification that the pH of the cell solution had not changed after the experiment (i.e. due to the injection of formaldehyde) ensured that this effect was not the consequence of change in pH.

hydrogenases which may be indicative of a possible physical barrier limiting the rate of diffusion of CO into and out of the enzyme.

The relationship between catalytic bias and sensitivity to CO is an interesting consideration. As previously mentioned the [FeFe]-hydrogenases are more biased towards H_2 production and more sensitive to CO than the [NiFe(Se)]-hydrogenases. A parallel can be drawn between the comparison of the bias and CO inhibition of [FeFe]- and [NiFe(Se)]-hydrogenases and the comparison of the catalytic bias and sensitivity to CO of the two [FeFe]-hydrogenases from *Clostridium pasteurianum*, *Cp*I and *Cp*II.[215] The physiological function of the *Cp*I is H_2 production whilst *Cp*II exhibits very low H_2 production activity.[††††] Also, *Cp*I is much more sensitive to CO than *Cp*II. The fact that this mimics the comparative characteristics of the "H_2-producing" [FeFe]-hydrogenases and the "H_2-oxidising" [NiFe(Se)]-hydrogenases allows us to speculate that there might be a correlation between physiological role in H_2 production (and thus catalytic bias towards H_2 production) and a heightened reactivity to CO.

The rates of inhibition of H_2 oxidation by the [FeFe]-hydrogenases were higher than those measured for the inhibition of H_2 production. Whilst the data in this chapter demonstrate that inhibition of the [FeFe]-hydrogenases occurs at potentials at which they evolve H_2, the results are commensurate, to a certain degree, with the notion, presented by Bennett et al.,[243] that the H_{red} state does not bind CO as the data show that CO is bound much less easily at -0.4 V. One reason that might explain the observation of *any* inhibition of the enzyme at -0.4 V is that H_{red} and H_{ox} are in equilibrium; even though the application of this potential will skew the equilibrium towards the H_{red} side,

[††††] The physiological role of *Cp*II remains a mystery. Adams et al. have postulated that it may actually be a breakdown product in the biosynthesis of *Cp*I.[215]

some H_{ox} will always be present during the catalytic cycle thus any loss of current occurs because the portion of the enzyme in the H_{ox} state is being inhibited and removed from the equilibrium, so it is only when H_{ox} is formed that inhibition occurs. This is depicted in Scheme 5.2. However, this inhibition is not as "direct" as it is at -0.05 V, which is perhaps why it is slower.

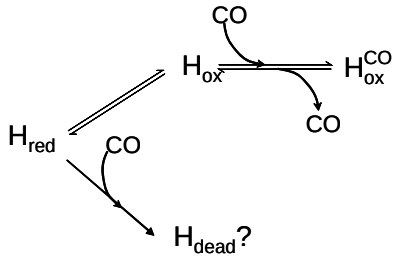

Scheme 5.2: Mechanism of binding of CO to the H-cluster of [FeFe]-hydrogenases

The fact that there is a consistent disparity in rate of inhibition by CO for H_2 oxidation and H_2 production (i.e. H_2 oxidation is inhibited much more rapidly than H_2 production) for all three [FeFe]-hydrogenases is interesting when considering the possibility of the rate of inhibition by CO being limited by a physical barrier, as is indicated by the data presented in Figure 5.18. This suggests either that the direction of catalysis (at the active site) limits the rate of inhibition by CO rather than the gas filter or that the structure of this filter is affected by potential. In the case of the former proposition, there are two possible effects which could lead to a retardation of inhibition of H_2 production relative to H_2 oxidation. Firstly, the position of the equilibrium between the H_{ox} and H_{red} state may be the crucial factor in determining the rate at which the enzyme becomes inhibited, as mentioned above. Alternatively, it may be that the conformation of the CN and CO ligands bound to Fe_D (the atom at which catalysis is supposed to occur) in H_{red} (assuming that H_{red} *does* bind CO, contrary to previous spectroscopic results) being different to that in H_{ox} has some part to play in affecting the rates of inhibition and inhibition constants of these two states. The increased steric hindrance

around Fe_D in the H_{red} state due to the shift of the bridging CO (present in H_{ox}) to the terminally-bound position might disfavour binding of a further ligand to Fe_D. Alternatively it may be that such steric restrictions prevent CO binding to H_{red} at all. The significant structural expansion of the H-cluster in the H_{red} state as compared to the H_{ox} state[67] might also be related to this effect.

The parallel between the potential dependence of $K_I^{app}(CO/H^+)$ for *Rm*MBH (section 5.3.2.1) and the fact that the CO binding of the [FeFe]-hydrogenases is more favourable in the H_2 oxidation domain over the H_2 production domain is noteworthy. This potential dependence of binding of CO to *Rm*MBH also mirrors the potential dependence of the binding of H_2 (Chapter 4, section 4.3.3).

The fact that the rates of recovery ($k_{recover}$) of *Dd*H, *Cr*HydA1 and *Ca*HydA are so similar argues against the notion that this "filter" limits this rate because there is only approximately 40% homology in the sequences of these enzymes. However, the disparity in the rates of CO inhibition ($k_{inhibit}$/[CO]) for these three enzymes suggests that there is at least some filtering effect. Examination of the $k_{inhibit}$/[CO] for H_2 production relative to the $k_{inhibit}$/[CO] for H_2 oxidation refines our understanding of the importance of the gas filter (characterized by k_{in} and k_{out} in Scheme 5.1) in limiting the rate of CO inhibition relative to the rate of reaction at the active site (characterized by k_2 and k_{-2}) for these three enzymes. Table 5.3 illustrates that, whilst the electronic effect (presumably on the active site) is most important for *Dd*H as the discrimination between the rates of CO inhibition of H_2 oxidation vs. H_2 production is strong ($k_{inhibit}(H_2oxidation)$: $k_{inhibit}(H_2$ production) = 63), the discrimination is much lower for *Ca*HydA ($k_{inhibit}(H_2oxidation)$: $k_{inhibit}(H_2$ production) = 3), thus furthering the notion

that the gas filter is more important for this enzyme. Again, *Cr*HydA1 fits in between *Dd*H and *Ca*HydA.

Comparison of the results presented in Figure 5.18 with those previously published on *Df*H and two of its mutants[162] (in which the mutation was made at the entry of the putative gas channel to the active-site) suggests the existence of such a filter. This kinetic study showed that the slow inhibition of a mutant of *Df*H with respect to the WT in experiments such as those shown in Figure 5.18 (i.e. upon injection of CO-saturated buffer) was the result of slow diffusion of the inhibitor to the active site rather than a difference in binding affinity.

However, the experiments exploring the photolability of the CO-inhibited state provide a counterpoint to the discussion in favour of a gas channel. The marked effect of light on *recovery* from CO inhibition of the [FeFe]-hydrogenases indicates that the rate of recovery is limited by breaking of the Fe-CO bond rather than efflux of CO from the H-cluster to the outside of the protein. In contrast with the transport of CO out of the protein which is not expected to be affected by light, Fe-CO complexes are well-known to be photosensitive.[249,251] Thus, whilst the inhibition may be limited by the gas filter (and to a greater extent in the order *Ca*HydA>*Cr*HydA1>*Dd*H), the kinetics of the Fe_D-CO bond-making and -breaking determine the rate of recovery. Further evidence for there being more than a simple gas channel limitation to the rate of reactions with the H-cluster will be presented in Chapter 6 which examines the response of these three [FeFe]-hydrogenases (amongst others) to O_2.

The model represented by Scheme 5.1 can help us to interpret the rate-determining stages of the process of binding and release of CO[248]; this model re-enforces the hypothesis that the gas channel cannot be the only limitation in inhibition by and recovery from CO. The model considers that the attack by CO involves two stages: the first stage is transport of CO from the external medium through the enzyme (for simplicity, this is shown as a single tunnel without branches or sites at which CO could be trapped) to a non-coordinating site close to the H-cluster (this is represented as CO----H); the second stage is migration of CO from the non-coordinating site to a coordination site that is assumed to be Fe_D (the actual inner-sphere binding reaction). The process of re-activation is the reverse of this reaction scheme.

The terms k_{in} and k_{out} are rates of transport of CO through the protein in either direction, and k_2 and k_{-2} are the elementary rates of binding and dissociation of CO, respectively, to Fe_D within the region of the active site pocket. With the simplification that k_{-2}[CO-Fe_D] is negligible until the reaction of inhibitor with enzyme is essentially complete (because the concentration of CO-Fe_D is low), the steady-state approximation with d[CO]/dt = 0 yields:

$$\text{Rate of inactivation} = \frac{k_{in}k_2[\text{CO}][\text{Fe}_D]}{k_{out} + k_2} \qquad \text{Equation 5.2}$$

where the pseudo first-order rate constant, $k_{inhibit}$ (as measured directly in experiments shown in Figure 5.13 and Figure 5.14), is:

$$k_{inhibit} = \frac{k_{in}k_2[\text{CO}]}{k_{out} + k_2} \qquad \text{Equation 5.3}$$

An implication of this model is that k_{in} and k_{out} should depend on the nature of the gas molecule and gas filter but not on the catalytic state of the H-cluster (the state predominating for a particular electrode potential, i.e. H_{ox} or H_{red}). Based on the

evidence that CO binds preferentially (and perhaps exclusively) to H_{ox},[243] it is reasonable to assume that k_2 for CO will be large for H_{ox} and small, even zero, for H_{red}.

Recognizing this is a simplistic model, let us now consider the following limiting scenarios: i) if $k_{out} \leq k_2$ (i.e. egress of CO from the enzyme is favoured over formation of the Fe_D-CO bond), $k_{inhibit} \sim k_{in}[CO]$ so the rate of inhibitor binding depends only on the external concentration of CO and rate of internal transport of CO; in this case little discrimination is expected based on the redox state of the H-cluster. Alternatively, ii), if $k_{out} >> k_2$, i.e. if the protein's internal structure does not provide an effective barrier to transport of CO, it follows that $k_{inhibit} = k_2 k_{in}[CO]/k_{out}$. In this scenario, the rate of inhibition depends not only on [CO] and the internal structure of the enzyme but also upon k_2 and therefore should also be faster for conditions favouring H_{ox} (H_2 oxidation) compared to H_{red} (H_2 production).

Recovery from CO follows the reverse sequence, and for $k_{in}[CO] = 0$ (because only the portion of the experiment after which [CO] = 0 is analysed to determine $k_{recover}$), Equation 5.4 is obtained

$$\text{Rate of recovery} = \frac{k_{out} k_{-2} [\text{CO - - - - - Fe}_D]}{k_{out} + k_2} \qquad \text{Equation 5.5}$$

and the first-order rate constant (as measured experimentally) is given by:

$$k_{recover} = \frac{k_{out} k_{-2}}{k_{out} + k_2} \qquad \text{Equation 5.6}$$

Under the limiting condition $k_{out} << k_2$, $k_{recover} = k_{out} k_{-2}/k_2$; whereas if $k_{out} >> k_2$, the rate of re-activation reduces to k_{-2} reflecting the likelihood that CO escapes from the enzyme (indicated by a high k_{out}) before it can re-coordinate (indicated by a high k_2). The data presented in this chapter, especially those demonstrating the photolability of

recovery from CO inhibition (Figure 5.19), suggest that the latter situation must generally be the case, with a more intermediate situation (a smaller k_{out} relative to k_2) applying for *Ca*HydA.

5.4.1.2. Irreversible CO inhibition of [FeFe]-hydrogenases

Whilst the gas filter may play an important part in limiting the rate of CO inhibition (characterized by $k_{inhibit}$) in both H_2 oxidation and production, the fact that irreversibility arises only whilst the enzyme is producing H_2 implies that two very different reactions with CO occur in the two states of the enzyme. The expansion of the H-cluster in the H_{red} state[252] may correlate with the irreversibility of CO-binding exhibited only in the H_2-production potential range.

The irreversible binding of CO when the potential is poised at -0.4 V is represented as formation of H_{dead} in Scheme 5.2. This finding is interesting in the light of the controversial[243] results from experiments performed on *Cp*I and *Cp*II by Adams[242] which describe irreversible binding of CO to *Cp*I. In this study, the irreversibly-bound CO-adduct was generated in the presence of sodium dithionite as a sacrificial electron donor maintaining the turnover of catalytic H_2 production; this adds weight to the hypothesis that the reversibility of CO inhibition is a function of the state of the enzyme, with that present when the enzyme is more reduced (and thus able to catalyse H_2 production) being the one that is susceptible to irreversible CO binding. This is the first electrochemical demonstration that binding of CO to hydrogenases can be irreversible. This feature is more conspicuous in the experiments performed on the *Cr*HydA1 and *Ca*HydA enzymes than on those performed on *Dd*H. Whilst it may occur to a very small degree for *Dd*H, the instability of films of this enzyme on the electrode

significantly convolutes the analysis. It is impossible to ascertain whether or not the small loss of current observed in Figure 5.4 when the enzyme has fully recovered from inhibition by 1% CO as compared to the current prior to inhibition is simply due to film loss in the elapsed 3000 s or due to a degree of irreversibility of binding. In the case of *Cr*HydA1 and *Ca*HydA, it is also shown that the reversibility is independent of the presence of H_2.

The mechanism of irreversible inhibition by CO remains a source for discussion but it is clear that the fact that irreversible CO-inhibition only occurs in the H^+ reduction direction implies that the activation pathway for removal of CO from the active site is modified only in this direction; either a sink in the reaction pathway or a very large activation barrier is reached, indicative of a "trapped" CO adduct. There a few possibilities for the mechanism of formation the trapped adduct:

1. Direct insertion of CO into the Fe-H bond (this hydride only being present under more strongly reducing conditions) and a possible subsequent attack by the putative N atom in the thiolate bridging ligand.

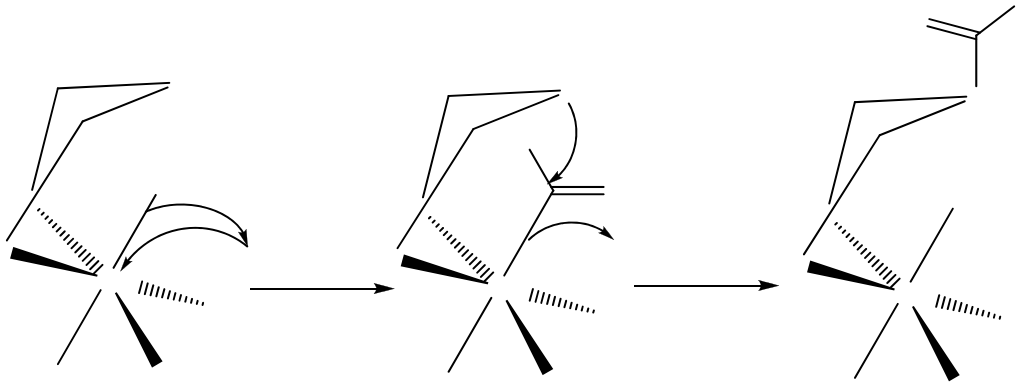

Scheme 5.3: A putative mechanism for irreversible CO inhibition of [FeFe]-hydrogenases by initial insertion of CO into the Fe-H bond to form a formyl adduct followed by a possible attack by the nitrogen atom in the thiolate bridging ligand. Only the Fe_D is shown for clarity.

2. Conserted migration of the hydride to one of the endogenous CO ligands and binding of exogenous CO (CO_{ex}) in the first instance. Note that this leaves the formyl adduct further way from the putative N atom in the thiolate ligand than in Scheme 5.3 thus interchange of the positions of the CO_{ex} and the formyl adduct must first take place before a potential nucleophilic attack on the formyl ligand as described above to occur.

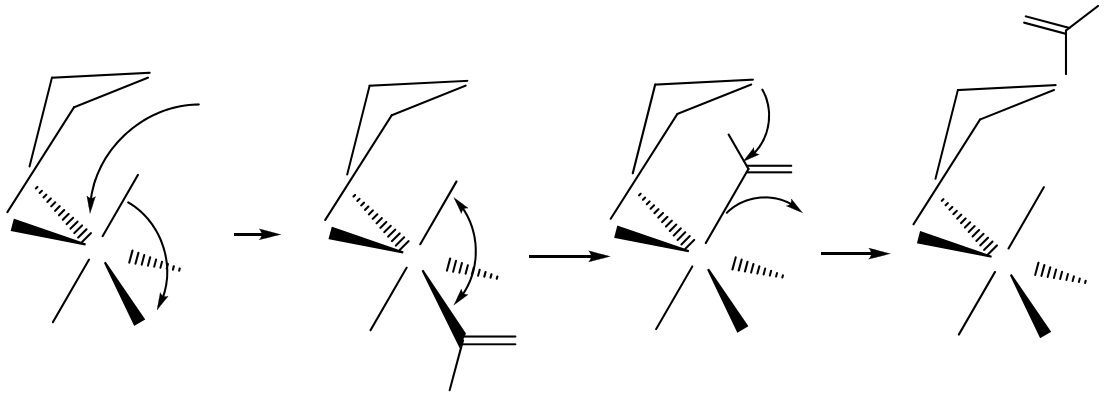

Scheme 5.4: A putative mechanism for irreversible CO inhibition by of [FeFe]-hydrogenases by conserted binding of exogenous CO (CO_{ex}) to Fe_D and migration of the hydride ligand to the CO ligand to which it is *cis*. Subsequent to a possible interconversion of the positions of CO_{ex} and the formyl ligand, attack by the thiolate N atom might proceed as in Scheme 5.3. Only the Fe_D is shown for clarity.

Thus, irreversible inhibition could result by the formation of a very stable formyl adduct preventing the binding of hydride at Fe_D or by alteration of the proton transfer pathway if the putative thiolate N atom is indeed involved in it.[66]

5.4.2. Inhibition by formaldehyde

Whilst the binding of the bimolecular π-acceptor ligands CO, H_2, and O_2 proceeds more favourably at higher potentials, the opposite is true of binding of formaldehyde. This strongly suggests that the mode of inhibition is different in this case. One possibility, aside from that shown in Reaction 5.1, is that formaldehyde could act as a Schiff base

NH

CO

and *reversibly* bind to a lysine, either in the active site cavity or in the gas filter, thus inhibiting catalysis (Reaction 5.2[253]).

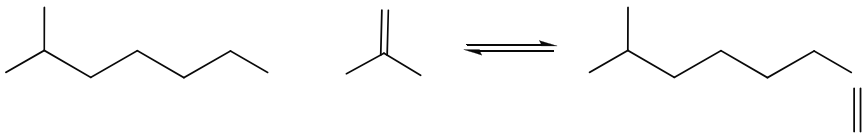

Reaction 5.2

One lysine and one glutamate residue are conserved throughout [FeFe]-hydrogenases in the protein motif around the active site.[35] Examples of how this lysine might fit into a potential proton transfer pathway involving the H-cluster Fe_D-CN ligand and a glutamate residue three residues along the chain (as proposed by Fontecilla-Camps et al.[66]) for *Dd*H, *Cr*HydA1, *Ca*HydA and *Cp*I are shown in Figure 5.17. Thus, inhibition would proceed via blockage of the proton transfer chain. Such transfer paths have been identified for both the [NiFe]-[66,81,116] and [FeFe]-hydrogenase.[119]

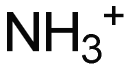

Binding of H_2CO could also occur at the putative N-atom (also thought to be involved in proton transfer[126,130]) in the bridgehead position of the bridging ligand in a similar fashion as that described by Reaction 5.2. However, it is not possible at this stage to identify the structure H_2CO-adduct; the experiments described above should be inspirational for future electrochemical and spectroscopic studies.

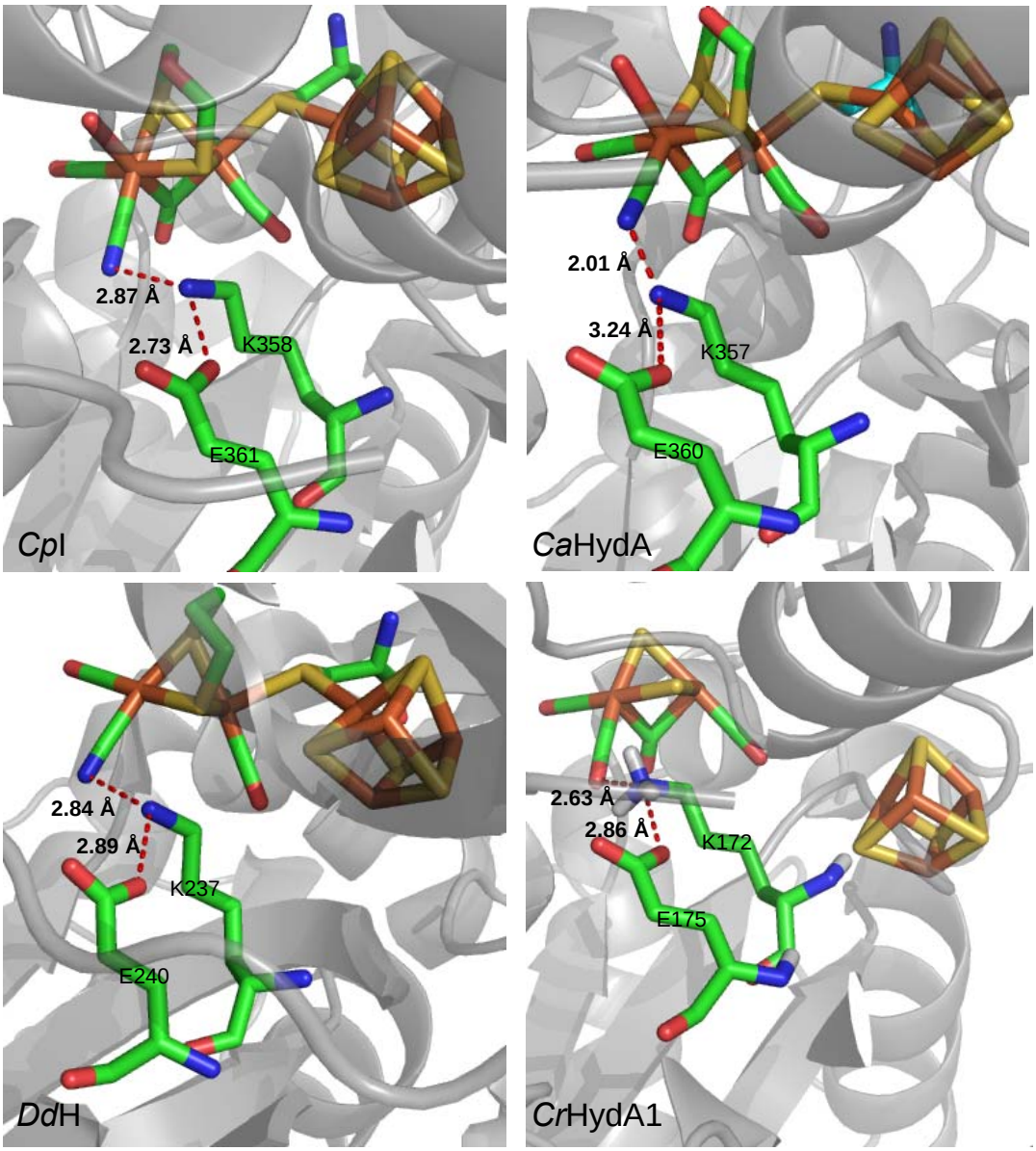

Figure 5.22: Structures of *Cp*I, *Ca*HydA, *Dd*H and *Cr*HydA1 showing the key lysine and glutamate residues involved in a putative proton transfer pathway. *Cp*I PDB code: 3C8Y.[122] *Ca*HydA model generated using MODBASE software[213] accessed at http://modbase.compbio.ucsf.edu/ModWeb20-html/modweb.html. *Dd*H PDB code: 1HFE.[119] *Cr*HydA1 model prepared using PyMOL by S. Stripp (U. Bochum))

Chapter 6:

Reactions of Hydrogenases with O_2

6.1. Abstract

The reactions of a range of hydrogenases with O_2 when poised to produce and oxidise H_2 are examined. Direct reduction of O_2 at graphite presents a problem for measurement of hydrogenase-catalysed H_2 production as O_2 is reduced at graphite at potentials below 0 V (see Chapter 2). Therefore, a method for distinguishing H_2 production activity from O_2 reduction at graphite was developed. *Re*MBH is shown to sustain H_2 production in the presence of high levels of O_2. It was found that the [NiFeSe]-hydrogenase *Db*H, which is more biased towards H_2 production than the [NiFe]-hydrogenases discussed in this thesis, is inactivated by very low concentrations of O_2 (5 μM) when it is oxidising H_2. However, the fact that *Db*H was found to reactivate very fast from O_2 at potentials below -0.25 V suggested that it would be capable of sustaining H_2 production in the presence of O_2 and this was confirmed by experiments performed in the H_2-production potential range. Results showing the response of [FeFe]-hydrogenases to O_2 are presented: these enzymes, especially *Ca*HydA, react much more slowly with O_2 than suggested by the reports of the O_2 sensitivity of [FeFe]-hydrogenase. It is shown that *Dd*H reacts at least ten times faster with O_2 when oxidising H_2 than when producing H_2 whilst this disparity in rates of reaction was not observed for *Ca*HydA. A comparison of these results is used to draw conclusions as to the rate-limiting step in the reactions with O_2 for the [FeFe]-hydrogenases. These rates are much slower than those obtained for inhibition by CO. This leads to the conclusion that, though a physical filter may limit the rate of reaction of such inhibitors with the [FeFe]-hydrogenases as suggested by the results presented in Chapter 5, a further reaction, such as the permanent modification of the active site, also lowers the rate at which these enzymes react with O_2. Lastly, CO is shown to protect

*Cr*HydA1 from complete inactivation by O_2 which implies that at some point in the mechanism of O_2 inactivation, O_2 must bind at the same site as CO, i.e. Fe_D.

6.2. Introduction

The response of different hydrogenases to O_2 varies greatly. Whilst the [NiFe]-hydrogenases from Knallgas bacteria *Ralstonia* are reversibly and only partially inhibited by O_2 and can continue to catalyse H_2 oxidation in air,[254,255] those from anaerobes, such as *Dg*H, require reductive reactivation to recover from exposure to O_2.[18,247] At the other extreme, the [FeFe]-hydrogenase are generally irreversibly damaged by O_2[18,36] with the [4Fe4S]-cluster in the H-cluster proposed to be the site of O_2 attack from EXAFS results.[211,221] However, there have been reports of partial reversibility of O_2 damage to *Ca*HydA[220] and the [FeFe]-hydrogenase from *Clostridium pasteurianum,* which at that point had not yet been identified as either *Cp*I or *Cp*II.[233]

This chapter aims to probe the origins of these discrepancies along the lines of three different mechanisms for O_2 tolerance[88] (as illustrated in Scheme 6.1), with a particular emphasis on the effect of O_2 on the states present during H_2 production:

A) ACCESS: A filter slows down the approach of O_2 to the active site.

B) REACTION: Exposure to O_2 does not form an irreversible adduct or an adduct that is slow to convert to the active form.

C) RECOVERY: O_2 binds much more easily to the enzyme when it is poised at certain potentials and/or can be reactivated much more rapidly by stepping the potential down below a certain level.

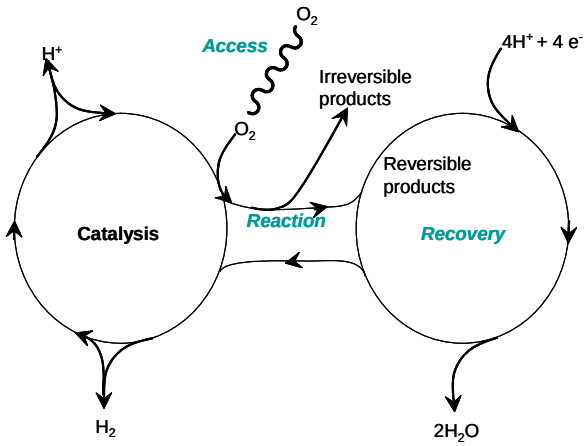

Scheme 6.1: Reactions of hydrogenase-catalysed H_2 production with O_2 to produce reversible and irreversible products.

For both [NiFe(Se)]- and [FeFe]-hydrogenases, O_2 has been shown to bind at the active site.[91,220,256] The mechanism of inactivation of the [NiFe]-hydrogenases has received more attention than that of the [FeFe]-hydrogenases. Lamle et al.[105] and Fontecilla-Camps[91] have argued that formation of the "Unready" Ni-A state only occurs in the presence of O_2 and that a partially reduced form of O_2 (hydroperoxo-) probably bridges the Ni and Fe atoms in the active site. This species is slow to reactivate, and would therefore be an "irreversible product" in the context of Scheme 6.1. Also formed upon exposure to O_2 is the Ni-B state for some enzyme molecules, and this can recover much more rapidly, therefore it is a "reversible product". The proportion of Ni-A to Ni-B is modulated by the electron richness of the environment the enzyme is experiencing when exposed to O_2; thus, under N_2 at higher potentials, a greater proportion of Ni-A is formed whereas lower potentials and the presence of H_2 favour the formation of Ni-B.[105] Intriguing exceptions to this are the membrane-bound hydrogenases from *Ralstonia* for which the "Unready" Ni-A state has not been observed.[257] By not forming the Ni-A species, which is slow to reactivate from O_2, these enzymes retain the ability to function in the aerobic environments experienced by the organisms from which they come. Other aspects of the O_2 sensitivity of [NiFe]-hydrogenases have also been

probed. Mutation of the residues close to the active site *Df*H have highlighted the importance of a potential gas channel in retarding O_2 inactivation.[162] The ligation of the [3Fe4S]-subcluster in the [NiFe]-hydrogenase from *Azotobacter vinelandii* was also shown to be crucial: a mutant bearing a serine in the place of a cysteine ligating the cluster was found to be much more tolerant to O_2 in terms of its H_2 oxidation activity and not to suffer from inhibition of H_2 production by H_2.[258]

Perusal of the literature on [FeFe]-hydrogenases informs on their susceptibility towards irreversible inactivation by O_2[32,73] involving complex redox chemistry, the products of which are still a matter of speculation.[221] In contrast, inhibition of these hydrogenases by CO is thought to be a simple competitive process[232,234,235] (at least in the case of H_2 oxidation - see Chapter 5) in which CO binds to Fe_D without significantly modifying the redox properties of the H-cluster. Thus, inhibition by CO is at least in part limited by diffusion of gas to the active site, therefore it can be used as a probe to reveal the kinetics of gas transfer across the enzyme. Molecules of CO have similar Lennard-Jones radii to those of O_2 (3.47 Å for O_2 and 3.69 Å for CO[231]); this implies that CO and O_2 could travel across the protein at similar rates if we assume that sterics limit the rate of transfer. In this chapter, the comparison of the rates of inactivation by O_2 with those for inhibition by CO are thus used to separate the kinetics of gas transfer of bi-molecules from those of the reaction of O_2 with the H-cluster. Additionally, the locus of O_2 attack is an important question addressed here.

6.2.1. Investigating H_2 production in the presence of O_2

With respect to the inactivation of hydrogenase-catalysed H_2 oxidation by O_2, less is known about the effects of O_2 on H_2 production as they cannot easily be probed in

solution or on an electrode. For the H_2 oxidation reaction, many electrochemical investigations[18,104,105,204,216,220] have been performed on the reactions of hydrogenases adsorbed onto graphite with O_2. This reaction occurs at potentials more positive than -0.35 V (at pH 6, 20 °C, 100% H_2). Most hydrogenases anaerobically inactivate at higher potentials (around 0 V, again depending on experimental conditions) but in most cases some H_2 oxidation is recorded above this potential. This means that the issue of direct reduction of O_2 at graphite complicating rates of inactivation of the hydrogenase has been by-passed in the aforementioned investigations by only performing electrochemical studies of this kind at potentials above 0 V. However, this excludes the possibility of interrogating hydrogenase-catalysed H_2 production in the presence of O_2. A novel method for distinguishing H_2 production from O_2 reduction is detailed in this chapter.[205,209,248] Hydrogenase-catalysed H^+ reduction (H_2 production) is distinguished by introducing a gaseous inhibitor into the oxygenated gas stream and measuring the rapid attenuation and restoration of current as catalysis is first blocked and then recovers as the inhibitor is flushed out.[205,209] In this case, this electrochemical method is superior to biochemical enzyme activity assay techniques involving soluble electron donors (e.g. sodium dithionite) and mediators (such as methyl viologen) as these react with and are removed by O_2. A schematic summarising the three stages in the experimental design is shown in Figure 6.1A.

This chapter shows typical results of experiments performed on a variety of hydrogenase chosen for this study to reflect the diversity of the behaviour of these enzymes in the presence of O_2, though many more experiments were performed than are included here. At one end of the spectrum of hydrogenases, the *Ralstonia* hydrogenases are amongst the least biased towards H_2 production that have been characterized

electrochemically (see Chapter 4, section 4.3.1), but they are amongst the most O_2-tolerant of the hydrogenases studied so far.[18] In fact, an artificial device involving a complex consisting of *Re*MBH ligated to a cyanobacterial Photosystem I has been exploited to produce H_2.[259] It thus followed that the investigation of hydrogenase-catalysed H_2 production in the presence of O_2 should begin by examining the reactivity of these enzymes to O_2 when catalysing H_2 production (see section 6.3.1). The behaviour of *Re*MBH, which is not thought to exhibit the Ni-A state on exposure to O_2, is contrasted to that of an enzyme which *does* convert into the Ni-A state under such conditions, *Dg*H (section 6.3.2). The catalytic bias for H_2 production exhibited by *Db*H (Figure 4.2) underlies the interest in investigating the possibility of this enzyme continuing to function in the direction of H_2 production in the presence of O_2. At the other end of the spectrum, the subject of the O_2 sensitivity of the [FeFe]-hydrogenases is important as these enzymes have been shown (in this thesis and elsewhere[5,18,88]) to be the most biased towards H_2 production. Thus, the effect of O_2 on H_2 production by an algal enzyme (*Cr*HydA1), an enzyme that produces H_2 as a by-product of fermentation (*Ca*HydA) and a H_2-oxidising [FeFe]-hydrogenase (*Dd*H) (an enzyme of known crystal structure for comparison) are examined in section 6.3.4.2.

Also investigated in this study is the comparative response of H_2 *oxidation* by *Db*H, *Dd*H, *Cr*HydA1 and *Ca*HydA to O_2. The kinetics of the attenuation of H_2 oxidation activity of [FeFe]-hydrogenases due to O_2 are also compared to the rate at which H_2 production activity diminishes and this comparison is used to strengthen our understanding of the limitations to the reaction with O_2 (see Discussion, section 6.4).

6.3. Results

6.3.1. H_2 production by [NiFe]-hydrogenase from an aerobe in the presence of O_2

Experiments designed to probe the ability of *Re*MBH to reduce H^+ in the presence of O_2 are shown in Figure 6.1B and Figure 6.2. The three key stages in the experiments exploring H_2 production in the presence of O_2 throughout this chapter are depicted in Figure 6.1A. As discussed in Chapter 5, H_2 production by the *Ralstonia* membrane-bound hydrogenases is much more strongly inhibited by H_2 than by CO[209] so H_2 was used as the inhibitor in these experiments. In both cases the experiment commenced with an atmosphere of N_2 in the headspace of the cell. After a constant current level was established, the headgas was changed to a mixture of 5% H_2 in N_2 (0.04 mM H_2), which resulted in a rapid loss of 90% of the current. The headgas was then switched back to 100% N_2 causing the H^+ reduction current slowly to recover. This marked the end of the first stage of the experiment. In stage 2, the headgas was first changed to 2% O_2 in N_2 (22 μM O_2), which resulted in a large increase in current, as expected, due to direct (non-enzymatic) O_2 reduction at graphite. At t = 1400 s, the headgas was changed to 2% O_2, 5% H_2, and 93% N_2; that is, a repeat of the first stage except in the presence of O_2. As before, a rapid loss of current is observed (0.15 μA), and this is of a similar magnitude to the attenuation observed during the anaerobic Stage 1 (0.17 μA). The headgas was switched back to 2% O_2 in N_2 to remove the inhibitory H_2, and the current recovered. In stage 3, anaerobic conditions were restored by replacing the headgas with N_2. The activity of the enzyme returned to the initial level recorded before O_2 was introduced into the cell, and the gas exchanges of Stage 1 were then repeated.

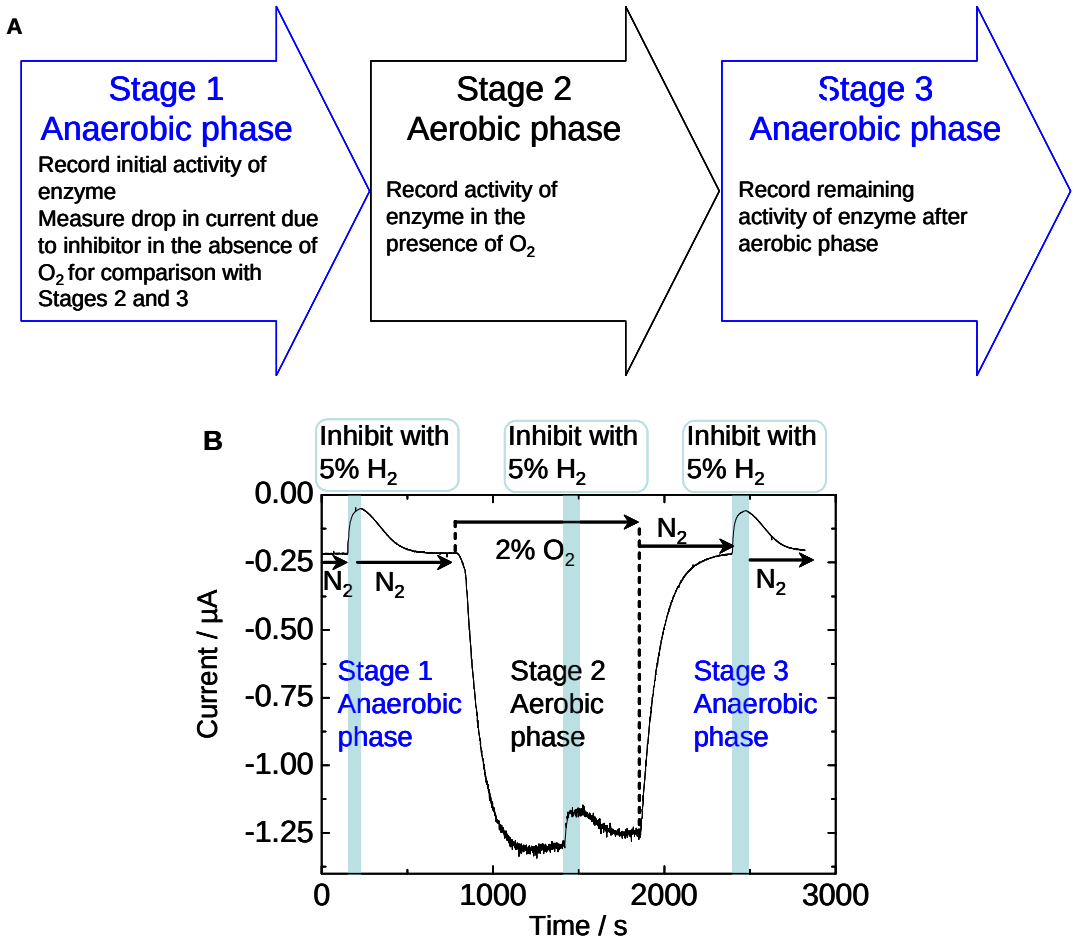

Figure 6.1: Chronoamperometry experiment designed to demonstrate H_2 production by *Re*MBH in the presence of 2% O_2 in the headspace. A schematic of the three stages and is shown in panel A and the experiment is shown in panel B. Experimental conditions: pH 5.5, 30 °C, 3000 rpm, -0.45 V. Gas mixtures as indicated; blue boxes highlight periods of inhibition by H_2 and N_2 is the carrier gas at all times.

A correction factor is required to calculate the actual level of O_2 experienced by the enzyme at the electrode surface due to the electrochemical consumption of O_2. Using the method described in Chapter 2 (section 2.8.1), it was calculated that more than 1% O_2 (16 µM) survives at the electrode surface under these conditions. The similar attenuation of current amplitudes in all three inhibition phases shows that the H^+ reduction activity of the enzyme is little affected 16 µM O_2. This is the first demonstration of H^+ reduction by a hydrogenase in the presence of O_2.[209] However, for technological applications of hydrogenases, activity at higher O_2 levels is desirable.

Figure 6.2 depicts a far more ambitious experiment with 21% O_2 present in the headgas (207 μM in solution) throughout Stage 2. Under the conditions of this experiment, it is estimated from the control experiments described in Chapter 2 that at least 13% O_2 (0.14 mM) survives at the electrode to be experienced by the hydrogenase. This experiment on *Re*MBH was carried out at 40 °C to enhance catalytic H_2 production and 10% H_2 was used as the inhibitor in this case. A similar effect was observed: the crucial attenuation of reduction current upon introduction of H_2 in the aerobic phase was clearly evident as before,[209] although the trace was noisier. Some activity may have been lost during the aerobic phase when H_2 was introduced and then removed, but note also that because >95% of the current here is due to O_2 reduction, even a small decrease in this component dominates the result (see the control experiment in Chapter 2, Figure 2.10, where a small change in the O_2 reduction rate is recorded between t = 800 and 1300 s; this may be the consequence of spoiling of the graphite surface by reduced O_2 species). The final stage of the experiment, measuring the H^+ reduction activity remaining after the aerobic phase, shows that more than 60% of the initial activity remains; at least part of the 40% attenuation in activity could be accounted for simply by film loss. In a final extreme trial, an experiment probing whether or not H_2 production could be sustained under an atmosphere of 40% O_2 (0.37 mM) was carried out, but the trace was too noisy to resolve the current due to enzymatic H_2 production under O_2.

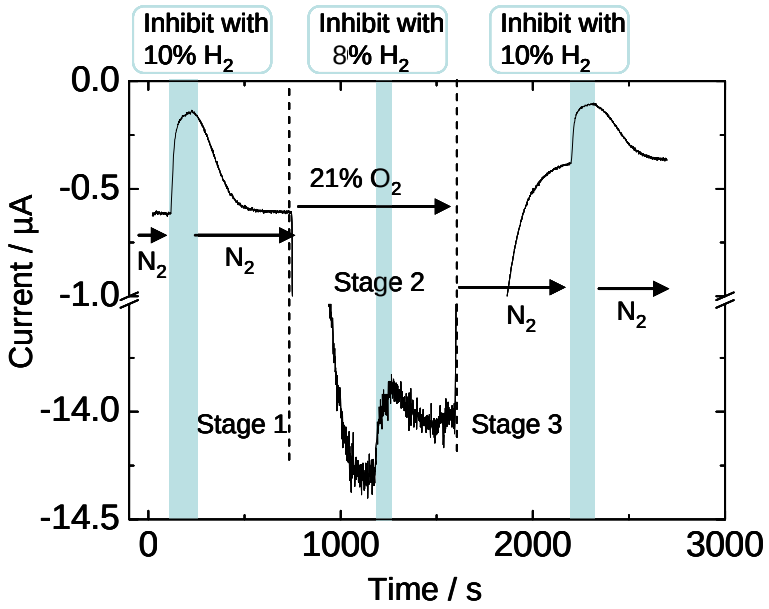

Figure 6.2: Chronoamperometry experiment designed to demonstrate H_2 production by *Re*MBH in the presence of 21% O_2 in the headspace. Experimental conditions: pH 5.5, 40 °C, electrode rotation rate 3000 rpm, -0.45 V. Gas mixtures as indicated; blue boxes highlight periods of inhibition by H_2, N_2 is the carrier gas at all times.

The O_2 inhibition of H_2 oxidation by *Re*MBH has been examined using PFE[18] and it has been shown to form a Ni-B-like state (which reactivates rapidly) upon exposure to O_2. Furthermore, release of inhibition of this enzyme from O_2 is accelerated by the application of increasingly negative potentials.[260] If some of the same states involved in the inhibition H_2 oxidation are relevant to the inhibition of H_2 production, the rapidity of the removal of any inhibitory O_2 (which allows catalysis to continue) may be related to the fact that the Ni-A state is not formed and that the low potential reactivates the Ni-B state to the active Ni-C state within the lifetime of the catalytic cycle.

6.3.2. H_2 production by [NiFe]-hydrogenase from an anaerobe in the presence of O_2

In contrast to *Re*MBH, *Dg*H is expressed by an *anaerobic* bacterium. A variety of techniques including FTIR,[247] EPR,[261] X-ray crystallography,[91] and PFE[18] have been

employed to characterize the various oxidation states of *Dg*H, and it was shown that this enzyme does exhibit the "Unready" Ni-A state.

The possibility for continued H_2 production by *Dg*H in the presence of O_2 was probed by performing experiments analogous to those described above. Given how slowly the Ni-A state of this enzyme is known to reactivate,[18] it was expected that H_2 production in the presence of O_2 would not be observed. Figure 6.3 shows an experiment in which *Dg*H is subjected to 1% O_2 at -0.4 V. As *Dg*H is much more strongly inhibited by CO than H_2[88] (see section 5.3.1.1), the inhibitor of choice in this case is 10% CO. As in the experiments shown in Figure 6.2, this concentration of inhibitor was chosen as it was found to be sufficient to inhibit the enzyme almost fully (~90%) as seen when the gas was changed to 10% CO in N_2 (highlighted in the light-blue box) from 100% N_2 in Stage 1 of the experiment. As the CO was subsequently flushed from the cell with N_2, the activity of the enzyme recovered and the current increased. When 1% O_2 was introduced into the cell in Stage 2 an immediate drop in current was observed, followed quickly by a plateau being reached. This is explained by the concurrence of two different processes: rapid inactivation of the hydrogenase and slower equilibration of O_2 with the cell solution. Reintroduction of CO into the cell in Stage 2 lead to a much smaller loss of current than was observed in the inhibition phase in Stage 1, thus confirming that the hydrogenase is active but to a much lesser degree than under anaerobic conditions. Removal of CO from the cell by flushing with the carrier 1% O_2 in N_2 lead to a small increase in current as the enzyme recovered from CO inhibition. When the O_2 was removed from the cell in Stage 3, an attenuation of current was recorded as a consequence of the loss of the component of the current that corresponded to O_2 reduction at graphite. Flushing 10% CO in N_2 back into the cell lead to a further

decrease in current, this time solely due to inhibition of the hydrogenase, as in Stage 1. The current increased rapidly for the first 500 s after switching the headgas back to N_2 as CO was removed from solution and inhibition of the enzyme was relieved. The current continued to increase slowly for a further 6000 s (see inset in Figure 6.3), consistent with slow reactivation of the Ni-A state observed after inhibition under H_2-oxidising conditions ($t_{1/2}$ = 35 min at 30 °C[18] and 29 min at 40 °C[247]).

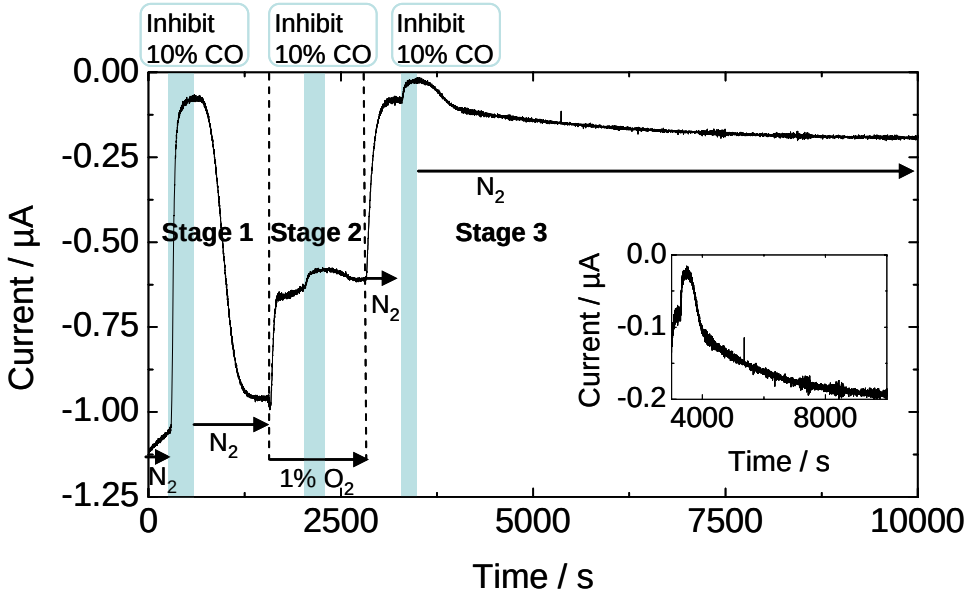

Figure 6.3: Chronoamperometry experiment designed to demonstrate H_2 production by *Dg*H in the presence of 1% O_2 in the headspace. Experimental conditions: pH 6, electrode rotation rate 3000 rpm, 20 °C, -0.4 V. Gas mixtures as indicated; blue boxes highlight periods of inhibition by CO and N_2 was the carrier gas at all times.

The experiment in Figure 6.3 shows that *Dg*H maintains some activity under 1% O_2 in the headgas (11.5 µM at the electrode), which is perhaps surprising given the sensitivity of this enzyme to O_2 under H_2-oxidising conditions, However, whereas *Re*MBH remains almost fully active under 21% O_2, *Dg*H is rendered almost completely inactive (~90%) by this low concentration of O_2. A separate experiment at 21% O_2 (Figure 6.4) confirmed that this enzyme was not capable of sustaining H_2 production in the presence of O_2 to the same degree as *Re*MBH under equivalent conditions (pH 5.5, 40 °C, Figure 6.2). A high concentration of the inhibitory CO was chosen for the experiment shown in Figure 6.4 to maximise the possibility of seeing a change in current due to inhibition

of the hydrogenase by CO in the presence of O_2. The set-up of the gas-feed into the cell was such that 100% CO was introduced to inhibit the enzyme in Stages 1 and 3 but as 21% O_2 was present in Stage 2, the percentage of CO in the headspace had to be reduced to 79%. This is equivalent to 964 μM CO in solution which far exceeds the $K_I^{app}(CO/H^+)$ measured for this enzyme (Chapter 5 - 3 μM), thus even this lower concentration of CO in solution should still have been sufficient to give rise to a noticeable attenuation in activity had the enzyme been active. However, as evidenced in Figure 6.4, no such drop of current was observed in Stage 2. (The slow decrease in current between 1300 and 1750 s resulting from a decrease in O_2 reduction with time was observed in many control experiments such as that shown in Figure 2.10). Furthermore, when O_2 was removed from the cell, virtually no current remained. The inset in Figure 6.4 shines a spotlight on the fact that very little activity remained after the aerobic phase. The tiny drop in current recorded when 100% CO was introduced in to the cell in Stage 3, attests to this.[‡‡‡‡]

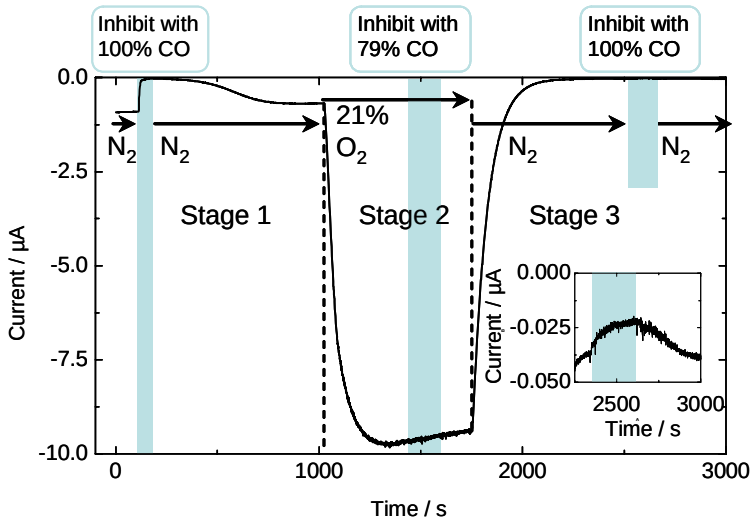

Figure 6.4: Chronoamperometry experiment designed to demonstrate H_2 production by *Dg*H in the presence of 21% O_2 in the headspace. Experimental conditions: pH 5.5, 40 °C, -0.4 V, electrode rotation rate 3000 rpm. Gas mixtures as indicated; blue boxes highlight periods of inhibition by CO and N_2 is the carrier gas at all times.

‡‡‡‡ Upon inhibition, the current did not decrease to zero; this was the result of the small current offset (~20 nA) on the blank electrode often observed at these low potentials.[216]

6.3.3. Reactions of a [NiFeSe]-hydrogenase with O_2

Valente et al. reported[89] that the [NiFeSe]-hydrogenase from *Dv* Hildenborough was more O_2-tolerant than expected by demonstrating that it could easily be aerobically purified. It has been suggested that steric blockage of the active site by Se (a larger atom than S) accounts for the increased O_2 tolerance of [NiFeSe]-hydrogenases.[66] To establish whether or not O_2 tolerance is a general feature of [NiFeSe]-hydrogenases, the behaviour of *Db*H was investigated. A study carried by Parkin et al.[205] identified the formation of two species upon inactivation of *Db*H with O_2 through cyclic voltammetry experiments similar to that shown in Figure 6.5 (see section 6.3.3.1).

6.3.3.1. H_2 oxidation by *Db*H in the presence of O_2

In the experiment shown in Figure 6.5, the potential was swept from -0.55 V to +0.24 V and an injection of O_2-saturated buffer was performed at a potential at which *Db*H catalyses H_2 oxidation; the current dropped immediately to zero following the O_2 injection. Once the potential reached +0.23 V, the potential was held for 5 minutes (to ensure that all the O_2 had been flushed out of solution) before being swept back to -0.55 V. This prevented a current due to O_2-reduction at graphite convoluting the observation of enzyme reactivation processes occurring below -0.1 V on the return scan, and ensured that the enzyme was reactivated under fully anaerobic conditions. The features corresponding to the two reactivation processes previously described are highlighted in the inset in Figure 6.5.

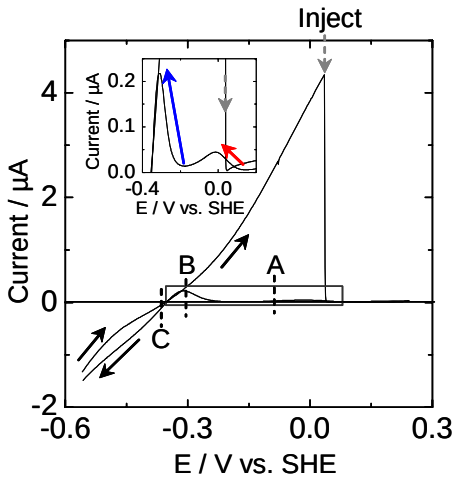

Figure 6.5: Experiments designed to probe recovery of *Db*H from aerobic inactivation. Inactivation was achieved by injection of O_2-saturated buffer to a final concentration of 16 µM O_2 in the cell at the point marked by the dashed grey arrow. Other conditions: pH 6, 30 ° C, 100% H_2 atmosphere, electrode rotation rate 3000 rpm, scan rate 1 mV/s. The points marked A, B and C by the vertical dashed lines indicate the points on the catalytic wave at which the experiments in Figure 6.6 panels A, B, and C (respectively) were performed. The black arrows mark the direction of the sweeps. The blue and red arrows mark the increase in activity representing reactivation of the Ni-A and Ni-B species, respectively.

The inset in Figure 6.5 clearly shows that the current corresponding to H_2-oxidation rose within two different potential ranges, (marked by the blue and red arrows) as the reductive sweep progressed, confirming the formation of two species upon aerobic inactivation. These two species were attributed to "Ready" Ni-B (the species reactivating at higher potentials) and "Unready" Ni-A (the species reactivating at more negative potentials) because of their relative ease of conversion to the active state upon reduction.[205]

A chronoamperometric study was undertaken to determine the rates of reactivation of these two species (Figure 6.6). Panel A shows an experiment aimed at resolving the rate of reactivation only of the species able to reactivate at the higher potential, thought to be the "Ready" Ni-B. Thus, reactivation was brought about at -0.11 V. At the start of the experiment, the potential was held at -0.55 V to ensure that the enzyme film was fully active. A negative current corresponding to H^+ reduction by the enzyme was

recorded at this potential. The potential was then stepped up to +0.34 V, and 150 µL of O_2-saturated buffer was immediately injected into the cell, initially containing 2 mL of buffered electrolyte (final concentration = 76 µM O_2 in solution). This inactivated the enzyme immediately such that the current dropped to zero. The potential was held at this level for 1200 s so as to allow all the O_2 to be removed before the potential was stepped down to -0.11 V to induce reactivation recorded as an increase in positive current due to recovery of H_2-oxidation activity. Panel B shows an experiment in which the first two potential steps were the same as in panel A[§§§§] (except that the potential was held at +0.34 V for an extra 800 s) and reactivation (in the third step) was induced by lowering the potential to -0.31 V to reactivate the remaining inactive enzyme, i.e. that in both the Ni-A and Ni-B states. In the experiment in panel C, the enzyme was reactivated at -0.38 V. Reference to Figure 6.5 shows that this potential is just within the potential domain in which *Db*H produces H_2. As H_2 is an inhibitor of H_2 production (see Chapter 4), this experiment was performed under Ar so as to minimise inhibition by H_2 complicating the reactivation from O_2 inactivation.

[§§§§] As the scale of the experiment shown in panel B is smaller than those of panels A and C, it can be seen that the current following the injection of the O_2-saturated buffer does not drop exactly to zero but to ~0.02 µA. This current is due to a small offset from the electrode at this potential rather than an remaining hydrogenase activity.

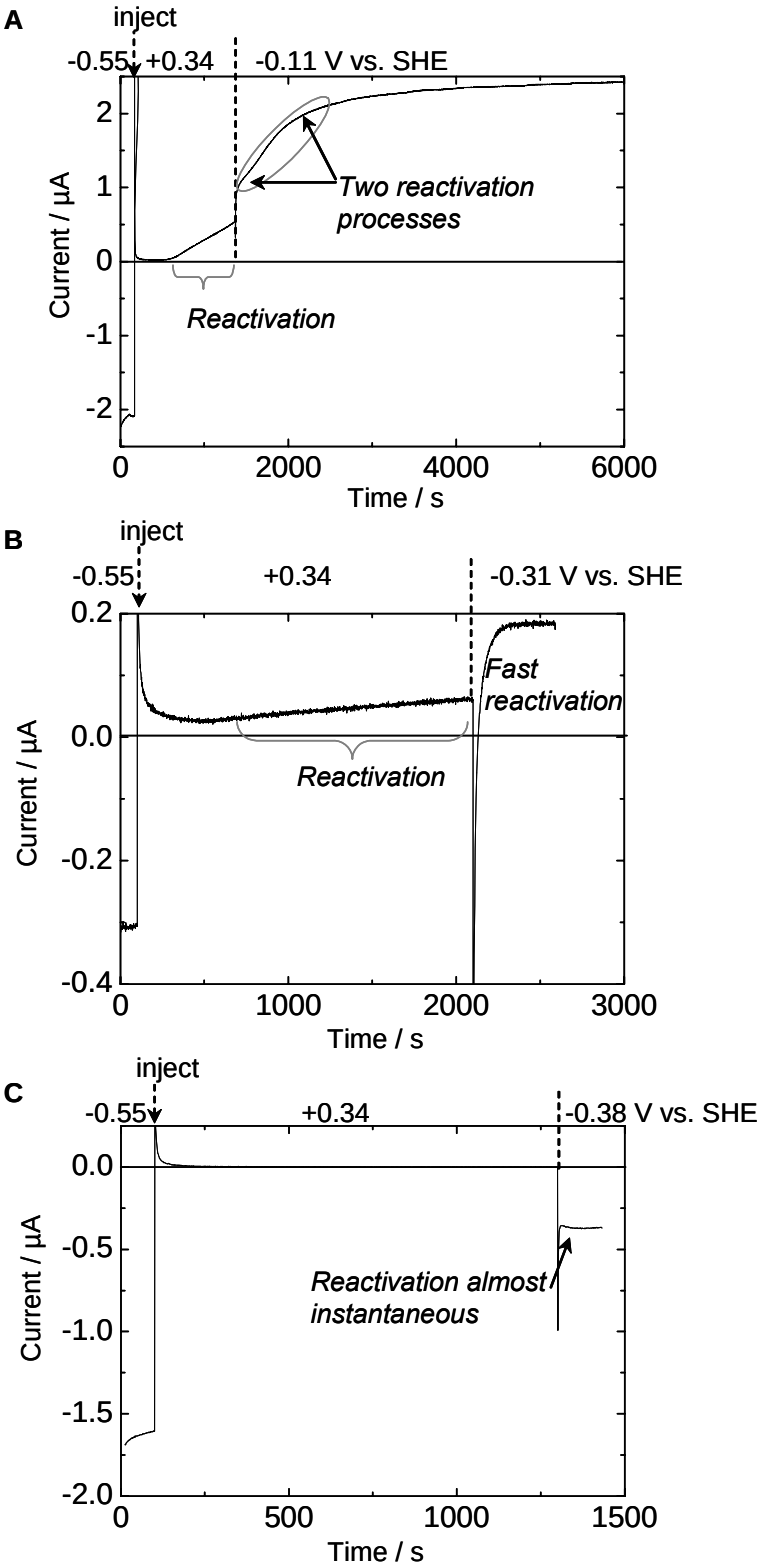

Figure 6.6: Experiments designed to investigate the potential dependence of reactivation of *Db*H from O_2 inactivation. The potential step sequence and the point of injection of O_2-saturated buffer (to give final concentrations of O_2 in solution of 76 µM for A and 52 µM for B and C) are as marked. Experimental conditions: pH 6, 30 °C, electrode rotation rate 2500 rpm, 100% H_2 atmosphere in panels A and B, 100% Ar atmosphere in panel C.

The slow increase in current whilst the potential was held at +0.34 V in the experiments shown in panels A and B indicates that the enzyme is actually able to reactivate at this high potential. This increase did not commence until approximately 400 s after the injection of the O_2-saturated buffer, probably correlating with the time taken for O_2 to flush out of the cell solution.

When the potential was stepped down to -0.11 V in panel A, the recovery of activity sped up substantially and the current appeared to increase in two phases, indicating that two different reactivation processes, corresponding to the two species formed upon aerobic inactivation, were underway. Whilst this experiment could thus not be used to determine the exact individual rates of the reactivation processes of the two species generated by aerobic inactivation as these processes overlapped in time, it does inform on the fact that both species *are* able to reactivate at a high potential, but the rates at which they reactivate differ. In cyclic voltammetry, this gives rise to the features shown in the inset in Figure 6.5 as the species appearing to recover over the lower potential range ("Unready" Ni-A) does not experience the higher potential range for a long enough period to reactivate and thus only reactivates within the timescale of the voltammetric experiment when the driving force is large enough.

Stepping the potential to -0.31 V in panel B induced a much more rapid and seemingly monophasic reactivation process. Panel C shows that reactivation at a slightly more negative potential, just at the positive limit of the range in which *Db*H produces H_2, is sufficiently reducing to reactivate the enzyme almost instantaneously.[205] Most of the enzyme was re-activated within the capacitive current 'spike' (i.e. the dead time caused by the potential step, usually less than 10 seconds[262]). This was confirmed in numerous

other experiments: using a more negative reactivation potential (below ~-0.38 V) all the reaction occurred within the dead time of the potential step. Re-activation after treatment with O_2 is therefore fast in this potential region, and *Db*H can clearly reactivate much faster than *Dg*H (half-life $t_{1/2}$ ~ 30 min).[18,247]

The fact that reactivation of *Db*H only occurs rapidly at electrode potentials close to the thermodynamic potential of the $2H^+/H_2$ couple suggests that this enzyme cannot oxidize H_2 in the presence of O_2. This is confirmed by the experiment shown in Figure 6.7 where the enzyme was held at 0 V under a 5% H_2 in N_2 atmosphere in the headspace and an injection of O_2 was performed, leading to a final concentration of 0.5% in the cell.[205] The low concentrations of H_2 in the headspace and of O_2 in solution after injection in this experiment were chosen so as to be closely comparable to the experiments performed under N_2 to investigate inactivation of H_2 production by *Db*H in the presence of O_2 (see below, Figure 6.8). This injection obliterated the activity within 2 s.

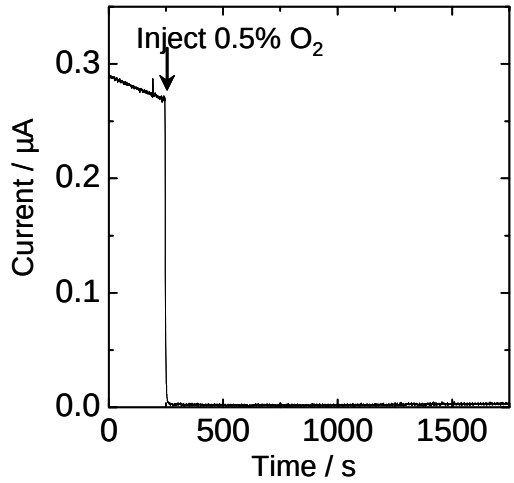

Figure 6.7: Inactivation of *Db*H at +0.24 V by injection of O_2-saturated buffer. Final concentration of O_2 = 0.5% (5.5 µM O_2 in solution). Experimental conditions: pH 6, 30 °C, 5% H_2 in N_2, electrode rotation rate 3000 rpm.

6.3.3.2. H_2 production by *Db*H in the presence of O_2

The rapidity of reactivation at potentials close to or below the thermodynamic potential of the $2H^+/H_2$ couple suggested that it might be possible to achieve sustainable H_2 production by *Db*H in the presence of small quantities of O_2. Therefore an experiment employing the method described above for the investigation of H_2 production by *Rm*MBH[209] and *Dg*H in the presence of O_2 was carried out on *Db*H (Figure 6.8).[205] As *Db*H is more strongly inhibited by CO than H_2 (see Figure 5.3), the inhibition phases were induced by flushing with CO in the headspace. A 1% fraction of CO in the headspace was sufficient to eliminate 90% of the activity.

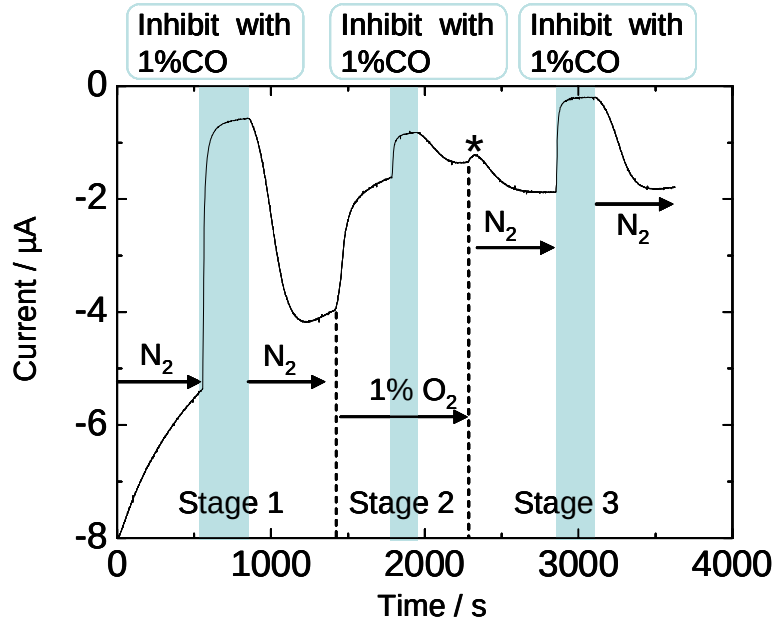

Figure 6.8: Chronoamperometry experiment designed to demonstrate H_2 production by *Db*H in the presence of 1% O_2 in the headspace, 30 °C. Experimental conditions: pH 6, electrode rotation rate 3000 rpm, -0.45 V. Gas mixtures as indicated; blue boxes highlight periods of inhibition by CO and the carrier gas is N_2 at all times.

The experiment commenced under 100% N_2: the steady loss of current in the first 500 s was the result of film loss. When 1% CO was introduced into the cell an immediate 90% drop in activity was recorded. The headgas was then changed back to 100% N_2 and an increase in current ensued. The introduction of 1% O_2 resulted in a sharp decrease in current which, again, tended to a steady level. The loss of current at this

stage is due to inhibition of *Db*H by O_2, but is superimposed on an increase in current due to graphite reduction of O_2. A further drop in current was observed when 1% CO was reintroduced into the cell, indicating that the enzyme was catalysing H^+ reduction (in the presence of O_2) prior to that point. When the CO was removed from the cell by flushing with 1% O_2 in N_2, the current rose as inhibition was released. Removal of O_2 from the cell by flushing with N_2 resulted in an initial decrease in current (indicated by *) due to depletion of O_2 to be reduced at graphite, followed by an increase in current due to recovery of *Db*H from inactivation by O_2. This recovery was substantially faster than that observed for *Dg*H in Figure 6.3; this is commensurate with the fact that *Db*H reactivates much more rapidly at low potentials than *Dg*H. This increase in current due to recovery of *Db*H activity appears slower than expected from the experiments shown in Figure 6.5 (in which the O_2 had been removed from the cell *prior* to reactivation by stepping the potential to -0.38 V) because O_2 was flushing out of solution *as* the enzyme reactivated. A final inhibition phase with 1% CO was performed to confirm that the enzyme is still active. When 1% CO was flushed into the cell, another 90% drop in current was recorded. The current then increased when the CO was removed by flushing with 100% N_2.

As described in Chapter 2, 1% O_2 in the headspace at -0.45 V leaves at least 0.5% O_2 to be experienced by the enzyme. It was determined that exposing the enzyme to 0.5% O_2 at +0.24 V represent an absolute minimum level of O_2 experienced at -0.45 V in the experiments shown in Figure 6.7. Whilst Figure 6.7 demonstrates that *Db*H cannot oxidise H_2 in the presence of 0.5% O_2, Figure 6.8 shows that it can *produce* H_2 under a minimum of 0.5% O_2.

The steady loss of current at the beginning of the experiment shown in Figure 6.8 is attributable to film loss. The method described above was employed in the experiment shown in Figure 6.9 but a lower temperature (20 °C) was applied; this induced a lower rate of film loss so the data are less convoluted by a steady loss of film over time. Since gas equilibration times and the inhibition of the enzyme are slower at this temperature, the experiment was conducted over a longer timescale.

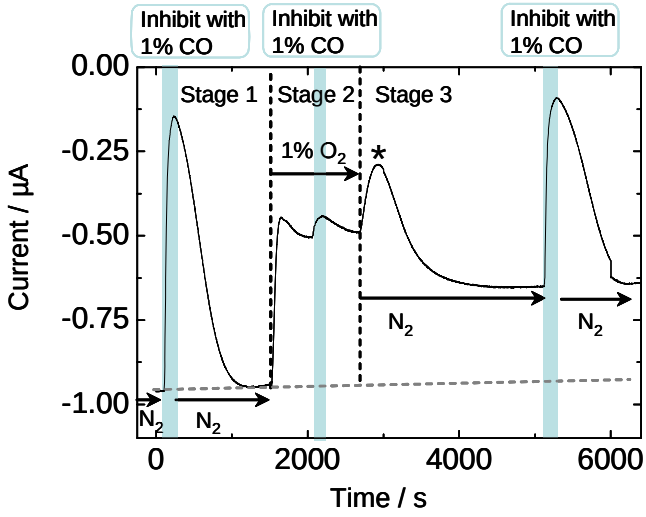

Figure 6.9: Chronoamperometry experiment designed to demonstrate H_2 production by *Db*H in the presence of 1% O_2, 20 °C. Experimental conditions: pH 6, electrode rotation rate 3000 rpm, -0.45 V. Gas mixtures as indicated; blue boxes highlight period of inhibition by CO and the carrier gas is N_2 at all times. The dashed grey line gives a visual guide to the progression of film loss throughout the experiments. The drop in current recorded at t = 6000 s is due to the passage of time in which the experiment (i.e. the recording of the current at -0.45 V) stopped and had to be restarted.

Upon introduction of O_2 at 1500 s the current resulting from H^+ reduction by *Db*H decreased immediately, reaching a minimum at 1600 s. This was due to rapid inhibition of hydrogenase-catalyzed H_2 production. The reduction current then slowly increased to a stable level of -0.55 µA because the current due to O_2 reduction increased as O_2 equilibrated with the solution. This feature was absent in Figure 6.8 because the magnitude of H_2 production current was much larger with respect to that from O_2 reduction; O_2 inhibition of H_2 production was therefore the predominant characteristic in this phase of the experiment shown in Figure 6.8. The feature marked * in Figure 6.8

(loss of reduction current upon immediate removal of O_2, followed by an increase in reduction current due to release of O_2 inhibition of the enzyme) was accentuated in Figure 6.9. This reflects the greater enzymatic current (with respect to the O_2 reduction current) observed in Figure 6.8 due to the higher temperature and, possibly, variation in enzyme film coverage on the electrode. Figure 6.9 also shows a projected line indicating the path of film loss. The discrepancy between projected and actual current at t = 6000 s suggests that some irreversible changes have occurred due to O_2.

Further experiments performed on *Db*H reveal that this enzyme is not able to sustain H_2 production at higher concentrations of O_2 as evidenced by the fact that current attenuation under 10% O_2 is very small when 1% CO is introduced in Stage 2 in Figure 6.10. When the CO was subsequently removed from the gas stream, no increase in current was observed, indicating that O_2 inactivation of the enzyme had annihilated the remaining H_2 production activity in the meantime. Upon removal of the O_2 from the cell, the current immediately decreased as expected in the first 500 s of Stage 3; however, the current increased after the O_2 had been flushed out until it reached a plateau (between t = 2800 s and 3500 s, see inset in Figure 6.10), indicating reactivation of the enzyme from O_2.

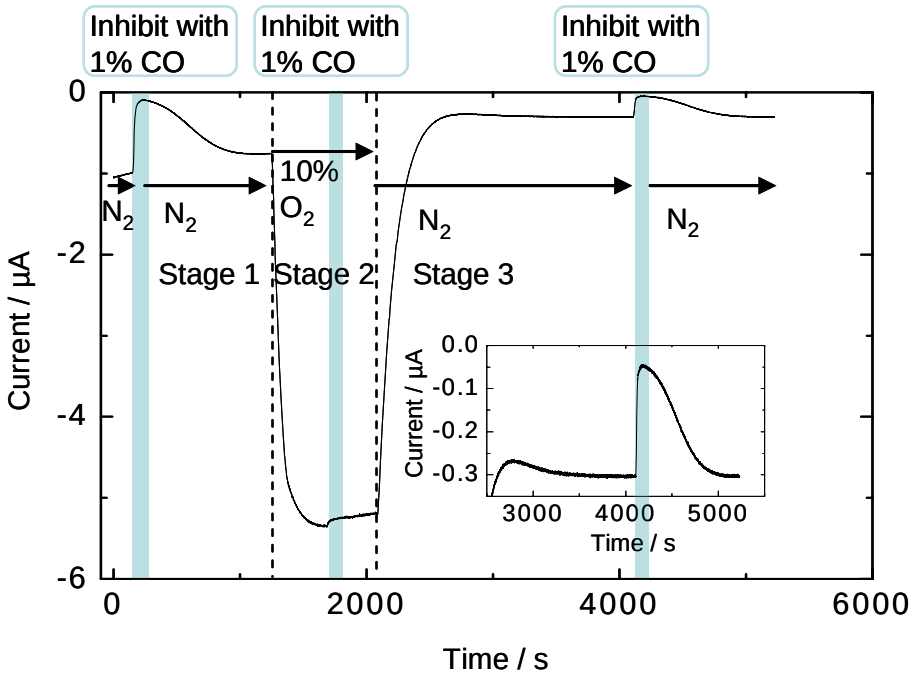

Figure 6.10: Chronoamperometry experiment designed to demonstrate H_2 production by *Db*H in the presence of 10% O_2. Experimental conditions: pH 6, 22 °C, electrode rotation rate 3000 rpm, -0.45 V. Gas mixtures as indicated; blue boxes highlight periods of inhibition by CO and the carrier gas is N_2 at all times.

The difference in appearance between Figure 6.9 and Figure 6.10 upon introduction of 1% O_2 into the cell requires explanation. In Figure 6.9, the current initially decreases as the enzyme is immediately inactivated and then increases as the O_2 equilibrates with solution and O_2 reduction becomes the principal component of the total current. In contrast, Figure 6.10 shows that flushing the cell with 10% O_2 leads to an immediate increase in current. This is because the predominant component of the current is the O_2 reduction at graphite as the concentration of O_2 is ten times higher than it is in the experiment shown in Figure 6.9.

6.3.4. Reactions of [FeFe]-hydrogenases with O_2

6.3.4.1. H_2 oxidation in the presence of O_2

A detailed study of the rates of inactivation of *Dd*H, *Cr*HydA1 and *Ca*HydA by O_2 was undertaken so as to compare the behaviour of these enzyme in the presence of O_2 when oxidising and producing H_2.[248] The potential at which these experiments were carried out was chosen to minimise O_2 reduction at graphite (which defined the more negative limit of the potential being applied) and anaerobic inactivation of the hydrogenase (which defined the more positive limit of the potential range). In fact, there is some overlap between the range of potentials at which O_2 is reduced at graphite and that at which anaerobic inactivation of the hydrogenases occurs. Thus, some experimental compromise (or rather a choice between a slight convolution due to a small underlying current generated by O_2 reduction and a rapid loss of enzyme activity due to high-potential inactivation occurring alongside aerobic inactivation) had to be made. In this instance, the former option was deemed favourable because the contribution due to the current from O_2 reduction was very low and control experiments on a blank electrode could be performed to subtract this component from the experiment (see Figure 2.12).

For a clear comparison of the effect of a given concentration of O_2 on *Dd*H, *Ca*HydA and *Cr*HydA1, only the experiments in which these enzymes were inactivated under 5% O_2 are shown in panels A, B, and C. The log-transform plots (Log(*i*) vs. time) for *all* the experiments at different [O_2] at 10 °C are shown in Figure 6.11D, E, and F from which the rate-constant *k* could be calculated. For each enzyme, the *k* values obtained at each concentration of O_2 (calculated from the gradient of the log transforms) are plotted in Figure 6.12C. As films of *Dd*H are so unstable on the electrode, the experiments comparing the three enzymes were performed at 10 °C. The lengthy experiments (> 2h)

probing the effect of O_2 on H_2 production by these enzymes (described below, section 6.3.3.2) were also carried out at this low temperature so as to avoid film loss complicating the current response over the time of the experiments. Results from experiments to determine the dependence of k for *Dd*H on [O_2] are shown in Figure 6.11A and D and Figure 6.12C. These were carried out at four different levels of O_2 (0.5, 2, 5 and 10% in the headspace). The log transform of the experiment performed under 10% O_2 is not included in Figure 6.11D because the reaction with O_2 was so fast that k was effectively incalculable. For *Cr*HydA1 and *Ca*HydA, the study of dependence of k on [O_2] was performed at 20 °C, a more physiologically relevant temperature. The results are shown in Figure 6.12.

An integral aspect of the design of these experiments was that mass-flow controllers should be used to ensure that the H_2 concentration in solution remained constant throughout the experiment, as with those involving inhibition by CO described in Chapter 5. This prevented the kinetics of the aerobic inactivation being complicated by simple substrate depletion. In the experiments shown in Figure 6.11, the experiments performed at 10 °C on *Dd*H, *Cr*HydA1 and *Ca*HydA commenced under 80% H_2, 20% N_2. When the headspace was flushed with 80% H_2, 15% N_2, 5% O_2, an attenuation of the current was recorded. In the case of *Dd*H and *Cr*HydA1, the rate of this current drop was found to be relatively rapid (as was the case for CO inhibition of all three enzymes – see Chapter 5), therefore, in initial experiments in which O_2 was introduced into the cell by simple gas exchange, the calculated rates of inactivation were complicated by the fact that the O_2 concentration was increasing as the activity was dropping. Thus, for *Dd*H and *Cr*HydA1 it was essential to ensure that the delivery of O_2 was instantaneous therefore O_2 was flushed into the headspace with a simultaneous

injection of 0.67 mL of buffer saturated with 80% H_2, 20% O_2 (at the point marked by the dashed arrow on Figure 6.11) into the 2 mL of solution initially present in the cell. As inactivation of *Ca*HydA was so slow, the injection was not necessary as the rate of equilibration of O_2 (introduced by gas-exchange) with the cell solution was far greater to that of inactivation (the rates are shown in Figure 6.11C and F). Once the current had dropped to zero, the headspace of the cell was then returned to 80% H_2, 20% N_2. Figure 6.12 shows experiments carried out at 20 °C on *Cr*HydA1 and *Ca*HydA using exactly the same method. For Figure 6.11A, B and C, Figure 6.12A and B, Figure 6.13A and B and Figure 6.14A, the current axis represents the experimentally recorded current minus the small contribution from O_2 reduction at graphite as calculated by the control experiments described in Chapter 2 (section 2.8.2). This ensures that the results accurately reflect kinetics of O_2 inactivation without convolution from O_2 reduction at the electrode. For each of the log-transform plots shown in Figure 6.11D, E, and F, Figure 6.12D and E, Figure 6.13C and D and Figure 6.14B, the log function is applied to the current normalised to the level recorded just prior to the injection for ease of comparison of the results at different concentration of O_2. This normalisation does not affect the rate constants calculated from the slope of the log-transform plots.

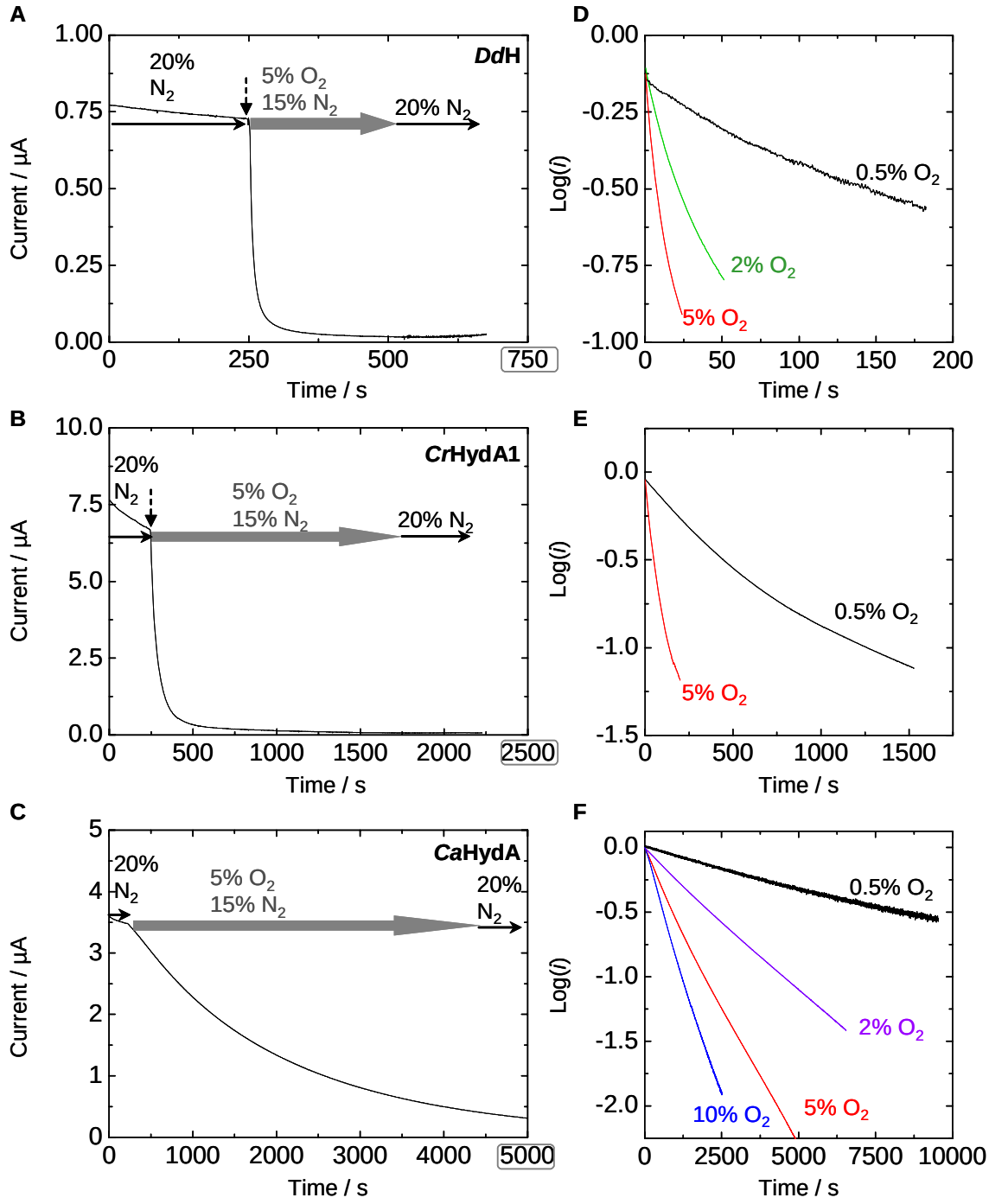

Figure 6.11: Comparison of rates of O_2 inactivation of H_2 oxidation by A) *Dd*H, B) *Cr*HydA1 and C) *Ca*HydA at 10 °C. Panels A and B) Inactivation of *Dd*H and *Cr*HydA1 (respectively) by simultaneous injection (marked by vertical dashed arrow) of 0.67 mL buffer saturated with 20% O_2 (80% H_2) into the 2 mL of buffer already in the cell and flushing of the headspace with the mixtures indicated. C) Inactivation of *Ca*HydA by flushing of the headspace with the mixtures indicated. Experimental conditions: pH 6, 10 °C, -0.05 V, electrode rotation rate 3000 rpm. Panels D, E and F show log transforms of the normalised currents for the experiments performed on inactivation of *Dd*H, *Cr*HydA1 and *Ca*HydA, respectively, at the [O_2] concentrations indicated. Time is shown as zero at the point at which O_2 was introduced into the cell.

For *Dd*H, the reaction was relatively fast ($t_{1/2}$ ~50 s when inactivation is induced by 4 μM O_2 in the cell), though still slower than for the [NiFe(Se)]-hydrogenases, for example *Db*H which is inhibited immediately on injection of O_2-saturated buffer to give the same final concentration in the cell (Figure 6.7). For *Cr*HydA1 and *Ca*HydA, the inactivation by O_2 proceeds much more slowly. In fact, even under 20% O_2 in the headspace of the cell, inactivation of *Ca*HydA has a half-life of 460 s at 10 °C.

When the O_2 was removed by flushing with 80% H_2, 20% N_2 a very small increase in current was recorded indicative of a very low degree of reactivation. On the scale of the experiments shown in Figure 6.11 this is only noticeable for *Dd*H (and even then, it is extremely subtle) and not noticeable at all in the experiments shown in Figure 6.12, but further examination of this effect in section 6.3.4.3 shows that all three [FeFe]-hydrogenases do reactivate to some degree. However, this degree of reactivation in no way equals that of the [NiFe(Se)]-hydrogenases which can recover up to 100% of their activity (for the *Ralstonia* enzymes for example) after exposure to O_2.[59,254]

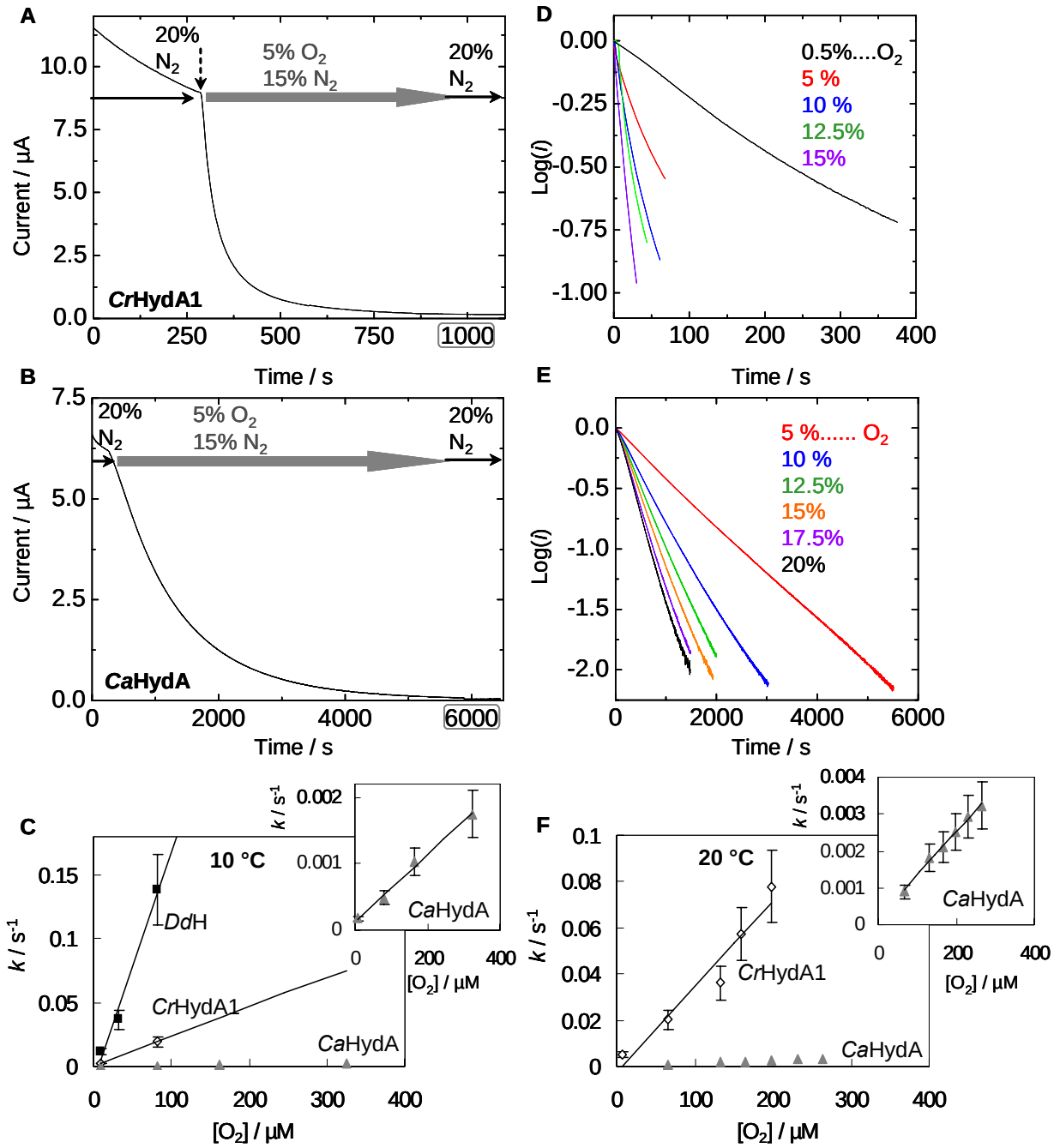

Figure 6.12: Comparison of rates of O_2 inactivation of A) *Cr*HydA1 and B) *Ca*HydA at 20°C. A) Inactivation of *Cr*HydA1 by simultaneous injection (marked by vertical dashed arrow) of 0.67 mL buffer saturated with 20% O_2 (80% H_2) into the 2 mL of buffer already in the cell and flushing of the headspace with the mixtures indicated. B) Inactivation of *Ca*HydA by flushing of the headspace with the mixtures indicated. Experimental conditions for A, B, D and E: pH 6, 20 °C, -0.05 V, electrode rotation rate 3000 rpm. Panels C and F) plots showing the dependence of the rate constant *k* for aerobic inactivation on [O_2] at 10 °C and 20 °C, respectively; insets show the *Ca*HydA results only. Panels D and E show log transforms of the normalised currents for the experiments performed on inactivation of *Cr*HydA1 and *Ca*HydA at the [O_2] concentrations indicated at 20 °C. Time is shown as zero from the point at which O_2 was introduced into the cell.

Whilst the log transforms of the experiments carried out on *Dd*H and *Cr*HydA1 are only linear for one to two half-lives and the error bars in the calculation for *k* are larger, the log transforms of the experiments performed on *Ca*HydA are linear for at least three half-lives and the error bars in this case are smaller. It is clear from Figure 6.12, panels C and F, that the dependence of *k* on the concentration of [O_2] is linear at both 10 °C and 20 °C. Moreover, increasing the temperature by 10 °C approximately doubles the rate of O_2 inactivation of *Cr*HydA1 and *Ca*HydA.

The study of the dependence of rate of inactivation by O_2 on the concentration of H_2 experienced by the enzyme can inform on the locus of O_2 attack. The experiments shown in Figure 6.13, panels A and B, were performed on *Cr*HydA1 and *Ca*HydA by using the method described above, under 8 and 80% H_2 in the headspace. The corresponding log transforms are shown in Figure 6.13, panels C and D. As inactivation is so much more rapid for *Dd*H, the subtle effect of H_2 concentration was not observable over the margin of error in the experiments so the results are not shown below.

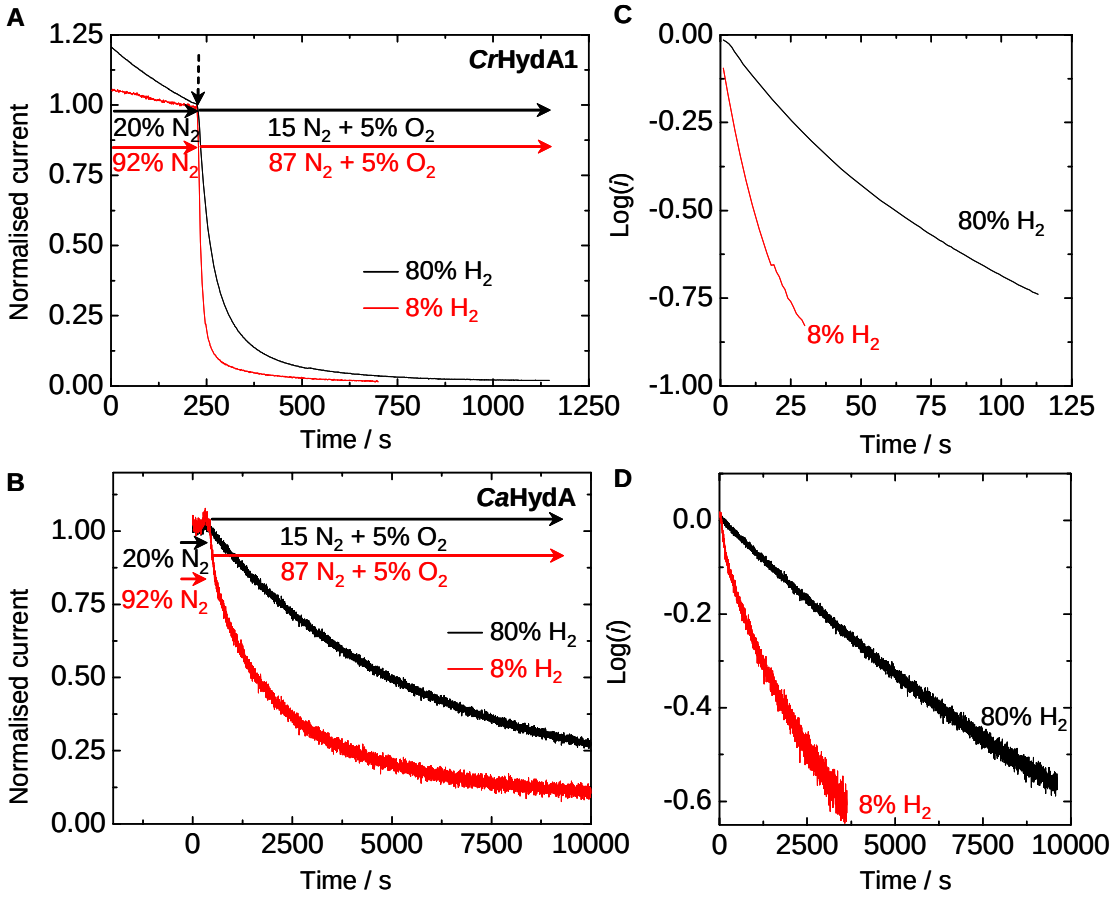

Figure 6.13: Dependence of the rate of O_2 inactivation of A) *Cr*HydA1 and B) *Ca*HydA on the concentration of H_2. A) Inactivation of *Cr*HydA1 by 5% O_2 in 8% (red trace) and 80% H_2 (black trace). Experimental conditions: pH 6, 20 °C, electrode rotation rate 3000 rpm, -0.05 V, gas mixtures as indicated and injection of 2 mL buffer saturated with 10% O_2, 82 % N_2, 8% H_2 (red trace) or 0.67 mL buffer saturated with 20% O_2, 80% H_2 (black trace) at the point indicated by the dashed arrow. B) Inactivation of *Ca*HydA by 0.5% O_2 in 8% (red trace) and 80% H_2 (black trace). Experimental conditions: pH 6, 10 °C, electrode rotation rate 3000 rpm, -0.05 V, gas mixtures as indicated. Panels C and D) log transform of experiments on *Cr*HydA1 and *Ca*HydA, respectively. Time is shown as zero at the point at which O_2 was introduced into the cell.

For *Cr*HydA1 and *Ca*HydA, inactivation proceeded more rapidly at 8% than at 80% H_2. The half-lives for inactivation are 25 s and 75 s for *Cr*HydA1 under 8% and 80% respectively and ~2000 s and 5000 s for *Ca*HydA under 8% and 80% respectively. This implies that H_2 protects the active site from O_2 to some degree. As H_2 is thought to bind to Fe_D,[146,244] it is likely that O_2 binds at this site at least at some point in the mechanism of O_2 inactivation (as also suggested by the set of experiments investigating the protective effect of CO against O_2 inactivation, section 6.3.4.4); this step may be rate-limiting at least at high concentrations of H_2. Alternatively, a high thermodynamic

drive for H_2 oxidation (i.e. high [H_2]) favouring catalytic turnover may prevent the formation of states that bind O_2.

Experiments were also performed to reveal the pH dependence of the O_2 inactivation of *Cr*HydA1 (Figure 6.14). Again, the method of simultaneous injection of O_2-saturated buffer and gas exchange described above was employed. Initial experiments performed at 20 °C did not demonstrate a pH dependence but lowering the temperature to 10 °C had a significant effect in unveiling this dependence. This may be because the concentration of H^+ is a limiting factor in the mechanism only at a lower temperature. Alternatively, it may result from the higher degree of scatter in the results from the experiments performed at 20 °C for which the rates are higher. Therefore, resolving subtle differences in *k* was not possible at 20 °C.

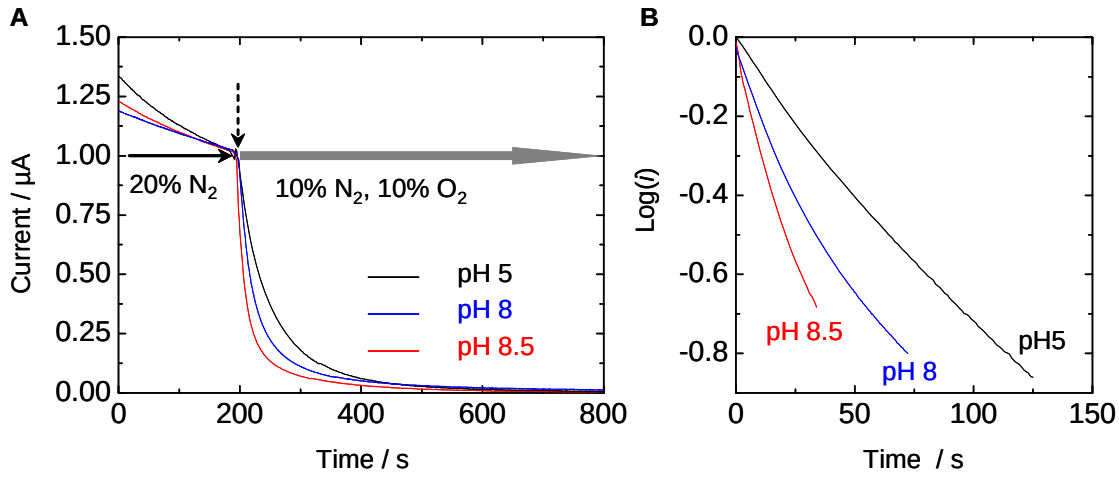

Figure 6.14: Experiments designed to probe the pH dependence of the rate of inactivation of *Cr*HydA1. A) Experimental conditions: 10 °C, -0.05 V, electrode rotation rate 3000 rpm, gas mixtures as indicated with 80% of the headspace atmosphere being H_2 at all times, dashed arrow marks the point of injection of 2 mL of buffer saturated with 20% O_2, 80% H_2 into the cell that contained 2 mL of buffer. B) Log transforms for experiments shown in A. Time is shown as zero at the point at which O_2 was introduced into the cell.

The experiments shown in Figure 6.14 demonstrate that inactivation by O_2 proceeded more slowly at lower pH. This indicates that H^+ as well as H_2 may be involved in protecting the active site against oxidative damage. With a greater supply of *Ca*HydA

and *Dd*H, the repetition of these experiments on these two enzymes would help to establish whether or not this is a general feature of the O_2 inactivation of [FeFe]-hydrogenases. Additionally, the change in the thermodynamic potential with pH should be taken into account in future experiments. Whilst the change in $2H^+/H_2$ potential due to the change in H_2 concentration in the experiments shown in Figure 6.13 was small (30 mV), a change from pH 5 to pH 8.5 (as in Figure 6.14) constitutes a change in the thermodynamic potential of 200 mV; therefore, future experiments performed at equivalent overpotentials from the $2H^+/H_2$ potential at each pH are necessary to obtain unconvoluted results on the effect of pH on the rate of O_2 inactivation.

6.3.4.2. H_2 production in the presence of O_2

Experiments to probe the possibility for continued H_2 production by *Dd*H, *Cr*HydA1 and *Ca*HydA in the presence of O_2 were performed using the method described above, with one alteration: once the O_2 was introduced in Stage 2, 2000 s were allowed to elapse before introduction of the inhibitor (CO) to allow for the slower time of O_2 inactivation of the [FeFe]-hydrogenases compared with the [NiFe(Se)]-hydrogenases.[248]

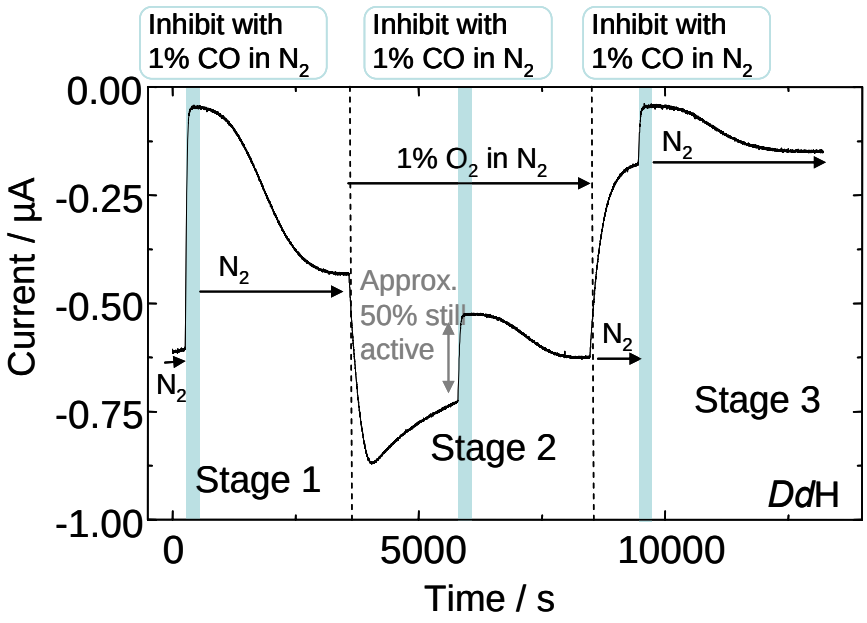

Figure 6.15: Chronoamperometry experiments designed to demonstrate H_2 production by *Dd*H at -0.4 V under 1% O_2. Other conditions: pH 6, 10 °C, electrode rotation rate 3000 rpm. Gas mixtures as indicated; blue boxes highlight periods of inhibition by CO and N_2 is the carrier gas at all times.

For all three enzymes, the experiment was commenced with 100% N_2 in the headspace. In Figure 6.15, when 1% CO was flushed into the cell a decrease in current was recorded resulting from inhibition of *Dd*H. Flushing the CO out with N_2 induced an increase in current due to recovery of H_2 production activity. When 1% O_2 was introduced into the headspace an initial increase in current was observed due to reduction of O_2 at graphite. However, after a 600 s the current began to drop. This is representative of the decrease in enzymatic H_2-production activity engendered by (slow) aerobic inactivation. When 1% CO was re-introduced into the cell, the magnitude of the loss of current was approximately 50% of the current recorded prior to exposure to O_2, showing that *Dd*H had retained around 50% of its activity at this point in the experiment. When CO was removed by flushing with 1% O_2 (in N_2), the current increased as H_2 production activity recovered (although aerobic inactivation continued throughout this phase). Removal of O_2 from the cell resulted in a drop in current due to loss of O_2 reduction at graphite. When the current reached a steady level, CO was

introduced into the cell one last time and the attenuation of the current further confirmed that the enzyme had survived exposure to O_2 for a hitherto unexpected length of time.

Similar experiments performed on *Cr*HydA1 and *Ca*HydA are shown in Figure 6.16. The concentration of inhibitor chosen in this case was 100% CO as these two enzymes are only slowly inhibited by 1% CO (see Figure 5.4). Another feature that differentiates the experiments in Figure 6.16 from that shown in Figure 6.15 is the greater degree of irreversible loss of activity of *Cr*HydA1 and *Ca*HydA due to exposure to CO at this potential (see section 5.3.3.1).

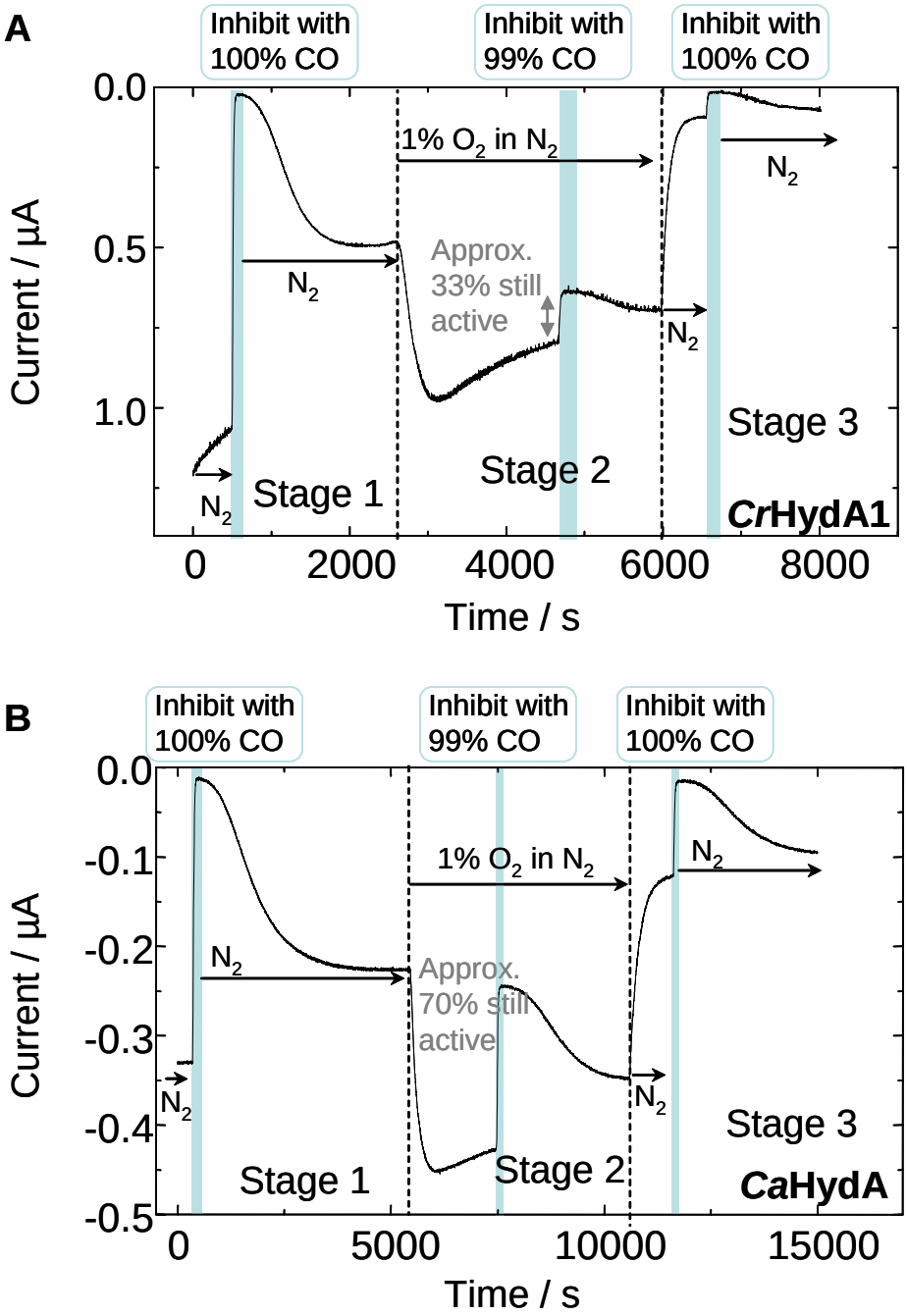

Figure 6.16: Chronoamperometry experiment designed to demonstrate H_2 production by A) *Cr*HydA1 and B) *Ca*HydA in the presence of 1% O_2. Other conditions: pH 6, 10 °C, electrode rotation rate 3000 rpm, -0.4 V. Gas mixtures as indicated; blue boxes highlight period of inhibition and N_2 is the carrier gas at all times.

The method of introduction of O_2 into the cell of the experiments performed at -0.05 V (section 6.3.4.1) and -0.4 V (above) was slightly different: whilst O_2 was introduced into the cell by gas exchange in the experiments shown in Figure 6.15 and Figure 6.16, the method of introduction of O_2 in the experiments performed at -0.05 V involved

injection of O_2-saturated buffer into the cell *as well* as gas exchange for *Dd*H and *Cr*HydA1 (see Figure 6.11 and Figure 6.12). However, the fact that 2000 s were allowed to elapse in the presence of O_2 (i.e. at least four times longer than is needed for the gas to equilibrate with the cell solution, judging by the control experiment shown in Figure 5.18) prior to introduction of CO in Stage 2 of the experiments at -0.4 V means that a comparison between the two sets of experiment is valid. Based on the experiments shown in Figure 6.15 and Figure 6.16, exposure of *Dd*H, *Cr*HydA1, and *Ca*HydA to O_2 for 2000 s lead to an approximate loss of 50%, 77% and 30% of their respective activities. While these experiments do not provide quantitative data on the level of inactivation, it is clear that all three hydrogenases retain a considerable degree of activity after exposure to at least 0.5% O_2 for more than half an hour at this potential. As will be discussed in the Discussion (section 6.4), this is in stark contrast with the reaction of *Cr*HydA1 and (especially) *Dd*H with O_2 at potentials at which they oxidise H_2 (section 6.3.4.1). The experiments performed at 10 °C at -0.05 V under 0.5% O_2 yielded half-lives for O_2 inactivation of 50 s for *Dd*H, 230 s for *Cr*HydA1 and 4000 s for *Ca*HydA (see section 6.3.4 and Table 6.1 for the corresponding rate constants). Whilst the rates of inactivation of H_2 production by these three enzymes (which are necessarily only rough estimates) are fairly similar, the rates of inactivation of H_2 oxidation vary greatly. For *Dd*H, there is an enormous disparity in the rates of inactivation of H_2 oxidation and H_2 production, with H_2 oxidation activity being annihilated much more rapidly. The difference (outside the boundary of error) in the rates for inactivation of these two processes (as characterized by the k(H_2 production)/k(H_2 oxidation) values quoted in Table 6.1) for *Cr*HydA1 is smaller and no difference is discernable at all for *Ca*HydA. This trend mimics that observed for the

discrimination of the rates of CO inhibition of H_2 oxidation vs. H_2 production (see Table 5.4).

	***Dd*H**	***Cr*HydA1**	***Ca*HydA**
k(H_2 oxidation) / s^{-1}	1.4 x 10^{-2}	3.1 x 10^{-3}	1.7 x 10^{-4}
k(H_2 production) / s^{-1}	3.5 x 10^{-4}	5.3 x 10^{-4}	2.5 x 10^{-4}
$\frac{k(H_2 \text{ oxidation})}{k(H_2 \text{ production})}$	40	6	~1

Table 6.1: Comparative pseudo-first order rate constants for inactivation of H_2 production and H_2 oxidation of *Dd*H, *Cr*HydA1 and *Ca*HydA by approximately 8 μM O_2. The half-lives quoted for the H_2 production reaction are approximates based on the percentage activity left after 2000 s in the presence of O_2 (Figure 6.15 and Figure 6.16). Experimental conditions for H_2 oxidation: 0.5% O_2 in the headgas, -0.05 V (data taken from experiments such as those shown in Figure 6.11). Experimental conditions for H_2 production: 1% O_2 in the headgas, -0.4 V. Other conditions: pH 6, 10 °C, electrode rotation rate 3000 rpm.

6.3.4.3. Reversibility of the reaction [FeFe]-hydrogenases with O_2

Whilst the vast majority of publications on inactivation of [FeFe]-hydrogenases by O_2 describe it as irreversible,[18,32,66,144,204] it has been argued that binding of O_2 to *Ca*HydA is partially reversible on the basis of PFE experiments performed by Léger et al.[220] The small degree of reversibility of O_2 inactivation mentioned in section 6.3.4.1 above observed for *Dd*H and *Ca*HydA was further examined using both cyclic voltammetry and chronoamperometry.

The experiments shown in Figure 6.17 were commenced under 80% H_2, 20% N_2 at -0.05 V. The 20% N_2 in the headspace was then exchanged for 20% O_2 in the experiment performed on *Cr*HydA1 and 19.5% N_2, 0.5% O_2 in the experiment performed on *Dd*H. This gave rise to a loss of current, indicating inactivation of both enzymes. Once the inactivation was complete, the O_2 was removed from the cell by flushing with N_2. When the remainder of the O_2 had been flushed from solution (i.e.

after a further 300 s), the potential was stepped down to -0.4 V for 50 s in the experiment on *Dd*H and 20 s in the experiment on *Cr*HydA1 and then stepped back up to -0.05 V in both cases.

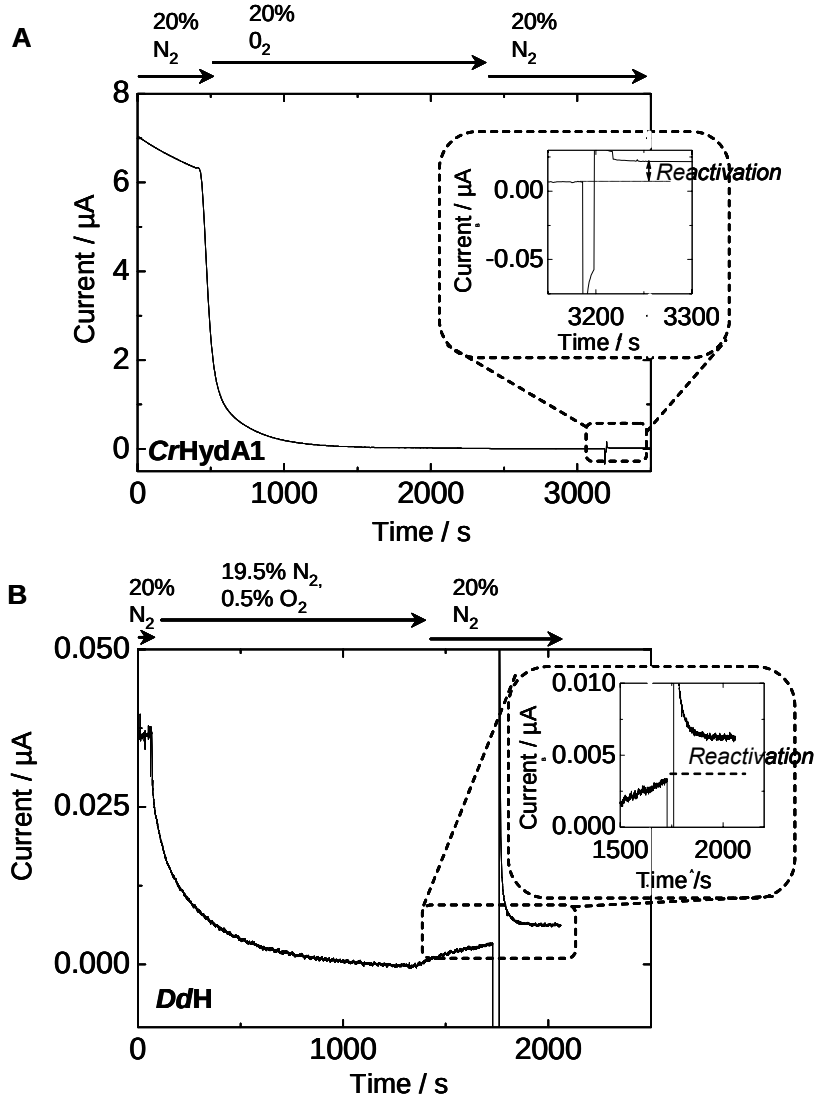

Figure 6.17: Examination of the recovery of A) *Cr*HydA1 and B) *Dd*H from O_2 inactivation by stepping the potential down to -0.4 V. Experimental conditions: for *Cr*HydA1 (A): pH 6, 23.5 °C, electrode rotation rate 3000 rpm, potential: -0.05 V from t = 0 s to t = 3185 s then -0.4 V from t = 3185 s to 3205 s then -0.05 V from 3205 s to t = 3500 s, gas mixtures as indicated with H_2 making up the remaining 80% of the headspace atmosphere. Experimental conditions: for *Dd*H (B): pH 6, 10 °C, electrode rotation rate 3000 rpm, potential: -0.05 V from t = 0 s to t = 1700 s then -0.4 V from t = 1700 s to 1750 s then -0.05 V from t = 1750 s to 2100 s, gas mixtures as indicated with H_2 making up the remaining 80% of the headspace atmosphere.

The potential step experiments shown in Figure 6.17 confirm that O_2 inactivation of *Cr*HydA1 as well as *Dd*H exhibit a very small degree of reversibility. The observation of reversibility is accentuated by the application of potentials at which these enzymes

produce H_2. As the O_2 is flushed from the cell, an increase in current is recorded, visible in the case of the experiment performed on *Dd*H because the initial current is much lower in this experiment than in the one performed on *Cr*HydA1 so this small increase of current is proportionally large. This increase is the result of reactivation of the hydrogenase. It is clear from the insets in Figure 6.17 that the current recorded at -0.05 V after the potential step down to -0.4 V is higher than it is prior to the step, thus demonstrating that the potential step has reactivated both *Dd*H and *Cr*HydA1 to some degree. The activity that *was* recovered during the low potential step returned extremely rapidly at -0.4 V. This is evident from the fact that the reductive current decreased due to film loss following the capacitive current spike (see inset in *Cr*HydA1 experiment) and the rapidity of this loss of current overtakes the increase in current due to reactivation. Furthermore, when the potential is stepped back to -0.05 V, no further increase in current was recorded. However, comparison of the magnitude of the oxidative current after exposure of the enzyme to O_2 with that recorded prior to introduction of O_2 into the cell (20% recovery for *Dd*H and 0.3% recovery for *Cr*HydA1) confirms that inactivation of these enzymes by O_2 is largely irreversible.

In Figure 6.18, a set of sequential cyclic voltammograms for *Ca*HydA under 80% H_2, 20% N_2 are shown. The first was recorded just after the enzyme was inactivated by O_2 at -0.05 V in an experiment such as the one shown in Figure 6.11 with about 5 minutes allowed for removal of O_2 from the cell prior to scanning. In the first (red) scan, the potential is swept reductively from +0.24 V to -0.2 V and back to +0.24 V. In all subsequent scans, the potential was swept forwards to -0.55 V and back to +0.24 V.

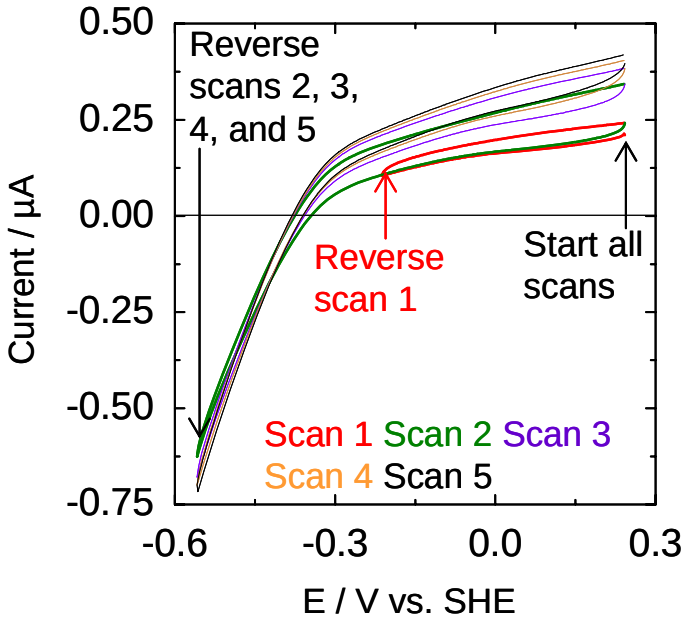

Figure 6.18: Examining the reversibility of binding to O_2 to *Ca*HydA by cyclic voltammetry. Experimental conditions: pH 6, 10 °C, electrode rotation rate 3000 rpm, scan rate 20 mV/s, 80% H_2, 20% N_2. All scans were started at +0.24 V. In the first scan the potential was swept down to -0.2 V before being reversed to +0.24 V. All subsequent scans were reversed at -0.55 V.

When the potential was scanned down to -0.55 V (scan 2), the current recorded on the return (oxidative) scan was substantially higher at +0.24 V than it was prior to the scan and the increase in this current was larger than that recorded prior to and after scanning down to -0.2 V (scan 1), again demonstrating that the application of lower potentials has promoted the reactivation of the enzyme. In the following scans, the current continued to increase, but the difference in current magnitudes at the very start and end of the scans decreased as the scan number increased until the activation process was essentially complete, at which point (after ~350 s) the scans nearly overlaid each other (scans 4 and 5).

As previously mentioned, it has been suggested that *Ca*HydA is capable of binding O_2 reversibly.[220] Figure 6.11, Figure 6.17 and Figure 6.18 clearly reveal that *Dd*H, *Cr*HydA1 and *Ca*HydA can recover a very small degree of activity after exposure to O_2, albeit to a lesser extent than is visually suggested by the experiments on *Ca*HydA

presented by Baffert et al,[220] thus a discussion of why the results presented above differ from the published results on *Ca*HydA is pertinent. The experimental protocol employed by Baffert involved simple injection of O_2-saturated buffer into the cell whilst H_2 flushed through the headspace, thus loss of current on injection resulted from substrate dilution *as well as* inactivation by O_2. The recovery of current after injection was thus at least in part due to the fact that the *Ca*HydA molecules which had not become inactivated were experiencing increasing concentrations of H_2 as the O_2 was flushed out of solution and were therefore able to turnover faster. Thus, the apparent recovery of activity in these experiments is convoluted. In a personal communication with the authors, the fact that the substrate depletion was taken into account in the computational modelling that lead to their conclusion of the high degree of reversibility of binding of O_2 was made evident (but no mention of this is made in the article[220]). In so far as the experiments detailed in 6.3.4.1 are not hampered by the artefact of substrate depletion, they are a substantial improvement on those described by Baffert in being less ambiguous.

6.3.4.4. Binding site of O_2

The experiments performed on *Cr*HydA1 shown in Figure 6.19 aimed to investigate the site of binding of O_2 by determining whether or not CO inhibition is protective against O_2 inactivation, as has been shown to be the case for *Ca*HydA.[220,232] As the Fe in the [4Fe4S]-subcluster of the H-cluster is high spin, it is not expected to bind CO, therefore inhibition of *Cr*HydA1 by CO must occur due to binding of CO to the [2Fe]-subcluster of the active site. If CO is found to protect the active site from O_2 damage, this suggests that the O_2 cannot bind because the position is already occupied by CO. However, if

CO does not protect from O_2 inactivation, these two inhibitors must bind at different loci.

Three experiments are overlaid in Figure 6.19B, a timeline of which is shown in Figure 6.19A. At the start of all three experiments, 80% H_2, 20% N_2 was flushed through the headspace of the cell and throughout the experiments 80% H_2 was maintained in the atmosphere. The remaining 20% was changed to 10% CO, 10 % N_2 (black line), 10% O_2, 10 % N_2 (blue line) or 10% CO, 10 % N_2 then 10% CO, 10% O_2 (red line), as represented in the timeline.

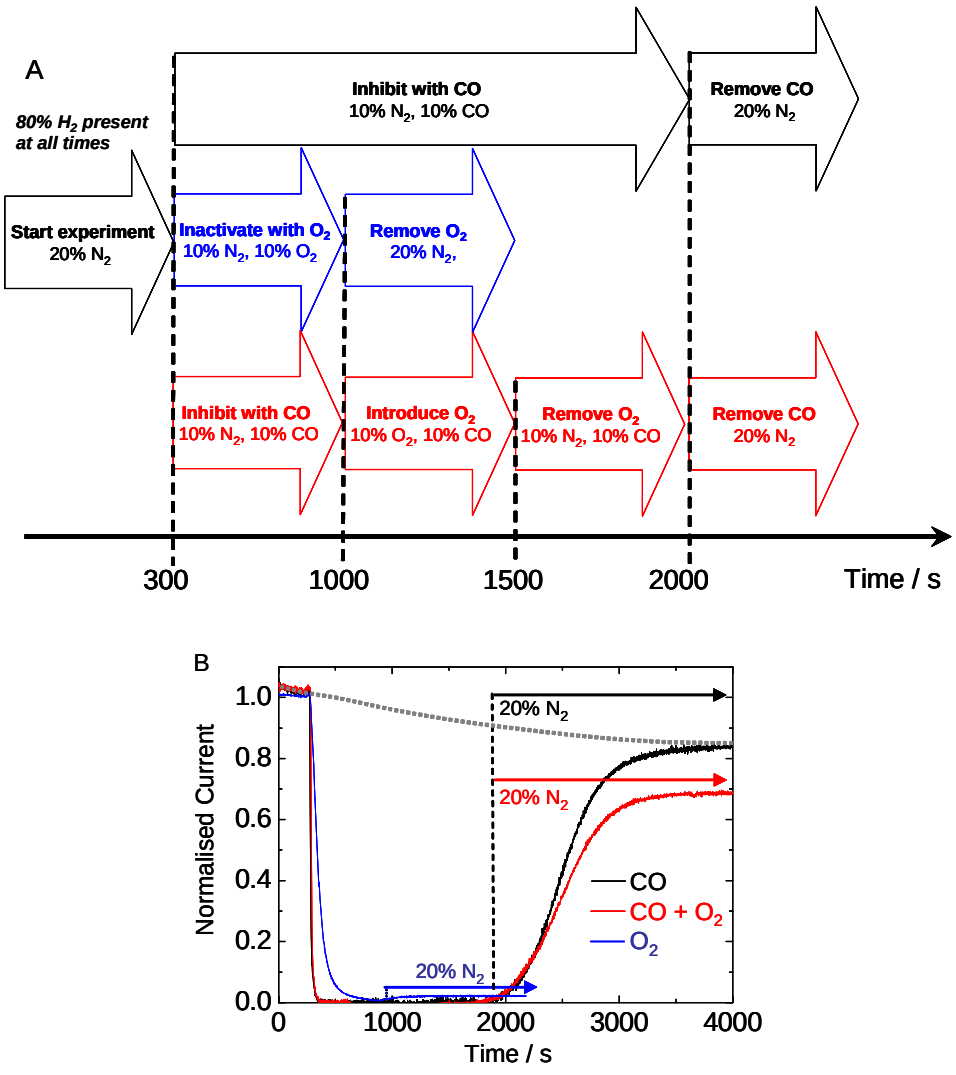

Figure 6.19: CO protection from O_2 damage to *Cr*HydA1 at -0.05 V under 80% H_2. A) schematic timeline of the gas changes and B) corresponding chronoamperometry traces for the three experiments. Panel B; black trace: the experiment starts under 80% H_2, 20% N_2, then the headspace gas is changed to

80% H_2, 10% N_2, 10% CO at t = 300 s. At t = 1900 s, the CO is flushed out with 80% H_2 20% N_2. Blue trace: the experiment starts under 80% H_2, 20% N_2, then the headspace gas is changed to 80% H_2, 10% N_2, 10% O_2 at t = 300 s. At t = 1000 s, the O_2 is flushed out with 80% H_2, 20% N_2, Red trace: the experiment starts under 80% H_2, 20% N_2, then the headspace gas is changed to 80% H_2, 10% N_2, 10% CO at t = 300 s. At t = 1000 s, the remaining 10 % N_2 is changed from 10% O_2. The O_2 is flushed out with 10% N_2 at t = 1500 s and the CO is flushed from the cell at t = 1900 s. Other conditions: pH 6, 20 °C, electrode rotation rate 3000 rpm. The grey dotted line gives a visual guide to the predicted trajectory of film loss.

The black trace shows the effect of changing the headspace mixture to 10% N_2, 10% CO (at t = 300 s). This leads to complete inhibition of the enzyme as evidenced by the fact that the current drops to zero. This inhibition is reversible, and when the 10% CO is removed from the cell by flushing with 20% N_2 the current rises to a level commensurate with complete recovery of the enzyme activity when film loss is taken into account. On the other hand, inactivation by O_2 is comparatively irreversible (blue trace). Flushing the 10% O_2 out of the cell from t = 1000 s did not lead to a more than negligible recovery of activity. The red trace shows an experiment in which the enzyme was inhibited with 10% CO before introduction and removal of 10% O_2 from the cell. Subsequent flushing of CO from the cell with 20% N_2 lead to a ~85% recovery of current.

The fact that there is near-complete recovery (~80%) of current in the red trace signifies that CO must have protected the enzyme from inactivation by O_2. Therefore, CO and O_2 must bind in the same position. This leads to the conclusion that O_2 must be able to bind to the [2Fe]-subcluster in the absence of CO.

6.4. Discussion

This chapter has surveyed the reactions of various hydrogenases with O_2 in the H_2 producing regime and when oxidising H_2 when comparison with this process was necessary. It was shown that the membrane-bound [NiFe]-hydrogenases from aerobic

Ralstonia bacteria are capable of sustaining H_2 production under high levels of O_2 (>138 μM in solution)[209] whilst the [NiFe]-hydrogenase from *Desulfovibrio gigas*, an anaerobic bacterium, was not able to sustain H_2 production in the presence of concentrations of O_2 higher than 1%. The [NiFeSe]-hydrogenase *Db*H also demonstrated continued H_2 production in the presence of O_2, albeit at a much reduced rate and under much lower levels of O_2[205] whilst being completely inactivated by equivalent concentrations of O_2 when oxidising H_2. This was commensurate with the rapidity of reactivation of this enzyme from damage by O_2 at potentials close to or below the $2H^+/H_2$ couple. There must therefore be an important electronic component in protecting the active site of *Db*H from O_2 damage. Increased O_2 tolerance of this enzyme over some [NiFe]-hydrogenases has been noted in the past, with the sterically restrictive size of the Se atom cited as a possible source of this tolerance.[66] Moreover, it was shown that at least two species are formed on aerobic inactivation of this enzyme, one of which – identified as "Ready" Ni-B – reactivates much more rapidly than the other – potentially an "Unready" Ni-A species.[205]

A further example of an electronic protection of the active site is the case of aerobic inactivation of *Dd*H which proceeds much more rapidly at potentials in the H_2 oxidation range than in the H_2 production region, though in both cases, aerobic damage is slower than for the [NiFe(Se)]-hydrogenases This behaviour contrasts with that of *Ca*HydA for which the disparity in the rates of aerobic inactivation of H_2 production and oxidation appears non-existent. As demonstrated by the rate constants quoted in Table 6.1, the discrimination between the rates of inactivation of H_2 production and H_2 oxidation by *Cr*HydA1 is less pronounced than that of *Dd*H but still observable. The fact that higher concentrations of H_2 were shown to slow the rate of O_2 inactivation may

be relevant to the underlying reasons for the relatively sluggish kinetics of O_2 inactivation of H_2 production. However, preliminary experiments designed to probe the extent of aerobic inactivation of H_2 production in the presence of O_2 such as those shown in Figure 6.16 performed with H_2 as the carrier gas (rather than N_2) were inconclusive, but it may be that the concentration of H_2 in the headspace is no longer rate-limiting when it is being produced at the active site.

Modelling the protein as a basic two-component system comprised of the active site and the protein "packaging" around it can help us to understand the difference between the three [FeFe]-hydrogenases. Whilst the approximate rates of inactivation of H_2 production are within the same range for all three enzymes (i.e. they all retain some activity after 2000 s in the presence of 1% O_2), the rates of inactivation of H_2 oxidation are greater for *Dd*H than they are for *Cr*HydA1 which are in turn greater than they are for *Ca*HydA (in agreement with Ghirardi et al.[32]). In fact, the rates obtained for the inactivation of H_2 oxidation by *Ca*HydA are extremely slow compared with other hydrogenases so far: the [NiFe(Se)]-hydrogenases *Db*H (as shown in section 6.3.3.1), *Df*H[216] and *Av*H[18] essentially react instantly with O_2.

The H-cluster of the three [FeFe]-hydrogenases is considered to be very similar for all three enzymes[67,142,143,147,263] (though subtle electronic differences were elucidated in EPR experiments[124]), thus suggesting that, if different rates of reaction with CO (see Discussion in Chapter 5) or O_2 are observed, this is likely to be a consequence the protein scaffold. This implies that aerobic inactivation of H_2 oxidation, which proceeds at very different rates for the three enzymes, is limited by the protein packaging, in other words, a possible 'gas channel' effect. A recent computational study has

suggested that the polarity and charge of residues surrounding the entry of the putative hydrophobic gas channel through which the O_2 might travel to reach the active site is critical in determining the O_2 sensitivity of [FeFe]-hydrogenases.[264]

On the other hand, aerobic inactivation of H_2 production occurs at similar rates for *Dd*H, *Cr*HydA1 and *Ca*HydA. If we concede that the three enzymes have gas channels of varying permeability due to the differences in their structures, then there must be a further limitation on the rate that applies to all three enzymes such that they react with O_2 at a similar rate when producing H_2. In this case it is possible that the rate of reaction is slowed by an electronic effect on the active site generated by the low potential. A number of observations made prior to this point in this thesis can be linked to the importance of such an electronic effect. For example, Figure 5.7 and Figure 5.8 show that CO inhibits H_2 production much more slowly than H_2 oxidation by *Dd*H, *Cr*HydA1 and *Ca*HydA. Considering the effect of diatomic inhibitors on the [NiFe(Se)]-hydrogenases, *Db*H preferentially binds O_2 when *oxidising* H_2. Additionally, the K_I^{app} values for CO- and H_2-inhibition of H_2 production by *Rm*MBH increase as the potential becomes more negative (see Chapter 4). These observations lend some support to the hypothesis that potential plays an important role in controlling both the thermodynamics and the kinetics of binding of diatomic molecules to hydrogenases. The similarity in rates of O_2 inactivation of H_2-production activity of the three enzymes may also relate to the direction of catalysis, i.e. when catalysing H_2 production, the very fact of forming H_2 at the active site becomes rate-limiting, but during H_2 oxidation the absence of this protective effect means that another component of the system (for example the gas filter in the protein packaging) determines the rate.

The comparative rates of inhibition of *Dd*H, *Cr*HydA1 and *Ca*HydA by CO add another dimension to this discussion. As shown in Figure 6.20**,** CO reacts much more rapidly than O_2 with the three [FeFe]-hydrogenases studied. As these two inhibitors are but a couple of atomic units apart in molecular weight and have similar radii (3.47 and 3.69 Å for O_2 and CO, respectively[231]), it can be assumed that O_2 should travel through a gas channel (or protein scaffold) at least as fast as CO if this process is limited simply by steric restrictions to species passing through the enzyme. (In fact, a computational study of the gas channels in myoglobin reported them to be more porous to O_2 than CO.[265]) Thus, any significant difference in the rates of reaction with O_2 and CO is more likely to relate to the reaction of these inhibitors at the active site.

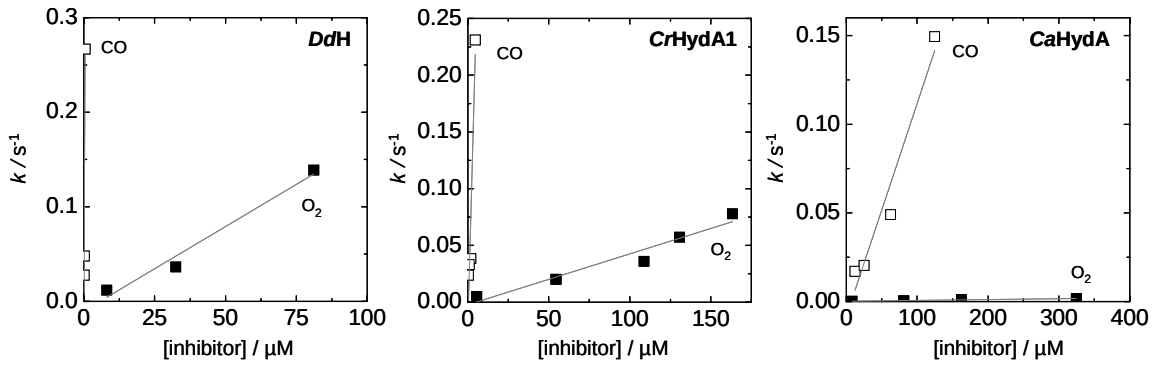

Figure 6.20: Comparison of rates of inactivation by CO and O_2 for *Dd*H, *Cr*HydA1 and *Ca*HydA taken from the O_2 experiments shown in Figure 6.11 for *Dd*H and *Ca*HydA and Figure 6.12 for *Cr*HydA1 and the CO experiments described in Chapter 5 (section 5.3.3.3). The CO data are represented by empty squares (□) and the O_2 data are represented by filled squares (■).The *Dd*H and *Ca*HydA results shown above are from experiments performed at 10 °C and those for *Cr*HydA1 are at 20 °C.

Reaction of [FeFe]-hydrogenases with CO is generally reversible[220,232,234,235] (except for the reaction of CO with *Ca*HydA and *Cr*HydA1 when these enzymes are poised to produce H_2, see Chapter 5). Whilst CO is unlikely to engage in any further chemistry after biding, the mechanism of irreversible modification of the H-cluster with O_2 is necessarily more complex, involving a possible reduction of O_2 to a reactive oxygen species (ROS); this complexity could be at the root of the difference between the rates of reaction with O_2 and CO. As the rate constant *k* for the inactivation of the [FeFe]-

hydrogenases by O_2 is dependent on the concentration of H_2, this suggests that the rate-limiting step must be the binding of O_2 at the site of binding of H_2 (i.e. the active site) rather than diffusion of O_2 to the active site unless H_2 is able to occupy and block the gas channel. The experiment demonstrating that CO protects from O_2 damage (Figure 6.19) fits perfectly into this picture: CO is known to be competitive with H_2[235] (which binds at Fe_D[155]) and to bind at Fe_D,[244] therefore the fact that exogenously-bound CO protects against O_2 confirms that binding of O_2 at Fe_D is a necessary step in the oxidative damage of [FeFe]-hydrogenases.

The nature of the as-yet uncharacterized O_2-adduct of the H-cluster is still a matter of speculation. One possibility that is considered here is degradation of the H-cluster [4Fe4S]-subcluster. Degradation of [4Fe4S]-clusters has been reported in numerous instances.[266-269] Specifically, ROS (which are likely to be more potent oxidising agents than O_2) such as superoxide are known to damage [FeS]-clusters.[270-274] Using EXAFS it is possible to distinguish FeFe distances from the [2Fe]-subcluster from those in the [4Fe4S]-cluster. The depletion of [4Fe4S] peak in the Fourier transform of the EXAFS spectrum of aerobically inactivated *Cr*HydA1 strongly suggests that the [4Fe4S]-cubane in the H-cluster of *Cr*HydA1 is damaged by O_2.[221] These data, in agreement with previous proposals on the damage of [FeS]-clusters by O_2 and ROS,[267,275] suggest degradation of the [4Fe4S]-cubane to a [3Fe4S]-cluster.[221] Whilst O_2 can damage [FeS]-cluster directly, these clusters are much more prone to reacting with ROS such as superoxide. Thus, a ROS generated by the reaction of O_2 with the active site could easily be damaging to the nearby cubane. Alternatively, partial O_2 reduction at the [2Fe]-subcluster could lead to long-range electron transfer from the cubane, causing irreversible oxidative damage. In this context, the oxidation level of the H-cluster (as

controlled by the potential) may dictate the nature of the ROS formed which in turn might control the rate of the resulting degradation of the [4Fe4S]-cluster. Damage by O_2 to these fragile moieties is irreversible and can lead to loss of a Fe atom and eventual breakdown of the cluster,[267] which will prohibit electron transfer and catalysis in turn. The [NiFe(Se)]-hydrogenases do not have a cubane ligated to the active site. The distance between the active site and the nearest [FeS]-cluster might act as a buffer zone, protecting against this irreversible damage.

Finally, this chapter has aimed to elucidate some of the mechanisms by which enzymes react with O_2 and by which they are protected from it:

- Hydrogenases from aerobic organisms such as *Ralstonia* bind O_2 only weakly and may not form the "Unready" Ni-A that is slow to reactivate.[257]
- The [NiFeSe]-hydrogenase *Db*H forms two kinetically-distinct species upon exposure to O_2 which are only reactivated rapidly at potentials close to the thermodynamic potential of the $2H^+/H_2$ couple. Whilst H_2 oxidation by this enzyme is thus incompatible with the presence of even a trace of O_2, H_2 production can be sustained at low levels of O_2. The reaction of this enzyme with O_2 is very rapid.
- The [FeFe]-hydrogenases react slowly with O_2, but the damage is largely irreversible. It is not unlikely that gas-filters play a role in limiting the rate at which O_2 causes the damage, especially in the case of *Cr*HydA1 and *Ca*HydA (which also react more slowly with CO than *Dd*H) but, given the comparative rapidity of the reaction of the [FeFe]-hydrogenases with CO, gas-filters cannot be the only rate-limiting factor. The potential at which the inactivation is

induced may determine the nature of a possible ROS formed at the active site and this in turn may control the rate of destruction of the ligated cubane.

Chapter 7:

Conclusion

This thesis and the publications[205,209,221,248] that have come as a corollary of it constitute a substantial body of research into the kinetics of inhibition of hydrogenases and the mechanistic implications thereof. A particular emphasis has been placed on the ability of a spectrum of hydrogenases to produce H_2 under different, challenging, conditions.

7.1. Bias towards H_2 production and binding of H_2

Cyclic voltammograms measured for a variety of hydrogenases under N_2 and H_2 illustrated their respective catalytic bias for H_2 production relative to H_2 oxidation. Generally, H_2 production is favoured by the [FeFe]-hydrogenases over the [NiFe(Se)]-hydrogenases. Moreover, the effect of H_2 as an inhibitor of H_2 production was more noticeable in experiments on [NiFe(Se)]-hydrogenases.

Product inhibition of hydrogenases, as quantified by the $K_I^{app}(H_2/H^+)$, is an important parameter to consider in assessing the technological use of [NiFe(Se)]-hydrogenases in comparison with the [FeFe]-hydrogenases. The clear relationship between strong product inhibition of H_2 production, a high affinity to bind H_2 for H_2 oxidation and a strong catalytic bias for H_2 oxidation over H_2 production was demonstrated. The intriguing exception was the C81A mutant of *Re*MBH, whose low affinity for H_2 when oxidising H_2 was neither matched by weak product inhibition nor an increased bias for H_2 production, suggesting that another characteristic of the *Ralstonia* enzymes limits their capacity to produce H_2. For both the [FeFe]- and [NiFe(Se)]-hydrogenases, the K_M was smaller than the $K_I^{app}(H_2/H^+)$; an extension of this is that the $K_I^{app}(H_2/H^+)$ became increasingly large as the potential was made more negative. This is coherent with the notion that binding of H_2 is advantageous when these enzymes are oxidising H_2

but detrimental to H_2 production, therefore, as the potential is made more negative and the driving force for H_2 production is increased, the binding of H_2 becomes less favourable.

7.2. Inhibition by CO

The *Ralstonia* enzymes are anomalous in being the only hydrogenases which bind H_2 more tightly than CO. The extreme opposite to these are the [FeFe]-hydrogenases which are hardly inhibited by H_2 when reducing H^+, in contrast to their inhibition by CO which only requires very low concentrations of CO. Additionally, they recover slowly from this inhibition. In fact, unlike the [NiFe(Se)]-hydrogenases, binding of CO to the state of the [FeFe]-hydrogenases which predominates at potentials at which the enzymes produce H_2 is partially irreversible and the more negative the electrode potential, the greater the degree of irreversibility. This finding should inspire further spectroscopic characterization of the permanently CO-inhibited state of the [FeFe]-hydrogenase so that the structure of this irreversible adduct might be determined.

Experiments assessing inhibition of the [FeFe]-hydrogenases by CO were used to survey a number of aspects of these enzymes. It was shown that the recovery from CO occurred more easily at potentials at which hydrogenases produce H_2 than at potentials at which they oxidise it, thus echoing the favourability of binding of H_2 throughout the potential range. Thus, it was shown that the electronics of the H-cluster are integrally linked to its ability to bind inhibitors. The rates at which *Dd*H, *Ca*HydA and *Cr*HydA1 were inhibited by CO were also slower at more reducing potentials. In this case, this may reflect the slower kinetics of a more complex irreversible reaction of the enzyme with CO occurring only at potentials at which the enzyme produces H_2.

Experiments in which CO-saturated buffer was injected into solution and allowed to flush out through the course of the experiments provided evidence for there being a physical barrier, the nature of which will depend on the structure of the enzyme, limiting the rate at which CO inhibits *Dd*H, *Cr*HydA1 and especially *Ca*HydA. However, the similarity of the kinetics of recovery of activity of *Dd*H, *Cr*HydA1 and *Ca*HydA suggests that a gas channel running through the protein scaffold is unlikely to limit the recovery as the sequence homology between these three enzymes is low (approximately 40%). Rather, the kinetics of Fe-CO cleavage govern the recovery from CO inhibition. Determination of the rates at which CO inhibited these enzymes allowed for some estimate of the rate at which diatomic molecules of the size of CO can penetrate these enzymes. Comparison of these rates with the much-slower rates obtained for the inactivation by O_2 (whose Lennard-Jones radius is very similar) confirmed the conclusion that a more complex modification of the protein, presumably at the active site, must occur to limit CO access as it is reasonable to assume that O_2 and CO travel across the protein at the same rate. Both CO and O_2 reacted most slowly with *Ca*HydA and most rapidly with *Dd*H.

7.3. Mechanism of oxidative damage to hydrogenases

The fact that CO protects *Ca*HydA and *Cr*HydA1 from O_2-damage indicates that both inhibitors bind at the same site. It is not known for CO to bind to [4Fe4S]-clusters but it has been shown to bind to Fe_D[139,147] thus suggesting that O_2 binds to this atom as well. However, EXAFS data[221] show O_2-damage to the cubane moiety of the H-cluster, thus, even though it was demonstrated that O_2 bound at Fe_D, some damage occurs at a different site. These observations imply two possible conclusions: 1) the presence of CO prevents O_2 from even penetrating the H-cluster enclave thus ultimately protecting

both the [2Fe]- and the [4Fe4S]-subclusters; 2) only the species, perhaps a superoxide, formed by O_2 attack at Fe_D, can attack the cubane. As N_2 does not protect from O_2 by its mere presence, option 2) seems more likely. Degradation of [4Fe4S]-clusters to [3Fe4S]-clusters[223,224] and complete breakdown of [2Fe2S]-clusters[276] due to highly oxidising potentials or exposure to O_2 is a well-documented[267,272] process. Two mechanisms for the destruction of the [4Fe4S]-cluster can be envisaged. In the first (A), ROS migrates from [2Fe]-subcluster to the [4Fe4S]-subcluster, complexes an Fe atom and abstracts it. In the second (B), the oxidising power of the ROS ligand generated by O_2 binding to the [2Fe]-centre induces long range electron transfer from the [4Fe4S]-cluster, and again, loss of an Fe atom ensues (see Scheme 7.1).

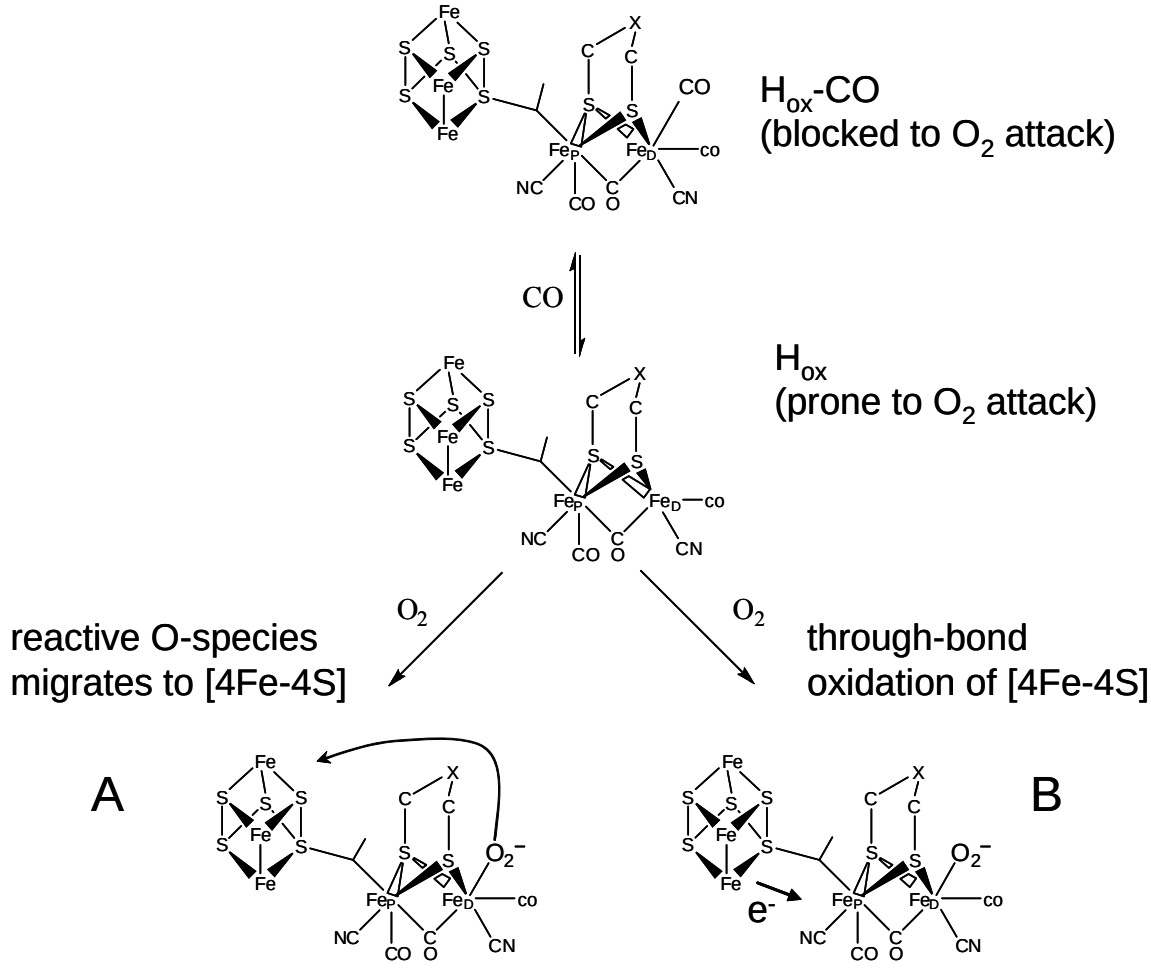

Scheme 7.1: Mechanism of protection of the active site from O_2 inactivation by CO and two possible routes to O_2-damage of the [4Fe4S]-cluster. A) Migration of ROS. B) Long-range electron transfer from the [4Fe4S]-cluster to the bound O_2-species.

Oxidative degradation of the algal enzymes *Cr*HydA1 and *Cs*HydA was also shown to occur at highly-oxidising potentials. The precedents for high-potential damage of [FeS]-clusters as demonstrated by PFE[223,224,276] coincide with the hypothesis that this may be at the origin of the irreversible anaerobic inactivation observed for the algal hydrogenases as well as aerobic inactivation. The occurrence of this form of degradation, which does not involve binding of O_2 (to form an ROS which migrates to the [4Fe4S]-cluster), lends some support to mechanism B for O_2 attack (Scheme 7.1) in which degradation is the result of long range electron transfer rather than direct attack by ROS at the [4Fe4S]-cluster. That irreversible damage by O_2 to the [NiFe(Se)]-hydrogenases does not occur to the same extent could thus reflect that, unlike the [FeFe]-hydrogenase, these hydrogenases do not have a cubane ligated *directly* to the active site. Additionally, like the bacterial [FeFe]-hydrogenase *Dd*H,[204] all the [NiFe(Se)]-hydrogenases studied by PFE[18,97] undergo *reversible* anaerobic inactivation. Whether or not this is related to the fact that all these enzymes, unlike *Cr*HydA1 and *Cs*HydA, possess a chain of [FeS]-clusters, which might offer some protection against oxidative damage, remains to be seen.

7.4. Probing H_2 production in the presence of O_2

A facile method for observing H_2 production in the presence of O_2 was detailed in this thesis and this constitutes one of the only techniques for following this process. Application of this method to a broad range of hydrogenases permits an extensive review of their aerobic H_2-producing abilities. In correlation with the well-established O_2-tolerant H_2 oxidation by the *Ralstonia* hydrogenases,[18,254,277] *Re*MBH was found to be the most O_2-tolerant H_2-producing enzyme, and exhibited continued H_2 production activity in the presence of at least 13% O_2 in the environment of the enzyme, but the H_2-

production activity was low, as it always is with this enzyme. Whilst *Dg*H is more biased towards H_2 production than *Re*MBH, it was not able to sustain H_2 production above 1% O_2 in the headspace, and recovery from even this low amount of O_2 was very slow. On the other hand, at potentials at which it produces H_2, the [NiFeSe]-hydrogenase *Db*H was shown to recover from O_2 inactivation almost immediately thus suggesting that H_2 production would be compatible with the presence of O_2. Indeed, this was found to be the case at low [O_2], but like *Dg*H, *Db*H cannot sustain H_2 production in the presence of higher [O_2]. The sluggish kinetics of O_2 inactivation of [FeFe]-hydrogenase-catalysed H_2 production were initially surprising considering how notoriously O_2-intolerant these enzymes are. These results were particularly unexpected in the case of *Dd*H since the H_2-oxidation activity of this hydrogenase was shown to be obliterated by O_2 rapidly relative to *Cr*HydA1 and *Ca*HydA. The difference in the rates of O_2 inactivation of H_2 oxidation vs. H_2 production was less marked for *Cr*HydA1 and non-existent for *Ca*HydA. Given that the H-clusters of *Dd*H, *Cr*HydA1 and *Ca*HydA are thought to be structurally similar,[67,141-143,147] this suggests that another factor limits the rate of reaction "upstream" from the active site, perhaps a gas filter, as suggested by the experiments in which CO-saturated buffer was injected into the cell (*vide supra*). However, the subtle electronic differences between the H-clusters of the algal hydrogenases *Cr*HydA1 and *Cs*HydA and the bacterial enzymes *Dd*H and *Cp*I demonstrated in EPR may also be related to the difference in their reactivities to diatomic inhibitors.[124,245]

7.5. Comparison of inhibition by CO, H_2, O_2, and formaldehyde

This thesis provides compelling evidence for the binding of diatomic molecules being more favourable at more positive potentials. The potential dependence of the rates of inactivation by O_2 (for *Dd*H – see Discussion in Chapter 6) and reactivation from exposure to O_2 (for *Db*H section 6.3.3.1) fits with the trends observed for binding of CO and H_2 to hydrogenases becoming increasingly unfavourable as the potential is made more negative.

For the three [FeFe]-hydrogenases studied, Figure 7.1A illustrates that the rate of inactivation of H_2 oxidation and production by CO are dependent on the hydrogenase whereas the rate of recovery from CO inhibition, whether during H_2 oxidation or H_2 production, is independent of the enzyme. Figure 7.1B demonstrates that the favourability of binding both O_2 and CO during H_2 oxidation over H_2 production is also dependent on the enzyme. The facts that *Ca*HydA is the most slowly inhibited by both CO and O_2 and that the ratios of favourability of binding these inhibitors during H_2 oxidation over H_2 production ($k_{inact}(O_2/H_2)/k_{inact}(O_2/H^+)$ and $k_{inact}(CO/H_2)/k_{inact}(CO/H^+)$, respectively – see Figure 7.1) are small with respect to that of *Dd*H combine to form a strong evidence base for the hypothesis that inhibition of *Ca*HydA is limited by a gas filter effect rather than formation of the Fe-inhibitor bond which should be dependent on the oxidation state of the Fe atom. For *Dd*H, there is a much more pronounced effect of potential on the kinetics of inhibition, thus suggesting that making and breaking the Fe-inhibitor bond is the rate-limiting step for this enzyme

On the other hand, the favourability ratio for CO inhibition over O_2 inactivation of H_2 oxidation ($k_{inact}(O_2/H_2)/k_{inact}(CO/H_2)$ in Figure 7.1) is fairly similar for all three enzymes. This may be the result of more rapid transport of CO through the enzyme or the fact that binding of CO is so much more favourable than binding of O_2 in all three cases that, even though there appear to be different rate-determining steps for all three enzymes, this is the predominant factor in determining the comparative kinetics of the two processes. This may result from the stability of the Fe-CO adduct due to the strength of the π-backbonding in the Fe-CO bond (with CO binding in a linear conformation) relative to the stability of Fe-O_2 adduct (in which O_2 binds in a bent conformation) which does not benefit from π-backbonding to the same degree.[278] Further spectroscopic and computational studies examining the active-site enclave and potential gas channels as well as genetic modifications to the direct environment of the active-site such as were performed on *Df*H[162] would be of great use in solving this puzzle.

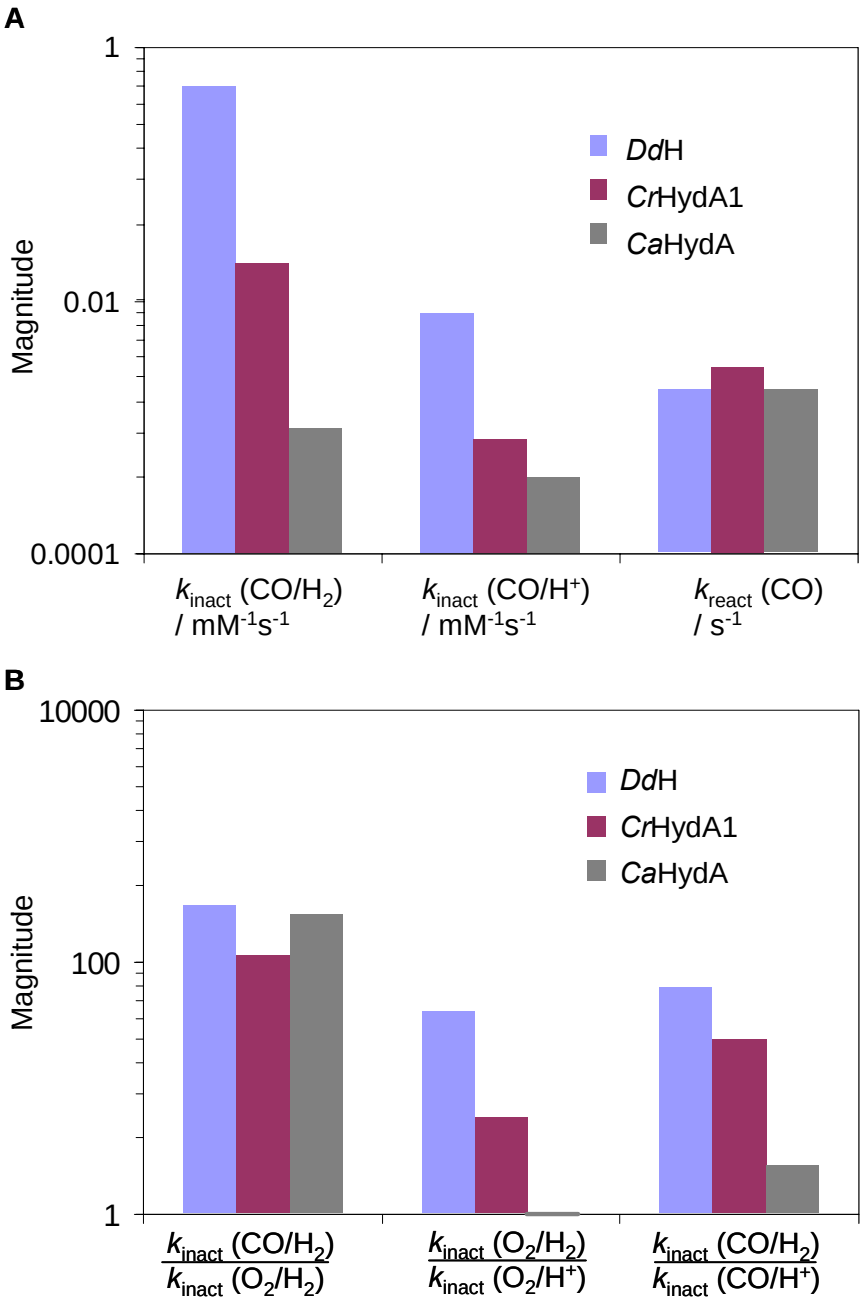

Figure 7.1: Bar charts representing notable comparisons between *Dd*H, *Cr*HydA1, and *Ca*HydA. A) The rates of CO inhibition of H_2 oxidation ($k_{inhibit}(CO/H_2)$ and H^+ reduction ($k_{inhibit}(CO/H^+)$ in comparison to the rates of recovery from CO inhibition ($k_{recover}(CO)$). As the rate of reactivation from CO inhibition is essentially independent of the process being catalysed, it is simply represented by an $k_{recover}(CO)$. B) The discrimination factors characterising the favourability of binding CO over O_2 ($k_{inhibit}(CO/H_2)$/ $k_{inact}(O_2/H_2)$), binding O_2 when the enzyme is catalysing H_2 oxidation over when it is catalysing H_2 production ($k_{inact}(O_2/H_2)$/ $k_{inact}(O_2/H^+)$) and binding CO when the enzyme is catalysing H_2 oxidation over when it is catalysing H_2 production ($k_{inhibit}(CO/H_2)$/ $k_{inhibit}(CO/H^+)$) for *Dd*H, *Cr*HydA1 and *Ca*HydA. The $k_{inact}(O_2/H_2)$/ $k_{inact}(O_2/H^+)$ ratios are approximate because the values of $k_{inact}(O_2/H^+)$ are estimates. This ratio is approximated to 1 for *Ca*HydA.

Intriguingly, the opposite potential dependence was observed for the favourability of binding of formaldehyde to *Cr*HydA1 to that observed for inhibition by CO, H_2 and O_2 of the hydrogenases studied in this thesis. This uncovers the possibility that, in this case, a different mode of binding, such as blockage of the proton transfer chain, is in place.

7.6. Future experiments

The work described in this thesis forms the basis for a number of different investigations. In the quest to understand the nature of the formaldehyde and irreversible CO adducts of [FeFe]-hydrogenases, spectroscopic, crystallographic and electrochemical methods applied to [FeFe]-hydrogenase mimics as well as the enzymes could be prove highly beneficial.

7.6.1. Spectroscopy

Whilst EPR[256] and infrared spectroscopy[144] have been used on a broad spectrum of hydrogenases, EXAFS has also recently been used to examine the structure of the active[211] and O_2-inactivated H-cluster of *Cr*HydA1.[221] Spectroscopic characterization of the formaldehyde adduct of the [NiFe(Se)]- and [FeFe]-hydrogenase could help identify the previously-described proton transfer pathways.[81,116,119,279] For the [FeFe]-hydrogenases, the heteroatom in the active site bridging dithiol ligand could also be identified if it were to bind formaldehyde.

The possibility of examining the spectroscopic properties of the H-cluster of *Cr*HydA1 and *Ca*HydA at specific potentials means that spectroelectrochemistry could be used to

probe the nature of the irreversible-CO adduct formed when these enzymes are inhibited by CO whilst catalysing H_2 production and whether or not the super-reduced state (H_{sred})[139] plays a role in its formation. As formaldehyde was found to inactivate H_2 production and H_2 oxidation at different rates, this technique could also inform on the differences from which this behaviour arises. Additionally, spectroelctrochemistry could also be highly informative in terms of the structure of the various species formed upon anaerobic inactivation.

7.6.2. X-ray crystallography

As with spectroscopy, crystallography could be used to identify the structure of the formaldehyde and irreversible CO adducts.

7.6.3. Electrochemistry

As the experiments probing anaerobic inactivation of the algal hydrogenases were often only performed on either *Cr*HydA1 or *Cs*HydA, performing equivalent experiments with the relevant enzyme would solidify the conclusions from this work. In particular, the refinement of the species formed on anaerobic inactivation was only performed on *Cr*HydA1, thus carrying similar experiments out on *Cs*HydA would point to the generality of this behaviour for algal enzymes. Performing experiments at the same *over*potentials with respect to the thermodynamic potentials under different conditions of H_2 and H^+ concentration would complement the experiments probing the kinetics and thermodynamics of reactivation of the species formed at high potential (see section 3.3.7). Comparison with a bacterial [FeFe]-hydrogenase which anaerobically inactivates

could cement this behaviour at highly oxidising potentials as a characteristic of the algal enzymes.

An electrochemical cell in which the electrolyte can rapidly be exchanged (by continual flushing) without needing to disturb the setup is currently under construction. This will help to deconvolute the reversibility of formaldehyde binding from film loss as the formaldehyde in solution will be removed with minimal perturbation to the enzyme film. This could also enhance the precision of the determination of the kinetics of recovery of the [FeFe]-hydrogenases from CO as the method described in section 5.3.3.3 (involving analysis of the kinetics of recovery after CO-inhibition by only taking the data after at least 600 s have elapsed since the CO *starts* to be flushed from the headspace into account) is somewhat crude. Given how tightly these enzymes bind CO, a more efficient method for removing the CO would make the assessment of the kinetics of recovery after inhibition (and thus supposedly in the absence of CO in solution) more accurate.

7.7. Concluding remarks

In this thesis, the first comprehensive electrochemical investigation of the [FeFe]-hydrogenases is described: the enzymatic activities and mechanisms of inactivation by O_2 and highly-oxidising potentials as well as the complexity of the states thus formed are electrochemically characterized and evaluated.

By considering the compendium of results reported herein, some notion of the "perfect hydrogenase for H_2 production" can be advanced. The ability of *Re*MBH to sustain H_2 production in high concentrations of O_2 makes it an attractive candidate at first glance,

but the turnover rates are low. On the other hand, the high catalytic rates for H_2 production of *Db*H in addition to its ability to recover rapidly from O_2 at low potentials make its active site an attractive centre for this process, despite its being more sensitive to H_2 inhibition of H_2 production than the [FeFe]-hydrogenases. The protein scaffold of *Ca*HydA appears to exhibit a tighter filter which restricts the rate at which diatomic molecules (including O_2) travel across the enzyme. In conclusion, an appealing notion for technological applications is the engineering of an enzyme with a *Ca*HydA-like architecture and a *Db*H-like active site in which no [4Fe4S]-cluster is ligated to the [NiFeSe]-active site. The publication of the structure of *Re*MBH will help us to ascertain the structural basis for its O_2 tolerance and thus refine the image of the "ideal" hydrogenase.

Appendices

Appendix I

Materials and methods

Enzymes

The laboratory of J.C. Fontecilla-Camps (Grenoble) supplied *Db*H,[82,280] *Df*H,[281] and *Dd*H[143] by performing the previously published protocols as referenced. The purification of *Dg*H[65] was performed under the direction of R. Cammack (King's College, London). The purification of *Ralstonia* was undertaken in the laboratory of B. Friedrich (Berlin).[222] The laboratory of T. Happe (Bochum) provided samples of *Cr*HydA1,[52] *Ca*HydA[16] and *Cs*HydA.

Film preparation

Films of *Db*H, *Dg*H and *Dd*H were prepared by either abrading the graphite surface with sand-paper (grade P800) or polishing with alumina on a moistened cotton ball and then sonicating the end of the electrode and rinsing with purified (Milli-Q) water before placing the electrode in a cryovial containing a concentrated solution of the enzyme. For the *Ralstonia* hydrogenases, *Cr*HydA1, *Ca*HydA and *Cs*HydA, the same procedure for abrasion or polishing was employed, but the enzyme was applied to the graphite tip of the electrode in 1 μL droplets by using an Eppendorf pipette.

Electrode preparation

The electrodes, as shown in Figure 2.7, consisted of a PGE tip (3 mm^2 cross-section, 5 mm long) attached by conductive silver-loaded glue to a steel rod encased in a nylon

casing. The graphite tip was held in place by an epoxy resin-hardener complex (Araldite).

Potentiostat

The Autolab PGSTAT 10 and Autolab PGSTAT 20 electrochemical analysers (Eco Chemie, The Netherlands) were employed as the potentiostats in conjunction with GPES software. The current was sampled at least every 0.0025 V and 1 s in cyclic voltammetry and chronoamperometry, respectively. An ECD (electrochemical detection) module was used in voltammetry to improve the signal-to-noise ratio.

Water-circulator

Experiments were thermostated by connecting the water-jacket of the electrochemical cell to a Neslab RTE 111 or RTE 101 water circulator.

Rotator

The electrode rotators were supplied by Eco Chemie (The Netherlands) or E. G. & G. (U.S.A).

Mass-Flow Controllers

Gas mixtures were delivered to the cell via mass-flow controllers from Sierra Tek, U.S.A. These were accurate to within 1% of their maximum flow rate (i.e. for the mass flow controller with a maximum flow rate of 100 standard cubic centimetre per minute (scc/min), it was accurate to within 1 scc/min

Glovebox

All experiments were performed inside anaerobic gloveboxes. The two gloveboxes used were provided by M Braun (Germany) and Vacuum Atmosphere (U.S.A). These maintain an atmosphere containing less than 2 ppm O_2.

Gases

Argon, N_2, 100% CO, and 1% CO in N_2 were supplied by BOC and Air products supplied Premier Grade H_2, O_2, 5% and 10% H_2 in N_2.

Solutions

Buffer solutions were prepared by titrating 50 mM Na_2HPO_4, 100 mM NaCl with 50 mM NaH_2PO_4, 100 mM NaCl to the right pH by using a pH meter (Russell 950, provided by Fisher U.K.). The NaCl was used as a supporting electrolyte. The pH meter was calibrated to the right temperature just before buffer preparation. The chemicals were of analytical grade and were provided by Sigma-Aldrich. The solutions were made up in deionised Milli-Q water with a resistivity of at least 18 mΩcm.

Data analysis

Fits to straight lines were performed in Origin© or Excel. For the Pourbaix diagrams in Chapter 3 (section 3.3.5), the solver tool in Excel was used to minimise the sum of the difference of squares of the real and fitted data.

Appendix II

Derivation of Equation 2.12

As the potential E varies as a function of time in a cyclic voltammogram, the change in surface coverage of the oxidised or reduced species with respect to time, $d\Gamma_{ox}/dt$ or $d\Gamma_{red}/dt$, is related to the change in surface coverage of the oxidised or reduced species with respect to potential, $d\Gamma_{ox}/dE$ or $d\Gamma_{red}/dE$, can be defined by multiplying by the change in potential with respect to the change in time, dE/dt, i.e. the scan rate ν.

$$\frac{d\Gamma_{ox}}{dt} = \nu \frac{d\Gamma_{ox}}{dE} \qquad \text{Equation II.1A}$$

$$\frac{d\Gamma_{ox}}{dt} = \nu \frac{d\Gamma_{ox}}{dE} \qquad \text{Equation II.1B}$$

Let us now return to Equations 2.7A and 2.7B

$$\Gamma_{red} = \frac{\Gamma}{1+\exp\left(\frac{nF\left(E-E^0\right)}{RT}\right)} \qquad \text{Equation 2.7A}$$

$$\Gamma_{ox} = \frac{\Gamma}{1+\exp\left(\frac{nF\left(E-E^0\right)}{RT}\right)} \qquad \text{Equation 2.7B}$$

Differentiating Equations 2.7A and 2.7B with respect to E gives Equations II.2A and II.3B respectively.

$$\frac{d\Gamma_{red}}{dE} = \frac{-\Gamma(nF\exp(nF(E-E^\circ)))}{\left(1+\exp\left(\frac{nF\left(E-E^0\right)}{RT}\right)\right)^2} \qquad \text{Equation II.2A}$$

$$\frac{d\Gamma_{ox}}{dE} = \frac{-\Gamma(nF\exp(nF(E-E°)))}{\left(1+\exp\left(\frac{nF\left(E-E^0\right)}{RT}\right)\right)^2} \qquad \text{Equation II.2B}$$

Therefore the differentials of Γ_{ox} and Γ_{red} with respect to time are given by Equations II.3A and II.3B

$$\frac{d\Gamma_{red}}{dt} = \nu\frac{-\Gamma(nF\exp(nF(E-E°)))}{\left(1+\exp\left(\frac{nF\left(E-E^0\right)}{RT}\right)\right)^2} \qquad \text{Equations II.3A}$$

$$\frac{d\Gamma_{ox}}{dt} = \nu\frac{-\Gamma(nF\exp(nF(E-E°)))}{\left(1+\exp\left(\frac{nF\left(E-E^0\right)}{RT}\right)\right)^2} \qquad \text{Equation II.3B}$$

Insertion of Equations II.3A and II.3B into Equation 2.9 gives Equation 2.12.

$$i = \pm n^2F^2A\Gamma\nu\frac{\left(\exp\left(\frac{nF(E-E°)}{RT}\right)\right)}{\left(1+\exp\left(\frac{nF\left(E-E^0\right)}{RT}\right)\right)^2} \qquad \text{Equation 2.12}$$

Appendix III

Explanation of the Pourbaix diagram (Chapter 3)

Calculation of number of electrons involved in inactivation and reactivation

Let us consider the reactivation process.

$$H_{ox}^{inact} + ne^- \leftrightarrow H_{ox} \qquad \text{Reaction 3.1}$$

The Nernst equation can be adapted to describe Reaction 3.1.

$$E = E^\circ - \frac{2.3RT}{nF}\left(\text{Log}\frac{[H_{ox}]}{[H_{ox}^{inact}]}\right) \qquad \text{Equation III.1}$$

The concentration of H_{ox} present is proportional to the rate of reaction, and thus to the current recorded, i.

$$H_{ox} \alpha\, i \qquad \text{Equation III.2}$$

The proportion of the enzyme present in the H_{ox}^{inact} state is equal to the total concentration of enzyme (which is proportional to the maximum current recorded on the backward reductive scans shown in Figure 3.8, i.e. after the enzyme has fully reactivated) minus that known to be present in the active H_{ox} state because it is observed electrochemically as i. Thus, $[H_{ox}^{inact}]$ can be defined as follows:

$$H_{ox}^{inact} \alpha\, i_{max} - i \qquad \text{Equation III.3}$$

Therefore, the Nernst equation can be rearranged.

$$E = E^\circ - \frac{2.3RT}{nF}\left(\text{Log}\frac{i}{i_{max} - i}\right) \qquad \text{Equation III.4}$$

Therefore, the plot of potential against Log(i/(i_{max}-i)) will have a gradient of -2.3RT/nF. These are shown Figure 3.8. The values of n obtained are tabulated below:

pH	n for *Cr*HydA1	n for *Cs*HydA
5	1.35	1.20
6	1.18	1.04
7	0.99	1.03
8	1.05	1.09
9	1.08	1.09

Table III.1: n values obtained for the anaerobic inactivation and reactivation process for *Cr*HydA1 and *Cs*HydA from experiments such as those shown in Figure 3.8.

Derivation of the mechanism and fit to the Pourbaix diagram

The dependence of E_{switch} on pH as demonstrated in the Pourbaix diagram shown in Figure 3.9 is informative in terms of the mechanisms of inactivation and reactivation. Below approximately pH 6, E_{switch} is independent of pH. However, above pH 6, E_{switch} shifts by approximately 60 mV per pH unit. The activation process can be defined by Reaction III.1 in which n' is the number of protons involved in reactivation.

$$H_{ox}^{inact} + n'H^+ + e^- \rightarrow H_{ox} \qquad \text{Reaction III.1}$$

We know that the difference between E_{switch} at a given pH ($E^{o}_{pH=x}$) and E_{switch} at one pH unit higher ($E^{o}_{pH=x+1}$) is equal to 60 mV. The Nernst equations corresponding to the process described by Reaction III.1 at a given pH (x) and another pH which is equal to x + 1 are Equations III.5a and III.5b in which E is the electrode potential.

$$E = E^{o}_{pH=x} - \frac{2.3RT}{nF}\left(\mathrm{Log}\frac{\left[H_{ox}\right]}{\left[H_{ox}^{inact}\right]\left[H^+\right]_x^{n'}}\right) \qquad \text{Equation III.5a}$$

$$E = E^{o}_{pH=x+1} - \frac{2.3RT}{nF}\left(\mathrm{L\,og}\frac{\left[H_{ox}\right]}{\left[H_{ox}^{inact}\right]\left[H^{+}\right]^{n'}_{x+1}}\right) \qquad \text{Equation III.5b}$$

Subtracting Equation III.5b from Equation III.5a and setting the result to 60 mV allows n' to be determined. Above about pH 6, n' is thus equal to 1. Below pH 6, E_{switch} becomes independent of pH (i.e. $n' = 0$). Using this information along with the fact that H_{ox} and H_{ox}^{inact} are known to be in the oxidation states $Fe^{2+}Fe^{+}$ and $Fe^{2+}Fe^{2+}$,[66] respectively, the reaction mechanism can be summarised by Figure III.1.

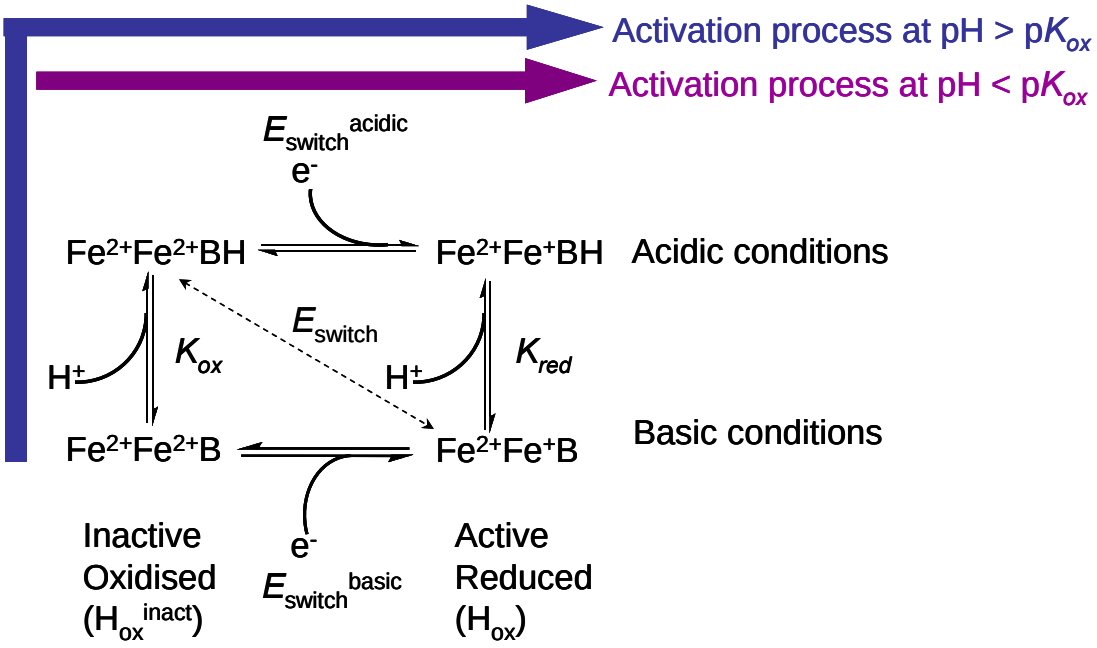

Figure III.1: Reaction mechanism for anaerobic inactivation and reactivation of *Cr*HydA1 and *Cs*HydA.

The system is thus characterized by two reduction potentials, E_{switch}^{acidic} and E_{switch}^{basic} for the equilibria involving an electron transfer and two equilibrium constants for the equilibria involving a proton transfer (K_{ox} and K_{red}). When the scan rate is slow enough, the species are at equilibrium and K_{ox} and K_{red} can thus be defined by Equations III.6 and III.7.

$$K_{ox} = \frac{\left[H^{+}\right]\left[Fe^{2+}Fe^{2+}B\right]}{\left[Fe^{2+}Fe^{2+}BH\right]} \qquad \text{Equation III.6}$$

$$K_{red} = \frac{\left[H^+\right]\left[Fe^{2+}Fe^{+}B\right]}{\left[Fe^{2+}Fe^{+}BH\right]} \qquad \text{Equation III.7}$$

The Nernst equation for the process of activation from H_{ox}^{iuact} to H_{ox} is given by Equation III.9 where [total oxidised species] = $[Fe^{2+}Fe^{2+}B]$ + $[Fe^{2+}Fe^{2+}BH]$ and [total reduced species] = $[Fe^{2+}Fe^{+}B]$ + $[Fe^{2+}Fe^{+}BH]$.

$$E = E_{switch} - \frac{2.3RT}{F}\mathrm{Log}\left(\frac{[\text{total oxidised species}]}{[\text{total reduced species}]}\right) \qquad \text{Equation III.8}$$

The Nernst equation describing E_{switch} in terms of the change from $Fe^{2+}Fe^{2+}BH$ to $Fe^{2+}Fe^{+}B$ can be derived using Equations III.6 and Equations III.7 as follows:

$$E = E_{switch} - \frac{2.3RT}{F}\mathrm{Log}\left(\frac{[Fe^{2+}Fe^{+}BH]\left([H^+]+K_{red}\right)}{[Fe^{2+}Fe^{2+}BH]\left([H^+]+K_{ox}\right)}\right) \qquad \text{Equation III.10}$$

$$E = E_{switch} - \frac{2.3RT}{F}\mathrm{Log}\left(\frac{[Fe^{2+}Fe^{+}BH]}{[Fe^{2+}Fe^{2+}BH]}\right) - \frac{2.3RT}{F}\mathrm{Log}\left(\frac{[H^+]+K_{red}}{[H^+]+K_{ox}}\right) \qquad \text{Equation III.11}$$

Under acidic conditions, we simply consider E as a function of E_{switch}^{acidic} and the Nernst equation is

$$E = E_{switch}^{acidic} - \frac{2.3RT}{F}\mathrm{Log}\left(\frac{[Fe^{2+}Fe^{+}BH]}{[Fe^{2+}Fe^{2+}BH]}\right) \qquad \text{Equation III.12}$$

Identifying Equation III.12 into Equation III.11 gives Equation III.13 which was used to fit the Pourbaix diagram.

$$E_{switch} = E_{switch}^{acidic} - \frac{2.3RT}{F}\mathrm{Log}\left(\frac{[H^+]+K_{ox}}{[H^+]+K_{red}}\right) \qquad \text{Equation III.13}$$

The pH equals the pK_{ox} when $[H^+] = K_{ox}$. This situation arises when $[Fe^{2+}Fe^{2+}B] = [Fe^{2+}Fe^{2+}BH]$ (see Equation III.6a), hence the placement of pK_{ox} on the Pourbaix diagram in Figure 3.9.

Appendix IV

Electrochemical calculation of K_M

The linearised form of the Michaelis-Menten equation, used as the basis for the Lineweaver-Burk plot, is given by Equation IV.1 in which the rate V_0 and the maximal rate V_{max} are defined by Equations IV.2 and IV.3

$$\frac{1}{V_0} = \frac{K_M}{V_{max}[S]} + \frac{1}{V_{max}} \qquad \text{Equation IV.1}$$

$$V_0 = k[S] \qquad \text{Equation IV.2}$$

$$V_{max} = k_{max}[S] \qquad \text{Equation IV.3}$$

In PFE, the rate constants k and k_{max} can be defined in terms of the current i and the corresponding maximal currents i_{max} (defined in Equation 2.14) by Equations IV.5 and IV.6 in which n is the number of electrons, F is the Faraday constant, A is the electrode area and Γ is the electroactive coverage of enzyme on the electrode.

$$\frac{i}{nFA\Gamma} = k \qquad \text{Equation IV.4}$$

$$\frac{i_{max}}{nFA\Gamma} = k_{max} \qquad \text{Equation IV.5}$$

Thus, implanting Equations IV.4 and IV.5 into Equations IV.2 and IV.3 and then inserting the result into Equation IV.1 gives the electrochemical version of the Michaelis-Menten equation, Equation 2.13.

$$\frac{1}{i} = \frac{K_M}{i_{cat}[S]} + \frac{1}{i_{cat}} \qquad \text{Equation 2.13}$$

Léger et al.[216] described experiments involving injection of an aliquot of buffer saturated with substrate into the cell and subsequent removal of the substrate by flushing the cell with an inert gas. In experiments, where the concentration of substrate is exponentially decreasing through the experiments (i.e. $[S] = [S]_0\exp(-t/\tau)$ where $[S]_0$ is the initial concentration of S at just after injection (t = 0) - see section 4.2.1), Equation 2.13 becomes Equation IV.6.

$$\frac{1}{i} = \frac{K_M}{i_{cat}[S]_0 \exp(-t/\tau)} + \frac{1}{i_{cat}} \qquad \text{Equation IV.6}$$

Calculation of K_I^{app}(inhibitor/substrate) *from experiments described in Chapter 3 and 5*

Let us return to Equation 3.2, used to calculate K_I^{app} for inhibition by H_2 in Chapter 3 and CO in Chapter 5 and Equation 4.5 from which it is derived.

$$(i_{N_2}/i_{inhibitor}) - 1 = \frac{[inhibitor]}{K_I^{app}(inhibitor/substrate)} \qquad \text{Equation 3.2}$$

$$\text{Log}((i_{N_2}/i_{inhibitor}) - 1) = \text{Log}(C_0/K_I^{app}(inhibitor/substrate)) - t/\tau \qquad \text{Equation 4.5}$$

In the Léger-type experiments in Chapter 4, the concentration of inhibitor is stepped by injecting inhibitor-saturated buffer into solution. The y-intercept of Equation 4.5 occurs at t = 0, i.e. just after the inhibitor-saturated buffer has been injected into the cell. In the experiments in Chapters 3 and 5, this is equivalent to the point at which the inhibitor present in the headspace of the cell has equilibrated with the solution and the current has reached its minimum. At this point, Equation 4.5 is simplified to

$$\text{Log}((i_{N_2}/i_{inhibitor}) - 1) = \text{Log}(C_0/K_I^{app}(inhibitor/substrate)) \qquad \text{Equation IV.3}$$

Taking the exponential of Equation IV.3 yields Equation 3.2.

Appendix V

Derivation of Equation 2.17

Let us consider the reactivation process described by Reaction 2.2 and define the total concentration of enzyme as being equal to the concentration of the "Inactive" species added to that of the "Active" species.

$$[\text{Total enzyme}] = [\text{Inactive}] + [\text{Active}] \qquad \text{Equation V.1}$$

The concentration of the "Inactive" species at $t = 0$ in the reactivation direction (i.e. when [Active] = 0), $[\text{Inactive}]_0$, is therefore equal to the total concentration of enzyme. When the reactivation process is complete (i.e. [Inactive] = 0 at, say, $t = \infty$) and all the enzyme has converted from the "Inactive" state to the "Active" state, [Active] is equal to $[\text{Inactive}]_0$. As [Active] at $t = \infty$ is proportional to i_{lim} and $[\text{Inactive}]_0$ must equal the concentration of "Active" species when the reactivation process is complete and i_{lim} has been reached, $i_{\text{lim}} \alpha [\text{Inactive}]_0$. As the concentration of the "Active" species throughout the reactivation process is proportional to i, [Inactive] must be proportional to i_{lim}-i throughout the reactivation process. Inserting these relations into Equation 2.16 gives Equation 2.17.

References

(1) *IPCC 2007: Summary for policy makers*; Cambridge University Press: Cambridge, 2007.
(2) Hoffman, P. *Tomorrow's Energy: Hydrogen, Fuel Cells and The Prospect of A Cleaner Planet*; MIT Press: Cambridge, Massachussetts, 2002.
(3) Jones, L. W. *Science* **1971**, *174*, 367-&.
(4) Grimes, C. A.; Varghese, O. K.; Ranjan, S. *Light, Water, Hydrogen: The Solar Generation of Hydrogen by Water and Photoelectrolysis*; Springer: New York, 2008.
(5) Cammack, R.; Frey, M.; Robson, R. *Hydrogen As a Fuel: Learning From Nature*; Taylor and Francis: London and New York, 2001.
(6) Bockris, J. O. M. *Science* **1972**, *176*, 1323-&.
(7) Ohta, T. In *Biohydrogen III*; Miyake, J., Igarashi, Y., Rögner, M., Eds.; Elsevier: Oxford, 2004, p 2-12.
(8) Deffeyes, K. *Huubert's peak: The Impending World Oil Shortage*; Princeton University Press: Oxford, 2003.
(9) Sorensen, B. *Hydrogen and Fuel Cells: Emerging Technologies and Applications*; Elsevier: London, 2005.
(10) Stephenson, M.; Stickland, L. H. *Biochem. J. (London)* **1931**, *25*, 205.
(11) Benemann, J. *Nat. Biotechnol.* **1996**, *14*, 1101-1103.
(12) Conrad, R. *Microbiol. Rev.* **1996**, *60*, 609-640.
(13) Lengeler, J.; Drews, G.; Schlegel, H. G. *Biology of the Prokaryotes*; Blackwell Science: Oxford, 1999.
(14) Mitchell, P. *Nature* **1961**, *191*, 144-&.
(15) Heidelberg, J. F.; Seshadri, R.; Haveman, S. A.; Hemme, C. L.; Paulsen, I. T.; Kolonay, J. F.; Eisen, J. A.; Ward, N.; Methe, B.; Brinkac, L. M.; Daugherty, S. C.; Deboy, R. T.; Dodson, R. J.; Durkin, A. S.; Madupu, R.; Nelson, W. C.; Sullivan, S. A.; Fouts, D.; Haft, D. H.; Selengut, J.; Peterson, J. D.; Davidsen, T. M.; Zafar, N.; Zhou, L.; Radune, D.; Dimitrov, G.; Hance, M.; Tran, K.; Khouri, H.; Gill, J.; Utterback, T. R.; Feldblyum, T. V.; Wall, J. D.; Voordouw, G.; Fraser, C. M. *Nat. Biotechnol.* **2004**, *22*, 554-559.
(16) Gorwa, M. F.; Croux, C.; Soucaille, P. *J. Bacteriol.* **1996**, *178*, 2668-2675.
(17) Appel, J.; Phunpruch, S.; Steinmuller, K.; Schulz, R. *Arch. Microbiol.* **2000**, *173*, 333-338.
(18) Vincent, K. A.; Parkin, A.; Lenz, O.; Albracht, S. P. J.; Fontecilla-Camps, J. C.; Cammack, R.; Friedrich, B.; Armstrong, F. A. *J. Am. Chem. Soc.* **2005**, *127*, 18179-18189.
(19) Odom, J. M.; Peck, H. D. *Annu. Rev. Microbiol.* **1984**, *38*, 551-592.
(20) Allakhverdiev, S. I.; Kreslavski, V. D.; Thavasi, V.; Zharmukhamedov, S. K.; Klimov, V. V.; Nagata, T.; Nishihara, H.; Ramakrishna, S. *Photochem. Photobiol. Sci.* **2009**, *8*, 148-156.
(21) Mertens, R.; Liese, A. *Curr. Opin. Biotechnol.* **2004**, *15*, 343-348.
(22) Adams, M. W. W.; Stiefel, E. I. *Science* **1998**, *282*, 1842.
(23) Lewis, N. S.; Nocera, D. G. *Proc. Nat. Acad. Sci.* **2006**, *103*, 15729-15735.
(24) Curtright, A. E.; Morgan, M. G.; Keith, D. W. *Environ. Sci. Technol.* **2008**, *42*, 9031-9038.
(25) *International energy outlook*; US Department of Energy: Washington DC, May 2007.
(26) Gaffron, H.; Rubin, J. *J. Gen. Physiol.* **1942**, *26*, 219-240.

(27) Tamagnini, P.; Leitao, E.; Oliveira, P.; Ferreira, D.; Pinto, F.; Harris, D. J.; Heidorn, T.; Lindblad, P. *FEMS Microbiol. Rev.* **2007**, *31*, 692-720.
(28) Gest, H.; Ormerod, J. G.; Ormerod, K. S. *Arch. Biochem. Biophys.* **1962**, *97*, 21-33.
(29) Zurrer, H.; Bachofen, R. *Appl. Environ. Microbiol.* **1979**, *37*, 789-793.
(30) Melnicki, M. R.; Bianchi, L.; De Philippis, R.; Melis, A. *Int. J. Hyd. En.* **2008**, *33*, 6525-6534.
(31) Hallenbeck, P. C.; Benemann, J. R. *Int. J. Hyd. En.* **2002**, *27*, 1185-1193.
(32) Ghirardi, M. L.; Posewitz, M. C.; Maness, P.-C.; Dubini, A.; Yu, J.; Seibert, M. *Annu. Rev. Plant Biol.* **2007**, *58*, 71-91.
(33) Hall, D. O.; Markov, S. A.; Watanabe, Y.; Rao, K. K. *Photosynthesis Res.* **1995**, *46*, 159-167.
(34) Happe, T.; Schutz, K.; Bohme, H. *J. Bacteriol.* **2000**, *182*, 1624-1631.
(35) Ghirardi, M. L.; Dubini, A.; Yu, J. P.; Maness, P. C. *Chem. Soc. Rev.* **2009**, *38*, 52-61.
(36) Lubitz, W.; Reijerse, E. J.; Messinger, J. *En. Environ. Sci.* **2008**, *1*, 15-31.
(37) Ghirardi, M. L.; Togasaki, R. K.; Seibert, M. *Appl. Biochem. Biotechnol.* **1997**, *63*, 141-151.
(38) Forestier, M.; King, P.; Zhang, L. P.; Posewitz, M.; Schwarzer, S.; Happe, T.; Ghirardi, M. L.; Seibert, M. *Eur. J. Biochem.* **2003**, *270*, 2750-2758.
(39) Happe, T.; Kaminski, A. *Eur. J. Biochem.* **2002**, *269*, 1022-1032.
(40) Barber, J.; Andersson, B. *Trends Biochem. Sci.* **1992**, *17*, 61-66.
(41) Surzycki, R.; Cournac, L.; Peltier, G.; Rochaix, J.-D. *Proc. Natl. Acad. Sci. U. S. A.* **2007**, *104*, 17548-17553.
(42) Kruse, O.; Rupprecht, J.; Bader, K.-P.; Thomas-Hall, S.; Schenk, P. M.; Finazzi, G.; Hankamer, B. *J. Biol. Chem.* **2005**, *280*, 34170-34176.
(43) Ghirardi, M. L.; King, P.; Kosourov, S.; Forestier, M.; Zhang, L.; Seibert, M. In *Artificial Photosynthesis*; Collings, A. F., Critchley, C., Eds.; Wiley Verlag: Germany, 2005.
(44) King, P. W.; Svedruzic, D.; Cohen, J.; Schulten, K.; Seibert, M.; Ghirardi, M. L. *Sol. Hyd. Nanotech.* **2006**, *6340*, U263-U271.
(45) Hambourger, M.; Gervaldo, M.; Svedruzic, D.; King, P. W.; Gust, D.; Ghirardi, M.; Moore, A. L.; Moore, T. A. *J. Am. Chem. Soc.* **2008**, *130*, 2015-2022.
(46) de la Garza, L.; Jeong, G.; Liddell, P. A.; Sotomura, T.; Moore, T. A.; Moore, A. L.; Gust, D. *J. Phys. Chem. B* **2003**, *107*, 10252-10260.
(47) Reisner, E.; Fontecilla-Camps, J. C.; Armstrong, F. A. *Chem. Comm.* **2009**, 550-552.
(48) Hallenbeck, P. C. *Water Sci. Technol.* **2005**, *52*, 21-9.
(49) Gfeller, R. P.; Gibbs, M. *Plant Physiol.* **1984**, *75*, 212-218.
(50) Maeda, T.; Sanchez-Torres, V.; Wood, T. K. *Appl. Microbiol. Biotechnol.* **2008**, *79*, 77-86.
(51) Demuez, M.; Cournac, L.; Guerrini, O.; Soucaille, P.; Girbal, L. *FEMS Microbiol. Lett.* **2007**, *275*, 113-121.
(52) von Abendroth, G.; Stripp, S.; Silakov, A.; Croux, C.; Soucaille, P.; Girbal, L.; Happe, T. *Int. J. Hyd. En.* **2008**, *33*, 6076-6081.
(53) Michel, C.; Giudici-Orticoni, M.-T.; Baymann, F.; Bruschi, M. *Water, Air, Soil Pollut. Focus* **2003**, *3*, 161-169.

(54) Macaskie, L. E.; Baxter-plant, V. S.; Creamer, N. J.; Humphries, A. C.; Mikheenko, I. P.; Mikheenko, P. M.; Penfold, D. W.; Yong, P. *Biochem. Soc. Trans.* **2005**, *33*, 76-79.
(55) Watrous, M. M.; Clark, S.; Kutty, R.; Huang, S. Q.; Rudolph, F. B.; Hughes, J. B.; Bennett, G. N. *Appl. Environ. Microbiol.* **2003**, *69*, 1542-1547.
(56) Adams, M. W. W.; Rao, K. K.; Hall, D. O. *Photobiochem. Photobiophys.* **1979**, *1*, 33-41.
(57) Jones, A. K.; Sillery, E.; Albracht, S. P. J.; Armstrong, F. A. *Chem. Comm.* **2002**, 866-867.
(58) Vincent, K. A.; Cracknell, J. A.; Clark, J. R.; Ludwig, M.; Lenz, O.; Friedrich, B.; Armstrong, F. A. *Chem. Comm.* **2006**, 5033-5035.
(59) Vincent, K. A.; Cracknell, J. A.; Lenz, O.; Zebger, I.; Friedrich, B.; Armstrong, F. A. *Proc. Natl. Acad. Sci. U. S. A.* **2005**, *102*, 16951-16954.
(60) Cracknell, J. A.; Vincent, K. A.; Armstrong, F. A. *Chem. Rev.* **2008**, *108*, 2439-2461.
(61) Peck, H. D.; Pietro, A. S.; Gest, H. *Proc. Natl. Acad. Sci. U. S. A.* **1956**, *42*, 13-19.
(62) Friedrich, C. G.; Schneider, K.; Friedrich, B. *J. Bacteriol.* **1982**, *152*, 42-48.
(63) Cammack, R.; Patil, D.; Aguirre, R.; Hatchikian, E. C. *FEBS Lett.* **1982**, *142*, 289-292.
(64) Graf, E. G.; Thauer, R. K. *FEBS Lett.* **1981**, *136*, 165-169.
(65) Legall, J.; Ljungdahl, P. O.; Moura, I.; Peck, H. D.; Xavier, A. V.; Moura, J. J. G.; Teixera, M.; Huynh, B. H.; Dervartanian, D. V. *Biochem. Biophys. Res. Commun.* **1982**, *106*, 610-616.
(66) Fontecilla-Camps, J. C.; Volbeda, A.; Cavazza, C.; Nicolet, Y. *Chem. Rev.* **2007**, *107*, 4273-4303.
(67) Adams, M. W. W. *Biochim. Biophys. Acta* **1990**, *1020*, 115-145.
(68) Sorgenfrei, O.; Linder, D.; Karas, M.; Klein, A. *Eur. J. Biochem.* **1993**, *213*, 1355-1358.
(69) Albracht, S. P. J. *Biochim. Biophys. Acta* **1994**, *1188*, 167-204.
(70) Shima, S.; Thauer, R. K. *Chem. Rec.* **2007**, *7*, 37-46.
(71) Vignais, P. M.; Billoud, B.; Meyer, J. *FEMS Microbiol. Rev.* **2001**, *25*, 455-501.
(72) Vignais, P. M.; Colbeau, A. *Curr. Issues Mol. Biol.* **2004**, *6*, 159-188.
(73) Vignais, P. M.; Billoud, B. *Chem. Rev.* **2007**, *107*, 4206-4272.
(74) Berkessel, A.; Thauer, R. K. *Angew. Chem. Int. Ed.* **1995**, *34*, 2247-2250.
(75) Adams, M. W. W.; Stiefel, E. I. *Curr. Opin. Chem. Biol.* **2000**, *4*, 214-220.
(76) Shima, S.; Lyon, E. J.; Thauer, R. K.; Mienert, B.; Bill, E. *J. Am. Chem. Soc.* **2005**, *127*, 10430-10435.
(77) Das, D.; Dutta, T.; Nath, K.; Kotay, S. M.; Das, A. K.; Veziroglu, T. N. *Curr. Sci.* **2006**, *90*, 1627-1637.
(78) Volbeda, A.; Charon, M. H.; Piras, C.; Hatchikian, E. C.; Frey, M.; Fontecilla-Camps, J. C. *Nature* **1995**, *373*, 580-587.
(79) Volbeda, A.; Garcia, E.; Piras, C.; De Lacey, A. L.; Fernandez, V. M.; Hatchikian, E. C.; Frey, M.; Fontecilla-Camps, J. C. *J. Am. Chem. Soc.* **1996**, *118*, 12989-12996.

(80) Volbeda, A.; Montet, Y.; Vernede, X.; Hatchikian, E. C.; Fontecilla-Camps, J. C. *Int. J. Hyd. En.* **2002**, *27*, 1449-1461.
(81) Matias, P. M.; Soares, C. M.; Saraiva, L. M.; Coelho, R.; Morais, J.; Gall, J. L.; Carrondo, M. A. *J. Biol. Inorg. Chem.* **2001**, *6*, 63 - 81
(82) Garcin, E.; Vernede, X.; Hatchikian, C.; Volbeda, A.; Frey, M.; Fontecilla-Camps, J. C. *Structure* **1999**, *7*, 557-566.
(83) Higuchi, Y.; Ogata, H.; Miki, K.; Yasuoka, N.; Yagi, T. *Structure* **1999**, *7*, 549-556.
(84) Happe, R. P.; Roseboom, W.; Albracht, S. P. J. *Eur. J. Biochem.* **1999**, *259*, 602-608.
(85) Pierik, A. J.; Roseboom, W.; Happe, R. P.; Bagley, K. A.; Albracht, S. P. J. *J. Biol. Chem.* **1999**, *274*, 3331-3337.
(86) Schroeder, O.; Bleijlevens, B.; Jongh, T. E.; Chen, Z.; Li, T.; Fischer, J.; Foerster, J.; Friedrich, C. G.; Bagley, K. A.; Albracht, S. P. J.; Lubitz, W. *J. Biol. Inorg. Chem.* **2007**, *12*, 212-233.
(87) Vincent, K. A.; Parkin, A.; Armstrong, F. A. *Chem. Rev.* **2007**, *107*, 4366-4413.
(88) Armstrong, F. A.; Belsey, N. A.; Cracknell, J. A.; Goldet, G.; Parkin, A.; Reisner, E.; Vincent, K. A.; Wait, A. F. *Chem. Soc. Rev.* **2009**, *38*, 36-51.
(89) Valente, F. M. A.; Oliveira, A. S. F.; Gnadt, N.; Pacheco, I.; Coelho, A. V.; Xavier, A. V.; Teixeira, M.; Soares, C. M.; Pereira, I. A. C. *J. Biol. Inorg. Chem.* **2005**, *10*, 667-682.
(90) Voordouw, G.; Menon, N. K.; Legall, J.; Choi, E. S.; Peck, H. D.; Przybyla, A. E. *J. Bacteriol.* **1989**, *171*, 2894-2899.
(91) Volbeda, A.; Martin, L.; Cavazza, C.; Matho, M.; Faber, B. W.; Roseboom, W.; Albracht, S. P. J.; Garcin, E.; Rousset, M.; Fontecilla-Camps, J. C. *J. Biol. Inorg. Chem.* **2005**, *10*, 239-249.
(92) Fichtner, C.; Laurich, C.; Bothe, E.; Lubitz, W. *Biochemistry* **2006**, *45*, 9706-9716.
(93) De Lacey, A. L.; Hatchikian, E. C.; Volbeda, A.; Frey, M.; Fontecilla-Camps, J. C.; Fernandez, V. M. *J. Am. Chem. Soc.* **1997**, *119*, 7181-7189.
(94) Bleijlevens, B.; Buhrke, T.; van der Linden, E.; Friedrich, B.; Albracht, S. P. J. *J. Biol. Chem.* **2004**, *279*, 46686-46691.
(95) Huyett, J. E.; Carepo, M.; Pamplona, A.; Franco, R.; Moura, I.; Moura, J. J. G.; Hoffman, B. M. *J. Am. Chem. Soc.* **1997**, *119*, 9291-9292.
(96) Maroney, M. J.; Bryngelson, P. A. *J. Biol. Inorg. Chem.* **2001**, *6*, 453-459.
(97) Jones, A. K.; Lamle, S. E.; Pershad, H. R.; Vincent, K. A.; Albracht, S. P. J.; Armstrong, F. A. *J. Am. Chem. Soc* **2003**, *125*, 8505-8514.
(98) Coremans, J.; Van der Zwaan, J. W.; Albracht, S. P. J. *Biochim. Biophys. Acta* **1992**, *1119*, 157-168.
(99) Kurkin, S.; George, S. J.; Thornley, R. N. F.; Albracht, S. P. J. *Biochemistry* **2004**, *43*, 6820-6831.
(100) Ogata, H.; Hirota, S.; Nakahara, A.; Komori, H.; Shibata, N.; Kato, T.; Kano, K.; Higuchi, Y. *Structure* **2005**, *13*, 1635-1642.
(101) Niu, S.; Thomson, L. M.; Hall, M. B. *J. Am. Chem. Soc* **1999**, *121*, 4000-4007.
(102) Teixeira, M.; Moura, I.; Xavier, A. V.; Dervartanian, D. V.; Legall, J.; Peck, H. D.; Huynh, B. H.; Moura, J. J. G. *Eur. J. Biochem.* **1983**, *130*, 481-484.

(103) Teixeira, M.; Moura, I.; Xavier, A. V.; Huynh, B. H.; Dervartanian, D. V.; Peck, H. D.; Legall, J.; Moura, J. J. G. *J. Biol. Chem.* **1985**, *260*, 8942-8950.
(104) Lamle, S. E.; Albracht, S. P. J.; Armstrong, F. A. *J. Am. Chem. Soc.* **2005**, *127*, 6595-6604.
(105) Lamle, S. E.; Albracht, S. P. J.; Armstrong, F. A. *J. Am. Chem. Soc.* **2004**, *126*, 14899-14909.
(106) Ogata, H.; Mizoguchi, Y.; Mizuno, N.; Miki, K.; Adachi, S.-i.; Yasuoka, N.; Yagi, T.; Yamauchi, O.; Hirota, S.; Higuchi, Y. *J. Am. Chem. Soc* **2002**, *124*, 11628-11635.
(107) Cammack, R.; Patil, D. S.; Hatchikian, E. C.; Fernandez, V. M. *Biochim. Biophys. Acta* **1987**, *912*, 98-109.
(108) Van der zwaan, J. W.; Albracht, S. P. J.; Fontijn, R. D.; Roelofs, Y. B. M. *Biochim. Biophys. Acta* **1986**, *872*, 208-215.
(109) Niu, S.; Hall, N. B. *Inorg. Chem.* **2001**, *40*, 6201-6203.
(110) Pavlov, M. *J. Am. Chem. Soc.* **1998**, *120*, 548.
(111) Siegbahn, P. E. M.; Blomberg, M. R. A.; Pavlov, M. W. N.; Crabtree, R. H. *J. Biol. Inorg. Chem.* **2001**, *6*, 460-466.
(112) Amara, P.; Volbeda, A.; Fontecilla-Camps, J. C.; Field, M. J. *J. Am. Chem. Soc* **1999**, *121*, 4468-4477.
(113) Kubas, G. J. *Acc. Chem. Res.* **1988**, *21*, 120-128.
(114) Bagley, K. A.; Duin, E. C.; Roseboom, W.; Albracht, S. P. J.; Woodruff, W. H. *Biochemistry* **1995**, *34*, 5527-5535.
(115) De Lacey, A. L.; Santamaria, E.; Hatchikian, E. C.; Fernandez, V. M. *Biochim. Biophys. Acta* **2000**, *1481*, 371-380.
(116) Dementin S; Burlat B; De Lacey, A. L.; Pardo, A.; Adryanczyk-Perrier, G.; Guigliarelli, B.; Fernandez, V. M.; Rousset, M. *J. Biol. Chem.* **2004**, *279*, 10508-10513.
(117) Meyer, J. *Cell. Mol. Life Sci.* **2007**, *64*, 1063-1084.
(118) Fontecilla-Camps, J. C.; Frey, M.; Garcin, E.; Hatchikian, C.; Montet, Y.; Piras, C.; Vernede, X.; Volbeda, A. *Biochimie* **1997**, *79*, 661-666.
(119) Nicolet, Y.; Piras, C.; Legrand, P.; Hatchikian, C.; Fontecilla-Camps, J. C. *Structure* **1999**, *7*, 13-23.
(120) Peters, J. W.; Lanzilotta, W. N.; Lemon, B. J.; Seefeldt, L. C. *Science* **1998**, *282*, 1853-1858.
(121) Hatchikian, E. C.; Magro, V.; Forget, N.; Nicolet, Y.; Fontecilla-Camps, J. C. *J. Bacteriol.* **1999**, *181*, 2947-2952.
(122) Pandey, A. S.; Harris, T. V.; Giles, L. J.; Peters, J. W.; Szilagyi, R. K. *J. Am. Chem. Soc.* **2008**, *130*, 4533-4540.
(123) Adams, M. W. W.; Eccleston, E.; Howard, J. B. *Proc. Natl. Acad. Sci. U. S. A.* **1989**, *86*, 4932-4936.
(124) Kamp, C.; Silakov, A.; Winkler, M.; Reijerse, E. J.; Lubitz, W.; Happe, T. *Biochim. Biophys. Acta - Bioenerg.* **2008**, *1777*, 410-416.
(125) Lemon, B. J.; Peters, J. W. In *Handbook of Metalloproteins*; Messerschmidt, A., Huber, R., Poulos, T., Wieghardt, K., Eds.; Wiley: Chichester, 2004; Vol. 2.
(126) Nicolet, Y.; De Lacey, A. L.; Vernede, X.; Fernandez, V. M.; Hatchikian, E. C.; Fontecilla-Camps, J. C. *J. Am. Chem. Soc.* **2001**, *123*, 1596-1601.
(127) Pierik, A. J.; Hulstein, M.; Hagen, W. R.; Albracht, S. P. J. *Eur. J. Biochem.* **1998**, *258*, 572-578.

(128) Kubas, G. J. *Chem. Rev.* **2007**, *107*, 4152-4205.
(129) Pereira, A. S.; Tavares, P.; Moura, I.; Moura, J. J. G.; Huynh, B. H. *J. Am. Chem. Soc.* **2001**, *123*, 2771-2782.
(130) Nicolet, Y.; Cavazza, C.; Fontecilla-Camps, J. C. *J. Inorg. Biochem.* **2002**, *91*, 1-8.
(131) Thomann, H.; Bernardo, M.; Adams, M. W. W. *J. Am. Chem. Soc.* **1991**, *113*, 7044-7046.
(132) Williams, R.; Cammack, R.; Hatchikian, E. C. *J. Chem. Soc. - Faraday Trans.* **1993**, *89*, 2869-2872.
(133) VanDam, P. J.; Reijerse, E. J.; Hagen, W. R. *Eur. J. Biochem.* **1997**, *248*, 355-361.
(134) Silakov, A.; Wenk, B.; Reijerse, E.; Lubitz, W. *Physical Chemistry and Chemical Physics* **2009**, *In press*.
(135) VanderSpek, T. M.; Arendsen, A. F.; Happe, R. P.; Yun, S. Y.; Bagley, K. A.; Stufkens, D. J.; Hagen, W. R.; Albracht, S. P. J. *Eur. J. Biochem.* **1996**, *237*, 629-634.
(136) Schwab, D. E.; Tard, C.; Brecht, E.; Peters, J. W.; Pickett, C. J.; Szilagyi, R. K. *Chem. Comm.* **2006**, 3696-3698.
(137) Nicolet, Y.; Lemon, B. J.; Fontecilla-Camps, J. C.; Peters, J. W. *Trends Biochem. Sci.* **2000**, *25*, 138-143.
(138) Lemon, B. J.; Peters, J. W. *Biochemistry* **1999**, *38*, 12969-12973.
(139) Roseboom, W.; Lacey, A. L.; Fernandez, V. M.; Hatchikian, E. C.; Albracht, S. P. J. *J. Biol. Inorg. Chem.* **2006**, *11*, 102-118.
(140) Nakamoto, K. In *Infrared and Raman Spectra of Inorganic Coordination Compounds. Part B*; John Wiley & Sons: New York, 1997.
(141) Patil, D. S.; Moura, J. J. G.; He, S. H.; Teixeira, M.; Prickril, B. C.; Dervartanian, D. V.; Peck, H. D.; Legall, J.; Huynh, B. H. *J. Biol. Chem.* **1988**, *263*, 18732-18738.
(142) Pierik, A. J.; Hagen, W. R.; Redeker, J. S.; Wolbert, R. B. G.; Boersma, M.; Verhagen, M. F. J. M.; Grande, H. J.; Veeger, C.; Mutsaers, P. H. A.; Sands, R. H.; Dunham, W. R. *Eur. J. Biochem.* **1992**, *209*, 63-72.
(143) Hatchikian, C.; Forget, N.; Fernandez, V. M.; Williams, R.; Cammack, R. *Eur. J. Biochem.* **1992**, *209*, 357-365.
(144) De Lacey, A. L.; Fernandez, V. M.; Rousset, M.; Cammack, R. *Chem. Rev.* **2007**, *107*, 4304-4330.
(145) Liu, Z.-P.; Hu, P. *J. Am. Chem. Soc.* **2002**, *124*, 5175-5182.
(146) Silakov, A.; Reijerse, E. J.; Albracht, S. P. J.; Hatchikian, E. C.; Lubitz, W. *J. Am. Chem. Soc.* **2007**, *129*, 11447-11458.
(147) De Lacey, A. L.; Stadler, C.; Cavazza, C.; Hatchikian, C.; Fernandez, V. M. *J. Am. Chem. Soc.* **2000**, *122*, 11232-11233.
(148) Albracht, S. P. J.; Roseboom, W.; Hatchikian, E. C. *J. Biol. Inorg. Chem.* **2006**, *11*, 88-101.
(149) Cao, Z.; Hall, M. B. *J. Am. Chem. Soc* **2001**, *123*, 3734-3742.
(150) Armstrong, F. A. *Curr. Opin. Chem. Biol.* **2004**, *8*, 133-140.
(151) Peters, J. W. *Curr. Opin. Struct. Biol.* **1999**, *9*, 670-676.
(152) Siegbahn, P. E. M.; Tye, J. W.; Hall, M. B. *Chem. Rev.* **2007**, *107*, 4414-4435.
(153) Zhou, T.; Mo, Y.; Liu, A.; Zhou, Z.; Tsai, K. R. *Inorg. Chem.* **2004**, *43*, 923-930.
(154) Fan, H.-J.; Hall, M. B. *J. Am. Chem. Soc.* **2001**, *123*, 3828-3829.

(155) Lemon, B. J.; Peters, J. W. *J. Am. Chem. Soc.* **2000**, *122*, 3793-3794.
(156) van Haaster, D. J.; Jongejan, J. A.; Hagedoorn, P.-L.; Hagen, W. R. *Int. J. Hyd. En.* **2006**, *31*, 1432-1438.
(157) Cohen, J.; Kim, K.; King, P.; Seibert, M.; Schulten, K. *Structure* **2005**, *13*, 1321-1329.
(158) Cohen, J.; Kim, K.; Posewitz, M.; Ghirardi, M. L.; Schulten, K.; Seibert, M.; King, P. *Biochem. Soc. Trans.* **2005**, *33*, 80-82.
(159) Frey, M.; Fontecilla-Camps, J. C. In *Handbook of Metalloproteins*; Messerschmidt, A., Huber, R., Poulos, T., Wieghardt, K., Eds.; Wiley: Chichester, 2004; Vol. 2.
(160) Montet, Y.; Amara, P.; Volbeda, A.; Vernede, X.; Hatchikian, E. C.; Field, M. J.; Frey, M.; FontecillaCamps, J. C. *Nat. Struct. Biol.* **1997**, *4*, 523-526.
(161) Teixeira, V. H.; Baptista, A. M.; Soares, C. M. *Biophys. J.* **2006**, *91*, 2035-2045.
(162) Leroux, F.; Dementin, S.; Burlatt, B.; Cournac, L.; Volbeda, A.; Champ, S.; Martin, L.; Guigliarelli, B.; Bertrand, P.; Fontecilla-Camps, J.; Rousset, M.; Léger, C. *Proc. Natl. Acad. Sci. U. S. A.* **2008**, *105*, 11188-11193.
(163) Buhrke, T.; Lenz, O.; Krauss, N.; Friedrich, B. *J. Biol. Chem.* **2005**, *280*, 23791-23796.
(164) Capon, J. F.; Gloaguen, F.; Petillon, F. Y.; Schollhammer, P.; Talarmin, J. *Eur. J. Inorg. Chem.* **2008**, 4671-4681.
(165) Rauchfuss, T. B. *Science* **2007**, *316*, 553-554.
(166) Gloaguen, F.; Rauchfuss, T. B. *Chem. Soc. Rev.* **2009**, *38*, 100-108.
(167) Tard, C.; Pickett, C. J. *Chem. Rev.* **2009**, *109*, 2245-2274.
(168) Kubas, G. J. *Metal Dihydrogen and Sigma- Bond Complexes*; Kluwer Academic: London, 2001.
(169) Tye, J. W.; Darensbourg, M. Y.; Hall, M. B. *Inorg. Chem.* **2008**, *47*, 2380-2388.
(170) Barton, B. E.; Olsen, M. T.; Rauchfuss, T. B. *J. Am. Chem. Soc.* **2008**, *130*, 16834-5.
(171) Curtis, C. J.; Miedaner, A.; Ciancanelli, R.; Ellis, W. W.; Noll, B. C.; DuBois, M. R.; DuBois, D. L. *Inorg. Chem.* **2003**, *42*, 216-227.
(172) Tard, C.; Liu, X.; Ibrahim, S. K.; Bruschi, M.; De Gioia, L.; Davies, S. C.; Yang, X.; Wang, L.-S.; Sawers, G.; Pickett, C. J. *Nature* **2005**, *433*, 610-613.
(173) Hu, X.; Brunschwig, B. S.; Peters, J. C. *J. Am. Chem. Soc.* **2007**, *129*, 8988-8998.
(174) Savéant, J. M. *Elements of molecular and biomolecular electrochemistry: an electrochemical approach to electron transfer*; Wiley-Interscience: Chichester, 2006.
(175) Eddowes, M. J.; Hill, H. A. O. *Journal of the Chemistry Society, Chemical Communications* **1977**, 771-772.
(176) Yeh, P.; Kawana, T. *Chem. Lett.* **1977**, 1145-1148.
(177) Armstrong, F. A. *Structure and Bonding* **1990**, *72*, 137-230.
(178) Brett, C. M. A.; Oliveira Brett, A. M. *Electrochemistry: Principles, Methods and Applications*; Oxford University Press: Oxford, 1993.
(179) Vincent, K. A.; Armstrong, F. A. *Inorg. Chem.* **2005**, *44*, 798-809.
(180) Hirst, J. *Biochim. Biophys. Acta - Bioenerg.* **2006**, *1757*, 225-239.
(181) Léger, C.; Bertrand, P. *Chem. Rev.* **2008**, *108*, 2379-2438.

(182) Hoeben, F. J. M.; Meijer, F. S.; Dekker, C.; Albracht, S. P. J.; Heering, H. A.; Lemay, S. G. *Acs Nano* **2008**, *2*, 2497-2504.
(183) Pershad, H. R.; Duff, J. L. C.; Heering, H. A.; Duin, E. C.; Albracht, S. P. J.; Armstrong, F. A. *Biochemistry* **1999**, *38*, 8992-8999.
(184) Page, C. C.; Moser, C. C.; Chen, X.; Dutton, P. L. *Nature* **1999**, *407*, 47-52.
(185) Armstrong, F. A.; Cox, P. A.; Hill, H. A. O.; Lowe, V. J.; Oliver, B. N. *J. Electroanal. Chem. and Interfac. Electrochem.* **1987**, *217*, 331-366.
(186) Gwyer, J. D.; Zhang, J. D.; Butt, J. N.; Ulstrupy, J. *Biophys. J.* **2006**, *91*, 3897-3906.
(187) Hasan, M. N.; Kwakernaak, C.; Sloof, W. G.; Hagen, W. R.; Heering, H. A. *J. Biol. Inorg. Chem.* **2006**, *11*, 651-662.
(188) McCreery, R. L. *Chem. Rev.* **2008**, *108*, 2646-2687.
(189) Fourmond, V.; Lautier, T.; Baffert, C.; Leroux, F.; Liebgott, P. P.; Dementin, S.; Rousset, M.; Arnoux, P.; Pignol, D.; Meynial-Salles, I.; Soucaille, P.; Bertrand, P.; Léger, C. *Anal. Chem.* **2009**, *81*, 2962-2968.
(190) Blanford, C. F.; Heath, R. S.; Armstrong, F. A. *Chem. Comm.* **2007**, 1710-1712.
(191) Rudiger, O.; Abad Jose, M.; Hatchikian, E. C.; Fernandez Victor, M.; De Lacey Antonio, L. *J. Am. Chem. Soc.* **2005**, *127*, 16008-9.
(192) Baymann, F.; Barlow, N. L.; Aubert, C.; Schoepp-Cothenet, B.; Leroy, G.; Armstrong, F. A. *FEBS Lett.* **2003**, *539*, 91-94.
(193) Schlereth, D. D. *J. Electroanal. Chem.* **1997**, *425*, 77-85.
(194) Jeuken, L. J. C.; Armstrong, F. A. *J. Phys. Chem. B* **2001**, *105*, 5271-5282.
(195) Bard, A. J.; Faulkner, L. R.; Wiley & Sons: Chichester, 2001.
(196) Armstrong, F. A.; Wilson, G. S. *Electrochim. Acta* **2000**, *45*, 2623-2645.
(197) Sucheta, A.; Cammack, R.; Weiner, J.; Armstrong, F. A. *Biochemistry* **1993**, *32*, 5455-5465.
(198) Hirst, J.; Armstrong, F. A. *Anal. Chem.* **1998**, *70*, 5062-5071.
(199) Heering, H. A.; Weiner, J. H.; Armstrong, F. A. *J. Am. Chem. Soc.* **1997**, *119*, 11628-11638.
(200) Mondal, M. S., Goodin, D. B., and Armstrong, F. A. *J. Am. Chem. Soc* **1998**, *120*, 6270-6276.
(201) Hudson, J. M.; Heffron, K.; Kotlyar, V.; Sher, Y.; Maklashina, E.; Cecchini, G.; Armstrong, F. A. *J. Am. Chem. Soc.* **2005**, *127*, 6977-6989.
(202) Pankhurst, K. L.; Mowat, C. G.; Rothery, E. L.; Hudson, J. M.; Jones, A. K.; Miles, C. S.; Walkinshaw, M. D.; Armstrong, F. A.; Reid, G. A.; Chapman, S. K. *J. Biol. Chem.* **2006**, *281*, 20589-20597.
(203) Léger, C.; Jones, A. K.; Albracht, S. P. J.; Armstrong, F. A. *J. Phys. Chem. B* **2002**, *106*, 13058-13063.
(204) Parkin, A.; Cavazza, C.; Fontecilla-Camps, J. C.; Armstrong, F. A. *J. Am. Chem. Soc.* **2006**, *128*, 16808-16815.
(205) Parkin, A.; Goldet, G.; Cavazza, C.; Fontecilla-Camps, J. C.; Armstrong, F. A. *J. Am. Chem. Soc.* **2008**, *130*, 13410-13416.
(206) Horwood, E. *Instrumental Methods in Electrochemistry*; Southhampton Electrochemistry Group: Chichester, 1993.
(207) Chen, S. In *Handbook of Electrochemistry*; Zoski, C. G., Ed.; Elsevier: Oxford, 2007.

(208) Léger, C.; Jones, A. K.; Roseboom, W.; Albracht, S. P. J.; Armstrong, F. A. *Biochemistry* **2002**, *41*, 15736-15746.
(209) Goldet, G.; Wait, A. F.; Cracknell, J. A.; Vincent, K. A.; Ludwig, M.; Lenz, O.; Friedrich, B. r.; Armstrong, F. A. *J. Am. Chem. Soc.* **2008**, *130*, 11106-11113.
(210) Lide, D. R. *C.R.C. Handbook of Chemistry and Physics* **1996-1997**, *77th Edition*.
(211) Stripp, S.; Sanganas, O.; Happe, T.; Haumann, M. *Biochemistry* **2009**, *48*, 5042-5049.
(212) Florin, L.; Tsokoglou, A.; Happe, T. *J. Biol. Chem.* **2001**, *276*, 6125-6132.
(213) Pieper, U.; Eswar, N.; Braberg, H.; Madhusudhan, M. S.; Davis, F. P.; Stuart, A. C.; Mirkovic, N.; Rossi, A.; Marti-Renom, M. A.; Fiser, A.; Webb, B.; Greenblatt, D.; Huang, C. C.; Ferrin, T. E.; Sali, A. *Nucleic Acids Res.* **2004**, *32*, D217-D222.
(214) van Haaster, D. J.; Hagedoorn, P. L.; Jongejan, J. A.; Hagen, W. R. *Biochem. Soc. Trans.* **2005**, *33*, 12-14.
(215) Adams, M. W.; Mortenson, L. E. *J. Biol. Chem.* **1984**, *259*, 7045-7055.
(216) Léger, C.; Dementin, S.; Bertrand, P.; Rousset, M.; Guigliarelli, B. *J. Am. Chem. Soc.* **2004**, *126*, 12162-12172.
(217) Jones, A. K.; Pershad, H. R.; Sillery, E.; Albracht, S. P. J.; Armstrong, F. A. *J. Inorg. Biochem.* **2001**, *86*, 283-283.
(218) Vincent, K. A.; Belsey, N. A.; Lubitz, W.; Armstrong, F. A. *J. Am. Chem. Soc.* **2006**, *128*, 7448-7449.
(219) Van Dijk, C.; Van Berkel-Arts, A.; Veeger, C. *FEBS Lett.* **1983**, *156*, 340-344.
(220) Baffert, C.; Demuez, M.; Cournac, L.; Burlat, B.; Guigliarelli, B.; Bertrand, P.; Girbal, L.; Léger, C. *Ang. Chem.-Int. Ed.* **2008**, *47*, 2052-2054.
(221) Stripp, S.; Goldet, G.; Brandmayr, C.; Vincent, K. A.; Haumann, M.; Armstrong, F. A.; Happe, T. *Proc. Natl. Acad. Sci. U.S.A.* **2009**, *In press*.
(222) Ludwig, M.; Cracknell, J. A.; Vincent, K. A.; Armstrong, F. A.; Lenz, O. *J. Biol. Chem.* **2009**, *284*, 465-477.
(223) Camba, R.; Armstrong, F. A. *Biochemistry* **2000**, *39*, 10587-10598.
(224) Tilley, G. J.; Camba, R.; Burgess, B. K.; Armstrong, F. A. *Biochem. J.* **2001**, *360*, 717-726.
(225) Fauque, G.; Peck, H. D., Jr.; Moura, J. J.; Huynh, B. H.; Berlier, Y.; DerVartanian, D. V.; Teixeira, M.; Przybyla, A. E.; Lespinat, P. A.; Moura, I. *FEMS Microbiol. Rev.* **1988**, *4*, 299-344.
(226) Parkin, A. *DPhil Thesis* University of Oxford, 2008.
(227) Teixeira, M.; Moura, I.; Fauque, G.; Dervartanian, D. V.; Legall, J.; Peck, H. D.; Moura, J. J. G.; Huynh, B. H. *Eur. J. Biochem.* **1990**, *189*, 381-386.
(228) Bingemann, R.; Klein, A. *Eur. J. Biochem.* **2000**, *267*, 6612-6618.
(229) Stadtman, T. C. *Annu. Rev. Biochem.* **1990**, *59*, 111-127.
(230) Axley, M. J.; Bock, A.; Stadtman, T. C. *Proc. Natl. Acad. Sci. U. S. A.* **1991**, *88*, 8450-8454.
(231) Poling, B.; Prausnitz, J. M. *The Properties of Gases and Liquids*; 5th ed. ed.; McGraw-Hill: New York, 2001.
(232) Erbes, D. L.; King, D.; Gibbs, M. *Plant Physiol.* **1979**, *63*, 1138-1142.
(233) Erbes, D. L.; Burris, R. H. *Biochim. Biophys. Acta - Enzymol.* **1978**, *525*, 45-54.

(234) Purec, L.; Krasna, A. I.; Rittenberg, D. *Biochemistry* **1962**, *1*, 270-275.
(235) Thauer, R. K.; Kaufer, B.; Zahringe.M; Jungerma.K *Eur. J. Biochem.* **1974**, *42*, 447-452.
(236) Griffin, R. J.; Chen, J. J.; Carmody, K.; Vutukuru, S.; Dabdub, D. *J. Geophys. Res. - Atmos.* **2007**, *112*.
(237) King, G. M.; Weber, C. F. *Nat. Rev. Microbiol.* **2007**, *5*, 107-118.
(238) Wu, M.; Ren, Q. H.; Durkin, A. S.; Daugherty, S. C.; Brinkac, L. M.; Dodson, R. J.; Madupu, R.; Sullivan, S. A.; Kolonay, J. F.; Nelson, W. C.; Tallon, L. J.; Jones, K. M.; Ulrich, L. E.; Gonzalez, J. M.; Zhulin, I. B.; Robb, F. T.; Eisen, J. A. *PLoS Genet.* **2005**, *1*, 563-574.
(239) Schneider, K.; Cammack, R.; Schlegel, H. G.; Hall, D. O. *Biochim. Biophys. Acta* **1979**, *578*, 445-461.
(240) Van der Linden, E.; Burgdorf, T.; Bernhard, M.; Bleijlevens, B.; Friedrich, B.; Albracht, S. P. J. *J. Biol. Inorg. Chem.* **2004**, *9*, 616-626.
(241) De Lacey, A. L.; Stadler, C.; Fernandez, V. N.; Hatchikian, E. C.; Fan, H. J.; Li, S. H.; Hall, M. B. *J. Biol. Inorg. Chem.* **2002**, *7*, 318-326.
(242) Adams, M. W. W. *J. Biol. Chem.* **1987**, *262*, 15054-15061.
(243) Bennett, B.; Lemon, B. J.; Peters, J. W. *Biochemistry* **2000**, *39*, 7455-7460.
(244) Lemon, B. J.; Peters, J. W. *Biochemistry* **1999**, *38*, 12969-12973.
(245) Silakov, A.; Wenk, B.; Reijerse, E.; Albracht, S. P. J.; Lubitz, W. *J. Biol. Inorg. Chem.* **2009**, *14*, 301-313.
(246) Chen, Z. J.; Lemon, B. J.; Huang, S.; Swartz, D. J.; Peters, J. W.; Bagley, K. A. *Biochemistry* **2002**, *41*, 2036-2043.
(247) De Lacey, A. L.; Pardo, A. L. A.; Fernández, V. M.; Dementin, S.; Adryanczyk-Perrier, G.; Hatchikian, E. C.; Rousset, M. *J. Biol. Inorg. Chem.* **2004**, *9*, 636-642.
(248) Goldet, G.; Brandmayr, C.; Stripp, S.; Cavazza, C.; Fontecilla-Camps, J. C.; Happe, T.; Armstrong, F. A. *J. Am. Chem. Soc.* **2009**, *in press*.
(249) Hoffman, B. M.; Gibson, Q. H. *Proc. Natl. Acad. Sci. U. S. A.* **1978**, *75*, 21-25.
(250) Kochanski, E. *Photoprocesses in transition metal complexes, biosystems and other molecules: experiment and theory*; Kluwer Academic Press: London, 1992.
(251) Haldane, J. S.; Lorrain Smith, J. *J. Physiol. (London)* **1896**, *20*, 497-520.
(252) Adams, M. W. W. *Biochim. Biophys. Acta* **1990**, *1020*, 115.
(253) Stryer, L. *Biochemistry*; Freeman: New York, 2005.
(254) Cracknell, J. A.; Vincent, K. A.; Ludwig, M.; Lenz, O.; Friedrich, B.; Armstrong, F. A. *J. Am. Chem. Soc.* **2008**, *130*, 424-425.
(255) Schink, B.; Probst, I. *Biochem. Biophys. Res. Commun.* **1980**, *95*, 1563-9.
(256) Lubitz, W.; Reijerse, E.; van Gastel, M. *Chem. Rev.* **2007**, *107*, 4331-4365.
(257) Saggu, M.; Zebger, I.; Ludwig, M.; Lenz, O.; Friedrich, B.; Hildebrandt, P.; Lendzian, F. *J. Biol. Chem.* **2009**, *284*, 16264-16276.
(258) McTavish, H.; Sayavedrasoto, L. A.; Arp, D. J. *J. Bacteriol.* **1995**, *177*, 3960-3964.
(259) Ihara, M.; Nishihara, H.; Yoon, K.-S.; Lenz, O.; Friedrich, B.; Nakamoto, H.; Kojima, K.; Honma, D.; Kamachi, T.; Okura, I. *Photochem. Photobiol.* **2006**, *82*, 676-682.

(260) Cracknell, J. A. *DPhil Thesis* University of Oxford, 2009.
(261) Cammack, R.; Patil, D.; Aguirre, R. *FEBS Lett.* **1982**, *142*, 289-292.
(262) Heering, H. A.; Mondal, M. S.; Armstrong, F. A. *Anal. Chem.* **1999**, *71*, 174-182.
(263) Patil, D. S.; Moura, J. J. G.; He, S. H.; Teixeira, M.; Prickril, B. C.; DerVartanian, D. V.; Peck, H. D., Jr.; LeGall, J.; Huynh Boi, H. *J. Biol. Chem.* **1988**, *263*, 18732-8.
(264) Tosatto, S. C. E.; Toppo, S.; Carbonera, D.; Giacometti, G. M.; Costantini, P. *Int. J. Hyd. En.* **2008**, *33*, 570-578.
(265) Cohen, J.; Arkhipov, A.; Braun, R.; Schulten, K. *Biophys. J.* **2006**, *91*, 1844-1857.
(266) Crack, J. C.; Le Brun, N. E.; Thomson, A. J.; Green, J.; Jervis, A. J. In *Globins and Other Nitric Oxide-Reactive Proteins, Part B*; Elsevier Academic Press Inc: San Diego, 2008; Vol. 437, p 191-209.
(267) Crack, J. C.; Green, J.; Cheesman, M. R.; Le Brun, N. E.; Thomson, A. J. *Proc. Natl. Acad. Sci. U. S. A.* **2007**, *104*, 2092-2097.
(268) Varghese, S.; Tang, Y.; Imlay, J. A. *J. Bacteriol.* **2003**, *185*, 221-230.
(269) Beinert, H.; Kiley, P. *FEBS Lett.* **1996**, *382*, 218-219.
(270) Flint, D. H.; Tuminello, J. F.; Emptage, M. H. *J. Biol. Chem.* **1993**, *268*, 22369-22376.
(271) Beinert, H.; Holm, R. H.; Munck, E. *Science* **1997**, *277*, 653-659.
(272) Imlay, J. A. *Mol. Microbiol.* **2006**, *59*, 1073-1082.
(273) Gardner, P. R.; Fridovich, I. *J. Biol. Chem.* **1991**, *266*, 1478-1483.
(274) Gardner, P. R.; Fridovich, I. *J. Biol. Chem.* **1991**, *266*, 19328-19333.
(275) Beinert, H.; Albracht, S. P. J. *Biochim. Biophys. Acta* **1982**, *683*, 245-277.
(276) Mitra, S.; Elliott, S. J. *Biochemistry* **2009**, *48*, 3813-3815.
(277) Cracknell, J. A.; Wait, A. F.; Lenz, O.; Friedrich, B.; Armstrong, F. A. *Proc. Natl. Acad. Sci. U.S.A.* **2009**, *Submitted*.
(278) Shriver, D. F.; Atkins, P. W. *Inorganic Chemistry*; 3rd edition ed.; Oxford University Press: Oxford, 1999.
(279) Fontecilla-Camps, J. C. *J. Biol. Inorg. Chem.* **1996**, *1*, 91-98.
(280) Teixeira, M.; Fauque, G.; Moura, I.; Lespinat, P. A.; Berlier, Y.; Prickril, B.; Peck, H. D., Jr.; Xavier, A. V.; Le Gall, J.; Moura, J. J. G. *Eur. J. Biochem.* **1987**, *167*, 47-58.
(281) Hatchikian, C. E.; Traore, A. S.; Fernandez, V. M.; Cammack, R. *Eur. J. Biochem.* **1990**, *187*, 635-643.